TEACH SPIN

Instruments Designed for Teaching

Diode Laser Spectroscopy

"Spectroscopy and Much More, Using Modern Optics"

DLS1-A

USER'S MANUAL

A PRODUCT OF TEACHSPIN, INC.

Designed in collaboration with
Professor Kenneth Libbrecht of the California Institute of Technology

DIODE LASER SPECTROSCOPY
Instructor/Student Manual Table of Contents

Introduction to TeachSpin's Diode Laser Spectroscopy

"Diode Laser Spectroscopy" was produced in collaboration with Professor Kenneth Libbrecht of the California Institute of Technology (Caltech).   Having used TeachSpin's Pulsed NMR and Optical Pumping in his advanced lab, Professor Libbrecht was convinced that TeachSpin would be able to build an apparatus that would make these experiments, which were a favorite with his students, available to the entire advanced laboratory community.   And the collaboration continues – shortly after DLS1-A was finished, Professor Libbrecht worked with us to create the Fabry-Perot Cavity accessory. And we are hoping to add even more.

Both the DLS1-A apparatus and this manual were produced in collaboration with Professor Libbrecht.   The varied "voices" will be apparent as your read the manual. Senior Scientist Dr. George Herold was responsible for much of the TeachSpin contribution to both the instrument design and this manual.

The first three student laboratory instruction manuals in the Experiments section come from the Caltech advanced lab. (You will find pdf versions of these documents on the Caltech advanced lab website.) The fourth experiment is in an article that was written for the American Journal of Physics by Professor David Van Baak of Calvin College, who is also a TeachSpin collaborating physicist.

We know you will be creating instruction manuals for this apparatus which are tailored to the specific needs of your own institution. We hope that, as you do so, you will make them available through your own lab websites or those of AAPT or ALPhA. They can then be shared both with people using this TeachSpin instrument and with other members of the advanced laboratory community who may have built similar experiments on their own.

We wish you and your students challenging, exciting, and satisfying adventures exploring Diode Laser Spectroscopy.

DIODE LASER SPECTROSCOPY

LASER PHYSICS

Diode Laser Physics

I. LASER BASICS

Beginning in the mid 1960's, before the development of semiconductor diode lasers, physicists mostly used tunable "dye" lasers in pioneering atomic physics experiments needing tunable laser light. Dye lasers use a chemical dye as the active medium, *i.e.* the material which produces the laser emission. A population inversion in the dye is created, typically, with a fixed-frequency "pump" laser. An individual dye will lase over a limited wavelength range, and different dyes are available to make tunable lasers at essentially all visible and near-infrared wavelengths. Unfortunately dye lasers are large, cumbersome instruments that are both very expensive to purchase (~$100,000.00) and expensive to operate and maintain. Some of the solid-state lasers used as dye laser replacements, such as the popular Ti:sapphire crystal (titanium-doped sapphire), work better than dyes, and other techniques using non-linear crystals exist to generate tunable laser light (Yariv 1991). However, while these may be less difficult to use than dye lasers they are still very expensive options.

The recent development of tunable, narrow-bandwidth, semiconductor diode lasers dramatically changed this picture. These lasers are inexpensive, easy to operate, and produce high-power, tunable, narrow-bandwidth radiation ($\Delta\nu < 1$ MHz, $\Delta\lambda < 1.5\times10^{-6}$ nm). For these reasons, tunable diode lasers have rapidly become commonplace in modern research laboratories.

Interior Diagram of TOLD9200 Series
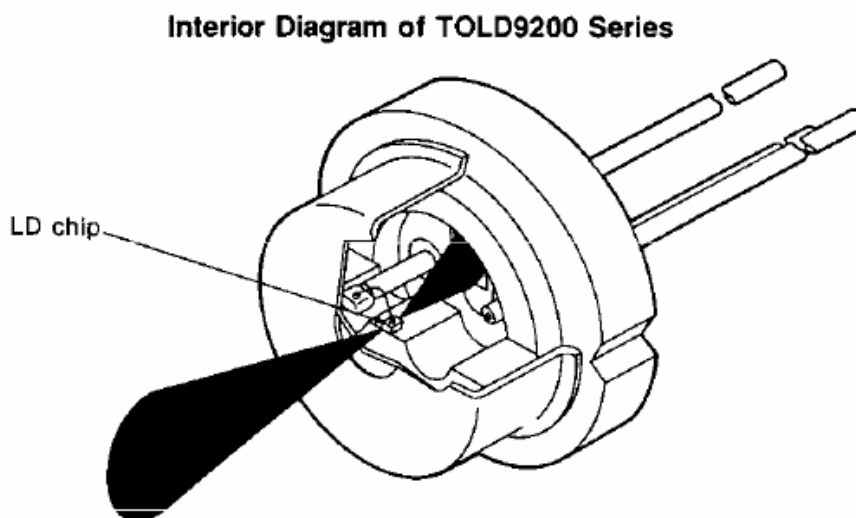
Figure 1: Cut-away view of a typical laser diode can, like those used in the TeachSpin laser

The basic physics of diode lasers is presented in several review articles and books, such as Wieman and Hollberg (1991) and Camparo (1985). Figure 1 shows a cut-away view of a typical diode laser, similar to the ones used in this experiment. The actual semiconductor device is a small chip (LD chip in Figure 1), bonded to a heat-sink. Tiny wires connect the

chip to the outside world. Most of the light emitted by the laser comes out the front facet, and a small amount also comes out the back facet. (The two facets are constructed to have different reflectivities). Often, a photodiode is placed at the back of the can, to monitor the laser output power. The main laser beam, which is elliptical and strongly diverging, comes out a window in the front of the laser diode can.

Figure 2 shows a more detailed view of a typical laser diode chip. Current is driven from the top to the bottom of the chip (see arrow in Figure 2), creating electron-hole pairs that recombine in the active layer, emitting light in the process. The light is confined to a narrow channel in the chip, ~2 microns high, ~10 microns wide, and about 400 microns long (wavy line in Figure 2). The facets of the chip, at the ends of the channel, act as partially reflecting mirrors enclosing the laser cavity.
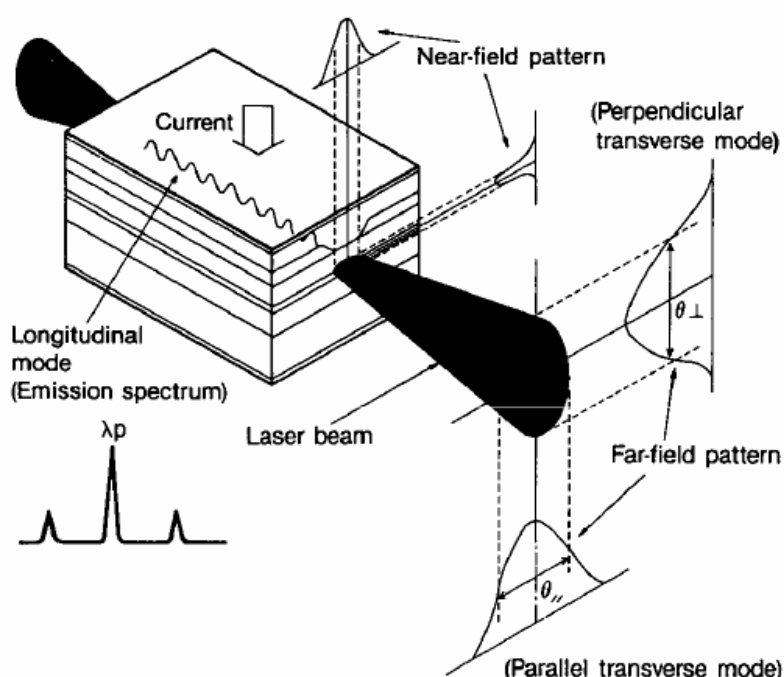
Figure 2: Schematic view of a laser diode chip

Figure 3 shows a schematic picture of the actual semiconductor layer structure in a diode laser. How all this *really* works, the nitty-gritty semiconductor technology, is not something we will concern ourselves with in this discussion. Since light generation in a diode laser results from the recombination of electron-hole pairs injected into an active layer at the diode's n-p junction, the wavelength of the emitted light is approximately that of the band gap of the material. The electron-hole population inversion is restricted to a narrow strip in the active layer, so the laser's optical gain is spatially localized. Gain is the amount that an optical wave is amplified by stimulated emission as it passes through the laser cavity. The diode heterostructure also serves as an optical waveguide; the active layer has a higher index of refraction than its surroundings, so light is confined to the channel by total internal refection. The cleaved facets at the end of the chip serve as the cavity mirrors and output couplers. These can be coated to increase or decrease the facet reflectivity.

SCHEMATIC STRUCTURE OF VISIBLE LASER DIODES

Electrode
Contact Layer (p-GaAs)
Blocking Layer (n-GaAs)
Cladding Layer (p-In(GaAl)P)
Active Layer (InGaP)
Cladding Layer (n-In(GaAl)P)
Substrate (n-GaAs)
Electrode

(a) Gain-Guided Laser

(b) Index-Guided Laser

Figure 3: Schematic picture of the internal semiconductor structure of some typical laser diodes. This view is looking into one facet of the laser cavity.

By careful construction of the diode cavity, the laser can be made to emit in a single longitudinal cavity mode (*i.e.* a standing wave inside the cavity, with a fixed number of nodes along the cavity axis and no nodes in the transverse direction). A "bare" diode laser has a linewidth of typically $\Delta v \sim 50$ MHz. The spatial mode of the laser, and thus the shape of the output beam, is defined by the narrow channel that confines the light. Since 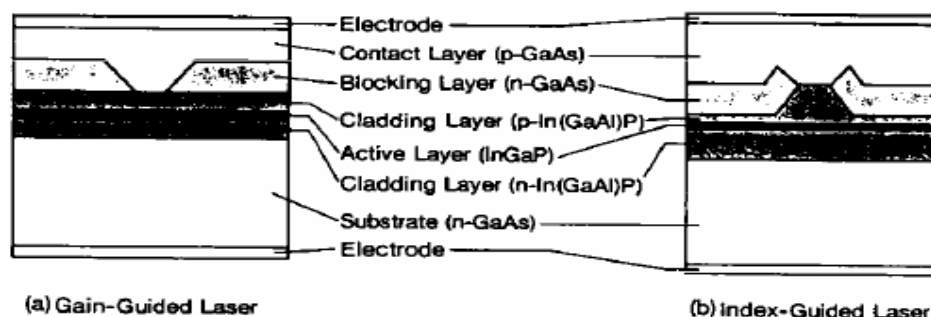the channel is rectangular, and not much larger than the light wavelength, the output beam is elliptical and strongly diverging (see Wieman and Hollberg 1991).

At low levels of injection current, the optical losses exceed the gain and a population inversion is not achieved. The light output is then broad-band, spontaneous emission, similar to that of an LED. But, above a "threshold" current, the laser emits a coherent beam, which increases in intensity linearly with injection current. The output power in coherent radiation can be as high as 50 percent of the input electrical power, which is very efficient compared with other methods of producing laser light.

Diode lasers have many uses; primary among these are retrieving data stored on optical disks (for instance all compact disk players use diode lasers) and sending light pulses down optical fibers for telecommunications. At present, one can purchase diode lasers that operate at wavelengths from the blue to the infrared; there is a big push in industrial labs to produce shorter wavelength lasers, in order to increase the density of optical disk storage. Power levels for single-mode diode lasers are typically a few mW, but can be as high as 1 Watt.

The TeachSpin diode lasers (Sanyo DL-7140-201S) emit up to 70 mW of output power near 785 nm. The back surface of the tiny semiconductor laser cavity is highly reflecting, while the front surface is often coated with a thin antireflection layer to enhance its transmission. (Only the manufacturer knows exactly how the facets are prepared; such details are often carefully guarded industrial trade secrets.)[*]

---

[*] It is possible to get an approximate measure of the reflection coefficient, R = 16.5% ± 5%. (See section A4-2 for details.)

II. LASERS WITH GRATING FEEDBACK or External Cavity Diode Lasers (ECDL)

A. Introduction

Bare diode lasers have two undesirable properties: 1) their linewidths ($\Delta\nu{\sim}50$ MHz) are large compared to the linewidths of atomic transitions (in our case $\Gamma{\sim}5$ MHz); and 2) they are extremely sensitive to optical feedback – as little as 10^{-6} of the output light scattered back into the laser may affect its frequency stability. As shown in Figure 4, we overcome both these problems by using a diode laser with a small amount of controlled feedback from a diffraction grating.
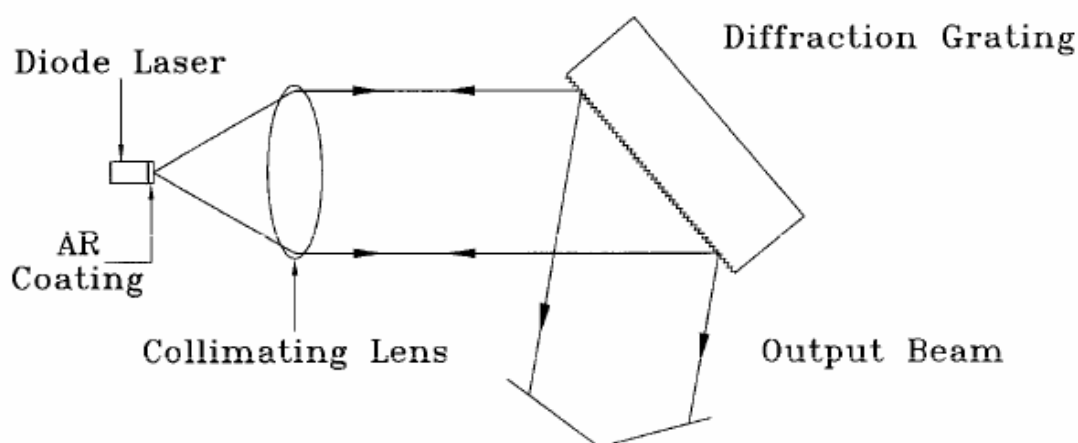
Figure 4: Basic configuration of the diode laser system

A lens in front of the laser collimates the output into a nearly nondiverging elliptical beam. After the lens, the beam strikes a diffraction grating, which is a holographic (no blaze) grating with 1800 lines/mm. Most of the light is directly reflected by the grating (m=0 grating order), but roughly 15 percent is reflected back into the laser (m=1 order). The grating forms an "external cavity" (*i.e.* external to the laser's own internal semiconductor cavity), which serves to frequency-stabilize and line-narrow the laser output (see Wieman and Hollberg 1991, and references therein, to understand how this happens). With the simple addition of the diffraction grating, the laser is much less sensitive to stray light feedback, and its linewidth will be reduced to $\Delta\nu < 1$ MHz, much smaller than the atomic transition linewidths we will be observing.

B. Laser Tuning:

With grating feedback, the frequency of the laser output depends on a number of factors. In order for you to effectively tune the laser to an atomic transition, it is helpful to understand how these factors determine the laser output frequency. The laser will tend to lase at the mode frequency with the greatest net gain (*i.e.* stimulated emission minus optical losses) (see Yariv 1991). Once the laser begins to lase in this mode, stimulated emission limits the number of electron-hole pairs which are available for lasing in other modes, and the result is a laser with a single-mode (*i.e.* single frequency) output beam. (Note: This does not always happen. Our lasers will sometimes lase in two or more modes at the same time, and sometimes the output

frequency will vary rapidly and chaotically over a broad frequency range. While these behavior patterns are interesting, and the subject of some amount of research, we will mainly try to find a place in parameter space where the laser operates in a single mode.) To determine the laser operating frequency (assuming single-mode operation), we need to find the frequency with the highest net gain. Figure 5 shows, schematically, the different contributions to the net gain. These contributions are best explored individually.
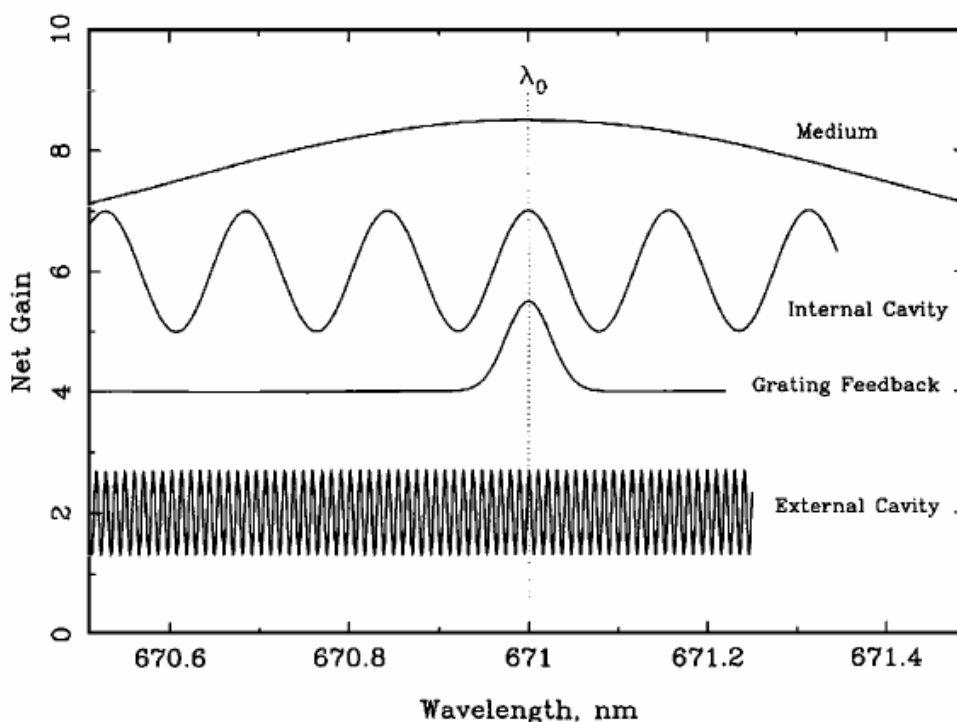
Figure 5: Schematic of the different contributions to the net optical gain of an arbitrary laser as a function of frequency. The curves are displaced relative to one another for clarity.

1. The medium gain

This depends on the properties of the semiconductor material from which the laser is made, in particular the band gap. The medium gain shows a broad peak in frequency space, whose position depends mainly on laser temperature. Since we are aiming for the rubidium atomic transition, we must set the laser temperature, using the temperature controller, so that it operates near 780 nm, the wavelength of the rubidium resonance lines. This temperature is recorded on the antistatic bag in which each diode is shipped. The temperature for the diode that was shipped in your laser is listed on the data sheet included in your manual.

A plot of Wavelength versus Temperature for a typical laser is shown in Figure 6. The overall slope of this data is about 0.23 nm $°C^{-1}$, which should be about equal for all the Sanyo diodes. From this slope and the temperature set point for 780 nm, you can determine an appropriate temperature for any desired wavelength for that specific diode. Once this is done, the medium gain curve is so broad that it is unimportant for determining the precise wavelength of the laser.
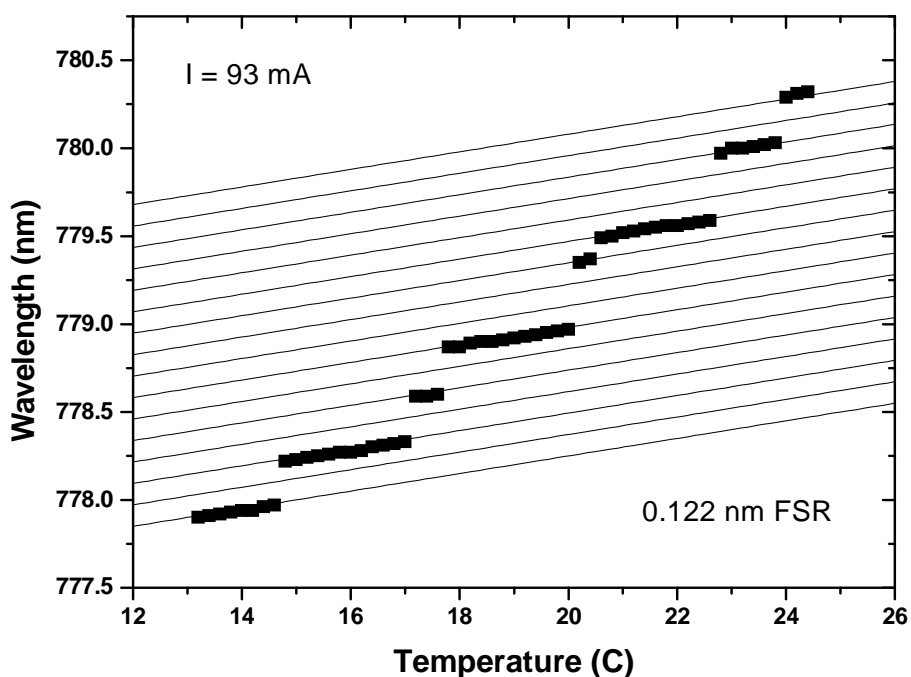
Figure 6: Output wavelength of a free-running (*i.e.* no external optical feedback) Sanyo DL-7140-200S diode laser as a function of diode temperature. (The behavior of other diode lasers is similar.)

2. The internal cavity

The diode junction forms a small Fabry-Perot etalon, or optical cavity, and like all optical cavities, it has a normal mode structure. This translates to an effective frequency-dependent net gain function which is periodic in frequency, as shown in Figure 5 (see Yariv 1991 or Möller 1988 for a discussion of optical cavities). The period is called the "free spectral range", and is given by $\Delta\nu_{FSR} = c/2Ln$, where c is the speed of light, n is the index of refraction ($n \approx 3.6$ in the semiconductor), and L is the cavity length. For this particular laser we have $\Delta\nu_{FSR} \approx 60$ GHz ($\Delta\lambda \approx 0.122$ nm). The internal cavity gain function will shift in frequency with changes in the diode temperature at roughly 0.05 nm $°C^{-1}$ this is measured from the small scale slope the individual steps in Figure 6. Unfortunately, the temperature of the laser head can not be changed very quickly. The thermal time constant of the laser head can be estimated to be on the order of 10 seconds.[*] The internal cavity modes will also change with the diode current. (See Figure 7.)

---

[*] Estimated from the mass ($\approx$170grams), heat capacity and thermal conductivity, assuimng the laser head is a solid cube of aluminum with the TEC on one face and the diode and temperature sensor at the center .

Figure 7: Free-running laser Wavelength versus Injection Current at a fixed temperature

The current affects a diode in two ways. First, increasing the current causes simple heating, which changes the temperature of the diode and thus the wavelength in much the same way as heating the laser head directly. With respect to wavelength, modulating the current can be thought of as a means of rapidly changing the diode temperature. This effect predominates 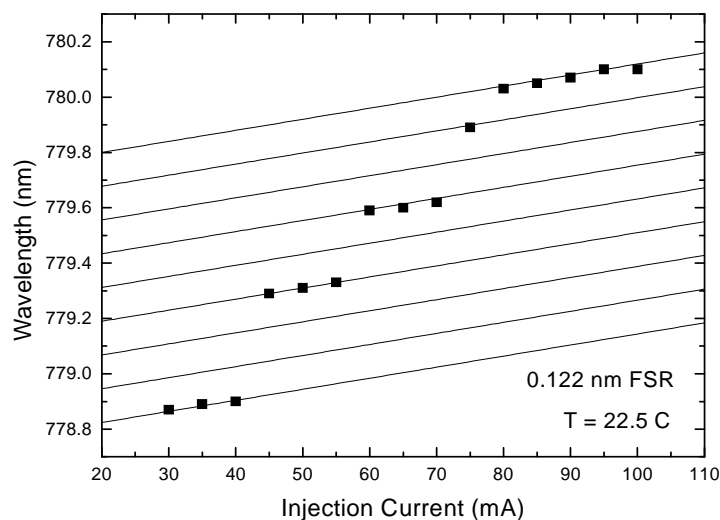for time scales longer than 1 μs and tunes at roughly 2 GHz/mA as shown in Figure 7. The second means by which the current changes the free-running laser wavelength is by changing the carrier concentration in the active region. This modulates the optical path length of the diode, with a tuning rate of about 200 MHz/mA, up to a maximum frequency that is set by the relaxation oscillation frequency of the diode, typically several GHz.

Taken together, Figures 5 - 7 demonstrate the interaction of several influences. Figure 6 shows a plot of the wavelength of a free-running laser as a function of temperature. As the temperature is increased, the maximum gain of both the medium and the internal cavity modes shown in Figure 5 will shift to longer wavelengths. They do not, however, shift at the same rate. This creates laser "mode hops" to different peaks of the cavity gain function. In practice, we would like to set the temperature and injection current so that the laser operates at the rubidium resonance frequency. But, as can be seen from Figure 6, this is not always possible with a free-running laser. With the addition of an external grating, the laser can be made to operate at any wavelength within a reasonably broad range.

3. The Grating Feedback

Since a grating disperses light, only light from a narrow wavelength band will be fed back into the laser for a fixed grating left/right (L/R) angle. (The grating up/down (U/D) angle should be set so that the light from the grating reflects back into the laser.) In this apparatus, the grating is used in a Littrow configuration where the first order diffraction is sent back into the diode. In this configuration, the wavelength can be found from $\lambda = 2\, d\, \sin\theta$, where d is

the line spacing of the grating and θ is the grating angle (measured from the normal). Assuming an ideal grating, where the resolving power is limited only by diffraction, the spectral width of the first order diffraction, $\Delta\nu$, will be given approximately by $\nu/\Delta\nu=N$, where ν is frequency and N is the number of grating lines subtended by the laser beam (see Möller 1988 or any general optics book, for a discussion of grating properties). For example, with a 0.3 cm laser beam width, we will find $N = 5400$ and $\Delta\nu \approx 70$ GHz. The position of this peak is determined by the grating L/R angle.

4. The external cavity

This is similar to (2) above, but with the external cavity, one end of which is the grating, and the other is the highly reflective back facet of the diode. Since the external cavity is much larger we have $\Delta\nu_{FSR} = c/2L \approx 10$ GHz. for a 15 mm external cavity length. (See Section A.4 and Figure A.4.1 for the relevant dimensions.) This curve shifts by moving the grating position, which we do either with the L/R knob on the laser head or with the piezo-electric transducer (PZT) in the grating mount.

In order to force the laser into single-mode laser operation at a predetermined wavelength λ_0 (e.g. an atomic resonance line), the gain from each of the components should peak at λ_0 as shown in Figures 5.

To get a more complete understanding of how these contributions interact, how the laser tunes as the grating angle is changed, we have tried to construct an accurate "best guess" picture of the shape of the various cavity modes in the laser. This picture is shown in Figure 8. Referring back to Figure 5, the grating feedback and external cavity gains have been merged into the single solid line of Figure 8. The broad medium gain has been left out of the plot. Figure 8 is a picture of the various cavity modes with all the gains having a maximum at the same frequency.
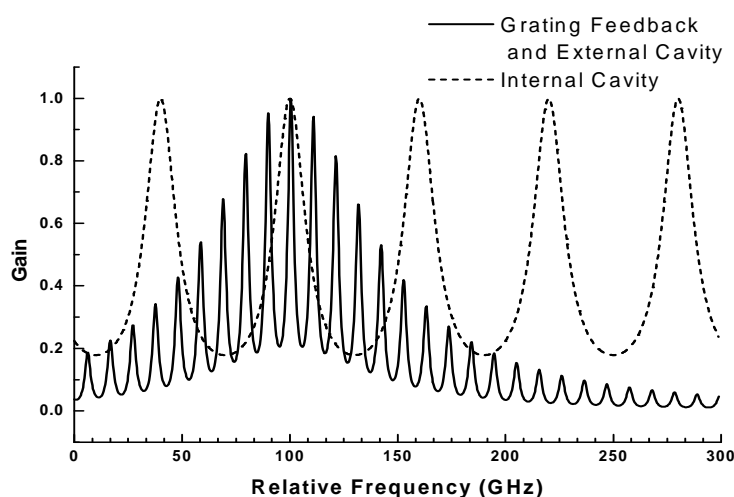
Figure 8: "Best guess" picture internal cavity, grating feed back and external cavity modes in the laser
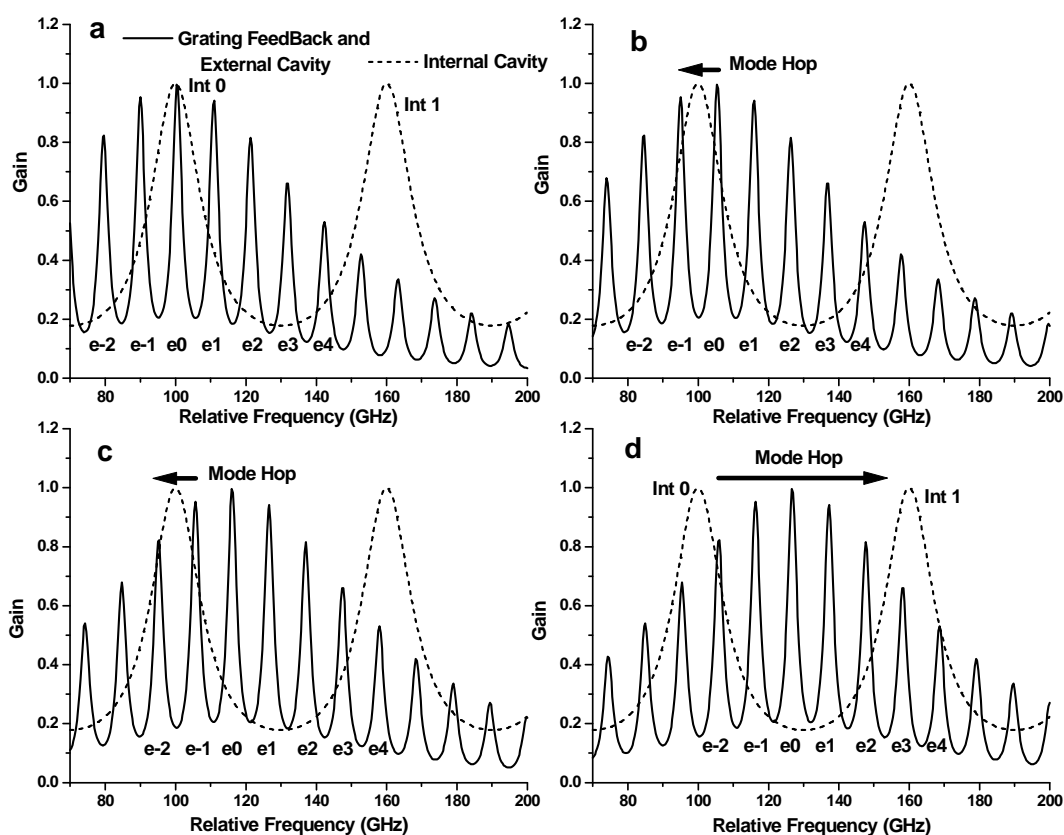
Figure 9: Series of graphs showing showing how the external and grating feed back mode shifts as the grating angle is changed.

Figure 9 shows a series of pictures of the External and Internal cavity modes as the grating angle is decreased. The pictures show only two of the internal modes labeled Int 0 and Int 1. For reference, we have also labeled some of the external modes e-2, e-1, e0, e1…e4. In Figure 9, Graph **a** is for the same grating angle shown in Figure 8, where the laser is oscillating in external mode e0. As the grating angle is decreased, mode e0 is shifted to higher frequency, shorter wavelength, until the point shown in graph b. At this point, the overall gain in external mode e-1 is about equal to that in mode e0 and, as the grating continues to move, the laser will jump into mode e-1. As the angle is decreased further, the laser will reach the point shown in graph c and the laser will hop to mode e-2. Finally, in graph d, the maximum of the grating feedback frequency is about half way between internal modes Int0 and Int1. As the angle continues to decrease, the laser will make a relatively larger mode hop and lase in external mode e3 under internal mode Int1.

You should notice that during this change in angle, the laser has swept through the same small frequency range "under" Int0 several times. After these changes, the laser moved to a new frequency defined by Int1 with a rather large gap of frequencies in between. To be able to cover the entire frequency range, we need to be able to change the position of the internal

modes. This is done by changing the laser current. To tune the laser to the correct wavelength for the rubidium transitions, both the correct grating angle and laser current must be found. The procedure for doing this is discussed in the next section. The next section will also describe a clever trick in which both the grating angle and laser current are swept simultaneously at rates such that both the internal mode Int0 and the maximum of the external modes e0 change in frequency together resulting in long (20 GHz) mode hop free scans. An understanding of the Figures 8 and 9 should help you visualize how this is accomplished.

III. REFERENCES.

Camparo, J. C. 1985, ”The Diode Laser in Atomic Physics,” *Cont. Phys*. **26**, 443.

Möller, K. D. 1988, *Optics*, (University Science Books).

Wieman, C. E. and Hollberg, L. 1991, “Using Diode Lasers for Atomic Physics,” *Rev. Sci. Instrum.* **62,** 1.

Yariv, A. 1991, *Optical Electronics*, 4th edition (Holt, Rinehart and Winston).

DIODE LASER SPECTROSCOPY

SPECTROSCOPY

Diode Laser Spectroscopy

I. BACKGROUND

One of the most important scientific applications of lasers is in the area of precision atomic and molecular spectroscopy. Spectroscopy is used not only to better understand the structure of atoms and molecules, but also to define standards in metrology. For example, the second is defined from atomic clocks using the 9192631770 Hz (exact, by definition) hyperfine transition frequency in atomic cesium, and the meter is (indirectly) defined from the wavelength of lasers locked to atomic reference lines. Furthermore, precision spectroscopy of atomic hydrogen and positronium is currently being pursued as a means of more accurately testing quantum electrodynamics (QED), which so far is in agreement with fundamental measurements to a high level of precision (theory and experiment agree to better than a part in 10^8). An excellent article describing precision spectroscopy of atomic hydrogen, the simplest atom, is Hänsch *et al*. 1979 (details are in References). Although it is a bit old, the article contains many ideas and techniques in precision spectroscopy that continue to be used and refined to this day.
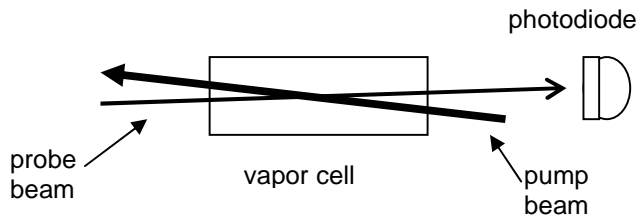
Figure 1: The basic saturated absorption spectroscopy set-up.

II. QUALITATIVE PICTURE OF SATURATED ABSORPTION SPECTROSCOPY – 2-LEVEL ATOMS.

Saturated absorption spectroscopy is one simple and frequently-used technique for measuring narrow-line atomic spectral features, limited only by the natural linewidth Γ of the transition (for the rubidium D lines $\Gamma \approx 6$ MHz), from an atomic vapor with large Doppler broadening of $\Delta \nu_{Dopp} \sim 1$ GHz. To see how saturated absorption spectroscopy works, consider the experimental set-up shown in Figure 1. Two lasers are sent through an atomic vapor cell from opposite directions; one, the "probe" beam, is very weak, while the other, the "pump" beam, is strong. Both beams are derived from the same laser, and therefore have the same frequency. As the laser frequency is scanned, the probe beam intensity is measured by a photodetector.

Figure 2 shows the spectra that might be recorded if 2-level atoms were in the vapor cell. The upper plot gives the probe beam absorption without the pump beam. Here one sees simple Doppler-broadened absorption. In our case, the Doppler width is much larger than the natural linewidth, $\Delta \nu_{Dopp} \gg \Gamma$, and the optical depth of the vapor is fairly small $\tau(\nu) \leq 1$.

The transmitted fraction of the probe is $e^{-\tau(\nu)}$, which defines the optical depth; τ is proportional to the atomic vapor density and the path length. As a result, the probe spectrum is essentially a simple Gaussian profile.

The lower plot in Figure 2 shows the spectrum *with* the pump beam. A spike appears right at the atomic resonance frequency. The reason this spike appears is as follows: If the laser frequency is $\nu_0 - \Delta\nu$, then the probe beam is absorbed only by atoms moving with longitudinal velocity $v \approx c\Delta\nu/\nu_0$, moving toward the probe beam. These atoms see the probe beam blue-shifted into resonance; other atoms are not in resonance with the probe beam, and so they do not contribute to the probe absorption. Because the pump beam is in the opposite direction, these same atoms see the pump beam red-shifted further from resonance, so they are unaffected by the pump beam. Thus for laser frequencies $\nu \neq \nu_0$, the probe absorption is the same with or without the pump beam. However, if $\nu = \nu_0$, then atoms with zero velocity, v = 0, contribute to the probe absorption.

These v = 0 atoms also see an on-resonance pump beam, which is strong enough to keep a

Fig. 2: **Absorption spectra for 2-level atoms, both without (upper) and with (lower) the pump beam.**

significant fraction of the atoms in the excited state, where they do not absorb the probe beam (in fact they increase the probe beam intensity via stimulated emission). Thus at $\nu = \nu_0$ the probe absorption is *less* than it was without the pump beam. (If the pump beam had infinite intensity, half of the atoms would be in the excited state at any given time, and there would be identically zero probe absorption. One would say these atoms were completely "saturated" by the pump beam, hence the name saturated absorption spectroscopy.) The advantage of this form of spectroscopy should be obvious ... one can measure sharp Doppler-free features in a Doppler-broadened vapor.

III. QUALITATIVE PICTURE OF SATURATED ABSORPTION SPECTROSCOPY – MULTI-LEVEL ATOMS.

If the atoms in the absorption cell had a single ground state and two excited states (typically an electronic level split by the hyperfine interaction), and the separation of the excited states was less than the Doppler width, then one would see a spectrum like that shown in Figure 3.

The peaks on the left and right are ordinary saturated absorption peaks at ν_1 and ν_2, the two resonance frequencies. The middle peak at $(\nu_1 + \nu_2)/2$ is called a "cross-over resonance."
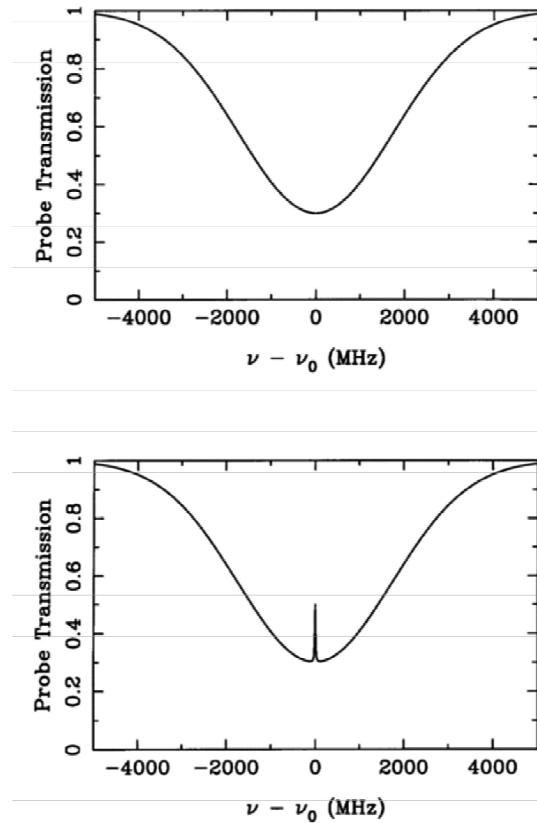
If you think about it for a while you can see where the extra peak comes from. It arises from atoms moving at velocities such that the pump is in resonance with one transition, and the probe is in resonance with the other transition. If you think about it a bit more you will see there are *two* velocity classes of atoms for which this is true – atoms moving toward the pump laser, and away from it.

If the atoms in the vapor cell had a single excited state, but two hyperfine ground states (we call them both "ground" states because neither can decay via an allowed transition), and the separation of the ground states was less than the Doppler width, then one might see a spectrum like in Figure 4. The extra cross-over dip results from a phenomenon called "optical pumping," which occurs because atoms in the excited state can decay into either of the two stable ground states. Thus, if atoms are initially in ground state $g1$, and one shines in a laser that excites $g1 \rightarrow e$, atoms will get excited from $g1 \rightarrow e$, over and over again until they once spontaneously decay to $g2$, where they will stay. The state $g2$ is called a "dark state" in this case, because atoms in $g2$ are not affected by the laser. We see that a laser exciting $g1 \rightarrow e$, will eventually optically pump all the atoms into $g2$.

To see how optical pumping produces the extra crossover dip, remember that only the pump laser can optically pump – the probe laser is by definition too weak. Also remember the atoms in the cell are not in steady state. When they hit the walls, they bounce off about equally distributed in both ground states, and the optical pumping only

Fig. 3: **Saturated absorption spectrum for atoms with a single ground state and two closely spaced excited states.**

Fig. 4: **Saturated absorption spectrum for atoms with a single excited state that can decay into either of two closely spaced excited states.**

operates for a short period of time as the atoms travel through the laser beams. If you think about it a while you can see there are two velocity classes of atoms that are responsible for the dip. For one velocity class the pump laser excites $g1 \rightarrow e$, which tends to pump atoms into $g2$. Then the probe laser, which excites $g2 \rightarrow e$ for these atoms, sees extra absorption. For the other velocity class the pump laser excites $g2 \rightarrow e$, $g1$ gets overpopulated, and again the probe laser (which now excites $g1 \rightarrow e$ for these atoms) sees more absorption.
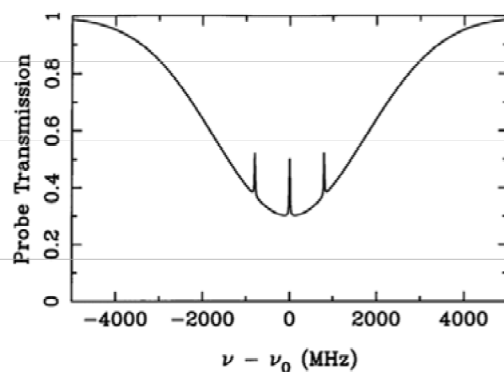
IV QUANTITATIVE PICTURE OF SATURATED ABSORPTION SPECTROSCOPY - 2-LEVEL ATOMS.

One can fairly easily write down the basic ideas needed to calculate a crude saturated absorption spectrum for 2-level atoms, which demonstrates much of the underlying physics. The main features are:

1) the transmission of the probe laser beam through the cell is $e^{-t(\nu)}$ and $\tau(\nu)$ is the optical depth of the vapor;

2) the contribution to $\tau(\nu)$ from one velocity class of atoms is given by

$$d\tau(\nu, \mathbf{v}) \sim (P_1 - P_2)F(\nu, \mathbf{v})dn(\mathbf{v})$$

where P_1 is the relative population of the ground state, P_2 is the relative population of the excited state ($P_1 + P_2 = 1$),

$$dn \sim e^{-m\mathbf{v}^2/2\kappa \mathrm{T}}d\mathbf{v}$$

is the Boltzmann distribution (for v along the beam axis), and

$$F(\nu, \mathbf{v}) = \frac{\Gamma/2\pi}{(\nu - \nu_0 + \nu_0 \mathbf{v}/c)^2 + \Gamma^2/4}$$

is the normalized Lorentzian absorption profile of an atom with natural linewidth Γ, including the Doppler shift. Putting this together, we have the differential contribution to the optical depth, for laser frequency ν and atomic velocity v:

$$d\tau(\nu, \mathbf{v}) = \tau_0 \frac{\nu_0}{c}(P_1 - P_2)F(\nu, \mathbf{v})e^{-m\mathbf{v}^2/2k\mathrm{T}}d\mathbf{v}.$$

The overall normalization comes in with the τ_0 factor, which is the optical depth at the center of resonance line, *i. e.* $\tau_0 = \int d\tau(\nu_0, \mathbf{v})$ with no pump laser (the integral is over all velocity classes). 3) The populations of the excited and ground states are given by $P_1 - P_2 = 1 - 2P_2$, and

$$P_2 = \frac{s/2}{1 + s + 4\delta^2/\Gamma^2}$$

where $s = I/I_{sat}$ and $\delta = \nu - \nu_0 - \nu_0 \mathbf{v}/c$. I_{sat} is called the saturation intensity (for obvious reasons ... if you consider the above formula for P_2 with $\delta = 0$, P_2 "saturates" $P_2 \to 1/2$ as $I/I_{sat} \to \infty$).

The value of I_{sat} is given by

$$I_{sat} = 2\pi^2 hc\Gamma/3\lambda^3.$$

For the case of rubidium, $\Gamma \approx 6$ MHz, giving $I_{sat} \approx 2$ mW/cm^2.

The underlying physics in points (1) and (2) should be recognizable to you. Point (3) results from the competition between spontaneous and stimulated emission. To see roughly how this comes about, write the population rate equations as

$$\dot{P}_1 = \Gamma P_2 - \alpha \mathrm{I}(P_1 - P_2)$$

$$\dot{P}_2 = -\Gamma P_2 + \alpha \mathrm{I}(P_1 - P_2)$$

where the first term is from spontaneous emission, with Γ equal to the excited state lifetime, and the second term is from stimulated emission, with α a normalization constant. Note that the stimulated emission is proportional to the intensity I. In the steady-state $\dot{P}_1 = \dot{P}_2 = 0$, giving

$$P_2 = \frac{\alpha \mathrm{I}/\Gamma}{1 + 2\alpha \mathrm{I}/\Gamma}$$

The term $\alpha I/\Gamma$ corresponds to the $s/2$ term above (note I_{sat} is proportional to Γ). A more complete derivation of the result, with all the normalization constants, is given in Milonni and Eberly (1988), and in Cohen-Tannoudji *et al.* (1992), but this gives you the basic idea.

Assuming a fixed vapor temperature, atomic mass, etc., the saturated absorption spectrum is determined by two adjustable external parameters, the pump intensity I_{pump} and the on-resonance optical depth τ_0. The latter is proportional to the vapor density inside the cell. Figure 5 shows calculated spectra at fixed laser intensity for different optical depths, and Figure 6 shows spectra at fixed optical depth for different laser intensities.

In Figure 5 one sees mainly what happens when the vapor density is increased in the cell. At low densities the probe absorption is slight, with a Gaussian profile, and the absorption increases as the vapor density increases. At very high vapor densities the absorption profile gets deeper and broader. It get broader simply because the absorption is so high near resonance that the probe is almost completely absorbed; for greater vapor densities the probe gets nearly completely absorbed even at frequencies fairly far from resonance; thus the width of the absorption profile appears broader. The saturated-absorption feature in Figure 5 does pretty much what you would expect. The probe absorption is reduced on resonance, due to the action of the pump laser. At very high vapor densities the saturated-absorption feature becomes smaller. This is because while the pump laser reduces the absorption, it doesn't eliminate it; thus at high vapor densities the probe is nearly completely absorbed even with the pump laser. The moral of this story is that the vapor density shouldn't be too low or high if you want to see some saturated-absorption features.

In Figure 6 one sees that if the pump intensity is low, the saturated-absorption feature is small, as one would expect. For larger pump intensities the feature grows in height and width. The width increases because at high laser intensities the effect of the pump laser saturates on resonance, and continues to grow off resonance; thus the width of the feature increases, an effect known as "power broadening."

Figure 6: Calculated saturated-absorption spectra for two-level atoms, for $(\tau, I/I_{sat}) = (1.0.1)$ $(1,1)$, $(1,10)$, $(1,100)$ and $(1,1000)$. Note at large laser intensities, the saturated absorption feature is "power broadened" as the line saturates.

Figure 5: Calculated saturated-absorption spectra for two-level atoms, for $(\tau, I/I_{sat}) = (0.1,10)$ $(0.316,10)$, $(1,10)$, $(3.16,10)$ and $(10,10)$. The two plots show the same spectra with the frequency axis at different scales. Note the overall Doppler-broadened absorption, with the small saturated-absorption feature at line center.

Finally, it should be noted that calculating the saturated absorption spectrum for real atoms, which must include optical pumping, many different atomic levels, atomic motion in the vapor cell, and the polarization of the laser beams, is considerably more subtle. A recent paper by Schmidt *et al.* (1994) shows much detailed data and calculations for the case of cesium.

Problem 1. Show that $\tau_0 = \int d\tau(\nu_0, \mathbf{v})$ when the pump laser intensity is zero, from the formula above. Hint: the integral is simplified by noting that $\Gamma << \Delta\nu_{Dopp}$.

Problem 2. The above calculations all assume that the pump laser has the same intensity from one end of the cell to another. This is okay for a first approximation, but calculating what really happens is an interesting problem. Consider a simple laser beam (the pump) shining through a vapor cell. If the laser intensity is weak, and the atoms are all pretty much in the ground state, then the laser intensity changes according to the equation $dI/dx = -\alpha I$, where $\alpha = \alpha(\nu)$ depends on the laser frequency, but not on position inside the cell. (In this case, α^{-1} is called the absorption length.) This equation has the solution $I(x) = I_{init}e^{-\alpha x}$, where I_{init} is the initial laser intensity. The transmission through the cell, $e^{-\alpha L}$, where L is the length of the cell, is what we called $e^{-\tau}$ above.

Your job in this problem is to work out what happens when the input laser beam is not weak, and thus we cannot assume that the atoms are all in the ground state. In this case $\alpha = \alpha(\nu, x)$, which makes the differential equation somewhat more interesting.

Assume the laser is on resonance for simplicity. Then the attenuation coefficient at any position x is proportional to $P_1 - P_2$, which in turn is proportional to $1/(1+s)$. Thus we have $\alpha(\nu_0, x) = \alpha_0/(1 + s(x))$.

In the weak beam limit $I << I_{sat}$ this reduces to our previous expression, so $\alpha_0 = \tau_0/L$. Write down an expression which relates the saturation parameter of the laser as it exits the cell s_{final}, the saturation parameter at the cell entrance $s_{initial}$, and the weak-limit optical depth τ_0. Check your expression by noting in the limit of finite τ_0 and small s you get $s_{final} = s_{initial}e^{-\tau_0}$. If $\tau_0 = 100$, how large must $s_{initial}$ be in order to have a transmission of 1/2 (i. e. $s_{final} = s_{initial}/2$)?

V. ATOMIC STRUCTURE OF RUBIDIUM

The ground-state electronic configuration of rubidium consists of closed shells plus a single 5s valence electron. This gives a spectrum which is similar to hydrogen (see attached Scientific American article). For the first excited state the 5s electron is moved up to 5p. Rubidium has two naturally occurring isotopes: [85]Rb (72 percent abundance), with nuclear spin quantum number $I = 5/2$, and [87]Rb (28 percent abundance), with $I = 3/2$.

The different energy levels are labeled by "term states", with the notation $^{2S+1}L'_J$, where S is the spin quantum number, L' is the spectroscopic notation for the angular momentum quantum number (i. e. S, P, D, ..., for orbital angular momentum quantum number $L = 0,1,2,$ ...), and $J = L + S$ is the total angular momentum quantum number. For the ground state of rubidium, $S = 1/2$ (since only a single electron contributes), and $L = 0$, giving $J = 1/2$ and the ground state, $^2S_{1/2}$. For the first excited state we have $S = 1/2$, and $L = 1$, giving $J = 1/2$ or $J = 3/2$, so there are two excited states $^2P_{1/2}$ and $^2P_{3/2}$. Spin-orbit coupling lifts splits the otherwise degenerate $P_{1/2}$ and $P_{3/2}$ levels. (See any good quantum mechanics or atomic physics text for a discussion of spin-orbit coupling.)

The dominant term in the interaction between the nuclear spin and the electron gives rise to the magnetic hyperfine splitting (this is described in many quantum mechanics textbooks). The form of the interaction term in the atomic Hamiltonian is $H_{hyp} \propto J \bullet I$, which results in an energy splitting

$$\Delta E = \frac{C}{2}\left[F(F+1) - I(I+1) - J(J+1)\right]$$

where $F = I + J$ is the total angular momentum quantum number including nuclear spin, and C is the "hyperfine structure constant."   Figures 7 and 8 show the lower S and P energy levels for ^{85}Rb and ^{87}Rb, including the hyperfine splitting.

Figure 7: (Left) Level diagrams for the D2 lines of the two stable rubidium isotopes.
(Right) Typical absorption spectrum for a rubidium vapor cell, with the different lines shown.
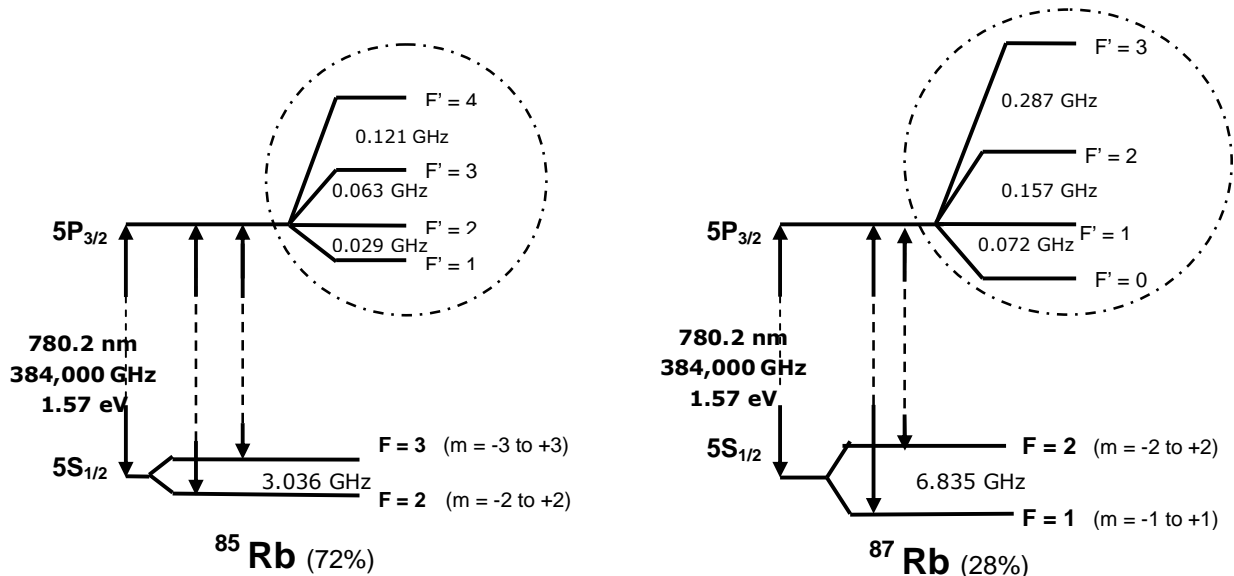
Figure 8:   More rubidium level diagrams, showing the hyperfine splittings of the ground and excited states.

VI.   REFERENCES

Cohen-Tannoudji, C., Duponi-Roc, J., and Grynberg, G. 1992.   Atom-Photon Interactons, (Wiley).

Hänsch, T. W., Schawlow, A. L., and Series, G. W. 1979, "The Spectrum of Atomic Hydrogen," *Scientific American* 240, 94 (March).

Milonni, P., and Eberly, J. 1988, *Lasers*, (Wiley).

Schmidt, O., Knaak, K.-M., Wynands, R., and Meschede, D. 1994, "Cesium Saturation Spectroscopy Revisited: How to Reverse Peaks and Oserve Narrow Resonances," *Appl. Phys. B*, 59, 167.

DIODE LASER SPECTROSCOPY

GETTING STARTED

OVERVIEW of the INSTRUMENT

INITIAL SETUP

FIRST EXPLORATIONS

I. Overview of the Instrument (See the Apparatus Section 5 for details.)

A. The Laser

TeachSpin's robust and reliable grating stabilized laser is both temperature and current regulated. When the grating is in place, it provides optical feedback that retroreflects the laser light to create an external cavity that stabilizes the laser to run at a controllable wavelength. A piezo stack, mounted in the grating support, allows the grating position to be modulated by an applied voltage. The laser temperature, laser current and piezo stack modulation are determined by individual modules of the Laser Diode Controller.

A Plexiglas cover over the laser provides isolation from air currents and protects the knobs used to adjust the angle of the grating from accidental changes. There are two holes in the cover to allow the laser beam to exit undisturbed both with and without the diffraction grating in place. (The grating can be removed to study the way the laser behaves without grating stabilization.)

B. The Detectors

Your apparatus is supplied with three photodiode detectors. The detectors contain current to voltage converters. The detector response is linear when the voltage output signal is between 0 and -11.0 Volts so you want to make sure you are no where near the -11.0 saturation voltage. A switch on the back of the detector allows you to change the gain setting from 10 MΩ to 333 Ω in ten steps. The detectors have separate signal and power cables. Three DETECTOR POWER plugs are on the front panel of the controller. You can send the detector signal directly to an oscilloscope or to the DETECTOR MODULE of the Controller.

C. The Absorption Cell Assembly

The absorption cell assembly consists on an outer glass cylinder, an insulation layer, a heater assembly, a "cold-finger", a thermocouple to monitor the temperature and the gas filled Rb cell itself. The cold-finger is a small piece of metal that fits over a small protrusion on the side of the cell. Because the metal is a good conductor and stays cooler than the cell, any excess rubidium will condense in the protrusion, rather than on the windows of the cell. The heater is both powered by and monitored from the controller.

D. The Magnetic Field Coils

The magnetic field coils are a Helmholtz pair which produces a uniform field at the Rubidium cell. They are used in experiments such as Resonant Faraday Rotation and Zeeman Splitting and must be powered by an external power supply. The Absorption Cell Assembly in mounted at the center, even when they are not in use.

E. The Controller

While almost all functions of the apparatus are controlled by the modules on the front on the Laser Diode Controller, the potentiometer used to set the laser temperature is on the back, to prevent accidental changes. The laser temperature determines the lasing frequency and will be set at the factory. The temperature should be touched only if, for some reason, a check of the Laser Temperature Set Point indicates it has been altered or the diode itself is changed.

The Modules – starting from the right

DETECTOR/LOW PASS/DC LEVEL: This module provides power for three detectors and offers two detector inputs and a series of Monitor options. You can look at either detector or a combined signal.

PIEZO CONTROLLER: This controls the piezo modulation, which determines the way the angle of the grating is changed and thus the change or "sweep" of the laser frequency. It includes a monitor output.

RAMP GENERATOR: This provides a bipolar variable amplitude and frequency triangle wave which can be used, via the RAMP OUTPUT connection, to modulate either or both the piezo stack and the laser current. The resulting changes in the grating angle and current produce the variation or "sweep" of the laser frequency. The RAMP GENERATOR module can supply a wide range of frequencies and amplitudes. The SYNC OUTPUT connection for the oscilloscope is located in this module.

CELL TEMPERATURE: The cell temperature is both set and monitored through keys on the LED display. It has been configured by TeachSpin. In case it is accidentally reset, see the Apparatus section for detailed help.

CURRENT: The current module controls the current to the laser. It houses a modulation input so that the current can be ramped along with the piezo stack and an attenuator to control the degree of modulation.

MONITORS: This set of connectors and indicators, located on the lower part of the cell temperature panel, provides a place to monitor, as a voltage, the set point temperature of the laser as well as the actual temperature and current. The indicator lights indicate the temperature of the laser in reference to the set point.

F. TV and Camera
The TV and camera will be used to observe both the light coming from the laser and the Rb fluorescence in the vapor cell. While invisible to our eyes, the 780 nm light can be detected by the camera and seen on the TV.

G. The Optics and Connectors
Your Diode Laser Spectroscopy system comes with a whole collection of bases supports, mirrors, polarizers, neutral density filters and beam splitters which can be combined in a wide variety of ways to do a wide range of experiments that is limited only by your imagination.

II. Initial Setup – What to do first (This may take one or two hours.)

These instructions will help you set up and align your laser for the first time. When you have carried out these detailed steps, your laser will be tuned to the Rubidium resonance lines. Once aligned, it is unlikely that the laser will need any more than minimal tweaking.

A. Unpacking and Setting Up the Laser
1. The room used for your diode laser should be able to be closed to other users, first so that you can dim the room lights, but most importantly so you can have absolute confidence that no stray laser beams can escape and potentially cause harm to anyone.

2. Unpack the various components from their shipping containers and place everything on a table with plenty of room to work.

3. Place the Controller at one end of the optical breadboard. (we find it easier to put the controller and laser on the right side of the board – the laser connection is behind the left end of the controller.)

4. Mount the laser on one end of the breadboard so that the beam will go across the board. (Before making placing the laser head on the board or making connections to it, ground yourself to remove electrostatic voltages.)

5. Remove the protective plug from the laser head 9-pin D-connector. Connect the laser to the controller using the 9-pin D-cable provided, which plugs into the back of the controller.

6. Make sure the laser power switch (located on the left side of the controller, on the front) is in the **off** position. Then plug in the laser controller power cord and turn on the main power switch (located in the back, near the power cord).

B. Setting up the Absorption Cell Assembly – the cell takes a while to get to optimum temperature so you want to have it heating up while you do other things.

1. Slide the Absorption Cell Assembly into the Magnetic Field Coils and secure it.

2. Place the assembly on the breadboard so that the laser beam will go through the cell. Put it eight inches or so away so that you have room to work between it and the laser.

3. Connect both cables from the cell assembly to the back of the controller. You will notice that the polarity of the banana plug heater wires does not matter. The polarity of the blue thermocouple connector, however, does matter. It will only plug into the blue receptacle one way.

4. When the power is turned on, the Cell Temperature controller (LED display on front panel) will first reset and then display the cell temperature. In five or ten minutes the cell temperature will be close to its factory established set-point temperature of 50 °C.[*] You may check and/or change the cell temperature set-point as follows:

    a) Press the leftmost button on the cell temperature controller. It is marked by a circular arrow. The temperature controller will read SP1.

    b) Press the rightmost button on the cell temperature controller. The cell set-point temperature (in degrees C) will now be displayed.

    c) You can press the up/down arrow buttons to change the set-point. Start with a temperature of 50 °C.

    d) Press the rightmost button. The display will read SP2

    e) Press the leftmost button twice. The display will read RUN momentarily, then it will read the cell temperature.

    f) The cell temperature should read near the set-point after several minutes. You may proceed with the next step before the final temperature is reached. The Cell Temperature controller is **not** critical to operation of your diode laser. It merely improves the signal strength by increasing the rubidium density in the cell. See Theory section for a plot of Rb pressure versus temperature.

---

[*] A starting temperature of 50 °C was chosen to give a nice strong absorption signal (about 90%). Once you become familiar with the system you may want to work at a lower temperature.

Trouble shooting: If the controller is not working as described please refer to the Apparatus section of the manual under Cell Temperature Controller for how to configure and set your controller. It is possible your controller became reset during shipping or by a student (the ever-present scapegoat).

C. Starting up the Laser

Operating note: The diode laser frequency depends on temperature. If not set correctly, you may not be able to get your laser to tune to the Rb resonance lines. The optimal temperature was determined at TeachSpin and is recorded on the data sheet.

1. Check the Diode Laser temperature:
   a) Use a voltmeter to read the TEMPERATURE SET-POINT in the MONITORS section of the controller chassis. This voltage should equal the Temperature Set-point recorded on the data sheet shipped with your laser. If it does not, adjust the 10-turn potentiometer on the back of the chassis to obtain the correct set-point.
   b) Make sure the LASER TEMPERATURE INDICATOR lights are both off. If either of these is on, then the laser temperature has not yet reached its set-point temperature. With a voltmeter connected to the LASER DIODE TEMPERATURE pin jacks, you may monitor the laser temperature.

2. PUT ON SAFETY GOGGLES. Your laser typically runs with an output optical power of 10-30 mW, all concentrated into a narrow, intense beam. Staring directly at the Sun sends about 1 mW into your eyes, **and this is already enough to cause permanent eye damage**. To make matters worse, the laser light has a wavelength close to 780 nm, which is nearly invisible. Practice proper laser safety – anyone that is in the room and can see the laser, should wear safety goggles when the laser is on.

3. Set the laser CURRENT potentiometer fully counterclockwise (low current) then turn the LASER POWER switch on.

D. Aligning the Laser

1. Locate the IR viewing card. The sensitive area of the IR card is a dull orange color. This contains a polymer that absorbs UV light from the ambient lights in the room, especially fluorescent lights. The polymer molecules are then excited into a metastable state, and incident IR light from the laser can induce a transition that emits visible light. (Note the IR card will not work well if the room lights are off for an extended period.) The IR card allows you to "see"(actually locate) the laser beam even when you are wearing your protective goggles, since the goggles do not block the visible light emitted by the polymer.

2. Hold the IR card at the laser output (the hole in the plastic cover of the laser) while you turn up the laser CURRENT knob. You will need to turn the knob 3-4 turns before the beam becomes detectable on the card.

3. Set up the TV and Assemble the TV camera:

   a) Put the TV monitor near the controller and set it up to display camera image.

   b) Connect the power cable of the camera to the 12V power supply provided, and connect the camera output cable to the TV monitor. You should see an image on the monitor.

   c) Place the TV camera, mounted on an optical post, into a post holder. Then the camera can conveniently be placed on the optical table with the laser and other optical components.
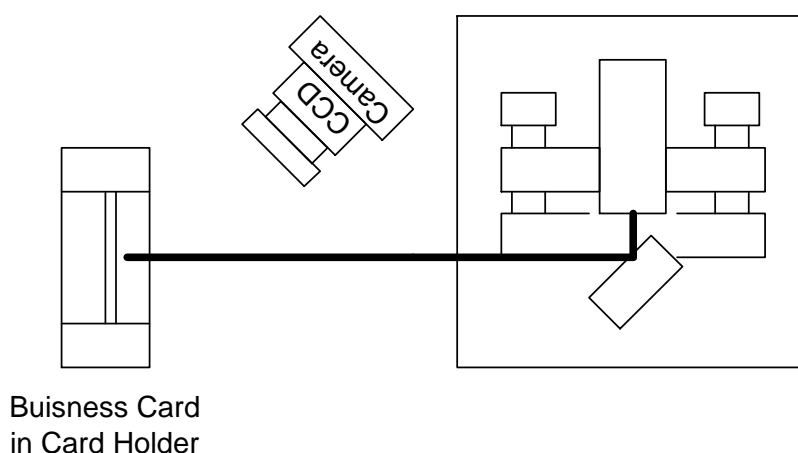
Buisness Card
in Card Holder

Figure 1. External Cavity Alignment

Operating note: The camera lens can be focused over a broad range of working distances, from infinity to as close as a few centimeters. The focus is adjusted by turning the lens. Do NOT shine the laser beam directly into the TV camera, for this may damage the CCD sensor.

4. Place a business card in the Neutral Density Filter holder and locate it so that it intercepts the laser beam see Figure 1. Focus the TV camera on the card. Dim the room lights and turn the laser current to zero. Now increase the current while watching the TV monitor. You will see a light spot that becomes slightly brighter as you increase the current. Your diode laser is below threshold, it is not lasing, but only acting as an LED. As you continue to increase the current you will observe a sudden brightening of the beam spot and the appearance of a speckle pattern characteristic of lasing.

Adjust the current so that the laser is just above threshold. You can measure the laser current with a voltmeter. A diode current of 50 mA. will give 5.0 Volt output on the LASER CURRENT in the MONITORS section. You can compare your measured value with the threshold current recorded on your data sheet. A lower threshold current represents better optical alignment. Do not be concerned if your threshold current is slightly higher than that recorded on your data sheet. You will align the cavity in the next few steps after which you can measure the threshold current again.

Note: Your laser was shipped with the laser aligned. It many cases it will need little if any adjustment. The following steps will allow you to check the alignment and optimize it, if necessary.

5. Look at the laser head itself. You will see two knobs protected by the plastic cover. The upper or top knob controls vertical alignment. The lower or side knob provides a wavelength selective horizontal alignment. Before beginning your alignment, it is important that you have read the first section of this manual Diode Laser Physics. It will be much easier to follow the procedure if you have some idea of the physics behind these adjustments. This may be the most difficult procedure you will need to follow in this experiment. For the uninitiated it is very easy to totally misalign the laser, which can be both frustrating and time consuming. If you are not familiar with diode laser adjustment, we ask that you follow each step closely. If you have trouble or do not observe what is described in a given step, do not go on to the next step! We have tried to anticipate possible problems and direct you to the solution. We also do not want to make you overly timid by this statement. Alignment of the external laser cavity is something that any experimental physicist can accomplish. You will need to become facile in the alignment, not only because your students may misalign the cavity, but also because eventually your diode will burn out, and you will have to replace it. This will involve an alignment of the cavity, starting from scratch.
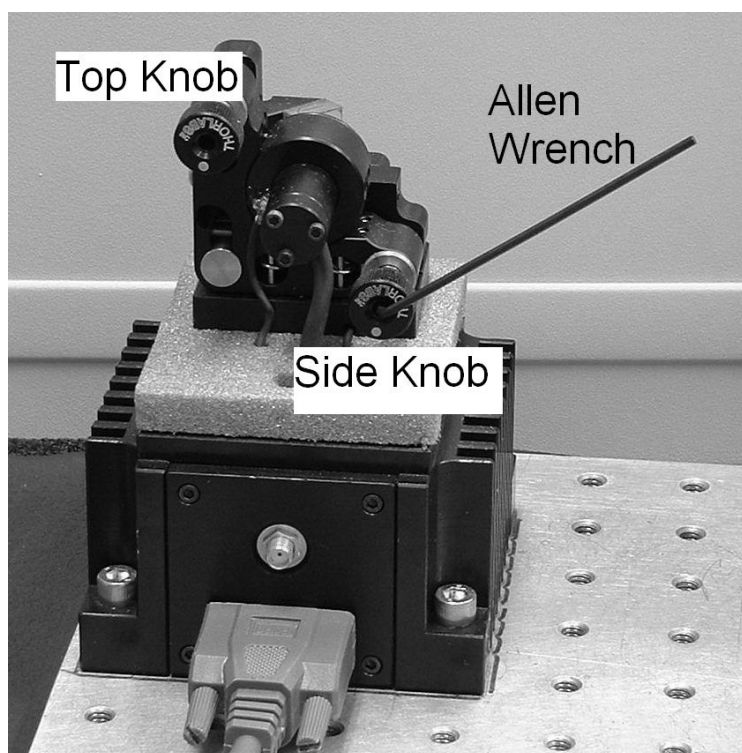

Figure 2:   Picture showing TOP and SIDE Knobs used to align grating. Allen wrench is shown in Side Knob.

6. Vertical Alignment: Remove the plastic cover from the laser and set the current so that the laser is just above threshold. Adjust the TOP knob while watching the laser spot on the card using the TV camera. Keep track of where this knob started, and DO NOT TURN THE KNOB MORE THAN ONE HALF TURN. You may find it useful to use the 5/64" Allen wrench placed in the back of the knob as a position indicator. It is also easier to make small adjustments of the knob by using the long arm of the Allen wrench as a lever.

You should see the laser spot change in intensity as the TOP knob is turned. If you rotate the TOP knob very slowly, you will notice that the bright "region" actually changes from bright to dim. These are modes of the laser. You should be able to distinguish six to ten of these modes, with fewer modes when the current is just above threshold. You are seeing different longitudinal modes in the external cavity defined by the grating and back facet of the diode. As you turn the top knob you are not only changing the grating angle but also the external cavity length. You have changed the cavity length by one half wave length when you move from one bright peak to the next.   You will need to have to set the current just above threshold to see this clearly. This may involve a few iterations of setting the TOP knob to give an intensity maximum and then adjusting the laser current.
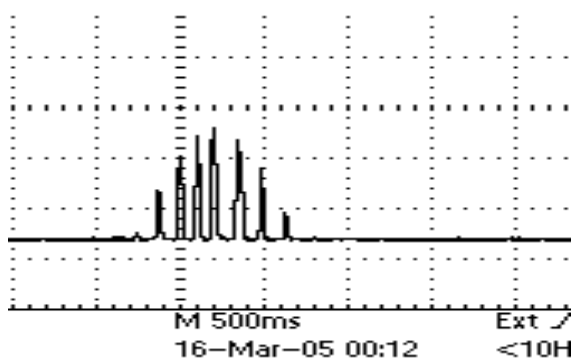

Figure 3, at the right, shows an oscilloscope trace of the intensity of the laser as the TOP knob is adjusted. It will give you an idea of how the brightness of the spots you are seeing is varying. It is hard to tell the middle ones apart. For best alignment leave the laser in the middle of this vertical mode pattern as best you can. It is not necessary to sit right on one of the mode maxima, but only near the center of the mode pattern. The correct mode maximum will be set later with the side horizontal adjustment knob and piezo voltage.

Note that finger pressure on the knob also changes the grating alignment, so remove your fingers often during this adjustment. If you find it difficult to turn the knob with a light touch, then you can use the Allen wrench placed in the back of the knob as a lever for adjustment.

It is not critical for operation of your laser that you achieve near perfect vertical alignment of the grating. You will get adequate laser performance by simply turning the TOP knob to the intensity maximum. However, it has been found that the better the alignment the better the operation of the laser. Better operation being defined as wider mode-hop-free scans.

If you are not able to see any change in laser intensity as you adjust the Top knob then STOP! Do not continue. Most likely both the SIDE and TOP knobs have both been moved by accident or during shipping. Please refer to "Aligning the external cavity" in the Apparatus section of the manual.

*Operating note : The TOP and SIDE knobs are used to align the grating with respect to the diode. The lines on the grating run vertically. Figure 2 shows the diode laser with the cover off and the 5/64" Allen wrench placed in the SIDE knob. The first order diffraction from the grating is directed back into the diode. The zero order reflection from the grating is the light you observe leaving the laser. The TOP knob rotates the grating about an axis that is parallel to the table top. Turning the TOP knob changes the vertical angle of the light diffracted from the grating. But to first order it **does** **not** change the wavelength of the light that is diffracted back into the laser. The SIDE knob rotates the grating about an axis that is perpendicular to the table top. Turning the SIDE knob **does** changes the wavelength of the light that is diffracted back into the diode.*

E. Setting up to Observe Rubidium Fluorescence

1. Remove the index card and position the Rubidium Absorption Cell Assembly so that the laser beam passes through the center of the cell. You may use the IR viewing card to trace the path of the beam.
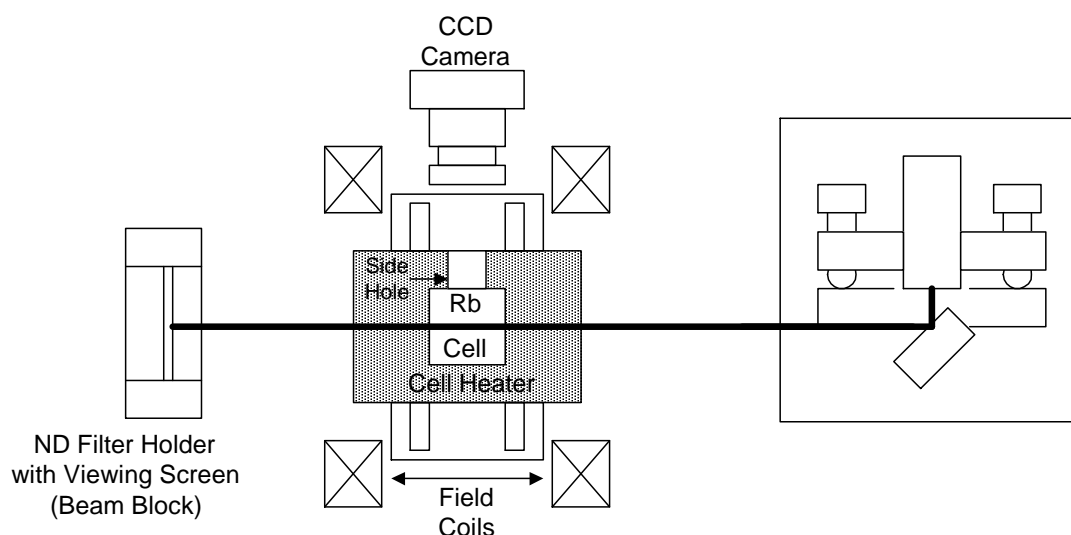

Figure 4. Setup for Observing Rubidium Florescence

2. Point the camera so it looks into the Rb cell from the Side Hole in the cell heater. If you place the camera up on the base of the cell holder you can position the camera so that it abuts the glass holder surrounding the Rb cell. It may also be helpful to dim the room lights since you will be looking for the fluorescence light emitted by the Rb atoms.

3. Set up the two channel oscilloscope that you will use for these experiments. Run a BNC cable from the RAMP OUTPUT of the RAMP GENERATOR module to an oscilloscope. Run a second cable from the RAMP GENERATOR SYNC. OUTPUT to the 'scope trigger. Observe the output on the 'scope as you adjust the RAMP GENERATOR settings.

4. Use The RAMP GENERATOR and PIEZO CONTROLLER to Set the Frequency Sweep

   a. Turn the ramp amplitude down and connect the RAMP OUTPUT from the oscilloscope to the modulation input connection on the PIEZO CONTROLLER MODULE. This is a good place to use one of the short BNC cables that came with the system.

   b. Connect the MONITOR OUTPUT of the PIEZO to Channel 1 of the oscilloscope. Turn the piezo OUTPUT OFFSET knob to zero. (The OUTPUT OFFSET changes the DC level of the monitor output. It does not change the voltage applied to the piezo stack. This control is used when locking the laser to an absorption feature and is not needed here.)

   c. Set the ramp generator frequency to about 10 Hz. Turn the piezo ATTENUATOR knob to one (1). Set the ramp generator AMPLITUDE knob to ten (10) and use the DC OFFSET knob of piezo controller to produce a large-amplitude triangle wave that is not clipped at the top or bottom. The piezo MONITOR OUTPUT should have a signal that runs from about 3 volts to about 8 volts.

Operating note: The PIEZO CONTROLLER drives a small piezoelectric stack that moves the optical feedback grating. This scans the laser frequency (see the Diode Laser Physics section of this manual for more on how this works).
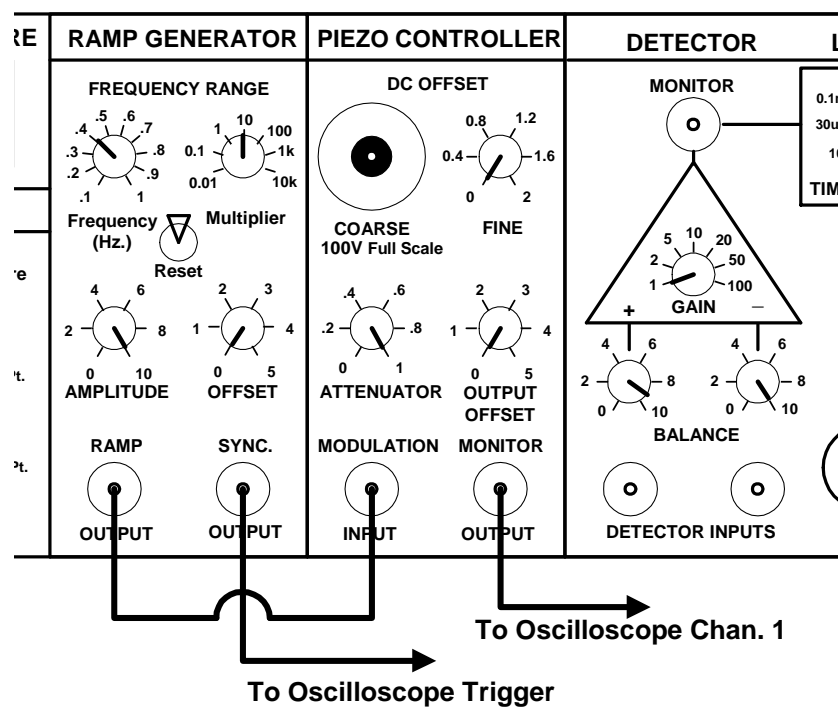

Figure 5: Modules showing connections for setting the frequency sweep.

F. Actually Finding the Rb Fluorescence, Initial Horizontal Adjustment

1. Set the laser current to the value listed on your data sheet. You will need to connect a voltmeter to the LASER CURRENT MONITOR to accurately set the current. If the horizontal grating position has not been changed much during shipping or because of accidental adjustment, then you will see a flashing streak of light within the cell on the TV monitor. This is rubidium fluorescence. Atoms of Rb in the cell, absorb laser light at the atomic resonance frequency and re-emitting it in all directions. *If you do not see any fluorescence, do not despair. You only need to make a slight adjustment of the SIDE knob.*

2. Put the 5/64" allen wrench (hex key) in the back of the SIDE knob and use it as a rotation marker. Remember the starting position of the wrench; you could even draw a little picture in your lab book. While you observe the TV screen looking for the fluorescence flash, slowly rotate the SIDE knob first one way and then the other. You should not need to rotate it more than one half turn in either direction.

3. If still no fluorescence is observed, then return the SIDE knob to the starting position, and adjust the current in 3mA increments (about 1/3 of a turn) both above and below the Laser current recorded on you data sheet. At each new current setting rotate the SIDE knob again, so that you don't lose your position, always return the knob to its starting position before changing the laser current. If you do NOT see any fluorescence, first repeat the above steps again, doing them with care. You might have someone else go through the steps as well. It's easy to miss some detail and thus not observe fluorescence. In particular check the laser temperature, the vertical alignment, and make sure you are sweeping the piezo.[*]

4. If you still see no florescence then you can try making bigger excursions in the grating angle with the side knob (plus and minus one whole turn). It may be that the Cavity became grossly misaligned during shipping, refer to section A4-2. in the appendix for details on aligning the external cavity.

5. Once you see the florescence flash move the SIDE knob so that the florescence is always visible. Now adjust the laser current to make the florescence as bright as possible.

G. Observing the Absorption Spectrum Using a Photodiode Detector

1. Connect a Photodiode Detector (PD) cable to the DETECTOR POWER output of the laser controller, and connect the Photodiode Detector output BNC to Channel two (2) of the oscilloscope. Set the Channel two (2) input coupling to DC, the gain to 5 Volts/div, and the vertical position so that ground is in the middle of the oscilloscope display. The signal from the Photodiode Detector is ***negative*** and saturates at about -11.0 volts. ***If you are uncomfortable observing a negative going signal, you can always use the invert function on your 'scope.***

---

[*] You can check that the piezo is actually moving by doing the following. With the Ramp generator connected to the Piezo modulation input, turn the AMPLITUDE of Ramp to zero, change the ramp frequency to about 3 kHz. And then increase the AMPLITUDE. You should be able to hear the piezo vibrate. WARNING: Do not leave the piezo running at high frequency and amplitude for a long time. It will cause heating and damage to the piezo.

2. Put the Photodiode Detector in place to intercept the laser beam coming through the Rb cell. You can move the PD for alignment. You will have to adjust the Gain on the back of the PD. Make sure that the beam is hitting the sensor and bolt the photodetector down.

    Operating note: In the present configuration there is a very high intensity beam (power per unit area) going through the Rb cell. This much power "saturates" the transition, resulting in very little total absorption of the beam.

3. Attenuate the Signal Reaching the Detector
    a) Assemble the glass neutral density filter in a fixed mirror holder and place it in a post holder. Please refer to the Optics section in the Apparatus Chapter of the manual if you are unfamiliar with putting optical components into mounts.
    b) Place the attenuator between the laser and the Rb cell (not between the cell and photodiode). Adjust the PD Gain so you can observe something on the 'scope showing that light is hitting the PD. For the best performance you want the PD Gain to be as high as possible without saturating the PD. This keeps the noise from the PD at a minimum. The PD gain changes in 1,3,10 steps, a signal level of 2 to 6 volts is reasonable. Block the beam with your hand to convince yourself that the PD is detecting the transmitted laser light.

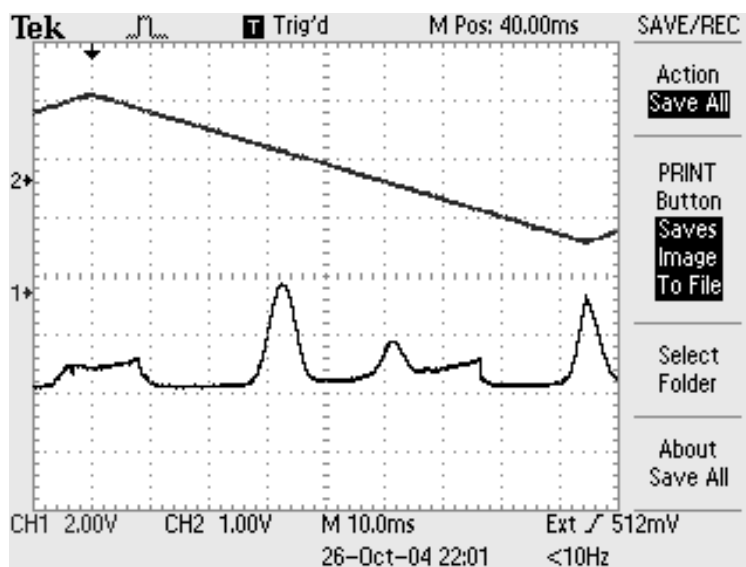   You should see a 'scope signal that looks something like this:

Figure 6: Upper trace (Channel 1) shows piezo monitor signal.
Lower trace (channel 2) shows Detector output. Note that signal is "negative going" so absorption features appear as spikes.

4. Interpreting the Oscilloscope Signals
    a) The upper trace shown in Figure 6 is the piezo monitor, which shows the voltage on the piezoelectric stack as a function of time. The lower trace is from the photodiode, showing absorption dips due to the Rb vapor. Because we have a negative going signal, these appear as spikes. If the laser scanned "perfectly" in frequency (that is no mode hopping), you would see just some fraction of the Rb absorption spectrum. The energy levels of [85]Rb and [87]Rb and the Doppler broaden spectrum are show below:
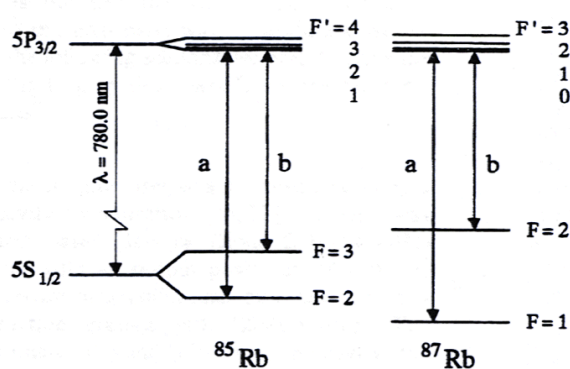

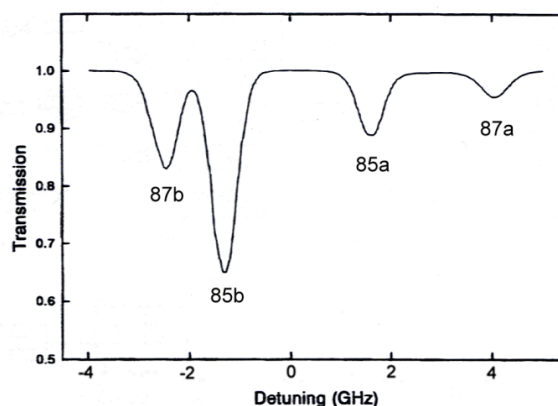Figure 7: Energy level Diagrams   Figure 8: Doppler broadened spectrum

    b) The absorption dips in your trace are interrupted by various "mode hops" – when the laser frequency jumps suddenly. Refer to the Diode Laser Physics section for a discussion of mode hops. Observe how the signal changes when you vary the laser current and the piezo drive parameters. Please explore the parameter space.

H. Horizontal Modes, Final Horizontal Adjustment

1. Adjust the laser current and piezo voltage so that a "nice" absorption spectrum is centered on the oscilloscope. This takes a little practice. As with the vertical adjustment, there are also horizontal modes. These modes are slightly different, in that turning the horizontal move through two or three of these modes by changing the piezo DC LEVEL voltage.
    a) Place the 5/64" allen wrench (hex key) in the back of the SIDE knob with the long arm of the allen wrench sticking out at about a 45° angle. (See picture at step 15). You will use the allen wrench as a lever to gently move through the horizontal modes.
    b) Watch the oscilloscope display as you gently push on the end of the allen wrench. You should be able to identify six to eight modes in which the Rb absorption is still visible on the oscilloscope. You want to set the Side knob in the middle of this mode pattern.
    c) You might notice that the modes at the ends have a shorter and more erratic scan over the Rb absorption. You do not need to make an exact adjustment with the Side knob as the Piezo DC OFFSET voltage can be used to fine tune to the mode. With proper alignment and laser current adjustment you should be able to set a scan that covers the first three lines in the absorption spectrum (87b, 85b, and 85a as shown in Figure 9).
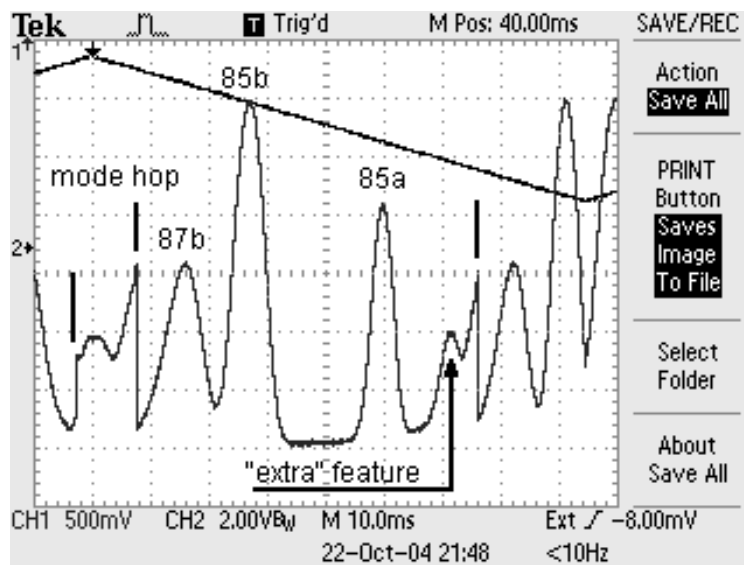
Figure 9: Scan showing first three absorption lines

2. You may notice a few "extra" features at the ends of a scan right before a mode hop. These feature look like (and are) replicas of the strong 85b and 87b absorptions and appear near where you would expect to find the 87a absorption.   The "extra" features are associated with relaxation oscillations in the diode laser. (See Diode Laser Physics Section). By reducing the laser current and adjusting the Piezo DC LEVEL, you should be able to get a nice scan showing the 85a and 87a features. This is shown in Figure 10.

Figure 10: Scan improved by adjustments to laser current and piezo DC level.

I. Using Simultaneous Current and Piezo Modulation to produce a larger scan range without mode hops. (See the Diode Laser Physics section for an explanation.)

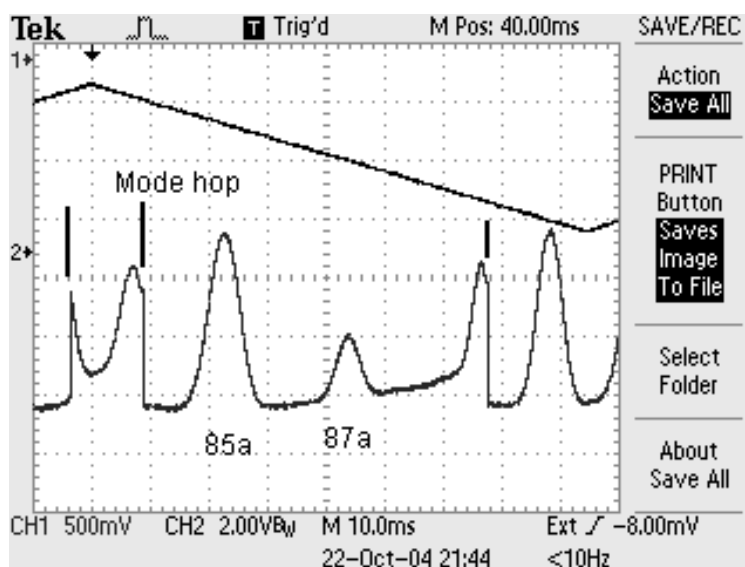1. Set the laser CURRENT ATTENUATOR knob to zero. Attach the BNC splitter "F" connector to the RAMP OUTPUT on the RAMP GENERATOR. Plug one BNC from the RAMP OUTPUT to the MODULATION INPUT of the PIEZO CONTROLLER, and the second BNC from RAMP OUTPUT to the CURRENT MODULATION INPUT.

2.   Turn the ramp generator amplitude up to maximum, and watch what happens when you turn up the current attenuator knob. With some tweaking you should be able to produce a full trace over the Rb spectrum. *The oscilloscope invert function has been used* to show the trace in what "looks" more like an absorption spectrum in the Figure 11. Note the correspondence to the expected atomic Rb spectrum shown in Figure 8
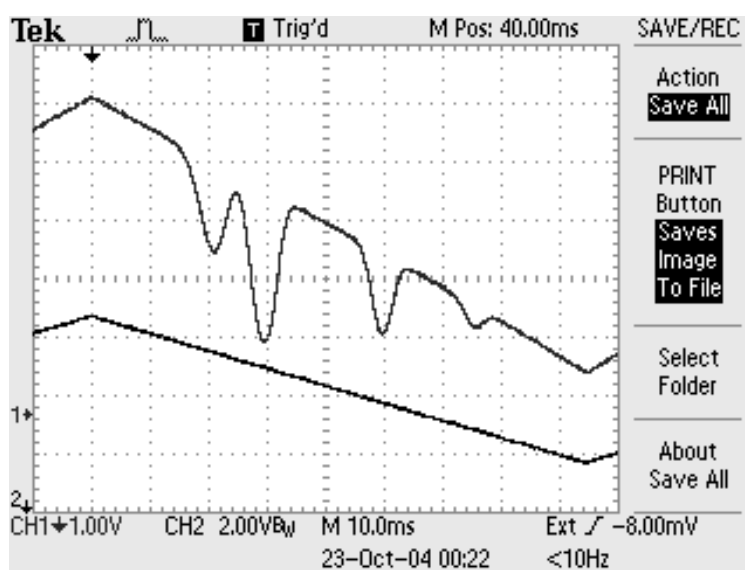
Figure 11: Expanded Scan Showing Four Absorption Lines

Operating point: The depth of the lines depends on the length of the Rb cell and the atomic density, the latter depending on cell temperature. You can explore this by changing the cell temperature.

3. You can see in the above that the background intensity changes considerably with the scan. This is because you are now scanning the laser intensity (via the current) together with the laser frequency (via the piezo). You can correct for this effect in a number of ways. One way is to digitally record a spectrum with the cell in place, and then record a second spectrum with the cell removed, and finally divide the two signals in software. This has the advantage that only a single photodetector is needed, but the disadvantage that the two traces are not recorded simultaneously. Another way to accomplish this is by using a second photodiode, as in the following layout.

3 - 14
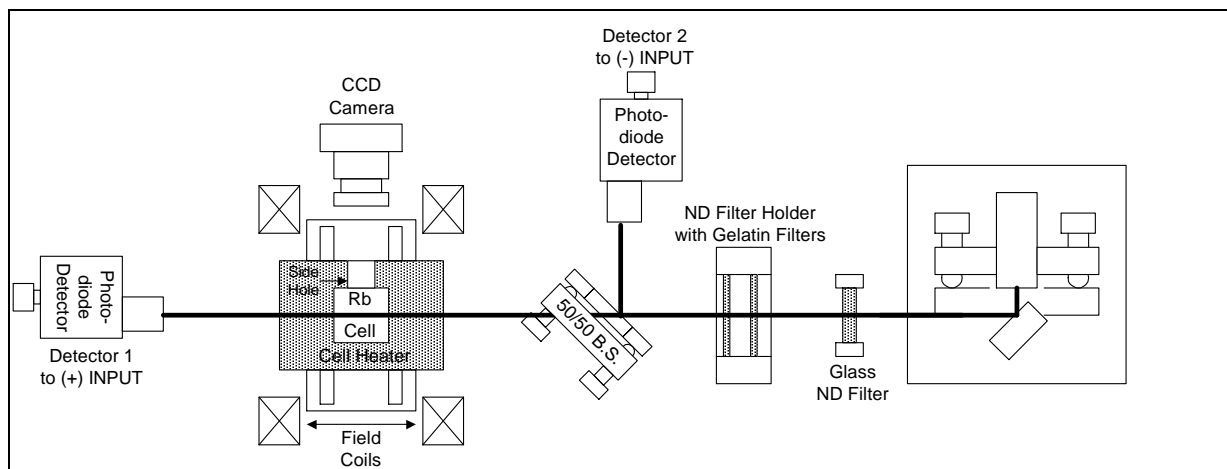
Figure 12: Apparatus set up to use two detectors

J. Using Two Photodiode Detectors to Compare a Beam directly from the Laser to one that has passed through rubidium vapor

1. You will need to place the 50/50 Beam splitter in a mirror mount. Please refer to the Optics section in the Apparatus Chapter of the manual if you are unfamiliar with putting optical components into mounts.

2. With this experimental configuration you will detect two simultaneous signals, one with and one without the Rb absorption, and then subtract the spectra. You will use the Detector electronics on the Laser Diode Controller.
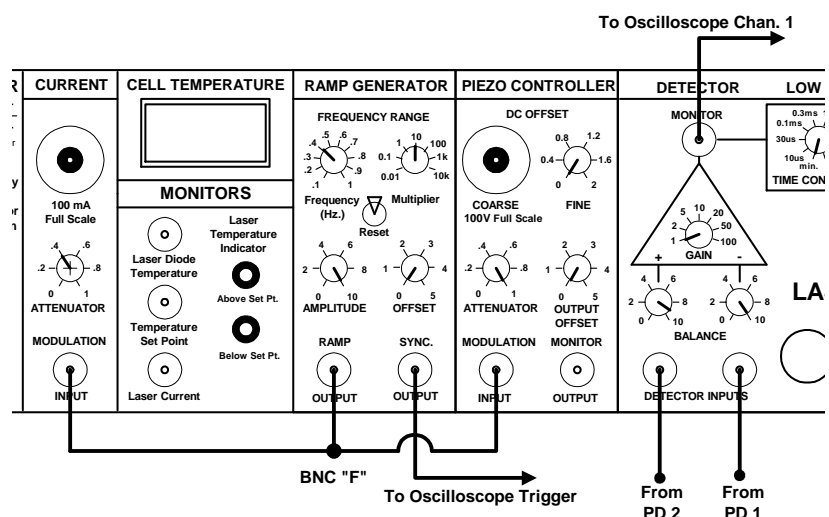
Figure 13: Controller Modules showing connections for using two photodiode detectors

3. Connect the BNC from the Photodiode Detector 1 to the right most (-) DETECTOR INPUT. (This will invert the signal from PD 1 so that absorptions will show as dips.) Set the BALANCE knob above the (-) INPUT to 1.0 (fully CW). Set the GAIN to 1. Connect a BNC Cable from the MONITOR connector above the gain triangle to Channel 1 on the 'scope.

3 - 15

Change the BALANCE knob and observe the effect on the 'scope. Position a second
Photodiode Detector to intercept the beam that has been split off by the Beam Splitter.
Connect the power cable of the detector to one of the open ports. Connect the BNC from
Photodiode Detector 2 to the (+) or left most DETECTOR INPUT. Set the BALANCE knob
above the (+) INPUT to 1.0 (fully CW) and turn BALANCE knob above the (-) INPUT to 0.
Adjust the Gain on the back of Photodiode Detector 2 for a "good" (2-6 volts) level signal
on the 'scope and position the photodiode for a maximum signal. Now increase the
BALANCE knob above the (-) INPUT to 1.0 and adjust the BALANCE to get a spectrum like
the one is Figure 14.
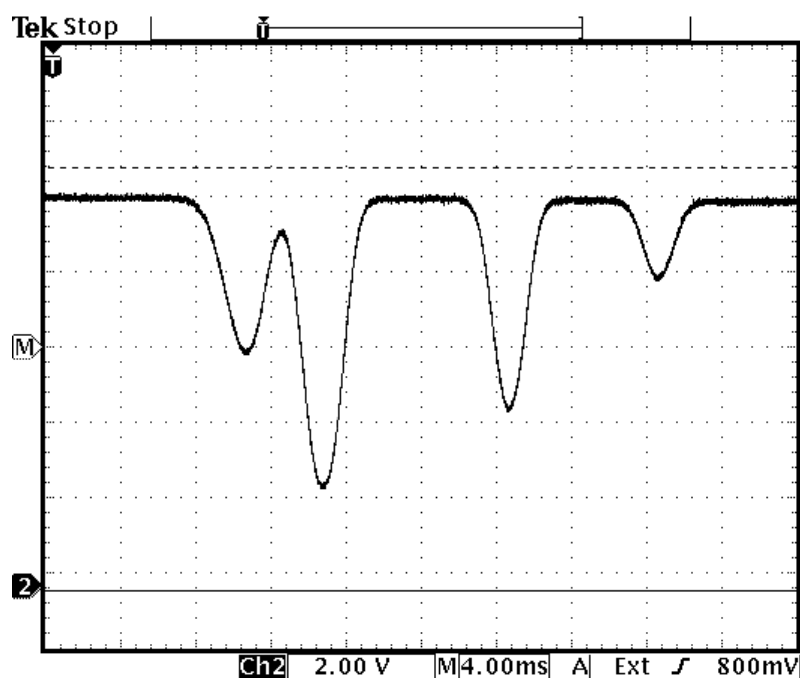
Figure 14: Trace for Channel 1 only showing the combined signal from the detectors.
Subtracting the signals removes the effect of "ramping" the current. The beams
reaching both detectors are varying at the same rate and the BALANCE controls are
used compensate for any difference in intensity.

The trace shows an excellent correspondence to the expected spectrum, with all four Rb
absorption dips on a flat background. Note, however, that the subtraction technique does not
immediately give an absolute measurement of absorption, while the digital method does.

*Operating note: You should always be wary that zero light on a photodiode may not
correspond to zero voltage output. You can check this by simply blocking the beam and
noting the voltage*

K. All Finished

At this point the initial alignment is complete, and you are ready to move on to the more sophisticated spectroscopy experiments. You may need to realign the grating feedback from time to time, following the above procedures. If not disturbed, however, the alignment will likely be stable for months.

L.   Shutting Down

If you are not using the laser for a few hours for some reason, you can you can leave the controller on.   Then the diode laser and the Rb cell will stay at their operating temperatures and be ready to go when you need it.

BUT TURN THE LASER CURRENT OFF. You should turn the laser current down, and the laser power switch off, whenever you leave the lab. This is a safety precaution, plus it will prolong the life of your laser. With use the diode laser will eventually burn out and need to be replaced, so leave the laser itself off when not in use.

It's okay to leave the ramp generator and piezo controller on and running at whatever setting you wish (for examples, the settings determined above). You can also leave the Rb cell temperature at whatever setting you wish. Then these will be set up when you want to use the laser – just turn on the laser power switch and turn up the current. After the laser warms up briefly, you should have essentially the same spectrum you had when you turned the laser current off.

We do not recommend leaving the controller on overnight and unattended even if the laser current has been turned off.

III. Observing Saturated Absorption

A. The Optical Plan

There are countless ways in which the optics could be configured to do observe the Saturated Absorptions Spectrum (SAS of Rubidium. A complete diagram of the configuration we will guide you in building is shown below in Figure 1. (A different layout is used in the lab notes from Caltech which are at the end of this manual.)
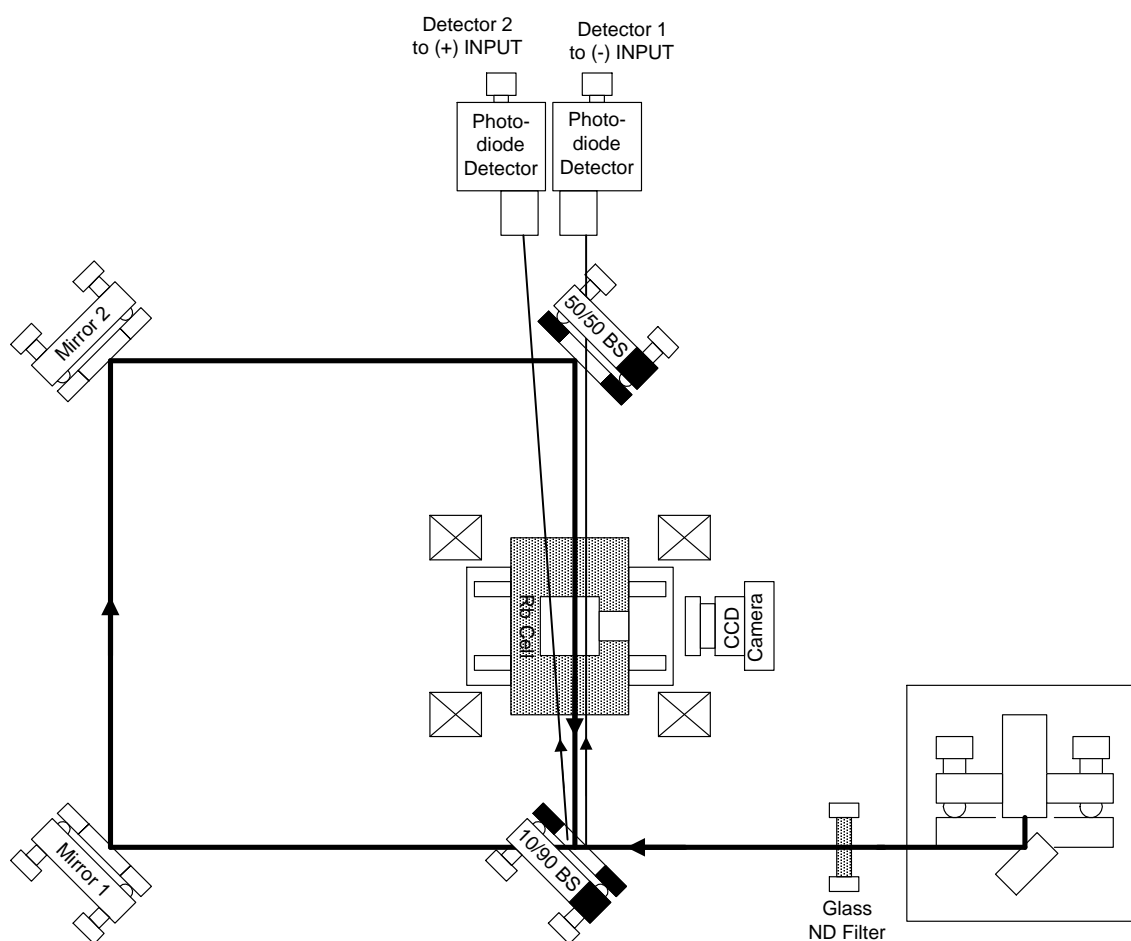
Figure 1. Complete SAS setup

B. Some Basics Before We Begin

1. Keep the beam height above the table constant as you bounce the beam off the mirrors. Since the center of the absorption cell and the laser are 4" (10 cm) above the table top, the beam should be there also. You can use the viewing card to check the beam height. Place the viewing card in the neutral density beam holder so that the marked line matches the top of the holder. Now, set the height so that the top edge of the holder, and thus the center of the viewing card, is 4 inches above the tabletop.
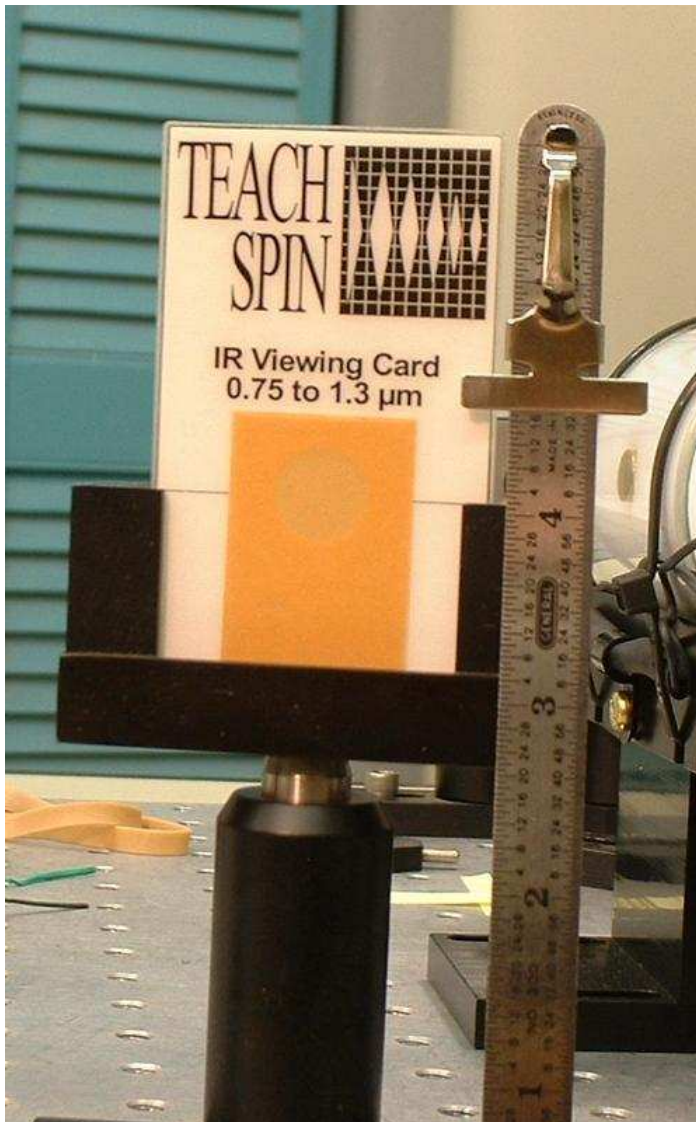
2. When placing optics, try to start with the beam centered in the optic. This gives you maximum adjustment range before the beam "walks off" the end of the optic and you have to reposition the mount.

3. When using the optical mounts to hold beam splitters, observe that there are two possible configurations of the mount. When looking at the mount from above, the upper adjustment screw can be placed on the right or the left. If placed on the wrong side, the support for the upper adjustment screw will block the transmitted beam. ***The upper screws are shown with a blackened edge in the figures below.*** To change orientations, you must remove the mount from the post and use the orthogonal mounting hole.

4. Spend a bit of time planning your optical layout before you start.

C. Placing the Components

Now that you have completed the Initial Setup and have observed the Doppler broadened absorption spectrum of Rubidium you are ready to look for saturated absorption.

1. Make sure you have two mounted mirrors, a 10/90 and a 50/50 beamsplitter assembled.

2. Reconfigure the apparatus you have been using into the layout shown in Figure 2. (This is only part of the complete SAS setup. We'll add the rest later.)

BE SURE TO HAVE A BEAM BLOCK IN PLACE AS SHOWN
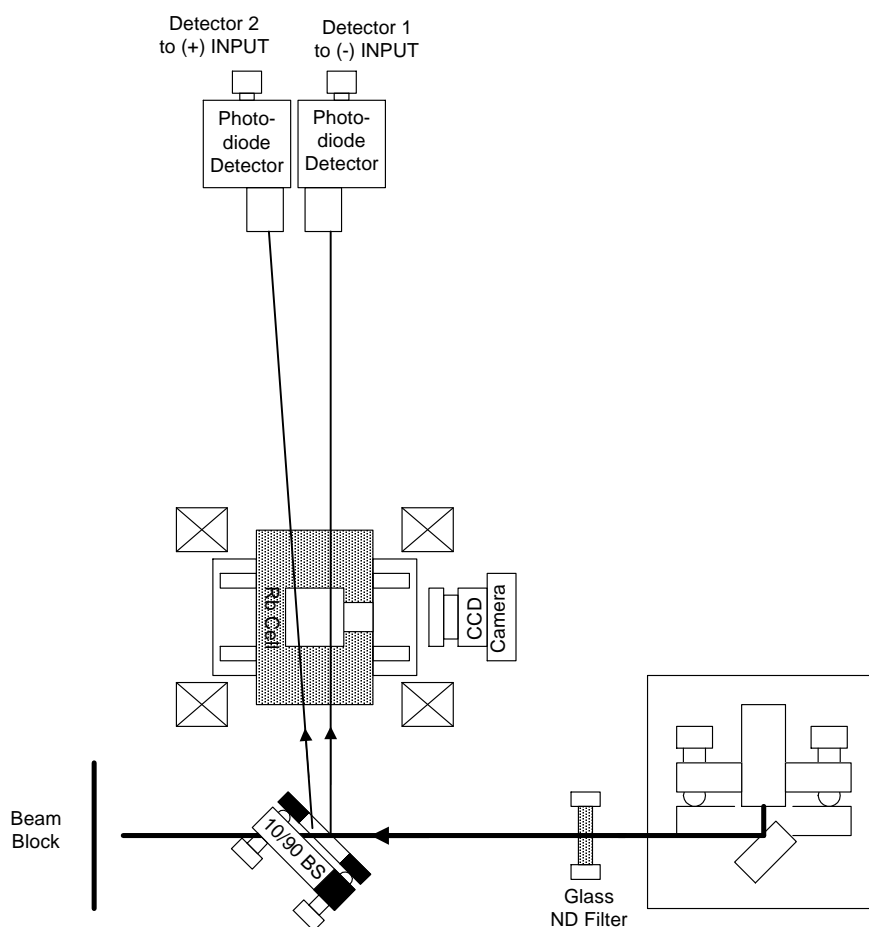
Figure 2. Start of SAS setup with 1^O wedged beam splitter in place

We have used the 1^O wedged beam splitter which yields two reflected beams, one from each face.   The small angle of the wedge causes the beams to diverge slowly so that both beams can travel through the cell to the two photodetectors. The second photodetector (PD) is not needed to "see" the SAS.   It is used in the final electronic subtraction to remove the absorptive background signal. If you do not intend to use this electronics "trick," you can leave the second detector out of the setup. Position the PD's to maximize the signal level from each.

Monitoring the output of the Detectors, you should observe the now familiar Rb absorption spectrum on your 'scope.

3.   Now, add the two turning mirrors to the setup, as shown in Figure 3. Move the Beam Blocker to the new location shown.
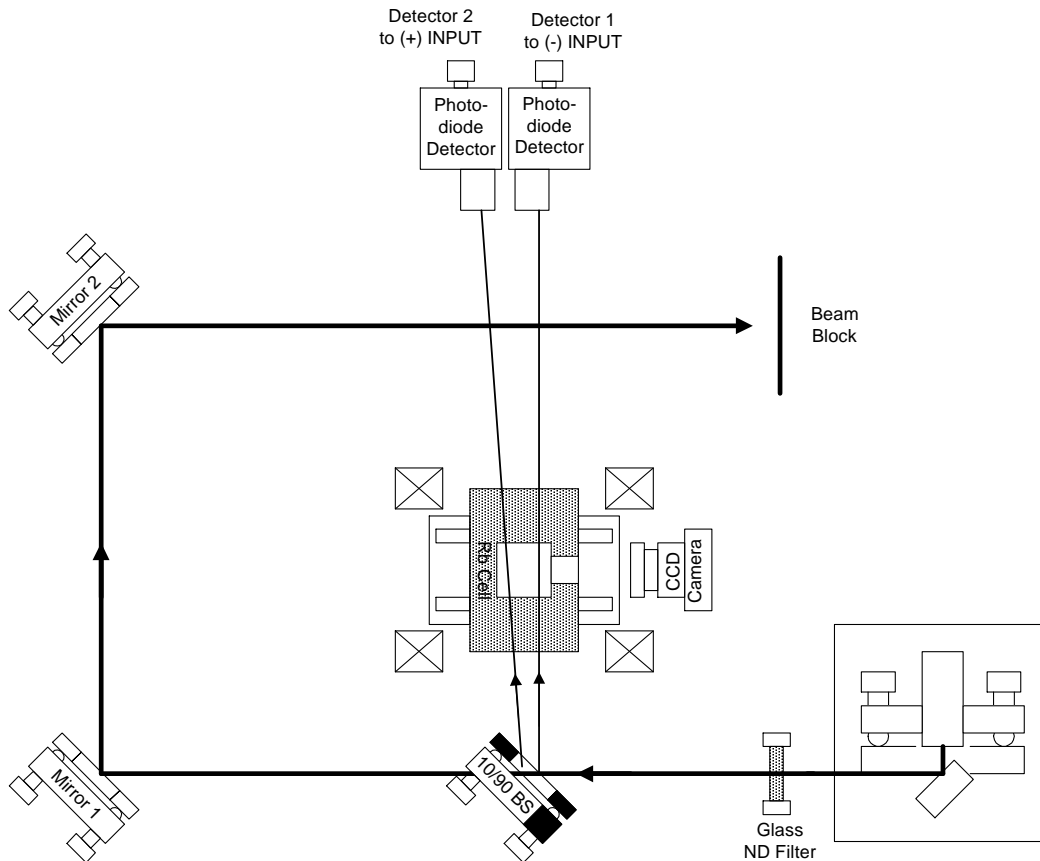
Figure 3. Turning mirrors added to setup.

D. Understanding the Functions of the Beams

We are now ready to add the important 50/50 beam splitter as shown in Figure 4. But first let's talk about the motivation for all the beams flying around. The initial 10%/90% beamsplitter has generated two weak 'probe' beams, and you've seen that each of them, passing through the cell to a photodetector, is a probe of the transmission of the cell. But the stronger beam transmitted through the 10/90 beamsplitter has now been brought around to the far side of the cell, and is ready to be sent through the cell, in the opposite direction of the probe beams, and overlapping one of the two probe beams inside the cell. (You want to overlap the beam going to Detector 1.) The stronger beam is called the 'pump' beam, and what it 'pumps' is the atoms being probed by only one of the two probe beams. Because we are using a 50/50 beamsplitter, only half the pump beam is sent through the cell, and only half of the probe beam gets through to the photodetector, PD1. The important function of the 50/50 BS, however, is to create the desired anti-parallelism of the pump beam and one of the probe beams.

There are two fine points to observe in Figure 4. First note the upper adjustment knob on the 50/50 BS mount is on the side such that the probe beam can pass through the mount. You should also observe that the mount is placed such that the beam going to Detector 1 passes through the 50/50 beam splitter, but the beam going to Detector 2 misses both the beam splitter and the edge of the mount that is holding the BS. With the 50/50 beam splitter in place, we are ready to align the strong pump beam so that it is anti-parallel to the weak probe beam going to detector 1. (You may want to read the appendix that has a short discussion of the algorithm used to position a beam in space.)

Remove the glass ND filter from the beam path. This will make it easier to see the two beams. Use the IR viewing card to observe the beams at position 1 which is right before the probe beam goes through the 50/50 BS. The IR viewing card has a circular hole on its backside so that you can observe beams from both directions.

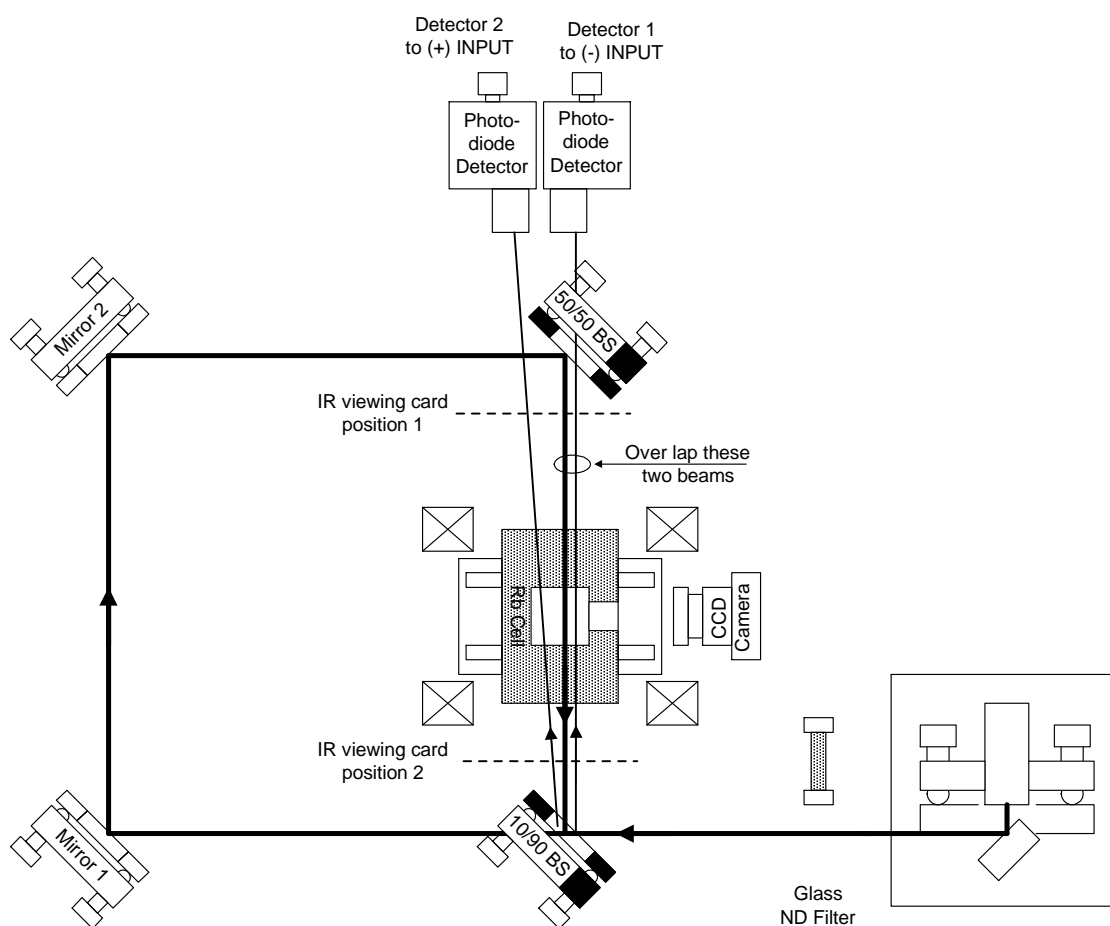Use the adjustment screws on Mirror 1 or 2 to overlap the two beam spots at position 1.

Figure 4. Aligning pump and probe beams.

Now, move the IR viewing card to position 2 (between the Rb cell and the 10/90 BS). Use the adjustment screws *on the 50/50 BS mount* to overlap the two beams at this position. It is very likely that the strong pump beam will not be visible at position 2 initially. You may have to loosen the screw that secures the post on the 50/50 BS and rotate it till you can find the beam.

If all else fails and you cannot get the beams to overlap easily, you can temporarily move the Rb cell and magnet off to the side so that you can trace the pump beam path from the 50/50 BS. Once the beams are overlapped at position 2, move back to position 1 and check the beams. Again use the mirrors to overlap the beams here. After a few iterations, you should be able to get the pump beam and one of the probe beams overlapping in space and anti-parallel in direction.

Now replace the glass ND filter (and the Rb cell, if you removed it) into the beam path. Look at the absorption signal on the oscilloscope. Expand the scale so that you can observe the two large absorption features. If your beams are close to being aligned, you will start to see some sharp spikes within the broad absorptions. See Figure 5. These "spikes" indicate that the ability of the rubidium atoms to absorb photons from the probe beam has been *diminished;* more light from the probe beam is actually reaching the detector. This is because atoms which, in the past, would have absorbed the probe beam photons are already in the excited state because they have absorbed photons from the "pump" beam. You may now try to maximize the size of these spikes by tweaking the adjustment screws on the mirrors and the 50/50 BS.

| (a) | (b) |
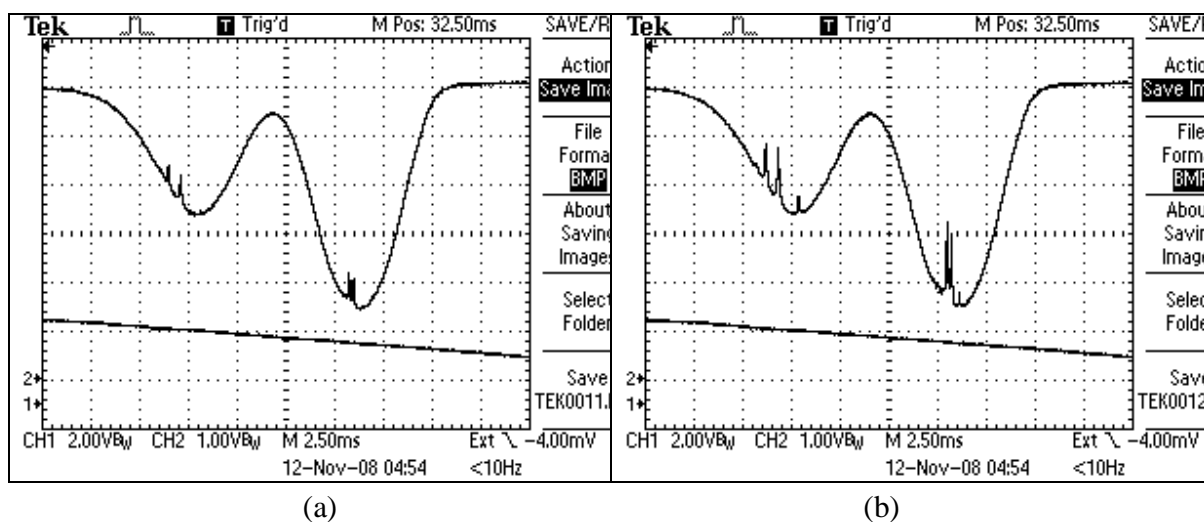
Figure 5. Observation of SAS features
       (a) Beams are partially overlapped and some SAS signal is visible
       (b) Signal after tweaking of mirrors and 50/50 beamsplitter.

If you are "too" good at this alignment, the two beams may be so perfectly anti-parallel that the strong pump beam comes through the cell and, bouncing off the 10/90, is reflected back into the laser. When this happens, the laser will no longer scan through the spectrum continuously, but in a series of steps. You may observe a spectrum that looks like that shown

in Figure 6.   This feedback is undesirable, but it does show that you have perfected the alignment of the two beams. Now you can slightly misalign the two beams such that the feedback does not corrupt the smooth scan of the laser.

You may have noticed that the Caltech lab notes show an opto-isolator right after the laser. The opto-isolator will stop this feedback from getting into the laser, but it is not essential for operation of the system.   Another technique to reduce feedback is to put more ND filters in the beam path. An added filter attenuates the reflected beam twice, once on the way out and again on the return trip.
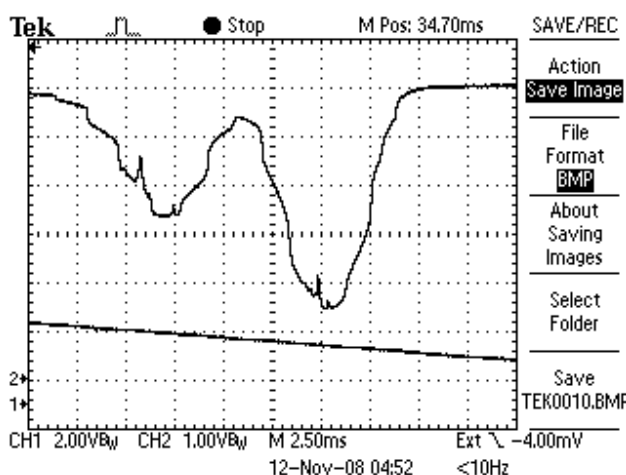
Figure 6.   When the anti-parallelism is too close to perfect, there is feedback into the laser that corrupts the frequency sweep. The 'staircase' appearance of the absorption profile is the indication of this.

If you have set up the second photodetector, you will now be able to use an electronics "trick" to isolate the SAS features. To preview this capability, send the two photodetector signals to the two channels of an oscilloscope, and adjust things until you can see what's similar about the two signals, and what's different. Now you are ready use the detector electronics section of your electronics box to isolate that difference. (You will be subtracting out most of the broad absorption signal.)

Put the signal from Detector 1 into the minus input and that from Detector 2 into the plus input of the detector section of the electronics box. Attach the monitor output to the 'scope. Set the plus balance control to zero and the minus balance control to one and observe the signal from Detector 1 on the 'scope. Adjust the gain on Detector 1 so that you have a large signal (several volts) but not so large as to saturate the detector (maximum signal less than 10 volts). Now, set the plus balance to one and the minus balance to zero and observe the signal form Detector 2. It will be inverted, with negative voltage values. Again adjust the gain of Detector 2 for a signal level that is comparable to that seen by Detector 1. Because the beam going to Detector 2 is not attenuated by the 50/50 beam splitter, the gain needed on Detector 2 will be less than that of Detector 1. (Typically Detector 1 needs a gain setting of 1.0 MΩ and Detector 2 a gain of 330 kΩ.)

Now set both balance knobs to one and then reduce the balance on the larger signal so that the Doppler broadened background is removed. This subtraction is never perfect, so there will always be some residual broad absorption signal remaining. You may now raise the gain setting on the difference signal and bring the SAS spikes up to the volt level. You are now ready to record some beautiful SAS traces.
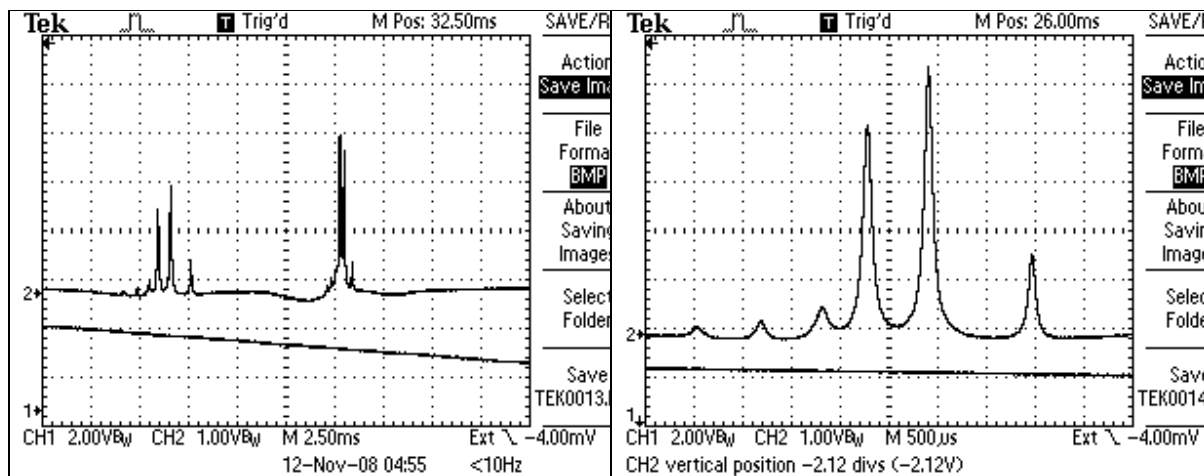
(a)   (b)

Figure 7.   SAS traces with background subtraction.
(a) Rb^{87} F=2 and Rb^{85} F=3
(b) Expanded view of Rb^{87} F=2.

It is interesting to study these signals as a function of the intensity in each of the beams. The above traces are power broadened. To observe the narrowest linewidths, you will have to work at very low optical power levels in both the pump and the probe beams. You can use neutral-density filters to attenuate the beams.   You will also need to darken your room to minimize ambient light falling into your photodetectors.

IV. Aligning a Michelson Interferometer
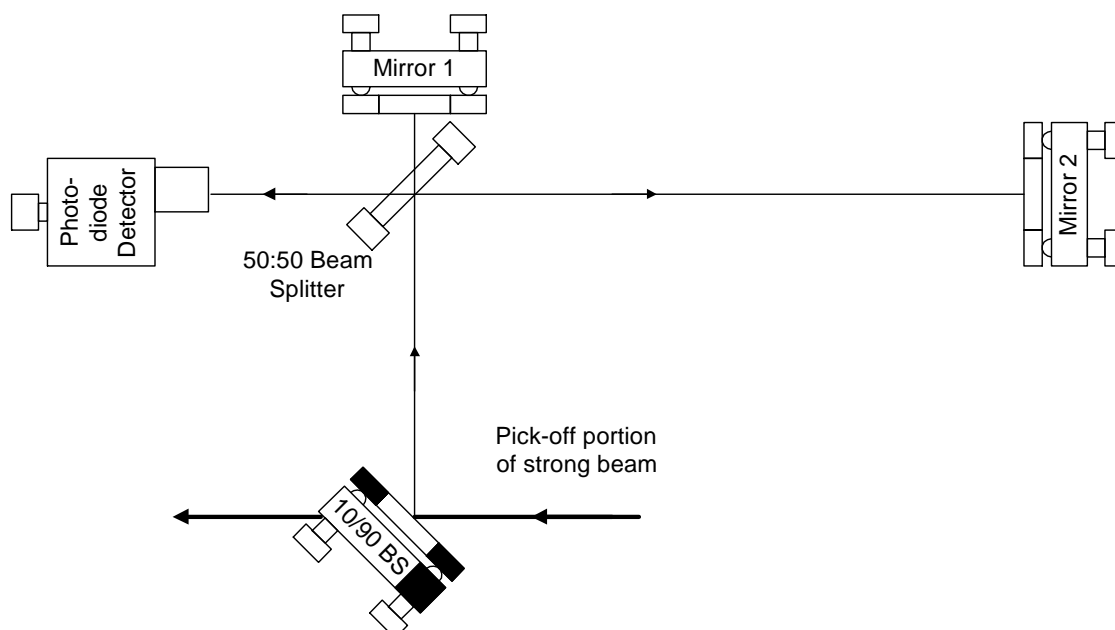
Figure 1: Overview of un-equal arm Michelson.

Find a spot on the table to lay out the Michelson interferometer (MI). You must use the filter holder to hold the 50/50 Beam Splitter (BS). A mirror mount will not allow the beam to come in and exit from all four directions.   This complicates the alignment as one can only make coarse adjustments of the 50/50 BS.

Keep Mirror 1 as close to the 50/50 BS as possible.

Use a wedged or flat piece of glass as the 10/90 BS to pick off a fraction of the laser beam.

Now look at Figure 2 below. We will use a business card with a hole punched in it to observe the reflected beam from each of the mirrors. Adjust the business card and card holder so that the incoming beam goes through the hole. Use the CCD camera to observe the beam reflected from the mirror. Adjust the mirror to send the out going beam back through the same hole.

Do this for both mirrors as shown in Figure 2.

Mirror 1

50:50 Beam
Splitter

CCD Camera

Business Card w/ hole
in Card Holder

CCD Camera

Mirror

50:50 Beam
Splitter

Mirror 2

Business Card w/ hole
in Card Holder
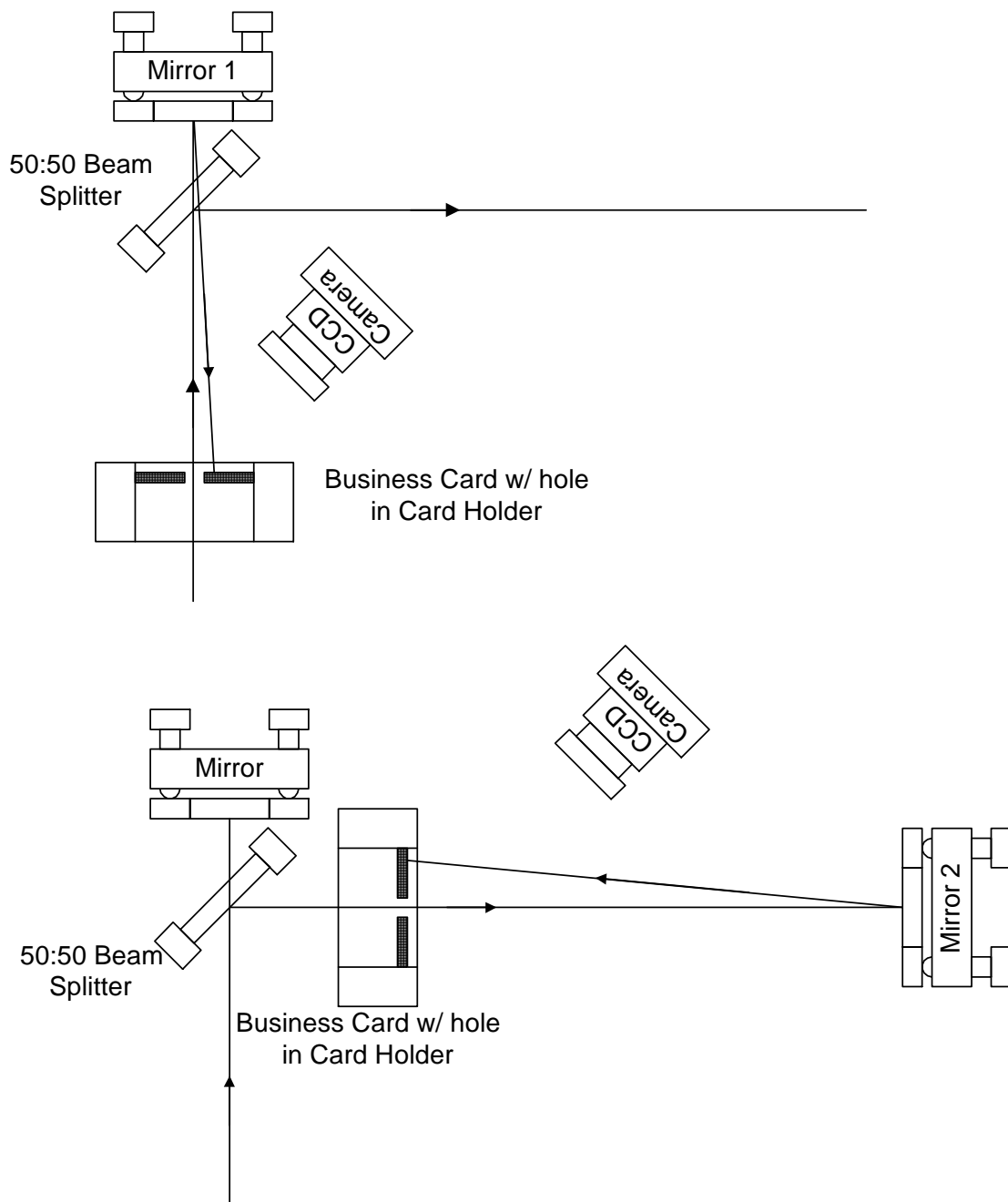
Figure 2: Use a business card with a hole punched in it to roughly align two mirrors.
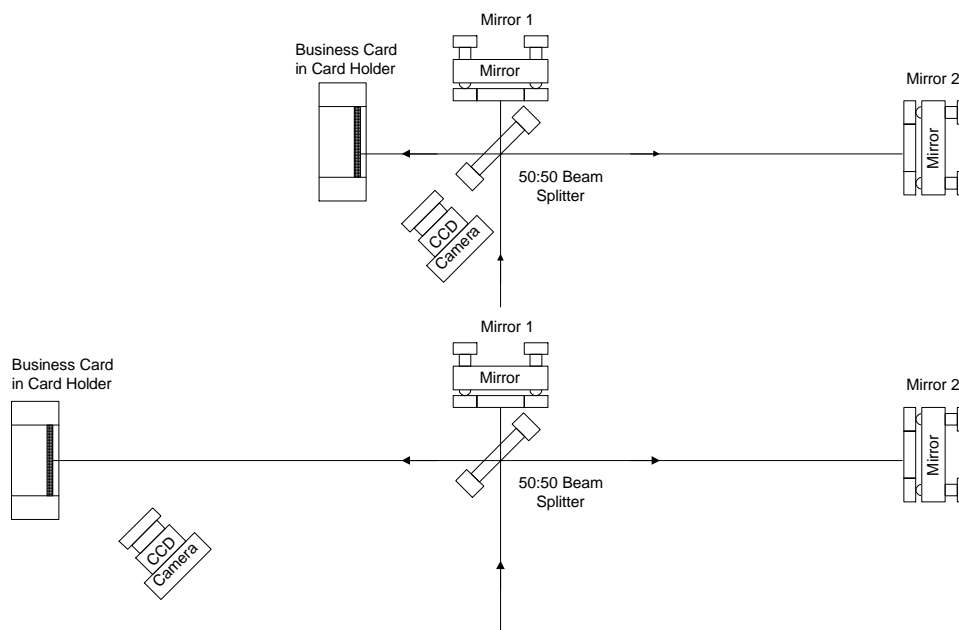
Figure 3 Iterative procedure to get two beam co-linear.

Now move the Card holder to the position shown in Figure 3. (Upper) You should see two beams on the card, one from each mirror.

With the card holder close to the 50/50 BS adjust mirror 2 to make the two beams over lap.

Then move the card holder to a position far from the 50/50 BS (a few feet, 1/2 meter or so.) Again, you should see two beams, now adjust mirror 1 to make the beams overlap.

Go back to the near position and repeat.

In a few iterations, you should start to see some fringes appear in the overlapped area of the two beams.

You will not see any fringes if the laser is scanning its wavelength, so turn off the wavelength scan during this part of the operation. (Set the Ramp Generator attenuator to zero.)

Once you see some fringes you can still repeat the above steps a few more times. If done correctly the fringe spacing should become larger as the alignment approaches optimum. Gently pushing on one of the mirror mounts should cause the fringe pattern to change.

Now put a photodiode in the beam and restart the laser scan. You should be able to see some nice periodic modulations of signal from the photodiode.

I find that a contrast ratio of 10% is about the best I can do. (minimum intensity is 10 % of maximum intensity.)

Other tips:

Remove the glass Neutral density filter from the laser beam when doing the alignment. This will help make the beams easier to see. You will have to replace the filter when you want to make scans.

Feed back from the interferometer can get back into the laser and corrupt the scan. If this is a problem adding more attenuators after the glass neutral density filter will help.

V. Appendix – Making Beams Collinear

Two points define a line, iterative procedure to align a laser beam to a "line in space".   The pictures are only for aligning in one dimension.

The process is shown in the Figures 1 – 4 below.   The objective is to get the laser beam, the narrow line, to be collinear to the "line in space" represented by the darker dashed line. The angles have been exaggerated to make it easier to see what is going on.

1. With the viewing card near to mirror M2, adjust angle of mirror M1 until the laser beam is intersecting with the desired "line in space". See Diagrams 1 and 2.

2. Now, move the viewing card to a distance far away from M2, as shown in Diagram 3.

3. Adjust the angle of mirror M2 so that laser beam again intersects the "line in space". You will notice that this makes the alignment at the first position, near M2, off a bit.

4. Now move the viewing card back to position shown in Diagram 1 and repeat.

You will probably have to repeat the process several times to get the beam where you want it. (That's iterative for you!) The closer the viewing card is to M2, the faster this procedure converges.

You might ask where the "line in space" that you are trying to match comes from. It could be another laser beam or, perhaps, a desired beam path defined by two irises.

1.)

Mirror

50/50 B.S.

IR Viewing Card

Line to match

2.)

Mirror

50/50 B.S.

IR Viewing Card

Line to match

3.)

Mirror

50/50 B.S.

Line to match

IR Viewing Card

4.)

Mirror

50/50 B.S.

Line to match

IR Viewing Card
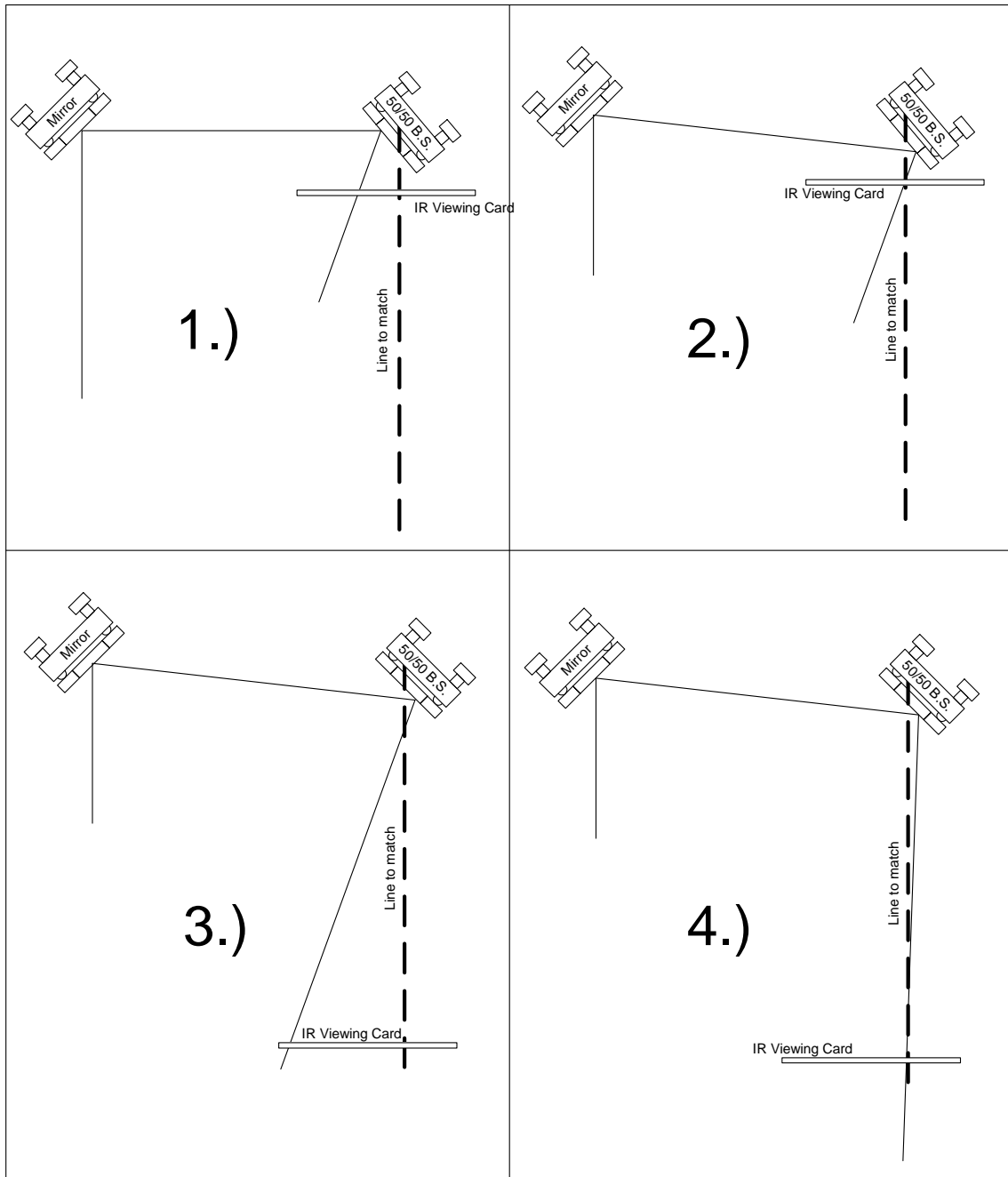
EXPERIMENTS SECTION
for
DIODE LASER SPECTROSCOPY

Experiments I – III were written for the Advanced Physics Laboratory of the California Institute of Technology. Pdf versions of these documents can be found on the Caltech advanced lab website.

Experiment IV can be found in an article written for the American Journal of Physics by Professor David Van Baak of Calvin College, who is also a TeachSpin collaborating physicist.

I.   Saturated Absorption Spectroscopy (Caltech)

II.   Interferometric Measurement of Resonant Absorption and Refractive Index in Rubidium (Caltech)

III. Resonant Light Propagation through an Atomic Vapor: The Maculuso-Corbino Effect (Caltech)

IV.   Resonant Faraday rotation as a probe of atomic dispersion, D.A. Van Baak, Am. J. Phys., Vol. 64, No. 6, June 1996

Ph 76 ADVANCED PHYSICS LABORATORY
– ATOMIC AND OPTICAL PHYSICS –

Saturated Absorption Spectroscopy

I. BACKGROUND

One of the most important scientific applications of lasers is in the area of precision atomic and molecular spectroscopy. Spectroscopy is used not only to better understand the structure of atoms and molecules, but also to define standards in metrology. For example, the second is defined from atomic clocks using the 9192631770 Hz (exact, by definition) hyperfine transition frequency in atomic cesium, and the meter is (indirectly) defined from the wavelength of lasers locked to atomic reference lines. Furthermore, precision spectroscopy of atomic hydrogen and positronium is currently being pursued as a means of more accurately testing quantum electrodynamics (QED), which so far is in agreement with fundamental measurements to a high level of precision (theory and experiment agree to better than a part in 10^8). An excellent article describing precision spectroscopy of atomic hydrogen, the simplest atom, is attached (Hänsch *et al.* 1979). Although it is a bit old, the article contains many ideas and techniques in precision spectroscopy that continue to be used and refined to this day.
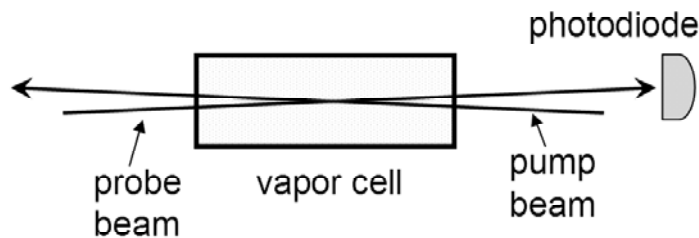
Figure 1. The basic saturated absorption spectroscopy set-up.

Qualitative Picture of Saturated Absorption Spectroscopy – 2-Level Atoms. Saturated absorption spectroscopy is one simple and frequently-used technique for measuring narrow-line atomic spectral features, limited only by the natural linewidth Γ of the transition (for the rubidium D lines $\Gamma \approx 6$ MHz), from an atomic vapor with large Doppler broadening of $\Delta\nu_{Dopp} \sim 1$ GHz. To see how saturated absorption spectroscopy works, consider the experimental set-up shown in Figure 1. Two lasers are sent through an atomic vapor cell from opposite directions; one, the "probe" beam, is very weak, while the other, the "pump" beam, is strong. Both beams are derived from the same laser, and therefore have the same frequency. As the laser frequency is scanned, the probe beam intensity is measured by a photodetector.

If one had 2-level atoms in the vapor cell, one might record spectra like those shown in Figure 2. The upper plot gives the probe beam absorption without the pump beam. Here one sees simple Doppler-

Figure 2. Probe absorption spectra for 2-level atoms, both without (upper) and with (lower) the pump beam.

broadened absorption; in our case the Doppler width is much larger than the natural linewidth, $\Delta \nu_{Dopp} >> \Gamma$, and the optical depth of the vapor is fairly small $\tau(\nu) \lesssim 1$ (the transmitted fraction of the probe is $e^{-\tau(\nu)}$, which defines the optical depth; τ is proportional to the atomic vapor density and the path length), so the probe spectrum is essentially a simple Gaussian profile.

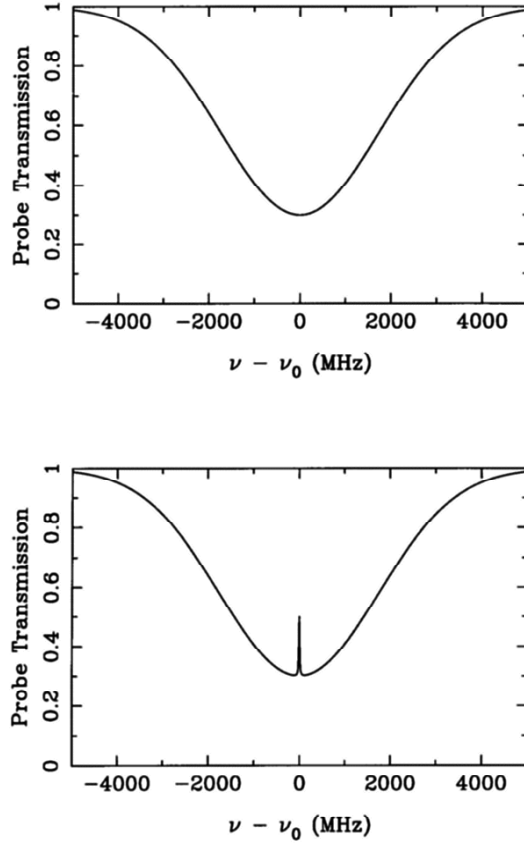The lower plot in Figure 2 shows the spectrum with the pump beam, showing an additional spike right at the atomic resonance frequency. The reason this spike appears is as follows: If the laser frequency is $\nu_0 - \Delta \nu$, then the probe beam is absorbed only by atoms moving with longitudinal velocity $v \approx c\Delta\nu/\nu_0$, moving toward the probe beam. These atoms see the probe beam blueshifted into resonance; other atoms are not in resonance with the probe beam, and so they do not contribute to the probe absorption. These same atoms see the pump beam red-shifted further from resonance (since the pump beam is in the opposite direction) so they are unaffected by the pump beam. Thus for laser frequencies $\nu \neq \nu_0$, the probe absorption is the same with or without the pump beam. However if $\nu = \nu_0$, then atoms with $v = 0$ contribute to the probe absorption. These $v = 0$ atoms also see an on-resonance pump beam, which is strong enough to keep a significant fraction of the atoms in the excited state, where they do not absorb the probe beam (in fact they increase the probe beam intensity via stimulated emission). Thus at $\nu = \nu_0$ the probe absorption is *less* than it was without the pump beam. (If the pump beam had infinite intensity, half of the atoms would

be in the excited state at any given time, and there would be identically zero probe absorption. One would say these atoms were completely "saturated" by the pump beam, hence the name saturated absorption spectroscopy.) The advantage of this form of spectroscopy should be obvious ... one can measure sharp Doppler-free features in a Doppler-broadened vapor.

Qualitative Picture of Saturated Absorption Spectroscopy – Multi-level Atoms. If the atoms in the absorption cell had a single ground state and two excited states (typically an electronic level split by the hyperfine interaction), and the separation of the excited states was less than the Doppler width, then one would see a spectrum like that shown in Figure 3. The peaks on the left and right are ordinary saturated absorption peaks at ν_1 and ν_2, the two resonance frequencies. The middle peak at $(\nu_1 + \nu_2)/2$ is called a "cross-over resonance." If you think about it for a while you can see where the extra peak comes from. It arises from atoms moving at velocities such that the pump is in resonance with one transition, and the probe is in resonance with the other transition. If you think about it a bit more you will see there are *two* velocity classes of atoms for which this is true – atoms moving toward the pump laser, and away from it.
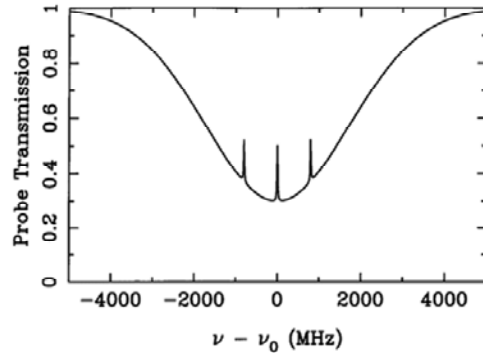

Figure 3. Saturated absorption spectrum for atoms with a single ground state and two closely spaced excited states.
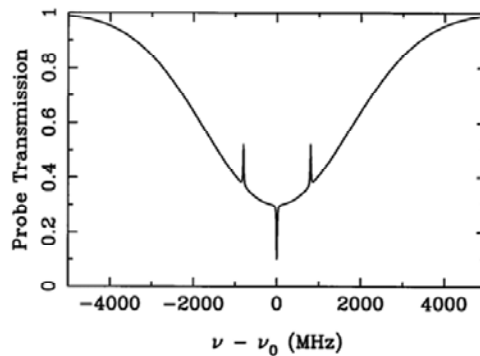

Figure 4. Saturated absorption spectrum for atoms with a single excited state that can decay into either of two closely spaced ground states.

If the atoms in the vapor cell had a single excited state but two hyperfine ground states (we call them both "ground" states because neither can decay via an allowed transition), and the separation of the ground states was less than the Doppler width, then one might see a spectrum like in Figure 4. The extra cross-over dip results from a phenomenon called "optical pumping," which occurs because atoms in the excited state can decay into either of the two stable ground states. Thus if atoms are initially in ground state $g1$, and one shines in a laser that excites $g1 \rightarrow e$, atoms will get excited from $g1 \rightarrow e$ over and over again until they once spontaneously decay to $g2$, where they will stay. The state $g2$ is called a "dark state" in this case, because atoms in $g2$ are not affected by the laser. We see that a laser exciting $g1 \rightarrow e$ will eventually optically pump all the atoms into $g2$.

To see how optical pumping produces the extra crossover dip, remember that only the pump laser can optically pump – the probe laser is by definition too weak. Also remember the atoms in the cell are not in steady state. When they hit the walls they bounce off about equally distributed in both ground states, and the optical pumping only operates for a short period of time as the atoms travel through the laser beams. If you think about it a while you can see there are two velocity classes of atoms that are responsible for the dip. For one velocity class the pump laser excites $g1 \rightarrow e$, which tends to pump atoms into $g2$. Then the probe laser, which excites $g2 \rightarrow e$ for these atoms, sees extra absorption. For the other velocity class the pump laser excites $g2 \rightarrow e$, $g1$ gets overpopulated, and again the probe laser (which now excites $g1 \rightarrow e$ for these atoms) sees more absorption.

Quantitative Picture of Saturated Absorption Spectroscopy – 2-Level Atoms. One can fairly easily write down the basic ideas needed to calculate a crude saturated absorption spectrum for 2-level atoms, which demonstrates much of the underlying physics. The main features are: 1) the transmission of the probe laser beam through the cell is $e^{-\tau(\nu)}$, $\tau(\nu)$ is the optical depth of the vapor; 2) the contribution to $\tau(\nu)$ from one velocity class of atoms is given by

$$d\tau(\nu, v) \sim (P_1 - P_2)F(\nu, v)dn(v)$$

where P_1 is the relative population of the ground state, P_2 is the relative population of the excited state $(P_1 + P_2 = 1)$,

$$dn \sim e^{-mv^2/2kT}dv$$

is the Boltzmann distribution (for v along the beam axis), and

$$F(\nu, v) = \frac{\Gamma/2\pi}{(\nu - \nu_0 + \nu_0 v/c)^2 + \Gamma^2/4}$$

is the normalized Lorentzian absorption profile of an atom with natural linewidth Γ, including the Doppler shift. Putting this together, we have the differential contribution to the optical depth, for laser frequency ν and atomic velocity v:

$$d\tau(\nu, v) = \tau_0 \frac{\nu_0}{c}(P_1 - P_2)F(\nu, v)e^{-mv^2/2kT}dv.$$

The overall normalization comes in with the τ_0 factor, which is the optical depth at the center of resonance line, $i.\ e.\ \tau_0 = \int d\tau(\nu_0, v)$ with no pump laser (the integral is over all velocity classes). 3) The populations of the excited and ground states are given by $P_1 - P_2 = 1 - 2P_2$, and

$$P_2 = \frac{s/2}{1 + s + 4\delta^2/\Gamma^2}$$

where $s = I/I_{sat}$ and $\delta = \nu - \nu_0 - \nu_0 v/c$. I_{sat} is called the saturation intensity (for obvious reasons ... if you consider the above formula for P_2 with $\delta = 0$, P_2 "saturates" $P_2 \rightarrow 1/2$ as $I/I_{sat} \rightarrow \infty$). The value of

I_{sat} is given by

$$I_{sat} = 2\pi^2 hc\Gamma/3\lambda^3.$$

For the case of rubidium, $\Gamma \approx 6$ MHz, giving $I_{sat} \approx 2$ mW/cm^2.

The underlying physics in points (1) and (2) should be recognizable to you. Point (3) results from the competition between spontaneous and stimulated emission. To see roughly how this comes about, write the population rate equations as

$$\dot{P}_1 = \Gamma P_2 - \alpha I(P_1 - P_2)$$
$$\dot{P}_2 = -\Gamma P_2 + \alpha I(P_1 - P_2)$$

where the first term is from spontaneous emission, with Γ equal to the excited state lifetime, and the second term is from stimulated emission, with α a normalization constant. Note that the stimulated emission is proportional to the intensity I. In the steady-state $\dot{P}_1 = \dot{P}_2 = 0$, giving

$$P_2 = \frac{\alpha I/\Gamma}{1 + 2\alpha I/\Gamma}$$

The term $\alpha I/\Gamma$ corresponds to the $s/2$ term above (note I_{sat} is proportional to Γ). A more complete derivation of the result, with all the normalization constants, is given in Milonni and Eberly (1988), and in Cohen-Tannoudji *et al.* (1992), but this gives you the basic idea.

Assuming a fixed vapor temperature, atomic mass, etc., the saturated absorption spectrum is determined by two adjustable external parameters, the pump intensity I_{pump} and the on-resonance optical depth τ_0. The latter is proportional to the vapor density inside the cell. Figure 5 shows calculated spectra at fixed laser intensity for different optical depths, and Figure 6 shows spectra at fixed optical depth for different laser intensities.

In Figure 5 one sees mainly what happens when the vapor density is increased in the cell. At low densities the probe absorption is slight, with a Gaussian profile, and the absorption increases as the vapor density increases. At very high vapor densities the absorption profile gets deeper and broader. It get broader simply because the absorption is so high near resonance that the probe is almost completely absorbed; for greater vapor densities the probe gets nearly completely absorbed even at frequencies fairly far from resonance; thus the width of the absorption profile appears broader. The saturated-absorption feature in Figure 5 does pretty much what you would expect. The probe absorption is reduced on resonance, due to the action of the pump laser. At very high vapor densities the saturated-absorption feature becomes smaller. This is because while the pump laser reduces the absorption, it doesn't eliminate it; thus at high vapor densities the probe is nearly completely absorbed even with the pump laser. The moral of this story is that the vapor density shouldn't be too low or high if you want to see some saturated-absorption features.

In Figure 6 one sees that if the pump intensity is low, the saturated-absorption feature is small, as one would expect. For larger pump intensities the feature grows in height and width. The width increases because at high laser intensities the effect of the pump laser saturates on resonance, and continues to grow off resonance; thus the width of the feature increases, an effect known as "power broadening."

Finally, it should be noted that calculating the saturated absorption spectrum for real atoms, which must include optical pumping, many different atomic levels, atomic motion in the vapor cell, and the polarization of the laser beams, is considerably more subtle. A recent paper by Schmidt *et al.* (1994) shows much detailed data and calculations for the case of cesium.

Problem 1. Show that $\tau_0 = \int d\tau(\nu_0, v)$ when the pump laser intensity is zero, from the formula above.
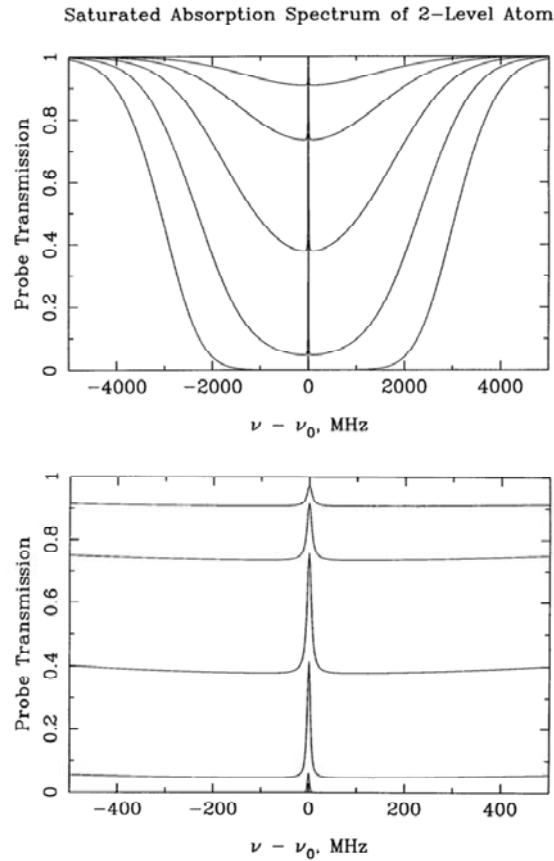
Saturated Absorption Spectrum of 2−Level Atom

Figure 5. Calculated saturated-absorption spectra for two-level atoms, for $(\tau, I/I_{sat}) = (0.1,10)$, $(0.316,10)$, $(1,10)$, $(3.16,10)$, and $(10,10)$. The two plots show the same spectra with the frequency axis at different scales. Note the overall Doppler-broadened absorption, with the small saturated-absorption feature at line center.

Hint: the integral is simplified by noting that $\Gamma \ll \Delta\nu_{Dopp}$.

Problem 2. The above calculations all assume that the pump laser has the same intensity from one end of the cell to another. This is okay for a first approximation, but calculating what really happens is an interesting problem. Consider a simple laser beam (the pump) shining through a vapor cell. If the laser intensity is weak, and the atoms are all pretty much in the ground state, then the laser intensity changes according to the equation $dI/dx = -\alpha I$, where $\alpha = \alpha(\nu)$ depends on the laser frequency, but not on position inside the cell (α^{-1} is called the absorption length in this case). This equation has the solution $I(x) = I_{init}e^{-\alpha x}$, where I_{init} is the initial laser intensity. The transmission through the cell, $e^{-\alpha L}$, where L is the length of the cell, is what we called $e^{-\tau}$ above.

Your job in this problem is to work out what happens when the input laser beam is not weak, and thus we cannot assume that the atoms are all in the ground state. In this case $\alpha = \alpha(\nu, x)$, which makes the differential equation somewhat more interesting. Assume the laser is on resonance for simplicity. Then the attenuation coefficient at any position x is proportional to $P_1 - P_2$, which in turn is proportional to
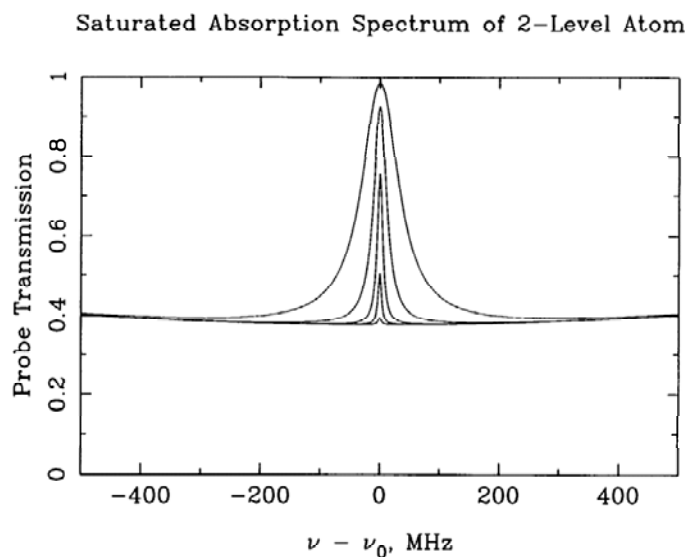
Saturated Absorption Spectrum of 2-Level Atom

Figure 6. Calculated saturated-absorption spectra for two-level atoms, for $(\tau, I/I_{sat}) = $ (1,0.1), (1,1), (1,10), (1,100), and (1,1000). Note at large laser intensities the saturated absorption feature is "power broadened" as the line saturates.

$1/(1 + s)$. Thus we have $\alpha(\nu_0, x) = \alpha_0/(1 + s(x))$. In the weak beam limit $I \ll I_{sat}$ this reduces to our previous expression, so $\alpha_0 = \tau_0/L$. Write down an expression which relates the saturation parameter of the laser as it exits the cell s_{final}, the saturation parameter at the cell entrance $s_{initial}$, and the weak-limit optical depth τ_0. Check your expression by noting in the limit of finite τ_0 and small s you get $s_{final} = s_{initial}e^{-\tau_0}$. If $\tau_0 = 100$, how large must $s_{initial}$ be in order to have a transmission of $1/2$ (i. e. $s_{final} = s_{initial}/2$)?

Atomic Structure of Rubidium. The ground-state electronic configuration of rubidium consists of closed shells plus a single 5s valence electron. This gives a spectrum which is similar to hydrogen (see attached Scientific American article). For the first excited state the 5s electron is moved up to 5p. Rubidium has two stable isotopes: ^{85}Rb (72 percent abundance), with nuclear spin quantum number $I = 5/2$, and ^{87}Rb (28 percent abundance), with $I = 3/2$.

The different energy levels are labeled by "term states", with the notation ${}^{2S+1}L'_J$, where S is the spin quantum number, L' is the spectroscopic notation for the angular momentum quantum number (i. e. S, P, D, ..., for orbital angular momentum quantum number $L = 0, 1, 2, \ldots$), and $J = L + S$ is the total angular momentum quantum number. For the ground state of rubidium $S = 1/2$ (since only a single electron contributes), and $L = 0$, giving $J = 1/2$ and the ground state ${}^2S_{1/2}$. For the first excited state we have $S = 1/2$, and $L = 1$, giving $J = 1/2$ or $J = 3/2$, so there are two excited states ${}^2P_{1/2}$ and ${}^2P_{3/2}$. Spin-orbit coupling lifts splits the otherwise degenerate $P_{1/2}$ and $P_{3/2}$ levels. (See any good quantum mechanics or atomic physics text for a discussion of spin-orbit coupling.)

The dominant term in the interaction between the nuclear spin and the electron gives rise to the magnetic hyperfine splitting (this is described in many quantum mechanics textbooks). The form of the interaction

term in the atomic Hamiltonian is $H_{hyp} \propto J \cdot I$, which results in an energy splitting

$$\Delta E = \frac{C}{2}[F(F+1) - I(I+1) - J(J+1)]$$

where $F = I + J$ is the total angular momentum quantum number including nuclear spin, and C is the "hyperfine structure constant." Figures 7 and 8 shows the lower S and P energy levels for ^{85}Rb and ^{87}Rb, including the hyperfine splitting.

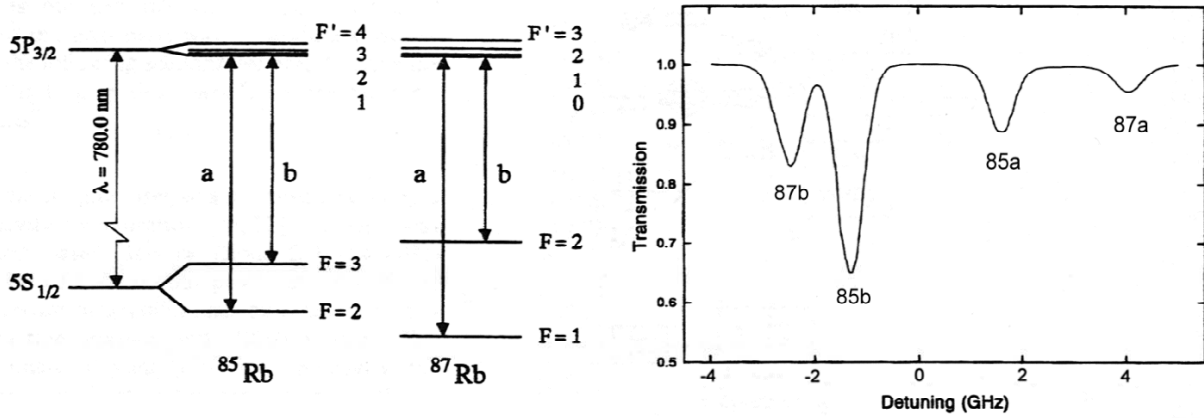Figure 7. (Left) Level diagrams for the D2 lines of the two stable rubidium isotopes. (Right) Typical absorption spectrum for a rubidium vapor cell, with the different lines shown.
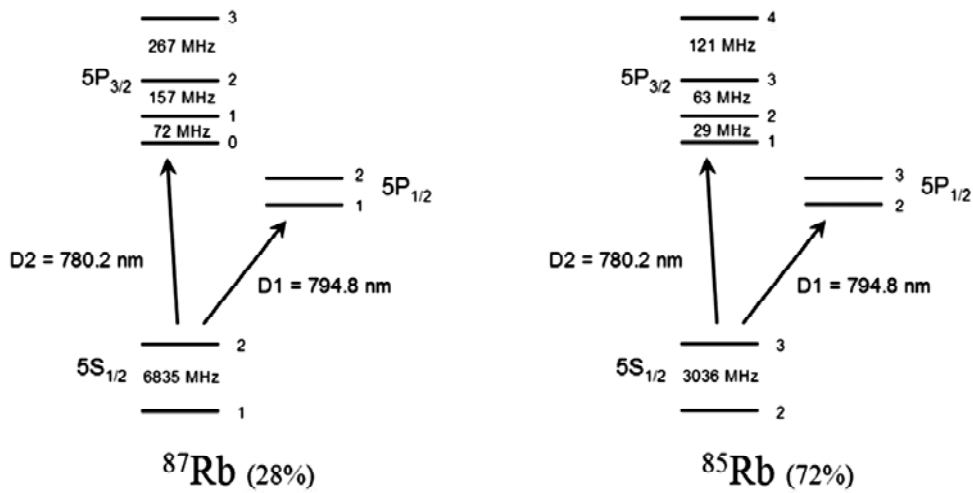

Figure 8. More rubidium level diagrams, showing the hyperfine splittings of the ground and excited states.

II. LABORATORY EXERCISES.

The goal of this section is first to observe and record saturated absorption spectra for as many of the
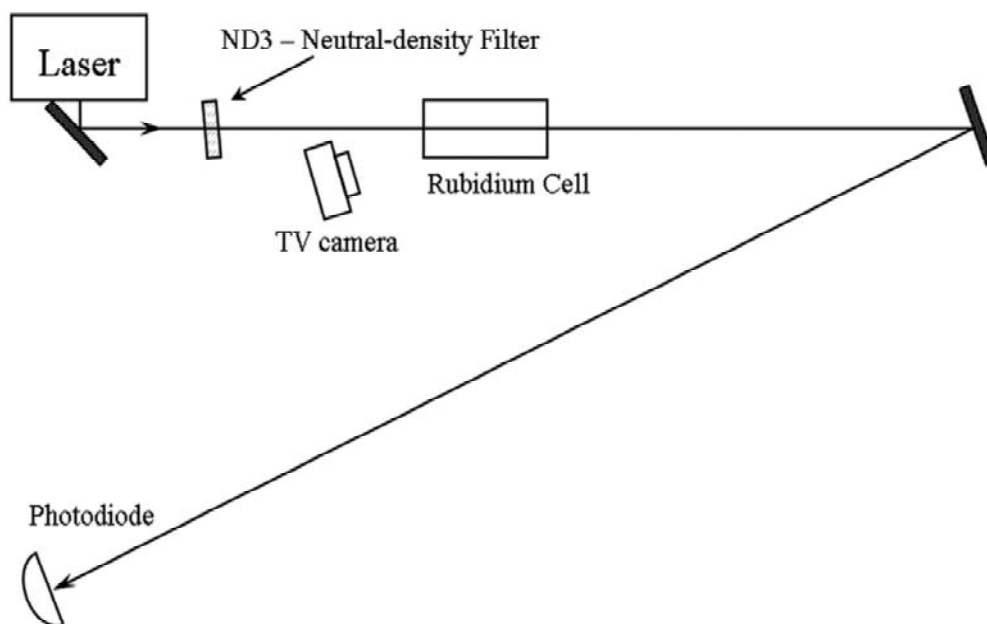
Figure 9. Recommended set-up to get the laser running on the rubidium resonance lines.

rubidium lines as you can, and then to see how well you can measure the $P_{3/2}$ hyperfine splitting of ^{87}Rb using a auxiliary interferometer as a length standard.

Remember that eye safety is important. First of all the laser operates at 780 nm, which is very close to being invisible. Thus you can shine a beam into your eye without noticing it. Also, the laser power is about 20 milliwatts, and all that power is concentrated in a narrow beam. Looking directly at the Sun puts about 1 milliwatt into your eye, and that much power is obviously painful. It is certainly possible to cause permanent eye damage using the Ph76 laser if you are not careful. Therefore – be careful. ALWAYS WEAR LASER GOGGLES WHEN THE LASER IS ON! As long as you keep the goggles on, your eyes will be protected.

Week 1 – Getting the Laser On Resonance.

The first step is to get the laser turned on and tuned to hit the rubidium lines. We see in Figure 7 that the lines span about 8 GHz, which can be compared with the laser frequency of $v = c/\lambda = 4 \times 10^{14}$ Hz. Thus to excite the atoms at all the laser frequency must be tuned to about a part in 10^5. Start with the simple set-up shown in Figure 8. The ND filter can be removed when aligning the laser beam.

Once you have the beam going about where you want it, sweep the high-voltage going to the grating PZT with a triangle wave, so that the voltage varies from about 0 to 100 volts. Use the HV/100 to monitor the high voltage on the oscilloscope. Sweeping this voltage sweeps the grating position using a small piezo-electric actuator (made from lead zirconate titanate, hence PZT). While the high voltage is scanning you should then also change the laser injection current up and down by hand. The current makes large changes in the laser frequency, while the PZT makes small changes (see the laser primer for details).

The plan is that with all this sweeping the laser will sweep over the rubidium lines and you will see some fluorescence inside the vapor cell. This will appear as a bright line inside the cell; don't be confused

by scattering off the windows of the cell. If you cannot see the atoms flashing at all, ask your TA for help. The laser may need some realignment, or you may just not be doing something right.

Once you see fluorescence, compare the photodiode output to the rubidium spectrum shown in Figure 7. Usually you can only get the laser to scan over part of this spectrum without mode hopping (see the laser primer). Record your best spectrum using the digital oscilloscope and print it out. At this point the laser is tuned to the rubidium lines. Before proceeding with the rest of the experiment, move the ND filter from its location in Figure 9 to a new position right in front of the photodiode. If you look closely you'll see the absorption lines are still there, but much weaker. How come? There are two reasons. First, optical pumping is faster with more laser power, so the atoms are more quickly pumped to the dark state. That makes the absorption less. Second, the atoms become saturated with the high power, just like you calculated above. That also reduces the absorption.
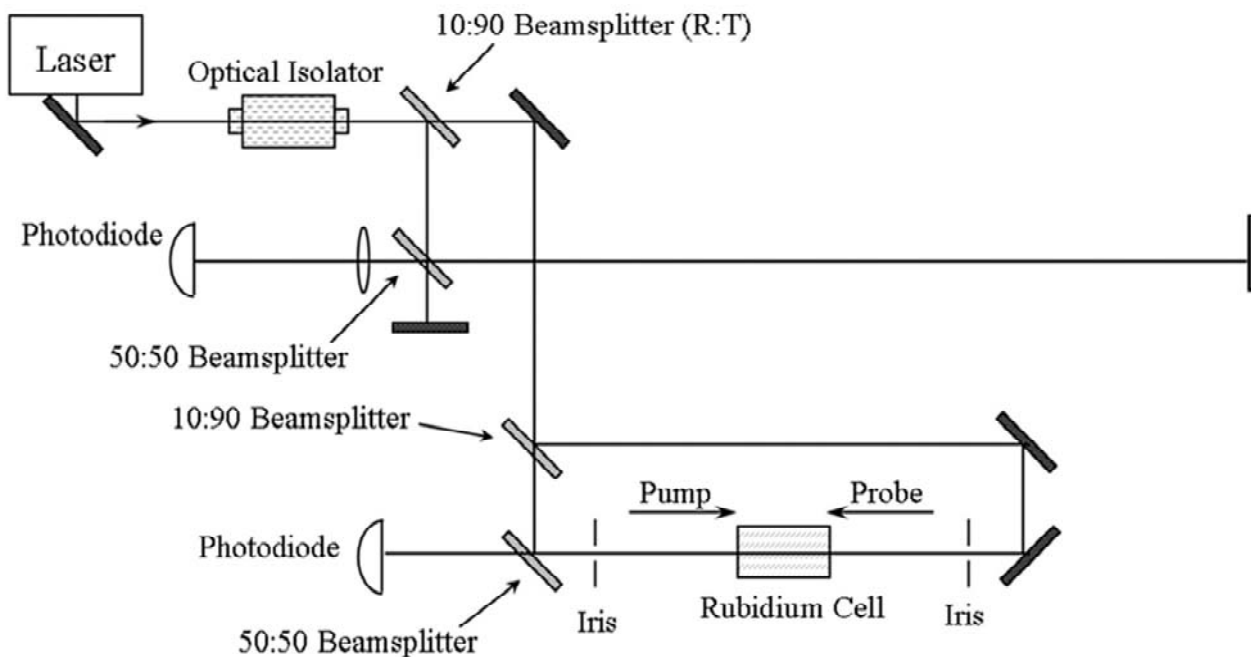
Figure 10. Recommended set-up to record rubidium saturated absorption spectra, and for measuring the hyperfine splittings.

Week 1 – Getting a Saturated Absorption Spectrum.

The suggested set-up for observing saturated absorption spectra is shown in Figure 10. Since the laser is on resonance from the last section, leave it alone while you change the set-up. Ignore the interferometer part for now; that comes in after you've gotten some spectra. The optical isolator is a device that contains a two polarizers, a special crystal, and strong permanent magnets (see Appendix I). The first polarizer is aligned with the polarization of the input laser (vertical), and simply transmits the beam. The crystal in the magnetic field rotates the polarization of the beam by about 45 degrees, using the Faraday effect, and the beam exits through the second polarizer, which is set at 45 degrees. A beam coming back toward the

laser sees all this in reverse; the beam polarization gets rotated in the crystal, so that the polarization is 90 degrees with respect to the vertical polarizer, and the beam is not transmitted. These devices are also sometimes called optical diodes, since light only passes through them in one direction. We use an optical isolator here to keep stray light (generated downstream...note the pump beam goes backward after it passes though the cell) from getting back to the diode laser, where is can adversely affect the frequency stability.

Note the 10:90 beamsplitter puts most of the laser power into the probe beam. The irises are an alignment guide; if you have both the pump and probe beams going through small irises, then you can be assured that the beams overlap in the rubidium cell. If you block the pump beam you should get a spectrum that looks pretty much the same as you had in the previous section.

Lab Exercise 1. Observe and record the best spectra you can for whatever rubidium lines you can see, especially the two strongest lines (87b and 85b in Figure 7). Get some nice spectra and put hard copies into your notebook. Note (but don't bother recording) that the saturated absorption features go away if you block the pump beam, as expected.

Week 2 – Measuring the Hyperfine Splitting.

Now finish the set-up in Figure 10 by adding the interferometer. (Turn off the laser frequency scanning while setting up the interferometer, so the fringes are stable.) Make the arm difference as long as you can. If you want you can add another mirror to the long arm to bounce it across the table. The longer the long arm, the better your measurement will be. Recombine the beams on the beamsplitter and send one of the output beams through a strong lens, so that the beam is expanded quite a bit. Align the overlap of the beams (in position as well as angle) until you see nice fringes on the expanded beam. Align the overlap so the fringes spacing is very large. Place the photodiode such that it only intercepts the light from one fringe of the interferometer.

If you now scan the laser frequency you should observe temporal fringes on the photodiode output. The fringe spacing can be computed from the arm length difference, which you should measure. When a beam travels a distance L it picks up a phase $\varphi = 2\pi L/\lambda$, so the electric field becomes

$$E = E_0 e^{i\omega t} e^{i\varphi}$$

When the beam is split in the interferometer, the two parts send down the two arms, and then recombined, the electric field is

$$
\begin{aligned}
E &= E_{arm1} + E_{arm2} \\
&= E_0 e^{i\omega t} \left[e^{i4\pi L_1/\lambda} + e^{i4\pi L_2/\lambda} \right]
\end{aligned}
$$

where L_1 and L_2 are the two arm lengths. The additional factor of two comes from the fact that the beam goes down the arm and back again. Squaring this to get the intensity we have

$$
\begin{aligned}
I &\sim \left| e^{i4\pi L_1/\lambda} + e^{i4\pi L_2/\lambda} \right|^2 \\
&\sim 1 + \cos\left(\frac{4\pi \triangle L}{\lambda} \right)
\end{aligned}
$$

where $\triangle L = L_1 - L_2$. If the laser frequency is constant, then the fringe pattern goes through one cycle every time the arm length changes by $\lambda/2$.

Problem 3. If $\triangle L$ is fixed, how much does the laser frequency have to change to send I through one brightness cycle? For your known $\triangle L$, what is the fringe period in MHz? From this you can convert your

measurement of $\triangle L$ into a calibration of the laser frequency scan.

Use the two oscilloscope traces to plot the interferometer fringes and the saturated absorption spectra at the same time, as you scan the laser frequency. Watch that the interferometer fringes are uniform as a function of PZT voltage; if not the nonlinearities could compromise your calibration. Zoom in on the hyperfine features you want to measure. You will need to know which features belong to which lines, so identify the features by comparing your spectra with the level diagrams in Figures 7 and 8. Print out some good spectra, measure the spacings of the various features using a ruler, and you can turn this all into a direct measurement of the hyperfine splittings. Try to do this for both lines 87b and 85b in Figure 7. Note there are no tricks or complicated math in any of this. You just have to understand what's going on, and not lose any factors of two. No fair adjusting the answer by factors of two until it agrees with the known splittings.

Lab Exercise 2. Measure and record the largest $P_{3/2}$ hyperfine splittings for ^{85}Rb and ^{87}Rb, in MHz. Estimate the accuracy of your measurement, knowing the various uncertainties you encountered along the way.

III. REFERENCES.

Cohen-Tannoudji, C., Dupont-Roc, J., and Grynberg, G. 1992, *Atom-Photon Interactions*, (Wiley).

Hänsch, T. W., Schawlow, A. L., and Series, G. W. 1979, "The Spectrum of Atomic Hydrogen," *Scientific American* **240**, 94 (March).

Milonni, P., and Eberly, J. 1988, *Lasers*, (Wiley).

Schmidt, O., Knaak, K.-M., Wynands, R., and Meschede, D. 1994, "Cesium Saturation Spectroscopy Revisited: How to Reverse Peaks and Observe Narrow Resonances," *Appl. Phys. B*, **59**, 167.
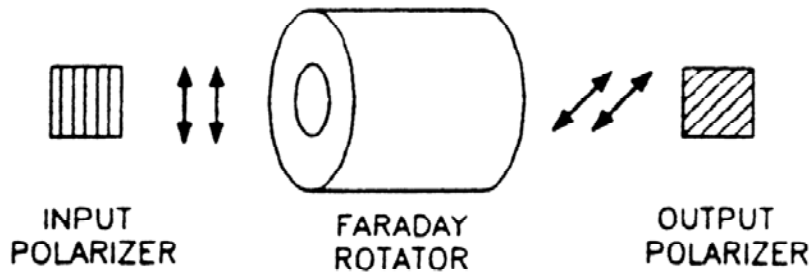
Appendix I – The Optical Isolator

Figure 11. Schematic picture of an optical isolator. Not shown is the large longitudinal magnetic field in the Faraday rotator produced by strong permanent magnets inside the device.

The optical isolator is a somewhat subtle device, which uses the Faraday effect. The Faraday effect is a rotation of the plane of polarization of a light beam in the presence of a strong magnetic field along the propagation axis. You can get a feel for this effect by considering a simple classical picture. An incoming light beam imposes an oscillating electric field on the electrons in the solid, which causes the electrons to oscillate. Normally the oscillating electrons re-radiate the light in the same direction as the original beam, which doesn't change the polarization of the light (it does change the phase, however, which is the cause of the material index of refraction). With the application of a strong longitudinal magnetic field, you can see that the Lorentz force $e \overrightarrow{v} \times \overrightarrow{B}$ will shift the motion of the electrons, and rotate their plane of oscillation. As the electrons re-radiate this tends to rotate the polarization of the light beam. Obviously a hand-wavy argument, but it gives you the right idea.

The optical isolator uses the Faraday effect to rotate the polarization angle of the input beam by 45 degrees, and the output beam exits through a 45-degree polarizer (see Figure 12). Note that the diode laser's beam is polarized, in our case along the vertical axis. If one reflects the beam back into the optical isolator, the polarization experiences another 45-degree rotation, in the same direction as the first, and the beam is then extinguished by the input polarizer. You can see that the rotations have the correct sense using the classical picture. Thus the overall effect is that of an "optical diode" – light can go through in one direction, but not in the reverse direction.

The Faraday effect is typically very weak, so the optical isolator uses a special crystal, which exhibits an anomalously large Faraday effect, and a very strong longitudinal magnetic field produced by state-of-the-art permanent magnets. Optical isolators have gotten much smaller over the last couple of decades as magnet technology has improved. The magnetic field is strong only near the axis of the device, which therefore has a small clear aperture. Also, too much light intensity will burn a spot in the Faraday crystal, so one must be careful not to focus the diode laser to a tight spot inside the optical isolator.

Ph 77 ADVANCED PHYSICS LABORATORY
– ATOMIC AND OPTICAL PHYSICS –

Interferometric Measurement of
Resonant Absorption and Refractive Index in Rubidium

I. BACKGROUND

In this lab you will observe the relation between resonant absorption and the refractive index in rubidium gas. To see how these are related, consider a simple model for a rubidium atom, namely that of a single electron bound by a harmonic force, acted upon by the electric field of an incident laser (see for example Jackson 1975, pg. 284, Marion and Heald 1980, pg. 282). Although crude, this model does allow us to write down the basic optical properties of a gas of atoms near an atomic resonance. In this picture, the equation of motion for the electron around the atom is

$$m[\ddot{x} + \gamma\dot{x} + \omega_0^2 x] = -eE(x, t)$$

where γ measures a phenomenological damping force. If the electric field varies in time as $Ee^{-i\omega t}$, then the dipole moment contributed by one atom is

$$
\begin{aligned}
p &= -ex \\
&= (e^2/m)(\omega_0^2 - \omega^2 - i\omega\gamma)^{-1}E \\
&= \epsilon_0 \chi_e E
\end{aligned}
$$

where χ_e is called the electric susceptibility. If there are N atoms per unit volume, then the (complex) dielectric constant of the gas is given by

$$
\begin{aligned}
\epsilon(\omega)/\epsilon_0 &= 1 + 4\pi\chi_e \\
&= 1 + \frac{4\pi N f e^2/m}{(\omega_0^2 - \omega^2 - i\omega\gamma)}
\end{aligned}
\tag{1}
$$

where f is a standard fudge factor, called the "oscillator strength" of the transition. Adding the oscillator strength factor makes this simple classical calculation agree with a more realistic quantum mechanical calculation. The oscillator strength is of order unity for strong transitions like the $S \to P$ rubidium lines, and is much smaller for forbidden atomic transitions. Both the oscillator strength and the damping factor γ are difficult to calculate for real atoms, since doing so requires quite a lot of detailed atomic physics.

Maxwell's equations (MKS units) for a propagating electromagnetic wave give us

$$\nabla^2 E - \mu\epsilon\frac{\partial^2 E}{\partial t^2} = 0$$

and we define an index of refraction $n = c/v = \sqrt{\epsilon\mu/\epsilon_0\mu_0}$, where v is the speed of wave propagation. Assuming $\mu/\mu_0 \simeq 1$ and the above expression for the dielectric constant ϵ/ϵ_0, we find ourselves with a complex index of refraction, which we write

$$n = \sqrt{\epsilon/\epsilon_0} = n_0(1 + i\kappa) \tag{2}$$

where n_0 and κ are real quantities. Evaluating Eqn. 1 gives

$$Re(\sqrt{\epsilon/\epsilon_0}) = n_0$$

$$\simeq 1 - \frac{2\pi(\omega^2 - \omega_0^2)Nfe^2/m}{(\omega^2 - \omega_0^2)^2 + \gamma^2\omega^2}$$

$$\simeq 1 - \frac{\pi\Delta\omega Nfe^2/m\omega_0}{\Delta\omega^2 + \gamma^2/4}$$

$$Im(\sqrt{\epsilon/\epsilon_0}) = n_0\kappa$$

$$\simeq \frac{2\pi Nf\omega\gamma e^2/m}{(\omega^2 - \omega_0^2)^2 + \gamma^2\omega^2}$$

$$\simeq \frac{\pi Nf\gamma e^2/2m\omega_0}{\Delta\omega^2 + \gamma^2/4}$$

where $\triangle\omega = \omega - \omega_0$. These are plotted in Figure 1. This is the index of refraction for a dilute atomic gas, which of course is proportional to the atom density.
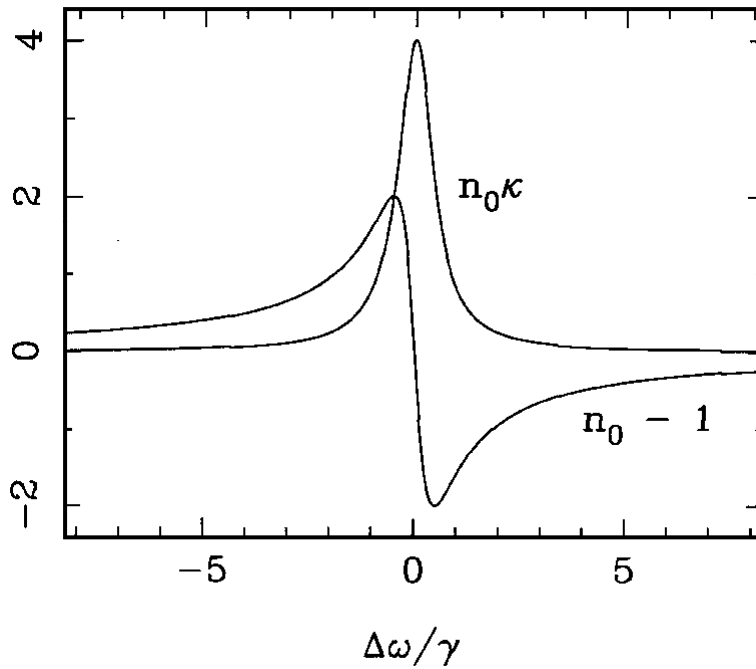
Figure 1. Plot of the absorption $n_0\kappa$ and refractive index change $n_0 - 1$ for a gas near an atomic resonance. Note the index change is proportional to the first derivative of the absorption.

An electromagnetic wave in the medium propagates according to

$$e^{-i(\omega t - nkz)} = e^{-kn_0\kappa z}e^{-i[\omega t - kn_0 z]} \tag{3}$$

where $k = \omega/c$. From this it can be seen that n_0 corresponds to the usual index of refraction, equal to c/v, while κ describes the attenuation of the wave. Note that a relation $n_0 - 1 \simeq -2\triangle\omega\kappa/\gamma$ exists between the index of refraction and the attenuation, which is independent of the oscillator strength of the atomic transition. This relation, showing that $n_0(\nu)$ and $\kappa(\nu)$ can be derived from one another, is an example of the more general *Kramers-Kronig relations*. A full quantum mechanical treatment also yields the same relation for the absorption and refractive index of a gas near an atomic resonance. The goal of this lab

is to measure both the absorption and index of refraction variations of rubidium gas around the $S \to P$ resonance lines. While absorption is easy to observe, refractive index changes are not, so an interferometric technique will be used to observe it.

Figure 2. The basic experimental set-up, consisting of a rubidium vapor cell in one arm of a Mach-Zehnder interferometer. The dotted lines represent 50:50 beamsplitters. The input laser scans across the (Doppler broadened) rubidium absorption line.
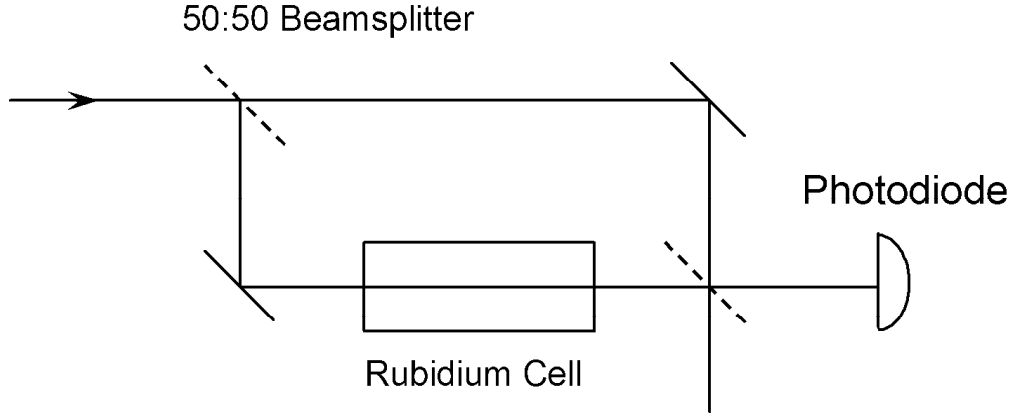
Let us examine the experimental set-up shown in Figure 2, consisting of a rubidium vapor cell in one arm of a Mach-Zehnder interferometer. The Mach-Zehnder interferometer is related to the Michelson interferometer, with which you are probably familiar. The input laser light is first split by a beamsplitter (we will assume both beamsplitters in the interferometer are perfect lossless 50:50 beamsplitters), and the two beams travel down different paths through the interferometer. They are recombined at the second beamsplitter, and the light intensity in one direction is measured with a photodetector. The intensity seen at the photodiode is sensitive to the relative phases of the two beams as they interfere at the second beamsplitter.

Your first job, *before* attempting the experiment, is to model the expected signal seen at the photodiode in Figure 2, as the laser frequency is scanned through the rubidium resonance line. If we consider the interferometer in Figure 2 without the rubidium cell, it is straightforward to calculate the photodiode signal. As the two beams propagate through the separate arms of the interferometer, each picks up a phase shift as it travels, given in Eqn. 3. Without the rubidium cell $n_0 = 1$ (neglecting the contribution from n_{air}) and $\kappa = 0$, giving simple free-space propagation e^{ikz}.

The output power hitting the photodiode comes from the combination of the two beams at the second beamsplitter, and is given by

$$
\begin{aligned}
\frac{I}{I_0} &= \frac{1}{4}\left|e^{ikL_1} + e^{ikL_2}\right|^2 \\
&= [1 + \cos(k\triangle L)]/2
\end{aligned}
$$

which is plotted in Figure 3. Since the beam splitters are perfect 50:50 beamsplitters, the beams in the two paths have equal intensity, so the photodiode output as a function of $\triangle L = L_2 - L_1$ varies from zero (destructive interference) to the initial laser intensity I_0 (constructive interference) as shown in the figure.
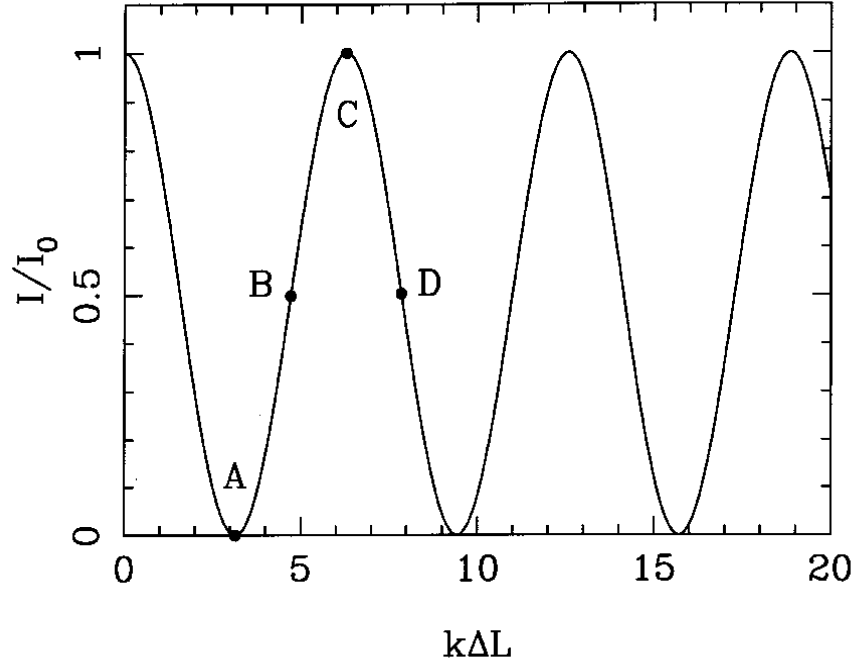
Figure 3. Photodiode output vs. $k\triangle L$, where $k = \omega/c = 2\pi/\lambda$, for a perfect Mach-Zehnder interferometer with no rubidium cell, at fixed laser frequency.

Next consider the effect of the rubidium cell on the propagation of a laser. From Eqn. 3, the total phase shift upon passing through the cell is

$$e^{-kn_0\kappa\Delta z}e^{ikn_0\Delta z} = e^{-kn_0\kappa\Delta z}e^{ik\Delta z}e^{ik(n_0-1)\Delta z}$$
$$= e^{-\tau}e^{ik\Delta z}e^{i\delta}$$

where $\triangle z$ is the length of the cell. The factor $e^{ik\Delta z}$ in this expression is the free-space propagation factor. The $e^{-\tau}$ factor comes from attenuation in the cell, with $\tau = kn_0\kappa\triangle z \approx k\kappa\triangle z$. Because we have a resonance line, τ depends on frequency and we can assume a Lorentzian line profile,

$$\tau = \frac{\tau_0\gamma^2}{\triangle\omega^2 + \gamma^2}$$

where τ_0 is the absorption at line center. The $e^{i\delta}$ factor is the additional phase shift from the refractive index of the rubidium atoms, with $\delta = k(n_0 - 1)\triangle z$. The atomic factors are related through $\delta = (n_0 - 1)\tau/\kappa = -2\triangle\omega\tau/\gamma$, which you should verify.

If we now put the rubidium cell in the interferometer, the photodiode output will be given by

$$\frac{I}{I_0} = \frac{1}{4}\left|e^{ikL_1} + e^{-\tau}e^{ikL_2}e^{i\delta}\right|^2$$
$$= [1 + e^{-2\tau} + 2e^{-\tau}\cos(k\triangle L + \delta)]/4.$$

Note that if the rubidium density is zero, then $\tau = \delta = 0$ and we have the same result as before. Note also that three terms in this equation are frequency dependent: τ, δ, and k. However, if $\triangle L$ is small then $k\triangle L$ changes very little as the laser frequency is scanned over a rubidium line, so we can assume $k\triangle L$ is

essentially constant as a function of laser frequency (see Problem 1).

Problem 1. Consider the photodiode output from the interferometer without the rubidium cell. Figure 3 shows the output at fixed laser frequency as a function of $\triangle L$. The maxima in this are referred to as "fringes," from their spatial structure (which you will see in the lab when you set up the interferometer). How small must $\triangle L$ be in order for the photodiode output to go through less than one fringe as the laser is scanned over the rubidium resonance line (call it 5 GHz)? To get the best results, you should try to set up your interferometer with $\triangle L$ less than this.

Problem 2. Compute the photodiode output as a function of laser frequency around the rubidium resonance line, $I(\triangle\omega)/I_0$, for the set-up shown in Figure 2. Assume the atoms in your cell are at rest (for ease of calculation) with some linewidth γ, so we can use the Lorentzian profile above for $\tau(\omega)$. Make three different plots of $I(\triangle\omega)/I_0$, one for each of three different values of the line-center optical depth: $\tau_0 = 0.4$, 2, and 20. Make your plots over the range $-20\gamma < \triangle\omega < 20\gamma$. Plot six curves on each plot, with values of $k\triangle L \bmod(2\pi)$ equal to $j\pi/5$, with $j = 0$ to 5. The first and last of these correspond to the positions A and C in Figure 3. Label your plots. You will be trying to reproduce these curves in the lab. (Check your calculations by comparing with the one calculated curve in Figure 5 below.) Why does $I(\triangle\omega = 0)/I_0$ go to 0.25 for large τ_0?

Amazingly enough, the generality of the Kramers-Kronig relations says that the above calculations relating $n_0 - 1$ and κ are true for a Doppler-broadened gas as well as for atoms at rest. Because of this, scanning the laser over the Gaussian profile of the Doppler-broadened gas will give results which are qualitatively similar to those you calculated in Problem 2 for the atoms' natural Lorentzian profile.

II. LABORATORY EXERCISES.
The Clausius-Clapeyron Relation. Before launching into the main part of the lab, we'll get warmed up by first measuring just the resonant absorption as a function of the rubidium cell temperature. Heating the cell increases the rubidium vapor density and thus increases the absorption. The rubidium vapor in the cell is in equilibrium with a small bit of solid rubidium on the cell wall, and the vapor pressure is given by the Clausius-Clapeyron relation

$$
\begin{aligned}
p(T) &= p_0 e^{-L/RT} \\
&= p_0 e^{-\ell/kT}
\end{aligned}
$$

where p_0 is a constant, T is the cell temperature in Kelvin, L is the latent heat of vaporization per mole, ℓ is the latent heat per atom, R is the gas constant, and k is Boltzmann's constant. This equation is derived from rather fundamental thermodynamic relations, but the derivation is a bit too involved to repeat here. Most good books on statistical mechanics derive it. For example, you can find it in Reif's book (see references below), which is still an excellent introduction to the subject.

Assuming the rubidium gas behaves like an ideal gas (a good assumption), the vapor density is proportional to $e^{-\ell/kT}$, and thus so is the optical depth $\tau(\omega)$. The light transmitted through the cell is equal to $I_{out}(\omega) = I_{in}e^{-\tau(\omega)}$ in the limit that I_{in}, the light incident on the cell, is much less than the saturation intensity (which was introduced in the previous lab, equal to about 2 mW/cm^2 for rubidium). Thus we have

$$
\frac{I_{out}(\omega)}{I_{in}} = \exp\left[-A(\omega)\exp(-\ell/kT)\right]
$$

where the function $A(\omega)$ contains the Doppler-broadened absorption profile of the gas. If we measure the

intensity of the line center only, then

$$\frac{I_{out}(\omega_0)}{I_{in}} = \exp\left[-A_0 \exp(-\ell/kT)\right]$$

where here A_0 is a constant for a given atomic transition. The goal of the first part of the lab will be to measure $I_{out}(\omega_0)/I_{in}$ at several different values of the cell temperature, and from these data extract the latent heat of vaporization of rubidium gas.

Start with the cell at room temperature (about 25C on the cell temperature controller). Scan the laser frequency and send the beam through the rubidium cell and onto a photodiode. Reduce the laser intensity by about 3-4 orders of magnitude by using absorption filters, in order to reduce the intensity well below the saturation value. Tune the laser so you can see all four of the rubidium transitions, although probably not all in a single sweep. Check how much background light is getting into the photodiode by blocking the laser beam. You may need to turn out the lights and shield the photodetector to keep the stray light down. Remember that zero volts on the photodiode may not mean zero light. All amplifiers have offsets, so you may need to compensate for the photodiode reading at zero light.

When you observe the photodiode signal on the 'scope, you will probably notice that $I_{out}(\omega_0)/I_{in}$ changes with laser settings, in particular with the laser current. This is because the laser doesn't always run in a single mode. When it runs multi-mode, some light is not resonant with the atoms and thus is not absorbed. This is a serious problem that limits how accurately you can measure $I_{out}(\omega_0)/I_{in}$. You can get pretty good results if you do the following: set the high voltage so the transition you want to observe is centered in the sweep, and then adjust the laser current to *minimize* $I_{out}(\omega_0)/I_{in}$.

If you think the laser is scanning okay and giving you accurate measurements, then start making measurements of $I_{out}(\omega_0)/I_{in}$ on the middle **85a** line as a function of temperature. Measure $I_{out}(\omega_0)$, $I_{out}(nonresonant) \approx I_{in}$ and I_{dark} at each temperature. You can take $I_{out}(nonresonant)$ to be an eyeball average of the intensity on either side of the line. Don't move the cell or any of the optics during the measurements; only adjust the laser settings a small amount in order to minimize $I_{out}(\omega_0)$. Make sure you measure especially carefully when $I_{out}(\omega_0)/I_{in}$ is small. Measure at temperatures from 25C to 75C in increments of 5-10C. You don't need to wait a long time to reach some particular temperature exactly; just make sure the temperature is fairly stable for each reading. The temperature is stable enough if it changes by less than 0.1C in 10 seconds.

When you have the data, you should get a straight line when you plot $\log(\log(I_{out}(\omega_0)/I_{in}))$ versus $1/T$ (why? - see above). Extract the latent heat of vaporation from the slope of this line. Express you answer in Joules/gram.

Also, plot $I_{out}(\omega_0)/I_{in}$ as a function of temperature, along with a curve going through the data using the Clausius-Clapeyron relation with the parameters you measured. If you plot the fit from about $T = -10C$ to $T = 80C$ you can also see the low-temperature structure of the absorption versus temperature.

The Kramers-Kronig Relation. Next, move on to the main event of observing the Kramers-Kronig relation in the lab by measuring Mach-Zehnder spectra like those you calculated in Problem 2. The first thing you should do in the lab is check your calculations with your TA. If your calculations aren't right, the lab will make no sense at all.

The optical set-up is shown in Figure 4. To begin the lab work, set up the Mach-Zehnder interferometer using the diode laser, just to get a feeling for what the fringe pattern looks like. Follow the set-up in Figure 4, starting out without the negative lens and without the neutral-density (ND) filter. Make sure the beam goes through the centers of the rubidium cell windows, where the optical quality is best. In keeping with

what you found in Problem 1 above, make sure the two arms of the interferometer are about the same length. Check that the laser is tuned on resonance by blocking one arm of the interferometer and putting the ND filter back in. You should then see a nice absorption spectrum on the photodiode when you scan the laser.

Adjust the mirrors so the two beams overlap on the second beamsplitter, and then adjust the second beamsplitter so the two beams are collinear. If the beams overlap well at the beamsplitter, and the also overlap some distance downstream from the beamsplitter, then you know they must overlap everywhere. Iterate these steps so the two beams are overlapping and collinear as best you can. At this point you should start to see fringes on the interfering beams. Put in the negative lens to expand the beam before it hits the photodiode. This makes it easier to see the fringe pattern, and you can adjust the interferometer so that broad fringes are seen. They should be broad enough so that the photodiode only samples a small part of a fringe.
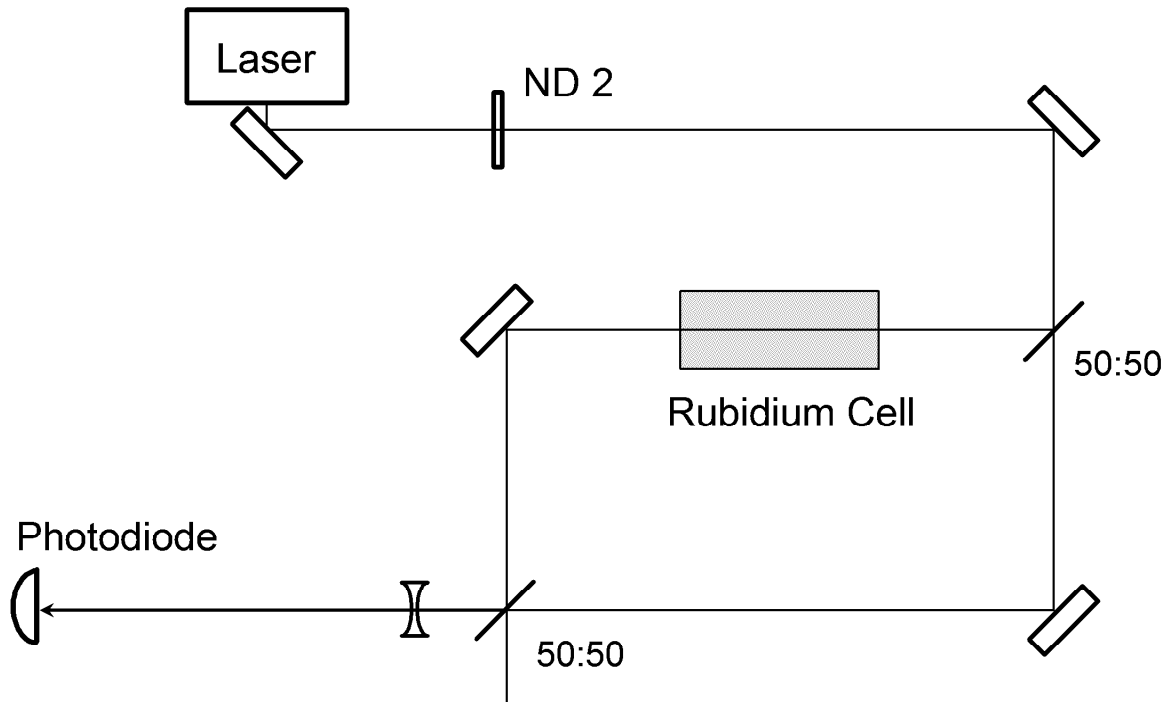
Figure 4. Optical layout for the main part of the lab. The ND filter should usually be removed when aligning the beams. Point the TV camera at the photodiode when looking at fringes.

You should also note that by gently pressing on the breadboard one can move the fringe pattern (effectively changing $\triangle L$ above). With the photodiode sampling the interfering beams and the laser off resonance, wiggle one of the mirrors with your finger (gently!) while watching the photodiode output on the oscilloscope. You should see a (time-dependent) fringe pattern that looks something like a that shown in Figure 3. Measure the fringe contrast, $(I_{\max} - I_{\min})/I_{\max}$. You can adjust the interferometer while wiggling the mirror to get high contrast fringes on the oscilloscope. You may find it necessary to play with the alignment a bit to get a good fringe contrast. For best results the contrast should be better than 0.8,

since your theory assumed a constrast of unity. When you get good fringes, capture the photodiode output (while wiggling the mirror) on the digital 'scope, and put a hard copy in your notebook.
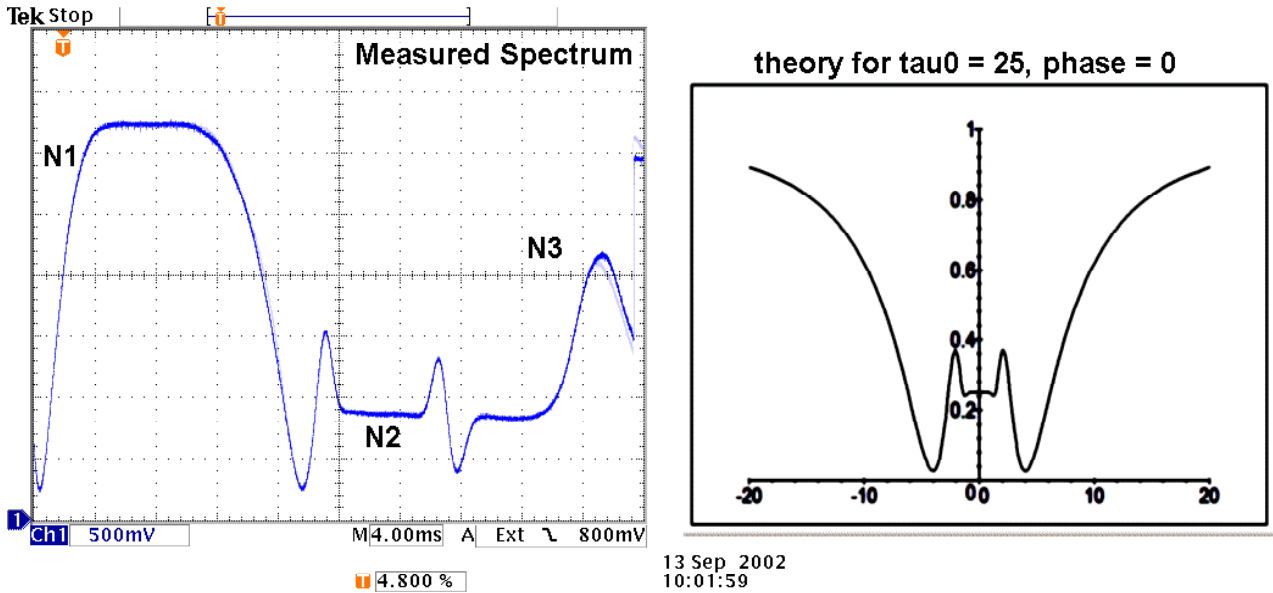

Figure 5. A comparison of a measured spectrum (left) with a calculated spectrum (right). The plot shows $I(\triangle\omega)/I_0$ versus $\triangle\omega/\gamma$. The calculation assumed $\tau = 25$ at line center and $k\triangle L= 0$. The measured spectrum is for the 85b line, but the adjacent 87b line complicates the right side of the spectrum (marked by N3). The center of the 85b line is at N2. The feature at N1 is an artifact of the laser scanning.

Next block the arm of the interferometer without the rubidium cell, in order to observe the rubidium absorption line without any interferometer effects. If all is going well, you should see a nice strong Doppler-broadened absorption line, without any serious mode hops. The ND filter is necessary to avoid saturating the line (which makes it broader). Tune the laser to get a nice strong 85b line, with the 87b line on the side. Have your TA check it out, and save a spectrum.

Now unblock the second arm of the interferometer, and watch the oscilloscope. As you push on the optical bench, you can see different points in the interferometer fringe pattern, and you should see an output something like what you calculated in Problem 2 for low τ. Play around with the interferometer until you understand what's going on and your spectra agree reasonably well with theory. Have your TA take a look at the spectra to see that everything looks good. Capture three good traces, corresponding roughly to points B, C, and D in Figure 3.

Lastly, heat the rubidium cell by turning the controller setting to 100C. Watch the spectra as the cell heats up. It will take about 15 minutes, but then you should begin seeing spectra that look like what you calculated for high τ. Figure 5 shows some typical results for one phase. The data will probably not be a perfect match to calculation, but the results should provide a reasonable demonstration of the Kramers-Kronig relations.

Take several spectra at high τ, at different phase angles. In particular, take spectra at $k\Delta L= 0$ and $k\Delta L= \pi$.

III. REFERENCES.

Jackson, J. D. 1975, *Classical Electrodynamics,* 2nd Edition.

Marion, J. B. and Heald, M. A. 1980, *Classical Electromagnetic Radiation,* 2nd Edition.

Reif, F, 1965, *Fundamentals of Statistical and Thermal Physics.*

Resonant Light Propagation through an Atomic Vapor: The Macaluso-Corbino Effect

Kenneth G. Libbrecht[1]

Norman Bridge Laboratory of Physics, California Institute of Technology 264-33, Pasadena, CA 91125

1. The Experiment

This experiment is extremely easy to set up, as is apparent from the optical layout shown in Figure 1. Note it would take just a few seconds to switch from a saturated absorption experiment to this one.
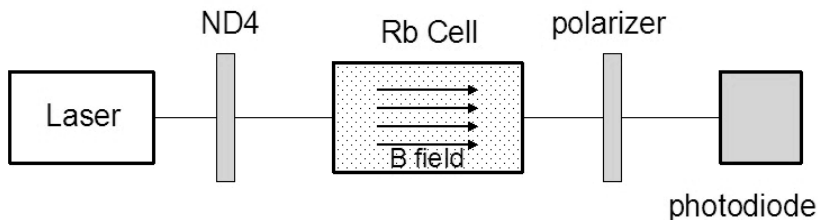

Figure 1. Basic optical layout. The large ND filter makes sure one is in the unsaturated regime. The light coming out of the laser is linearly polarized, so only one polarizer is needed.

Figure 2 shows the light transmitted through the cell as a function of frequency when the B field is not present and the polarizer is at some random angle. Rotating the polarizer only changes the overall scale of the figure. Nothing here but simple resonant absorption.

Figure 4 shows the light transmitted with 1.3 amps going through the coils and with three different polarizer angles. The theory still needs work when the polarizer angle is zero, probably because the theory is too simplistic for a multilevel atom. But it gives reasonable results when the polarizer is not quite at zero angle.

2. Analysis

We have the complex index of refraction for an atomic gas, given by

$$
\begin{aligned}
n &= n_0(1 + i\kappa) \\
&= n_0 + in_0\kappa
\end{aligned}
$$

where n_0 and κ are real quantities given by

$$
\begin{aligned}
n_0 &\simeq 1 - \frac{2\pi(\omega^2 - \omega_0^2)Nfe^2/m}{(\omega^2 - \omega_0^2)^2 + \gamma^2\omega^2} \\
&\simeq 1 - \frac{\pi\Delta\omega Nfe^2/m\omega_0}{\Delta\omega^2 + \gamma^2/4}
\end{aligned}
$$

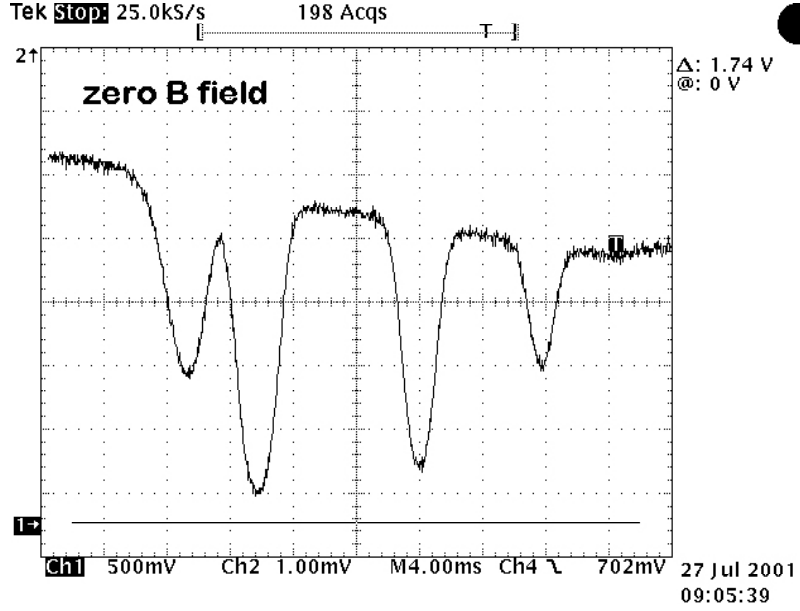[1] *kgl@caltech.edu*; URL: http://www.its.caltech.edu/~atomic/

Figure 2. Transmitted light as a function of frequency, scanning over all four rubidium absorption lines. The B-field is zero and the cell temperature is about 40 C. The background slope comes from scanning the laser current together with the scan of the grating position.

$$\simeq \quad 1 - \frac{A\Delta\omega}{\Delta\omega^2 + \gamma^2/4}$$

$$n_0\kappa \quad \simeq \quad \frac{2\pi N f \omega \gamma e^2/m}{(\omega^2 - \omega_0^2)^2 + \gamma^2\omega^2}$$

$$\simeq \quad \frac{\pi N f \gamma e^2/2m\omega_0}{\Delta\omega^2 + \gamma^2/4}$$

$$\simeq \quad \frac{A\gamma/2}{\Delta\omega^2 + \gamma^2/4}$$

near the atomic resonance, where $\Delta\omega = \omega - \omega_0$. These are plotted in Figure 3. This is the index of refraction for a dilute atomic gas, which of course is proportional to the atom density N. Note that a relation $n_0 - 1 \simeq -2\Delta\omega\kappa/\gamma$ exists between the index of refraction and the attenuation, which is independent of the oscillator strength of the atomic transition. This relation, showing that $n_0(\nu)$ and $\kappa(\nu)$ can be derived from one another, is an example of the more general *Kramers-Kronig relations*. A full quantum mechanical treatment also yields the same relation for the absorption and refractive index of a gas near an atomic resonance.

An electromagnetic wave in the medium propagates according to

$$e^{-i(\omega t - nkz)} = e^{-kn_0\kappa z}e^{-i[\omega t - kn_0 z]} \tag{1}$$

where $k = \omega/c$. From this it can be seen that n_0 corresponds to the usual index of refraction, equal to c/v, while κ describes the attenuation of the wave. Then the complex electric field amplitude can be written $E_0 \exp(-\tau)$ after passing through the cell, where E_0 is the initial field amplitude and

$$\tau(\omega) = kn_0\kappa(\omega)L - ik[n_0(\omega) - 1]L$$

where we have taken out the constant phase shift kL. Using $n_0 - 1 \simeq -2\Delta\omega\kappa/\gamma$ this becomes

$$\tau \quad \simeq \quad kn_0\kappa L + \frac{i2k\Delta\omega\kappa L}{\gamma}$$
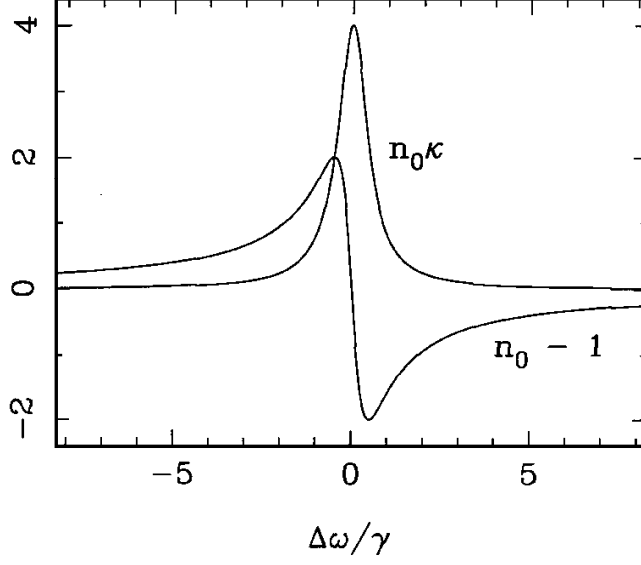
2

Figure 3. Plot of the absorption $n_0\kappa$ and refractive index change $n_0 - 1$ for a gas near an atomic resonance. Note the index change is proportional to the first derivative of the absorption.

$$
\begin{aligned}
\tau(\omega) &\simeq kn_0\kappa(\omega)L\left[1+i\frac{2\Delta\omega}{\gamma}\right] \\
&\simeq \frac{\tau_0}{2}G\left(\Delta\omega\right)\left[1+i\frac{2\Delta\omega}{\gamma}\right]
\end{aligned}
$$

where τ_0 is the optical depth at line center (defined from the intensity and not field) and $G\left(\omega\right)$ is the normalized line profile

$$
G\left(\Delta\omega\right) = \frac{\gamma^2/4}{\Delta\omega^2 + \gamma^2/4}
$$

We can write the electric field in linearly polarized light as

$$
\begin{aligned}
\overrightarrow{E_x} &= \widehat{x}E_0e^{i(\omega t - kz)} \\
\overrightarrow{E_y} &= \widehat{y}E_0e^{i(\omega t - kz)}
\end{aligned}
$$

and circularly polarized light

$$
\begin{aligned}
\overrightarrow{E_+} &= \frac{1}{\sqrt{2}}\left[\widehat{x}E_0e^{i(\omega t - kz)} + i\widehat{y}E_0e^{i(\omega t - kz)}\right] \\
&= \frac{1}{\sqrt{2}}\left[\overrightarrow{E_x} + i\overrightarrow{E_y}\right] \\
\overrightarrow{E_-} &= \frac{1}{\sqrt{2}}\left[\widehat{x}E_0e^{i(\omega t - kz)} - i\widehat{y}E_0e^{i(\omega t - kz)}\right] \\
&= \frac{1}{\sqrt{2}}\left[\overrightarrow{E_x} - i\overrightarrow{E_y}\right]
\end{aligned}
$$

so

$$
\begin{aligned}
\overrightarrow{E_x} &= \frac{1}{\sqrt{2}}\left[\overrightarrow{E_+} + \overrightarrow{E_-}\right] \\
\overrightarrow{E_y} &= \frac{-i}{\sqrt{2}}\left[\overrightarrow{E_+} - \overrightarrow{E_-}\right]
\end{aligned}
$$

We can represent a polarizer using matrix notation, in which the output fields, after going

3

through the polarizer, are

$$
\begin{bmatrix} E_x \\ E_y \end{bmatrix}_{out} = \begin{bmatrix} 1 & 0 \\ 0 & 0 \end{bmatrix} \begin{bmatrix} E_x \\ E_y \end{bmatrix}_{in}
$$

$$
\begin{bmatrix} E_x \\ E_y \end{bmatrix}_{out} = \begin{bmatrix} 0 & 0 \\ 0 & 1 \end{bmatrix} \begin{bmatrix} E_x \\ E_y \end{bmatrix}_{in}
$$

for x and y polarizers. If we use a y polarizer rotated by an angle θ, the matrix becomes

$$
\begin{bmatrix} \cos\theta & \sin\theta \\ -\sin\theta & \cos\theta \end{bmatrix} \begin{bmatrix} 0 & 0 \\ 0 & 1 \end{bmatrix} \begin{bmatrix} \cos\theta & -\sin\theta \\ \sin\theta & \cos\theta \end{bmatrix}
$$

$$
\approx \begin{bmatrix} 0 & \theta \\ \theta & 1 \end{bmatrix}
$$

the latter for small θ.

Now we put all the pieces together. We start with x polarized light and represent it in terms of two circular polarizations

$$
\overrightarrow{E_{in}} = \begin{bmatrix} 1 \\ 0 \end{bmatrix}
$$

$$
= \frac{1}{\sqrt{2}} \left\{ \frac{1}{\sqrt{2}} \begin{bmatrix} 1 \\ i \end{bmatrix} + \frac{1}{\sqrt{2}} \begin{bmatrix} 1 \\ -i \end{bmatrix} \right\}
$$

$$
= \frac{1}{2} \left\{ \begin{bmatrix} 1 \\ i \end{bmatrix} + \begin{bmatrix} 1 \\ -i \end{bmatrix} \right\}
$$

When this light enters the cell, the different circular polarizations propagate differently because of the Zeeman splitting. Thus the field becomes

$$
\overrightarrow{E} = \frac{1}{2} \left\{ \begin{bmatrix} 1 \\ i \end{bmatrix} \exp\left(-\tau_+\right) + \begin{bmatrix} 1 \\ -i \end{bmatrix} \exp\left(-\tau_-\right) \right\}
$$

$$
= \frac{1}{2} \begin{bmatrix} \exp\left(-\tau_+\right) + \exp\left(-\tau_-\right) \\ i\exp\left(-\tau_+\right) - i\exp\left(-\tau_-\right) \end{bmatrix}
$$

where

$$
\tau_\pm \simeq \frac{\tau_0}{2} G\left(\Delta\omega \pm \delta\right) \left[1 + i\frac{2}{\gamma}\left(\Delta\omega \pm \delta\right) \right]
$$

and $\delta \propto B$ is the frequency shift from the Zeeman splitting.

Finally, we hit this with the output polarizer and the final field is

$$
\overrightarrow{E_{final}} \simeq \frac{1}{2} \begin{bmatrix} 0 & \theta \\ \theta & 1 \end{bmatrix} \begin{bmatrix} \exp\left(-\tau_+\right) + \exp\left(-\tau_-\right) \\ i\exp\left(-\tau_+\right) - i\exp\left(-\tau_-\right) \end{bmatrix}
$$

$$
\simeq \frac{1}{2} \begin{bmatrix} i\theta\left(\exp\left(-\tau_+\right) - \exp\left(-\tau_-\right)\right) \\ \theta\left(\exp\left(-\tau_+\right) + \exp\left(-\tau_-\right)\right) + i\left(\exp\left(-\tau_+\right) - \exp\left(-\tau_-\right)\right) \end{bmatrix}
$$

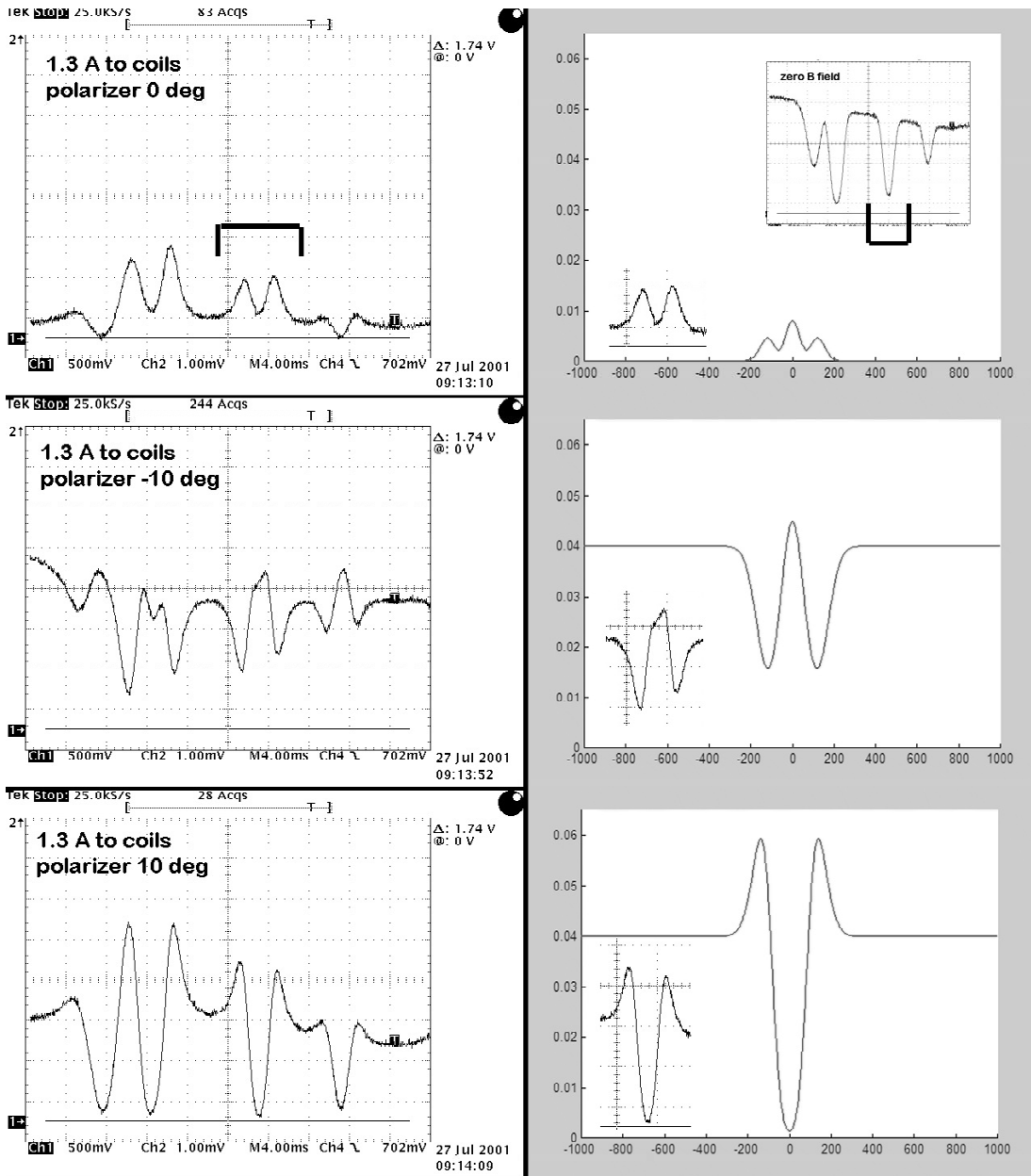The final intensity is then the absolute square of this field.

Figure 4. Left: Data showing light transmission as a function of laser frequency with 1.3 A going through the coils. The polarizer angle was 0 (top), -10 degrees (middle), and 10 degress (bottom). Right: A model of one absorption line (indicated) under conditions like those for the data.

5

whose only impact on the electric field is a global reversal of its direction, should not alter the relative spacing of field lines in a CFLD. Since the sign-reversed version of Fig. 6 must show uniform spacing of the outgoing field lines on the +4 charge, equatorial clumping does not show the invariance under charge reversal that would be expected of a true field property.

[9] Phillip M. Rinard, Delbert Brandley, and Keith Pennebaker, "Plotting Field Intensity and Equipotential Lines," Am. J. Phys. **42**, 792–793 (1974).

[10] While charge distributions lacking a monopole moment possess divergent field lines, such as the $\theta = 0$ and $\theta = \pi$ lines in the dipole, such lines are few in number and can be avoided by the proper choice of θ_0. By contrast, the number of divergent lines associated with a false monopole moment is proportional to N, and is unaffected by the choice of θ_0. In several figures, including the dipole CFLD of Fig. 1(a), gaps on negative charges were avoided by setting θ_0 to a value very close to 0, producing an apparently divergent field line that eventually reappears at the opposite end of the diagram and terminates on a negative charge.

[11] Edwin A. Abbot, *Flatland: A Romance of Many Dimensions by a Square* (Seeley & Co., London, 1884). For a more technical discussion of two-dimensional science, see A. K. Dewdney, *The Planiverse: Computer Contact with a Two-dimensional World* (Poseidon, New York, 1984). While this article was in press, the authors were made aware of the recent note of T. E. Freeman, "One-, two-, or three-dimensional fields?," Am. J. Phys.

63, 273–274 (1995). Freeman shows a field line diagram with a false monopole moment and correctly observes that the distortion would disappear in a two-dimensional universe.

[12] Boundary clumping can be avoided in a distribution with one negative and several positive charges by reversing the sign of each charge. A form of boundary clumping can be seen in charge distributions containing a single positive charge, but the problem originates solely from numerical errors that are easily avoided.

[13] The problem of distributing points uniformly on a sphere is discussed in the Internet document sphere.faq, produced by Dave Rusin. The document is located at: http://www.math.niu.edu:80/~rusin/papers/spheres/sphere.faq. Uniform tilings are not achieved on golf balls or geodesic domes which either employ multiple tiling elements or contain defects at the north pole or at the equatorial "weld" line.

[14] Reference 13 describes methods of obtaining nearly uniform distributions of an arbitrary number of points on the surface of a sphere.

[15] If field line diagrams are seen as primarily serving visualization and pedagogic purposes (rather than serving as a practical research/design tool) it may be time to reevaluate their pedagogic worth. Tornkvist *et al.* suggest that, independent of any imperfections that may be present in CFLDS, students often misinterpret these diagrams. S. Tornkvist, A. Petterson, and G. Transtromer, "Confusion by representation: On students' comprehension of the electric field concept," Am. J. Phys. **61**, 335–338 (1993).

Resonant Faraday rotation as a probe of atomic dispersion

D. A. Van Baak
Department of Physics, Calvin College, Grand Rapids, Michigan 49546

The Faraday effect (the rotation of the plane of polarization of light as it propagates through a sample parallel to a static magnetic field) is readily detected in room-temperature rubidium vapor by a diode-laser experiment near the D_2 resonance line at 780 nm, and the theoretical treatment of this effect provides an unusually clear insight into the relation between absorption and dispersion in the interaction of light with matter. © *1996 American Association of Physics Teachers.*

I. INTRODUCTION

Impelled by a belief in the unity of the forces of nature, Michael Faraday sought, and in 1845 provided, the first phenomenological evidence for a connection between light and magnetism when he discovered the effect that still bears his name. He found that plane-polarized light, propagating through matter parallel to a static magnetic field, underwent a systematic rotation of its plane of polarization. The effect, though unambiguous, is typically not large, with rotation per unit distance per unit field of order 10 rad/m T (≈ 0.03 arcmin/cm Oe) in ordinary glass samples in the midvisible; this "Verdet constant" is itself a function of wavelength, typically growing dramatically toward the blue end of the visible spectrum. Not until the atomic-electron hypothesis toward the end of the 19th century was it possible to provide a more detailed model for Faraday rotation; Becquerel predicted a Verdet constant related to the dispersion $dn/d\lambda$ of the material. A modern picture of Faraday rotation emerges from the quantum-mechanical response of an atom to a magnetic field; in this picture the atomic absorption and disper-

sion are both affected by the field, and in this sense the Faraday effect is to dispersion what the Zeeman effect is to absorption (or emission).

Given the small magnitude of Faraday rotation in bulk condensed matter, it might seem impossible to detect the effect for a much more dilute gas sample. It is the connection between absorption and dispersion that contradicts this expectation; both effects are subject to enormous enhancements near atomic resonances. This paper will work out the theory of Faraday rotation for light interacting with a simple model system, and will derive the behavior of the Verdet constant both far from, and very near, an atomic resonance. The calculation, in turn, is motivated by the possibility of observing resonant Faraday rotation in an atomic vapor, in this case by the interaction of 780 nm diode-laser radiation with a room-temperature sample of rubidium vapor. The notable and detailed agreement between observed rotation signals, and those computed from a theory involving atomic dispersion, demonstrates the reality of dispersion, and its intimate connection with absorption. Since the absorption and fluorescence of rubidium vapor under diode-laser excitation is an

emerging classic experiment in diode-laser optics, and since only very modest extra equipment is needed to display Faraday rotation, a growing number of students will be able to appreciate directly this probe of the dispersion that always accompanies atomic absorption.

Faraday's own account of his discovery is available in a reprint edition;[1] discussions of it in biographical[2] and bibliographical[3] contexts are also available. The enhancement of the Faraday effect near resonance lines in atomic vapors was discovered in 1898 by Macaluso and Corbino[4] and has been applied in modern times to create narrow-band optical filters.[5] Two earlier papers in this Journal describe Faraday-rotation experiments in bulk matter;[6,7] this effect has also become the basis of optical isolators.[8] The derivation worked out in this paper has been guided by that of Preston and Dietz,[9] who however are motivated by experiments on nonresonant rotation in bulk matter.

Section II of this paper gives a quantum-mechanical treatment of Faraday rotation in a dilute vapor of a model atomic system. Section III discusses the instrumental requirements for diode-laser spectroscopy of rubidium vapor in general, and the added requirements for Faraday-rotation experiments in particular. Section IV presents and discusses typical experimental results, and Sec. V presents conclusions and applications.

II. THEORY

We divide this derivation of Faraday rotation into four parts. The first step is to consider the propagation of linearly polarized light through a medium, resolving it into two oppositely directed circularly polarized fields which are assumed to propagate independently. The second step is to relate the macroscopic index of refraction, and the attenuation, of the two circular polarization components in a medium to the microscopic susceptibility of the atoms in the sample. The third step introduces the simplest quantum-mechanical system for which the susceptibility can be computed, and extracts the results for Faraday rotation. Finally this section takes up the effects of Doppler broadening on the signals computed from the model.

The first step of the theory resembles Fresnel's method for understanding optical rotation in chiral media, in which an incident linearly polarized field is decomposed into two oppositely directed circularly polarized fields of equal amplitude; the fundamental assumption is that each circularly polarized field propagates independently (but differently) through the medium. Here we will suppose that each of the two circular polarizations has its own index of refraction and attenuation coefficient, and work out the results for propagation.

We introduce the two circularly polarized fields[10] propagating in the $+\mathbf{z}$ direction (real parts understood):

$$\mathbf{E}_{\pm}(z,t)=E_0(\hat{\mathbf{x}}\pm i\hat{\mathbf{y}})\exp i(kz-\omega t) \qquad (1)$$

and write the incident field as the superposition

$$\mathbf{E}(0,t)=\mathbf{E}_+(0,t)+\mathbf{E}_-(0,t)=2E_0\,\hat{\mathbf{x}}\exp i(k0-\omega t), \qquad (2)$$

which is clearly a linearly polarized field with polarization along x. Now we assume that the fields $\mathbf{E}_{\pm}$ propagate with indices of refraction $n_{\pm}$ and attenuation constants $\beta_{\pm}$ respectively. Then the wave number k is given by

$$k_{\pm}=\frac{2\pi}{\lambda/n_{\pm}}=\frac{2\pi}{\lambda}\,n_{\pm}, \qquad (3)$$

where λ is the *vacuum* wavelength of the light, and the incident field propagates through a sample of length L to give the emergent field

$$\mathbf{E}(L,t)=E_0\,\exp(-\beta_+L)(\hat{\mathbf{x}}+i\hat{\mathbf{y}})\exp i\left(\frac{2\pi}{\lambda}\,n_+L-\omega t\right)$$
$$+E_0\,\exp(-\beta_-L)(\hat{\mathbf{x}}-i\hat{\mathbf{y}})\exp i\left(\frac{2\pi}{\lambda}\,n_-L-\omega t\right). \qquad (4)$$

In the usual case of equal attenuations for the two polarizations $(\beta_+=\beta_-=\beta)$, this reduces to

$$\mathbf{E}(L,t)=2E_0\,\exp(-\beta L)(\hat{\mathbf{x}}\cos\Delta\theta-\hat{\mathbf{y}}\sin\Delta\theta)$$
$$\times\exp i\left(\frac{2\pi}{\lambda}\frac{n_++n_-}{2}L-\omega t\right), \qquad (5)$$

which clearly represents a linearly polarized wave whose direction of polarization has been rotated through the Faraday rotation angle $\Delta\theta$, given by

$$\Delta\theta=\frac{2\pi}{\lambda}\left(\frac{n_+-n_-}{2}\right)L. \qquad (6)$$

In Sec. III we will see how this rotation signal $\Delta\theta$ can be extracted from (4) even when differential attenuation is present.

The second stage of the theoretical derivation is to relate the macroscopic parameters n and β to the microscopic behavior of the sample. This can be achieved by assuming that the medium as a whole develops, in response to the electric field $\mathbf{E}$, an electric polarization $\mathbf{P}$ given by

$$\mathbf{P}=\epsilon_0\chi\mathbf{E}, \qquad (7)$$

where for a dilute-gas sample we do not need to distinguish between the incident and the "local" value of the electric field. The electric susceptibility χ defined by (7) is a dimensionless, complex, and frequency-dependent scalar quantity characterizing the sample. Under this assumption, Maxwell's equations give the relationship between wave number k and frequency ω for any monochromatic plane wave propagating through the material:

$$\left(\frac{kc}{\omega}\right)^2=1+\chi. \qquad (8)$$

In the limit of low density, we will see that $|\chi|$ is so small even near resonance that we can adequately write

$$\frac{kc}{\omega}=1+\frac{\chi}{2}; \qquad (9)$$

then the usual decomposition of χ into real and imaginary parts

$$\chi=\chi'+i\chi'' \qquad (10)$$

gives the results

$$n=1+\frac{\chi'}{2}\quad\text{and}\quad\beta=\frac{2\pi}{\lambda}\frac{\chi''}{2}. \qquad (11)$$

Thus the macroscopic propagation constants n and β have been related to the real and imaginary parts of the microscopic susceptibility, respectively.

The third part of the derivation is to assume a model for the medium and to compute its electric susceptibility. The
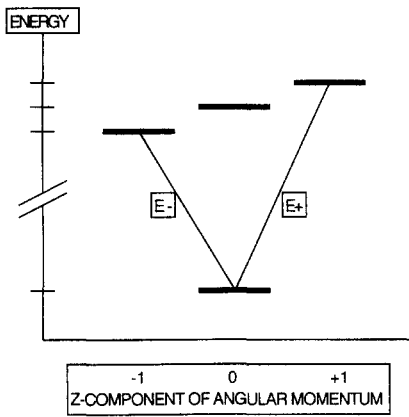
Fig. 1. The model atomic system used in this paper to compute absorption, dispersion, and Faraday rotation in a dilute vapor. The ground state is nondegenerate, and the excited state has three magnetic sublevels, here shown as slightly split by an external magnetic field.

simplest model system is a gas of independent atoms, of number density N, with each atom having a nondegenerate ground state and an excited state forming a Zeeman triplet, as shown in Fig. 1. This is exemplified by a $^1S_0-^1P_1$ transition of an atom with no nuclear spin or hyperfine structure; such an atom shows the "normal" Zeeman effect, and in the presence of a magnetic field $\mathbf{B}=B\hat{z}$ the upper-state sublevels split as shown in Fig. 1, with $m=\pm1$ states undergoing energy shift

$$\Delta E = \pm \mu_B B, \tag{12}$$

where $\mu_B = e\hbar/2m_e$ is the Bohr magneton. Then transitions from the (unshifted) ground state to the $m=\pm1$ excited states will occur at Bohr frequencies

$$\nu_{0\pm} = \nu_0 + \frac{\Delta E}{h} = \nu_0 \pm \frac{\mu_B B}{h} = \nu_0 \pm \frac{e}{4\pi m_e} B. \tag{13}$$

For the electric fields introduced in (1), the electric-dipole selection rules allow the fields $E_\pm$ to induce only the resonant upward transitions with $\Delta m = \pm 1$ respectively. Thus each circular polarization will separately interact with its own two-level system, and so each polarization will propagate with its own index of refraction and attenuation constant, as was assumed above. These numbers, in turn, will be those arising from the susceptibility of a generic two-level atomic system, which is given as a function of optical frequency ν by[11]

$$\chi(\nu) = \frac{N\lambda^3}{16\pi^3\tau} \frac{1}{\nu_0 - \nu - i\Delta\nu/2}, \tag{14}$$

where $\lambda = c/\nu$, ν_0 is the Bohr frequency of the transition, $\Delta\nu = (2\pi\tau)^{-1}$ is its "natural linewidth" (full-width at half-maximum, in ordinary frequency), and τ is the spontaneous-decay lifetime of the upper state.

Then from the result (11) above, we can write the attenuation constant for the electric field as

$$\beta(\nu) = \frac{N\lambda^2}{16\pi^2\tau} \frac{\Delta\nu/2}{(\nu-\nu_0)^2+(\Delta\nu/2)^2}, \tag{15}$$

which shows the conventional Lorentzian line shape. It gives peak absorption at line center, where $\nu=\nu_0$ and $\lambda=\lambda_0=c/\nu_0$; here β reaches the value

$$\beta_{\max} = \frac{N\lambda_0^2}{16\pi^2\tau} \frac{2}{\Delta\nu} = \frac{N\lambda_0^2}{4\pi}. \tag{16}$$

Again from the earlier result (11), we can deduce for the index of refraction $n(\nu)$ of the sample the curve

$$n(\nu) - 1 = \frac{N\lambda^3}{32\pi^3\tau} \frac{\nu_0 - \nu}{(\nu-\nu_0)^2+(\Delta\nu/2)^2}, \tag{17}$$

which shows a dispersive dependence on frequency, with positive values occurring below the resonant frequency, and a peak departure of index n from unity occurring at frequencies $\nu=\nu_0\pm\Delta\nu/2$, of size

$$|n-1|_{\max} = \frac{N\lambda_0^3}{32\pi^3\tau} \frac{1}{\Delta\nu} = \frac{N\lambda_0^3}{16\pi^2} = \beta_{\max} \frac{\lambda_0}{4\pi}. \tag{18}$$

This tightly related behavior of absorption and dispersion has distinct implications for an experiment seeking to detect atomic dispersion; for example, if a sample of length L is dense enough to attenuate, at line center, the fields to e^{-1} (or the transmitted power to $e^{-2}=13.5\%$), then it has $\beta_{\max}L=1$, so

$$|n-1|_{\max} = \frac{\lambda_0}{4\pi L}, \tag{19}$$

which is very small indeed for plausible sample lengths. If one tries to detect this deviation of refractive index from unity by interferometric means, then the phase shift (relative to vacuum) that will accumulate in a one-way trip through this sample is

$$\Delta\phi = \frac{2\pi}{\lambda} |n-1|L, \quad \text{so} \quad \Delta\phi_{\max} = \frac{2\pi}{\lambda_0} \frac{\lambda_0}{4\pi L} L = \frac{1}{2} \text{ (radian)}. \tag{20}$$

This phase shift is only 8% of the 2π radians required to produce a single interferometric fringe, and it would have to be detected in the face of the deep absorption accompanying it. Conventional detection of atomic dispersion is carried out much farther from line center, using samples of much greater optical thickness, and relying on the fact that dispersion drops off with detuning less rapidly than does absorption. We will see that Faraday rotation offers an indirect, but vastly easier, way to detect atomic dispersion, even for optically thin samples, and that the Faraday rotation signal can be followed right through resonance.

The absorption and dispersion signals thus far computed are shown in Fig. 2, in which axes have been normalized to "natural" values. The horizontal axis gives frequency in units of the natural linewidth $\Delta\nu$, so that the absorption signal reaches half-maximum, and the dispersion signal reaches its extrema, at ordinate $\pm1/2$. The dispersion-shaped signal gives $n(\nu)-1$ in the units shown; for reference, the room-temperature number density of rubidium[12] is near $N=2.5\times10^{16}$ m^{-3}, so that at a resonant wavelength of $\lambda_0=0.78\times10^{-6}$ m, the factor $N\lambda_0^3/8\pi^2$ has value 15×10^{-5}. This means the computed index of refraction is confined to the range $1\pm(75\times10^{-6})$, and it shows that the $|\chi|\ll1$ assumption made above is retrospectively justified.

With all these preliminaries, we can now calculate the Faraday rotation signal and its frequency dependence. Given the separate resonant frequencies (13) for the oppositely directed circularly polarized fields $E_\pm$, we can form the difference of refractive indices called for in (6), and write
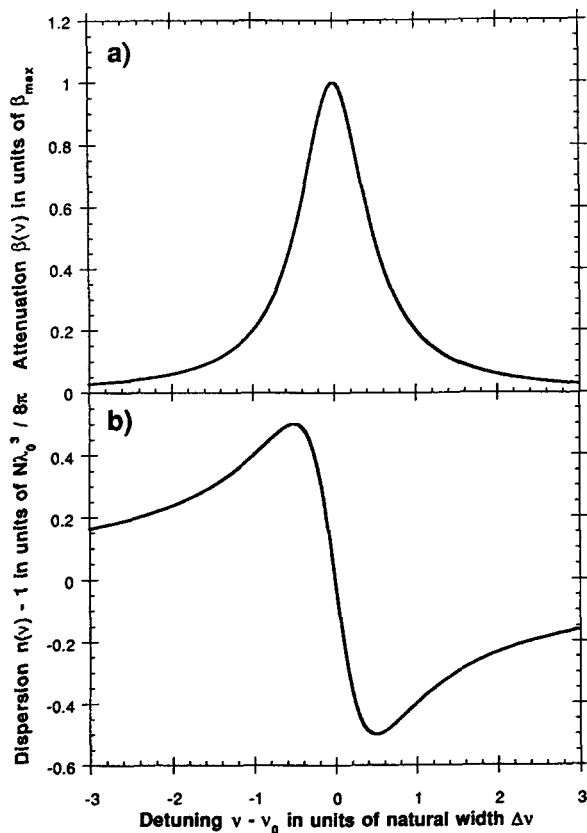
Fig. 2. Graphs of the absorption (a) and dispersion (b) signals computed for the model two-level atomic system, in the absence of Doppler broadening. The curves arise from Eqs. (15) and (17) respectively; the horizontal scale is in units of the "natural linewidth" $\Delta\nu$, and the vertical scales are in units natural to the problem.
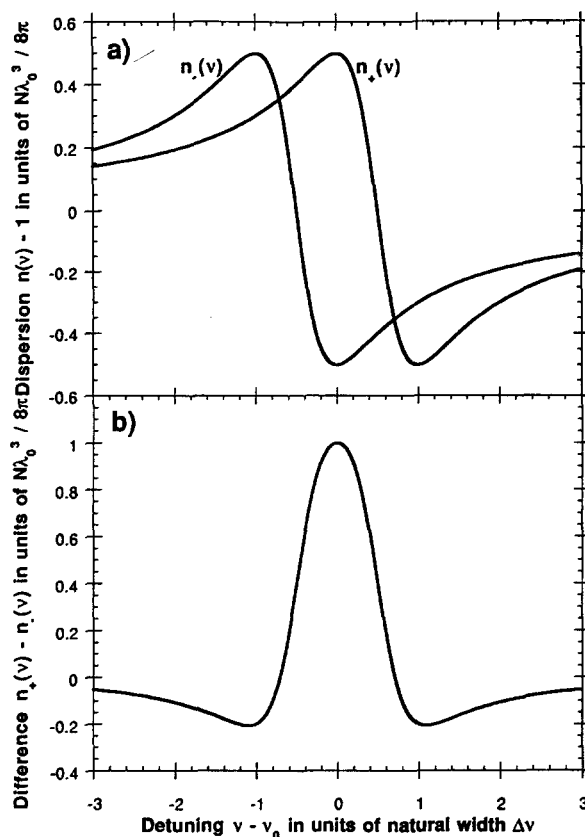

Fig. 3. (a) Dispersion curves for the two circular polarizations of light in the Zeeman-split model atomic system in the absence of Doppler broadening, computed for the particular choice of magnetic field strength $(e/4\pi m_e)B = \Delta\nu/2$. (b) The Faraday-rotation angle computed from the curves in (a), showing the characteristic symmetric signal predicted for resonant Faraday rotation.

$$\Delta\theta(\nu) = \frac{N\lambda^2 L}{32\pi^2\tau}\left[\frac{\nu_{0+}-\nu}{(\nu_{0+}-\nu)^2+(\Delta\nu/2)^2}\right.$$

$$\left. -\frac{\nu_{0-}-\nu}{(\nu_{0-}-\nu)^2+(\Delta\nu/2)^2}\right]. \tag{21}$$

Figure 3 shows the general character of the Faraday rotation signal deduced from this result; its frequency dependence arises from the difference of two (offset) dispersion signals, so that the $\Delta\theta(\nu)$ signal has a symmetric form, centered at the unshifted line center ν_0. The analytic form of the Faraday rotation signal is thus a bit complicated, but two special cases are worth extracting.

The first is applicable whenever the magnetic field (and thus the Zeeman shift) is small enough; it makes use of the general result

$$f(x+\epsilon) - f(x-\epsilon) = 2\epsilon f'(x) + O(\epsilon^3), \tag{22}$$

which [using (17)] allows (21) to be written (to lowest order in B) as

$$\Delta\theta = VBL, \quad \text{with } V = \frac{1}{\lambda}\frac{e}{2m_e}\frac{dn}{d\nu} = -\frac{e}{2m_e c}\nu\frac{dn}{d\nu}. \tag{23}$$

Thus the Faraday rotation $\Delta\theta$ is predicted to be proportional to the strength of the magnetic field and the sample length, with a proportionality factor V called the Verdet constant; and V is predicted to have a frequency dependence $-\nu\,dn/d\nu$, or $\lambda\,dn/d\lambda$, in agreement with the Becquerel formula.[13]

Actual materials with electronic structure much more complicated than that modelled here do in fact follow the Becquerel form of V quite closely, except for a multiplicative correction factor (the magneto-optic constant γ) generally somewhat smaller than unity.[14] It is worth noting that the wavelength dependence of Faraday rotation is given by the dimensionless quantity $\lambda\,dn/d\lambda$, and that its scale is fixed by the combination of fundamental constants

$$\frac{e}{2m_e c} = 293.34 \text{ rad/T m} = 1.0084 \text{ arcmin/Oe cm}. \tag{24}$$

These results for small field B also make it clear why Faraday rotation can be so enormously enhanced near an atomic resonance. First, the index of refraction n departs maximally from unity near a resonance, and second, it does so with a dispersive shape, going from maximum to minimum in a frequency span of only the natural linewidth. Thus a quotient like $\Delta n/\Delta\nu$ has, near resonance, the largest possible numerator and a very small denominator. In terms of the graph of Fig. 3(a), ordinary nonresonant Faraday rotation depends on a tiny difference between two refractive indices, each of which is separately very close to one; but resonant Faraday rotation involves the difference of two refractive indices, each of which is near its maximum possible departure from unity, and whose departures from unity are of *opposite sign*.

This enhancement of Faraday rotation at a resonance motivates the examination of a second special case of (21), namely, the Faraday rotation at the center of the (zero-field) atomic resonance, at $\nu = \nu_0$. The result is

$$\Delta\theta|_{\nu=\nu_0} = \frac{N\lambda_0^2 L}{32\pi^2\tau} 2 \frac{kB}{(kB)^2 + (\Delta\nu/2)^2}, \tag{25}$$

where $k = e/4\pi m_e = 13.996$ GHz/T; this function grows linearly with B (for $kB \ll \Delta\nu/2$), reaches a maximum at $kB = \Delta\nu/2$, and then decreases gradually. The initial linear dependence of Faraday rotation on B allows the extraction of an at-resonance Verdet constant of

$$V_{res} = \frac{1}{L}\frac{d(\Delta\theta)}{dB}\bigg|_{B=0} = \frac{N\lambda_0^2}{32\pi^2\tau} 2 \frac{k}{(\Delta\nu/2)^2} = \frac{N\lambda_0^2}{4\pi}\frac{e}{m_e}\tau, \tag{26}$$

which for values of experimental interest like $N = 2.5\times10^{16}$ m^{-3}, $\lambda_0 = 0.78\times10^{-6}$ m, $e/m_e = 1.76\times10^{11}$ C/kg, and $\tau = 25.5\times10^{-9}$ s (Ref. 15) yields the enormous value of $V = 5.4\times10^6$ rad/T m. Thus despite a gas density some 12 orders of magnitude smaller than that of typical solids, the resonant Faraday effect yields a computed Verdet constant about 5 orders of magnitude larger than that seen in bulk matter!

The maximum value of Faraday rotation at $kB = \Delta\nu/2$ in (25) arises from the particular circumstance depicted in Fig. 3(a), where the dispersion curves for n_+ and n_- are split apart by the Zeeman effect until the maximum of one lies immediately above the minimum of the other; this maximizes the difference $n_+ - n_-$ and thus the Faraday rotation. The maximum value of the rotation angle is given by

$$\Delta\theta_{max} = \frac{N\lambda_0^2 L}{32\pi^2\tau}\frac{2}{\Delta\nu} = \frac{N\lambda_0^2 L}{8\pi}. \tag{27}$$

If we again suppose that the sample density and length have been chosen so as to attenuate transmitted light by factor e^{-2} at resonance (when the magnetic field is off), then the relation $\beta_{max}L = 1$ again applies, and from (16) the maximum Faraday rotation obtainable with this sample is

$$\Delta\theta_{max} = \frac{N\lambda_0^2 L}{8\pi} = \frac{4\pi}{8\pi} = \frac{1}{2} \text{ (radian)}. \tag{28}$$

Once again, the intimate relationship between absorption and dispersion has imposed a maximum on the signal obtainable with a sample of a given optical thickness, and once again the observable signal is limited to one-half radian. But this Faraday rotation of 0.5 rad is vastly easier to detect experimentally than the 0.5 rad of phase shift derived in (20) above. First, no interferometric setup is required to obtain the Faraday-rotation signal, but rather the mere one-way transmission of linearly polarized light through a sample; second, the signal to be extracted is not the phase shift of a fringe pattern, but the much more concrete rotation in space of the plane of polarization of the transmitted light.

The absorption, dispersion, and Faraday-rotation signals computed thus far are complicated, in experimental practice, by the Doppler effect. Rather than a sample of atoms all at rest and all sharing a common resonant frequency ν_0 (or its Zeeman-shifted equivalent), the experimenter confronts a sample of atoms of mass m, sharing common rest frequency ν_{00}, but spread out in velocity component v_z according to the (one-dimensional) Maxwell distribution, a Gaussian

$$g(v_z) \sim \exp\left\{-\frac{mv_z^2/2}{k_B T}\right\}, \tag{29}$$

where k_B is Boltzmann's constant and T is the absolute temperature of the sample. The effect of this distribution in velocity is to create a distribution of apparent resonant frequencies ν_0, where the (first-order) Doppler shift gives

$$\nu_0 = \nu_{00}(1 + v_z/c), \quad \text{so} \quad v_z = \lambda_0(\nu_0 - \nu_{00}). \tag{30}$$

Thus the sample effectively contains a whole collection of distinguishable kinds of atoms, with distribution of resonant frequencies

$$g(\nu_0) \sim \exp\left\{-\frac{m}{2k_B T}\lambda_0^2(\nu_0 - \nu_{00})^2\right\}. \tag{31}$$

Defining the "Doppler width" $\Delta\nu_D$ as the full width at half-maximum of this distribution, we get

$$\Delta\nu_D = \left[\frac{8k_B T \ln 2}{m\lambda_0^2}\right]^{1/2}, \tag{32}$$

and the Doppler distribution, normalized to unit area, becomes

$$g(\nu_0) = \left[\frac{4\ln 2}{\pi\Delta\nu_D^2}\right]^{1/2}\exp\left\{-\ln 2\left(\frac{\nu_0 - \nu_{00}}{\Delta\nu_D/2}\right)^2\right\}. \tag{33}$$

The utility of this normalized distribution is that results previously calculated for motionless atoms, all of one resonant frequency ν_0, can be transformed to results applicable to the actual Doppler distribution of atoms by a simple convolution. For example, the previously computed index of refraction $n(\nu;\nu_0)$, a function of frequency ν for a given line center ν_0, changes to

$$n(\nu) = \int_{-\infty}^{\infty} g(\nu_0) d\nu_0\, n(\nu;\nu_0). \tag{34}$$

Similar convolutions apply to the attenuation and the Faraday-rotation signals $\beta(\nu)$ and $\Delta\theta(\nu)$. In the limit that the Doppler width $\Delta\nu_D$ is negligible, the distribution function $g(\nu_0)$ turns into the delta function $\delta(\nu_0 - \nu_{00})$, and the convolution reproduces the original results. Alternatively, in the limit that the laser frequency's detuning from resonance $\nu - \nu_{00}$ is much larger than either the Doppler width or any Zeeman shift, this delta-function approximation is a good one; thus the Becquerel result derived above remains valid for ordinary nonresonant Faraday rotation. But for the experimental situation described in Sec. III, the case of interest is at the other extreme, with the room-temperature Doppler width exceeding the natural linewidth by a factor of about 100. This has dramatic consequences for the width and size of the absorption, dispersion, and Faraday-rotation signals. The Appendix discusses suitable numerical methods for performing the convolution integrals, but we go on here to present some of the results.

The results easiest to intuit are for absorption. The convolution defined by (34) preserves the total area under the absorption curve, and intuition hints, and computation confirms, that its width will increase from the natural linewidth to very nearly the Doppler width. The consequence is that the absorption at line center must decrease by about the same factor of 100 by which the linewidth increases. Less intuitively obvious are the results for dispersion, though clearly the convolution must smear out the width of the narrow dispersion feature by a similar large factor. Numerical evalua-
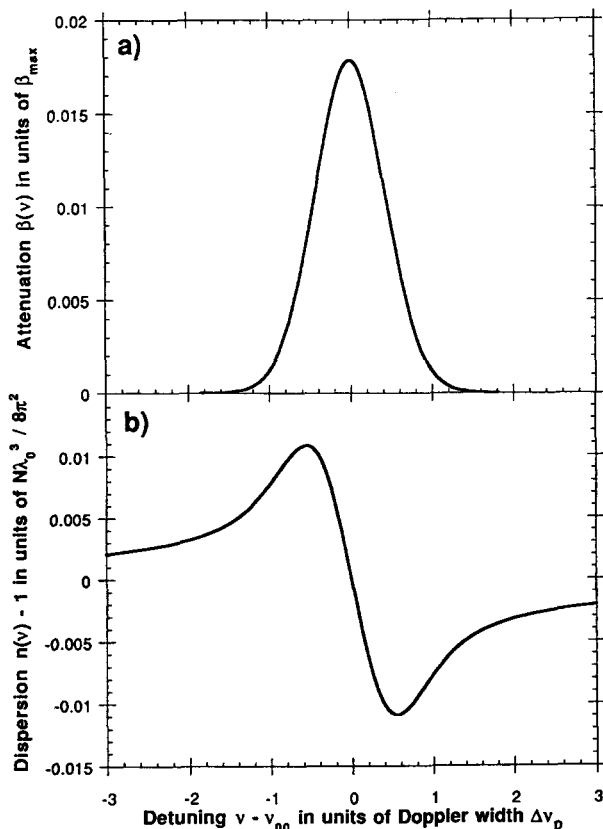
Fig. 4. Graphs of the absorption (a) and dispersion (b) signals computed for the model two-level atomic system, in the presence of Doppler broadening. The curves were computed via (34) and the numerical methods of the Appendix; the horizontal scale is in units of the "Doppler width" $\Delta \nu_D$, and the vertical scales are in the same units as those of Fig. 2. The curves are computed assuming a Doppler width $\Delta \nu_D$ of 511 MHz and a natural linewidth $\Delta \nu$ of 6.24 MHz.
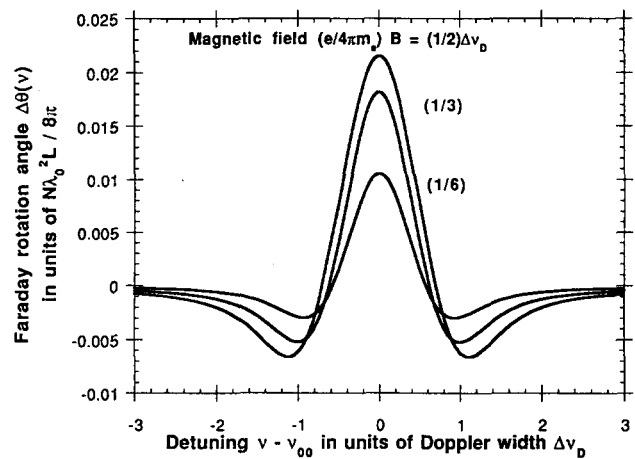

Fig. 5. Faraday rotation angles computed for the model problem of this paper, in the presence of Doppler broadening, for three values of magnetic field strength B: $(e/4\pi m_e) B = \Delta \nu_D/6$, $\Delta \nu_D/3$, and $\Delta \nu_D/2$.

tions confirm this, with the broadened dispersion curve reaching its extrema just outside the frequencies at which the absorption curve reaches its half-maxima. Just as for the absorption curve, so too for the dispersion: this hundredfold increase in width is accompanied by a decrease in height by a similar factor. The results are shown in Fig. 4, which resemble the unbroadened curves of Fig. 2 in character, but which are smaller in vertical scale. Remarkably enough, the dispersion *per unit absorption* is scarcely affected by Doppler broadening; in fact, for a Doppler-broadened sample of density sufficient to give the same absorption at line center, the dispersion (at its extrema) is actually some 23% larger than in the unbroadened case.

Since the Faraday-rotation signal is related to the difference between two dispersion signals, the same results apply to it. The large increase in horizontal scale implies that the magnetic field required to maximize the line-center Faraday rotation will be increased by a similar factor, giving the requirement $kB \approx \Delta \nu_D/2$; for the case of interest, $\Delta \nu_D \approx 500$ MHz, so that a field of about 18 mT (180 Gauss) is required. The previous results for Faraday rotation per unit absorption still apply, with the Doppler-related correction noted above; a sample giving e^{-2} transmission at zero-field line center is predicted to display maximum Faraday rotation of (0.5 rad) $\times (1.23) \approx 35°$.

Finally, Fig. 5 gives some computed results for Faraday rotation as a function of laser frequency, for some different

values of magnetic field. Each curve is symmetric around the zero-field line center, and each has long tails of sign opposite to that of the central peak. Since these long tails describe the ordinary off-resonant Faraday rotation, and since Faraday found that the *direction* of off-resonant rotation is the same as that of the (conventional) current in the solenoid producing the field, we deduce that resonant Faraday rotation should have a direction *opposite* to that of the current producing the field; this prediction is readily checked experimentally. Since the Faraday-rotation signal is the difference of two antisymmetric dispersion signals, the Faraday-rotation signals also share their property of having zero net area under their graphs. Thus broadband light cannot be used to display the phenomenon of resonant Faraday rotation; the light interacting with the atoms needs to have a spectral distribution no wider than the Doppler width of the transition.

III. APPARATUS

It is the availability of low power but tunable diode lasers that makes this resonant-Faraday-rotation experiment feasible in the undergraduate laboratory. The diode lasers produced by the millions for compact-disc players have nominal output power 3 mW and wavelength 780 nm; the further facts that their output is of very narrow spectral width (of order 20 to 50 MHz) and also tunable (by changing the diode temperature or injection current) make them wonderfully useful spectroscopic sources. The happy coincidence of their nominal wavelength with the strongest resonance line in the rubidium spectrum, and the extremely convenient vapor pressure of rubidium at room temperature, make diode-laser experiments in rubidium vapor extraordinarily simple and straightforward. Even once-exotic phenomena like Doppler-free spectroscopy via saturated absorption can easily be performed on a benchtop in real time.[16]

The instrumental requirements for diode-laser spectroscopy of rubidium in general can be divided into four categories: laser source, rubidium cell, optical detectors, and ancillary electronics.

For the laser source in such experiments we have used consumer-market laser diodes such as the Mitsubishi ML4102 and Sharp LT022MC devices. Although nominally of 780-nm output wavelength, in fact these devices can be

(discontinuously) temperature tuned at average rate about +0.25 nm/K or −1000 GHz/K, so that diodes of various nominal wavelength can be tuned to near the desired 780-nm wavelength. The nuisance is that these diode lasers exhibit "mode hops" such that any given device has probability below 50% of being tunable to a target wavelength; the easiest solution is to buy and test multiple diodes and find one which does not mode-hop past the desired frequency. In any given mode, these lasers exhibit typical tuning rates of about −120 GHz/K as their case temperature is varied, and −2 GHz/mA as their injection current is varied. In order to vary, and then stabilize, the laser-diode temperature, we have used two-stage thermoelectric servomechanisms,[17] although single-stage systems would likely suffice in this application. In order to perform real-time scanning of the laser frequency, we vary the diode-laser current about its average value of order 60 mA by a sawtooth modulation of audio frequency and peak-to-peak amplitude of about 5 mA; this gives (in addition to a characteristic but undesired modulation of the optical power output) a sawtooth scan of optical frequency over a range of about 10 GHz. This is sufficient to scan over the rubidium resonance line's hyperfine-structure pattern. Finally, since the light emerging from the diode laser is strongly divergent, we use an optimized lens[18] mounted just in front of it to produce a collimated beam of transverse dimensions about 2×5 mm². Such a lens can easily be adjusted to produce a beam with a divergence negligible over a meter's flight path; the elliptical cross-section and residual astigmatism common to most diode laser beams do not present a problem in this experiment. However, the large optical intensity of order 5 mW in just a few square millimeters means that optical signals in rubidium can be readily saturated. For experiments such as Doppler-free saturated absorption, this is desirable; but for Faraday-rotation experiments, this can be avoided either by using a less tightly focused laser beam, or by using neutral-density filters to attenuate the laser beam. A suitable level of attenuation is easily found empirically by noting, with decreasing values of laser-beam intensity, an approach to a asymptotic value for the fractional absorption at a rubidium resonance.

The rubidium cell used in such experiments can be of 1- to 3-cm diameter and 5- to 10-cm length; for polarization-sensitive experiments it is very convenient for the cell to have flat end windows at near-normal incidence. Since typical experiments can be done with the rubidium near room temperature, exotic glass is not required. The data below were all obtained with a cell of 25-mm (outside) diameter, 51-mm (inside) length, made of Pyrex glass, and filled with rubidium of natural isotopic abundance, in vacuum (no buffer gas).[19]

The simplest optical detectors for use near 780 nm are silicon photodiodes. These are available in a wide range of shapes and sizes, but all share the remarkably high quantum efficiency (>50%) of silicon p-n photojunctions at these near-infrared wavelengths. The detectors can be operated at zero potential difference, such that they act like ideal current sources, with responsivity of order 0.5 A/W; it is convenient to use operational amplifiers as current-to-voltage converters to generate voltage outputs of order 1 V per milliwatt of incident optical power. Such detector/amplifier combinations can easily have response times under 10 μs, and display output noise equivalent to optical inputs well under 1 μW.

The ancillary electronics needed for this sort of experiment include the servomechanism for diode-laser tempera-

ture control, the stable but agile current source of order 0–100 mA, 0–3 V needed to drive the diode laser, and an audio-frequency oscillator to modulate the diode-laser current and thus its output frequency. Remarkably, most of the experiments of interest can be accomplished with signal-capturing electronics no more complicated than a dual-trace oscilloscope; given the laser power and detector noise levels available, even nonlinear optical effects such as saturated absorption can be displayed in real time on an oscilloscope display.

Given such capabilities, only modest additional equipment is needed to perform the Faraday-rotation experiment described here: one needs only a source of magnetic field, and a somewhat more complicated polarization-sensitive optical detector system. The magnetic fields required are of moderate size, up to perhaps 20 mT (200 Gauss), and are easily produced by air-core solenoidal coils. The homogeneity requirements are also easily satisfied, since the fields need to be uniform only over the few-millimeter transverse extent, and the few-centimeter length, of the laser-illuminated rubidium vapor. The data displayed below were obtained using two old short-solenoid coils,[20] each of length 90 mm and effective diameter 112 mm, arranged as an approximate Helmholtz pair. The coils were put in parallel to match the capabilities of an available power supply, and required 41 V at 1.3 A to produce the desired magnetic field. The gap between the coils allowed a Hall-effect Gaussmeter probe to be inserted from the side of the coil, where it could measure the longitudinal field right next to the rubidium cell; alternatively, for a coil system of simpler geometry, the magnetic field could be computed from the measured coil dimensions and current.

The Faraday-rotation experiment clearly requires that the laser light used be linearly polarized upon reaching the sample cell, and that its (rotated) direction of linear polarization be analyzed subsequent to the cell. The input-polarization requirement could be satisfied in many ways, but the simplest is merely to use the intrinsic polarization of the diode-laser emission: for a diode laser at rated power, the nominal polarization purity of >100:1 is easily sufficient for the experiment described here. Thus a linear polarizer suitable for 780 nm (Ref. 21) is only optional; another luxury is a 780-nm half-wave plate, allowing the input polarization to be rotated as desired.

The requirement of detecting the rotation of polarization is a bit more complicated. If the light emerging from the sample cell were purely linearly polarized, then its direction of polarization could be found (at any one wavelength) by searching for extinction with a rotatable linear polarizer used as analyzer. But there are two objections to this classical technique: first, in the presence of differential absorption, the output light is in general elliptically polarized [as (4) shows] so that exact extinction cannot be achieved; and second, this technique does not lend itself to an automated procedure giving a real-time display of polarization-rotation as a function of laser frequency. So for this application we have instead built a simple polarimeter[22] based on a polarizing beamsplitter cube[23] and two photodiodes, arranged as shown in Fig. 6. For input light parallel to the axis shown, and lying in the wavelength range of the device, the beamsplitter approximates very nearly the intended function of transmitting all of the input light of one linear polarization, and deflecting through a right angle all of the input light of the orthogonal linear polarization. In practice, the laser beam used is of
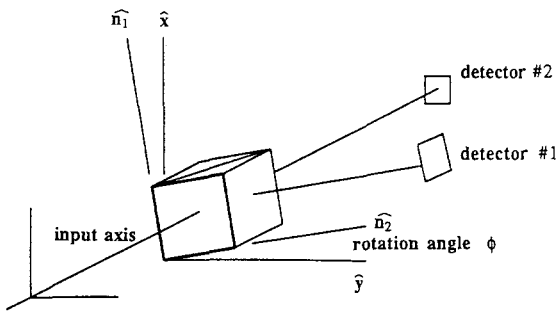
Fig. 6. The polarization analyzer used to gather the Faraday-rotation data of this paper, composed of a polarizing-beamsplitter cube and two detectors arranged to capture the optical power exiting its two output faces. Also displayed are the lab-fixed transverse coordinate axes $\hat{x}$ and $\hat{y}$, and the cube-fixed axes $\hat{n}_1$ and $\hat{n}_2$.

much smaller transverse, angular, and wavelength extent than the acceptance limits of the beamsplitter, and the two output beams from the beamsplitter are easily captured on modest-area photodiodes.[24] Each photodiode current is separately converted to a voltage,[25] so that two separate real-time voltages, proportional to powers in two orthogonal optical linear polarizations, are simultaneously available for oscilloscope display. The beamsplitter and the two photodiodes are all held together in a cylindrical structure, forming a rigid "analyzer" that can be rotated about a mechanical axis coinciding with the laser beam to be analyzed.

Given a light beam exiting the Faraday medium of the form (4), it is easy to work out the response of the polarization analyzer just described. The simplest case of pure Faraday rotation (with no differential absorption) yields a linearly polarized beam, with polarization axis rotated by angle $\Delta\theta$ from its original x direction. So if in Fig. 6 the analyzer's axes were rotated by $\phi=45°$ away from the $\hat{x}$ and $\hat{y}$ directions, it is easy to see that the transmitted and deflected beams would be of equal amplitude in the absence of Faraday rotation; but in the presence of Faraday rotation, one beam would increase, and the other decrease, in amplitude. This is the motivation for taking the difference of the two intensities as the experimental signal. For a general orientation of the analyzer, with the upper face's normal turned through angle ϕ from the x direction, we can define the "eigen-axes" of the beamsplitter to be

$$\hat{n}_1 = \hat{x}\cos\phi - \hat{y}\sin\phi, \quad \hat{n}_2 = \hat{x}\sin\phi + \hat{y}\cos\phi, \quad (35)$$

in the sense that light of pure linear polarization along $\hat{n}_1$ will be entirely deflected, and light of pure linear polarization along $\hat{n}_2$ will be entirely transmitted, by the polarizer. Defining the signal of interest to be the difference in the power emerging from the two faces of the beamsplitter, we have

$$S \equiv P_1 - P_2 = \frac{1}{2}|\mathbf{E}(L,t)\cdot\hat{n}_1|^2 - \frac{1}{2}|\mathbf{E}(L,t)\cdot\hat{n}_2|^2. \quad (36)$$

Here, $\mathbf{E}$ is the (complex) electric field incident on the beamsplitter, and we have used the result $|\mathbf{E}|^2/2$ for the time-averaged power of a field written in complex representation. For an electric field of the form (4), the result that emerges is

$$S = 2E_0^2 \exp[-(\beta_+ + \beta_-)L]\cos 2(\Delta\theta - \phi), \quad (37)$$

which depends on the same rotation angle $\Delta\theta$ defined in (6), despite the presence of differential absorption $(\beta_+ \neq \beta_-)$. For the natural choice $\phi=45°$, this simplifies to

$$S = 2E_0^2 \exp[-(\beta_+ + \beta_-)L]\sin 2\Delta\theta. \quad (38)$$

This shows that a readily extracted experimental signal is directly related to the sine of twice the Faraday rotation angle $\Delta\theta$ defined by (6). The meaning of the leading coefficient $2E_0^2$ is clearly seen operationally by imagining zero absorption, zero Faraday rotation, and the analyzer set to the $\phi=0°$ or 90° positions, since then (37) gives "baseline signals"

$$S_{\max,\min} = \pm S_0 = \pm 2E_0^2. \quad (39)$$

Then, if the analyzer is set to angle $\phi=45°+\epsilon$, one readily finds

$$S = S_0 \exp[-(\beta_+ + \beta_-)L]\sin 2(\Delta\theta - \epsilon), \quad (40)$$

which can be used in three ways. The first application is a method for setting the angle ϕ to the desired 45°: the procedure is to turn off the magnetic field (so that the Faraday rotation $\Delta\theta$ is zero); then the signal S is seen to vanish only when $\sin(-2\epsilon)=0$, i.e., when $\epsilon=0$ or $\phi=45°$. The second application is a method for measuring the Faraday rotation angle $\Delta\theta$ directly: if (for any given laser frequency) the analyzer is turned from the previously established $\phi=45°$ location to that angle at which the observed signal S is driven to zero, then (40) shows that

$$2(\Delta\theta - \epsilon) = 0, \quad \text{or} \quad \epsilon = \Delta\theta; \quad (41)$$

i.e., the analyzer has just been turned through exactly the Faraday rotation angle $\Delta\theta$. The third application is a way to get a real-time display related to the instantaneous Faraday rotation as the laser is scanned; this is obtained by rotating the analyzer to $\phi=45°$, by sending voltage signals proportional to P_1 and P_2 to a dual-trace oscilloscope, and by arranging for a vertical deflection proportional to their difference and a horizontal deflection driven by the same low-frequency oscillator that drives the frequency sweep of the laser.

IV. DATA AND DISCUSSION

We turn now to data derived from diode-laser spectroscopy of rubidium vapor, and a discussion of it in terms of the model so far developed.

For purposes of orientation, it is important first to acquire simple absorption data; this can be easily done with the apparatus described above by turning the magnetic field off and by orienting the polarization analyzer (to the $\phi=0$ position) so that the incoming linearly polarized light is entirely transmitted to one of the two photodetectors. Then the intensity of the transmitted light, as a function of laser-diode current, exhibits a graph like that of Fig. 7. This graph, and those to follow, was obtained by operating the diode laser with a sum of a fixed dc, and a sawtooth-modulated ac, injection current. Increasing current is to the right; the diode laser responds to greater current by exhibiting greater output power, and larger output wavelength. The increasing output power is displayed in the linearly rising signal in the figure; the increasing wavelength, or decreasing optical frequency, is chosen to scan over the rubidium D_2 resonance line at 780 nm. The upsloping optical signal (interpolated through the narrow absorption features displayed) is exactly the signal S_0 defined above, since it is obtained for polarimeter angle $\phi=0°$, for no absorption, and for zero magnetic field; knowledge of S_0, and its (unintended) variation with laser frequency, allows a theoretical model to include laser power variation. Of course,
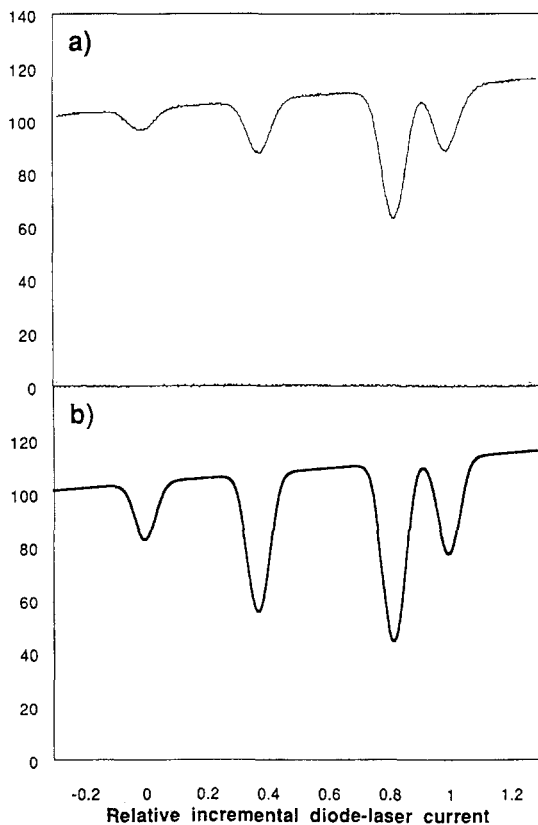
Fig. 7. (a) Intensity of (linearly polarized) light transmitted though a cell of rubidium vapor, as a function of relative incremental current in the diode-laser light source. The central value of diode-laser current has been empirically selected to give a central optical frequency near 384 200 GHz, and the width of the sweep has been selected to give a scan of about 10 GHz in optical frequency. Optical frequency *decreases* to the right; cell length $L=51$ mm, temperature=298 K; magnetic field zero. (b) Theory for this transmission signal, computed using the model described in the text. The horizontal scale, and the size and slope of the baseline, have been adjusted to match the data, but the shapes and sizes of the absorption dips are calculated from, not fit to, the model.

the more interesting content of the data of Fig. 7 is the set of narrow absorption features displayed; this is a high-resolution view of the Rb D_2 line. The scan was taken at low enough intensity (<0.4 mW in a spot about 3×6 mm^2) to avoid the saturation of the absorption features; the scan duration was under 2 ms.

The very first conclusion to be drawn is that rubidium is not as simple as the model introduced so far, since the data show not one, but rather four absorption dips. The structure observed is readily explained in terms of the actual structure of the rubidium D_2 line. This line arises from the $5s\ ^2S_{1/2}-5p\ ^2P_{3/2}$ transition out of the ground state; the combination of the isotopic composition of natural rubidium, and the hyperfine structure of the states involved, give rise to the lines displayed. The two inner lines arise from the 72.15% abundant ^{85}Rb isotope, and the outer ones from the 27.85% abundant ^{87}Rb isotope. The two inner lines are separated by about 3.6 GHz, the ^{85}Rb ground-state hyperfine splitting; similarly the outer lines are separated by about 6.8 GHz. For the purposes of this paper, these splittings can be taken as well known,[26] and they serve as a convenient way to calibrate the optical frequency scale. Each of the four observed absorption dips is broadened by two mechanisms: common to all is the room-temperature Doppler broadening of about 0.51 GHz, and different for each is the (unresolved) upper-state hyperfine structure, which ranges from 0.09 to 0.42 GHz for the various lines.

Clearly, enough is known about rubidium to permit a complete quantum-mechanical calculation of absorption, dispersion, and Faraday rotation;[27] such calculations are simplified by the cylindrical symmetry of the problem, which leaves the magnetic quantum number m_F a good quantum number even in the presence of the magnetic field, and which preserves the selection rules of $\Delta m_F = \pm 1$ for the fields described by $\mathbf{E}_{\pm}$. But such exact calculations are not particularly illuminating, and for the purposes of this paper we will instead "adapt reality to the model" by the following prescription. We will treat not only the two isotopes, but also the two ground-state hyperfine populations of each isotope, as separate noninteracting populations; we will ignore the upper-state hyperfine structure entirely; and we will assume that the transitions out of the ground state obeying the $\Delta m_F = \pm 1$ selection rules follow a simple Zeeman shift given by (13). In other words, we will treat the data as if rubidium were a mixture of four distinguishable kinds of the model atoms treated in the theory section above; the expected relative populations of the four "species" are given in Table I.

With this heavy-handed approximation, we can readily predict the expected size of the absorption signals; using the number densities of Table I for each of the four notional species of rubidium, we can use (15) to evaluate the absorption exponents $2\beta(\nu)L$ for the four species present, and then subject these to Doppler broadening by the methods of the

Table I. Statistical weights and number densities for the four "species" of rubidium giving rise to the four absorption features in Fig. 7. The features are labeled by the convention of Ref. 26, and are given in order of decreasing optical frequency.

Feature	Isotope and F value	Isotopic abundance	Statistical weight[a]	Overall weight	Number density[b]
(iv)	^{87}Rb, $F=1$	0.2785	3/8	0.1044	0.26×10^{16}
(iii)	^{85}Rb, $F=2$	0.7215	5/12	0.3006	0.75×10^{16}
(ii)	^{85}Rb, $F=3$	0.7215	7/12	0.4209	1.05×10^{16}
(i)	^{87}Rb, $F=2$	0.2785	5/8	0.1741	0.44×10^{16}

[a]Statistical weight is computed from $(2F+1)/2(2I+1)$, where $2F+1$ is the number of degenerate magnetic sublevels in a ground-state hyperfine level of a given F value, and $2(2I+1)$ is the total number of ground-state sublevels.

[b]Number densities (in m^{-3}) are computed assuming rubidium temperature $T=25$ °C=298 K, and overall rubidium number density 2.5×10^{16} m^{-3} (from Ref. 12).
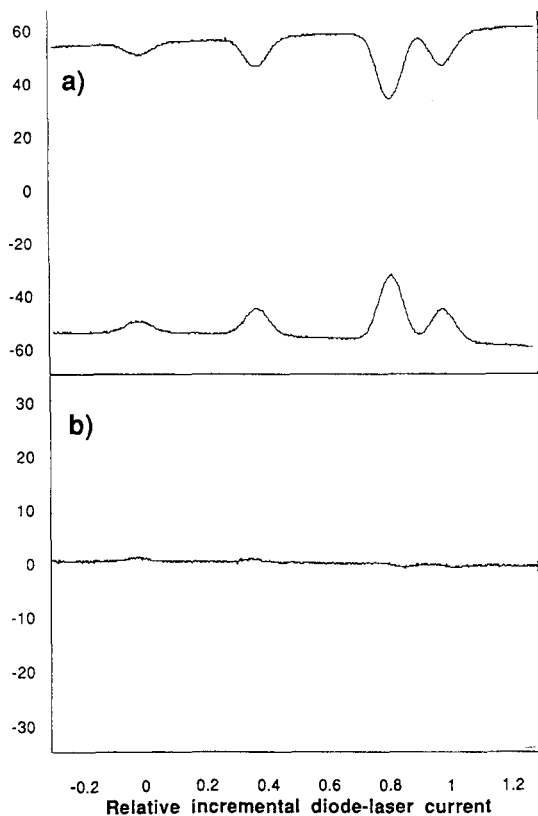
Fig. 8. (a) The signals obtained from the two photodetectors of the polarization analyzer of Fig. 6, under conditions of polarizer angle $\phi=45°$, zero magnetic field, and one signal electronically inverted. (b) The sum of the two signals of (a), further expanded vertically by a factor of 2; this is the signal representing zero Faraday rotation.

Fig. 9. (a) The experimental Faraday-rotation signal for three values of magnetic field strength ($B=5$, 10, and 15 mT), obtained at the same scale as the "baseline" data of Fig. 8(b). (b) Theoretical Faraday-rotation signals expected for this experimental situation, computed using the model described in the text. The theory uses the same horizontal and vertical scaling as in Fig. 7(b), and no adjustable parameters.

Appendix. Summing these and using the $B=0$, $\Delta\theta=\phi=0$ version of (37) above then gives a theoretical model for the absorption signal predicted for the sample. Figure 7(b) shows the results, where the horizontal axis, and the vertical scale and baseline slope, have been scaled to match the data, but in which no other parameters are adjusted. Comparing the data and the model, we see fine agreement in the shape of the absorption signals, showing that the computed Doppler broadening is really being observed; but the agreement in absolute and relative intensities is not so good. This may perhaps be attributed to optical pumping of the sample; though the light intensity is low enough to avoid saturation (depletion of the ground-state population), it may not be low enough to avoid optical pumping (redistribution of the ground-state magnetic sublevels' population).

Now there are only two experimental changes needed to display Faraday rotation with this system. The first is to rotate the polarization analyzer to the $\phi=45°$ position, to view the signals from both photodetectors, to invert one of them, and to display both on a dual-trace oscilloscope. The resulting displays are shown in Fig. 8, where the two signals are shown before and after algebraic addition on the 'scope. As expected, the two separate signals are nearly identical, and the sum signal is nearly zero, on the 'scope. The second change is to raise the magnetic field from its previous zero value to a succession of fixed values. The results for the previously vanishing "sum signal" on the 'scope are displayed in Fig. 9(a), for which the 'scope gain is the same as it was in Fig. 8(b). Each of the traces displays a set of four
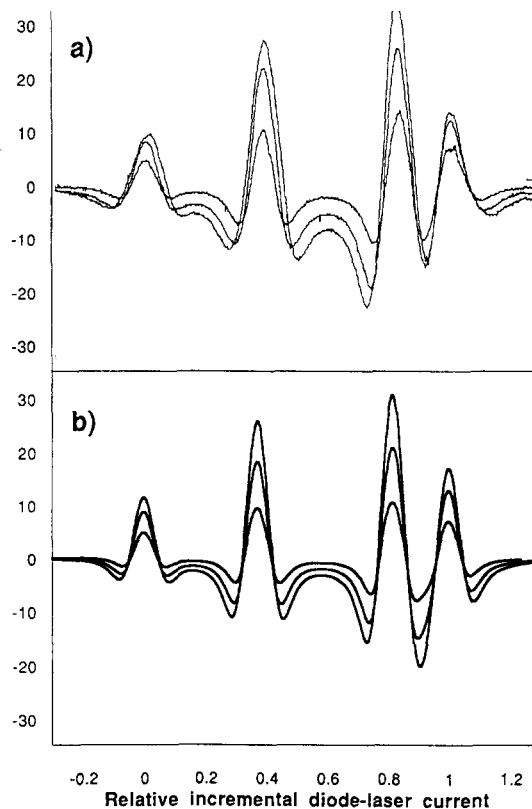
signals, each arising at the location of one of the four zero-field absorption features; each of the four signals resembles the symmetric resonant-Faraday-rotation signals predicted by theory and depicted in Fig. 5. Each of these traces was obtained in one single sweep of total duration less than 2 ms, so the Faraday rotation thus displayed is truly a real-time phenomenon; in fact the inductive time constant of the magnetic-field coils is the factor limiting the rate at which the Faraday-effect display on the oscilloscope can be changed!

For purposes of more detailed comparison with the theory, the theoretical prediction (40) was evaluated under the following assumptions: The leading factor S_0 (representing the characteristic variation in intensity that accompanies a diode laser's tuning) was taken from the pure absorption data above; the attenuation constants β_+ and β_- were taken from Doppler-broadened and Zeeman-shifted versions of (15), and the Faraday rotation angle $\Delta\theta$ was taken from the Doppler-broadened version of (21). This was done for four features, assumed to be located at the positions of the four zero-field absorption phenomena, and assumed to arise from species of the number densities given in Table I. Again, the quantities $(\beta_+ + \beta_-)$ and $\Delta\theta$ in (40) are linear in number density N, so they can be summed over the assumed four species to give values applicable to the whole sample; then evaluating the exponential and sine functions in (40) gives a result comparable to the data. The results are shown in Fig. 9(b), which displays a set of theoretical simulations of the actual experi-

ment. There are no new parameters adjusted in computing the Faraday signal, since the scaling of Fig. 7 suffices to fix all the necessary quantities. The agreement of the two halves of Fig. 9 illustrates that a simple model of atomic dispersion is indeed sufficient for a detailed description of resonant Faraday rotation; there is surprisingly good agreement in the details of the vertical scale of the signals, and some disagreement in the details of the broadening and saturation of the Faraday rotation signals with increasing magnetic field.

V. CONCLUSIONS AND APPLICATIONS

We have shown that the Faraday effect is readily detected in a diode-laser experiment in rubidium vapor, and that it has both an unusually large size and a particularly interesting structure in the immediate vicinity of the D_2 resonance line. We have also shown that a relatively simple theory can describe most of the features of the resonant structure, and this illustrates the intimate connection between absorption and dispersion in this resonant interaction of light and matter.

It is worth contemplating how the theoretical and experimental work discussed in this paper could be extended. An obvious extension to the theory would be to replace the simple atomic model used above with a quantum-mechanical model of actual rubidium, complete with the hyperfine structure of both the ground and excited states, and the correct magnetic-field dependence of all the energy levels. This has been done for the analogous D_2 line in cesium (in connection with experiments in parity violation),[28] and affords a useful exercise in matrix diagonalization. This, however, would still not give a perfect description of the experiment, since at easily accessible levels of laser intensity there arise nonlinear effects such as optical pumping, saturation, and velocity redistribution.[29]

On the experimental side, one could imagine a Doppler-free Faraday-effect experiment, using a "pump beam" to isolate one velocity class, and a "probe beam" passing through the same sample to measure Faraday rotation. Such an experimental arrangement would represent the use of the method of polarization spectroscopy[30] in the presence of a magnetic field. With the limitation of Doppler broadening removed, the next obstacle to spectroscopic resolution would be the intrinsic linewidth of free-running laser diodes. This limit could in turn be surpassed through the use of extended-cavity diode-laser systems of very narrow spectral widths; this would leave the natural linewidth of rubidium transitions as the limit on spectroscopic resolution.

There are other experimental arrangements that could be tried; much higher rubidium densities are easily accessible at moderately elevated temperatures. A larger departure would be investigation of the Voigt effect, the study of polarization rotation using a magnetic field transverse (rather than parallel) to the direction of light propagation.[31]

It is also worth remarking on a fascinating technological application of the Faraday effect for producing optical filters of extremely narrow bandwidth, but high peak transmission and wide field of view. The simplest of such filters is a sandwich with a rather high-density vapor cell between a pair of crossed linear polarizers. Such a filter would be opaque at all wavelengths in the absence of a magnetic field; in the presence of a suitable field, it is still opaque far from a resonance line (since the Faraday rotation is very small at large detuning) and right near a resonance line (since absorption in the vapor is very large there). But because absorption drops off with detuning more rapidly than does the Faraday-

rotation signal, it is possible for the cell to offer small absorption at two points on either side of the resonance where Faraday rotation is still as large as 90°. The result is that the sandwich becomes nearly transparent to light in two spectral regions each only a few GHz wide; this represents a passband whose width is only a few parts per million of the optical frequency. Filters like these have been proposed for systems involving laser communication with submerged submarines.[32]

APPENDIX

The presence of Doppler broadening leads to the need to evaluate convolution integrals of the form

$$\int_{-\infty}^{\infty} g(\nu_0)d\nu_0 \frac{(\Delta\nu/2) \text{ or } (\nu_0-\nu)}{(\nu_0-\nu)^2+(\Delta\nu/2)^2}$$

for absorption and dispersion signals, respectively, where $g(\nu_0)$ is the normalized Gaussian function defined by (33). The further case of the Faraday-rotation signal can be handled as a difference of two dispersion signals with distinct line centers. The Doppler broadening of Lorentzian absorption signals leads to the well-known "Voigt profile," and a recent article[33] describes various methods for computing these. Given the need to compute the broadening of both absorption and dispersion signals, and given modern computational environments, the best route to a solution seems to be via the complex error function.

The change of variable

$$t=\frac{2\sqrt{\ln 2}}{\Delta\nu_D}(\nu_0-\nu_{00})$$

transforms the integral above into the standard form

$$\frac{1}{\sqrt{\pi}}\int_{-\infty}^{\infty}\exp(-t^2)dt$$

$$\times\frac{(\Delta\nu/2) \text{ or } [\nu_{00}+(\Delta\nu_D/2\sqrt{\ln 2})t-\nu]}{[\nu-\nu_{00}-(\Delta\nu_D/2\sqrt{\ln 2})t]^2+(\Delta\nu/2)^2}$$

$$=\frac{2}{\Delta\nu_D}\sqrt{\frac{\ln 2}{\pi}}\int_{-\infty}^{\infty}e^{-t^2}dt\frac{y \text{ or } (t-x)}{(x-t)^2+(y)^2},$$

where

$$x=\frac{2\sqrt{\ln 2}}{\Delta\nu_D}(\nu-\nu_{00}) \quad \text{and} \quad y=\frac{2\sqrt{\ln 2}}{\Delta\nu_D}\frac{\Delta\nu}{2}.$$

Integrals of this form lack antiderivatives, but are related to the "complex error function" $w(z)$ defined[34] by

$$w(z)=\exp(-z^2)\text{erfc}(-iz)=\exp(-z^2)[1-\text{erf}(-iz)].$$

In fact the latest integral above is given very simply by[35]

$$\int_{-\infty}^{\infty} e^{-t^2} dt \, \frac{y \text{ or } (t-x)}{(x-t)^2+(y)^2}$$

$$= \pi\{\text{Re } w(x+iy) \text{ or } -\text{Im } w(x+iy)\}.$$

Since the complex function $w(z)$, or at least erf(z), is available as a library function in some modern numerical analysis packages, and since the real and imaginary parts of $w(z)$ simultaneously provide the broadening of the absorption and dispersion lineshapes respectively, this computational method has been used to generate the signals required in this paper. In the case of interest, the y parameter has the fixed and small value of about 0.0102, and the x parameter reaches about ± 33 for detuning $\nu - \nu_{00}$ of ± 10 GHz.

[1] Michael Faraday, *Experimental Researches in Electricity*, paragraphs 2146–2242 [in Vol. III of the reprint edition (Dover, New York, 1965)].

[2] E. Scott Barr, "Men and milestones in optics. V: Michael Faraday," Appl. Opt. **6**, 631–637 (1967).

[3] E. D. Palik and B. W. Henvis, "A bibliography of magnetooptics of solids," Appl. Opt. **6**, 603–630 (1967).

[4] D. Macaluso and O. M. Corbino, "On a new effect on light traversing certain metallic vapors in a magnetic field," C. R. Acad. Sci. **127**, 548 (1898).

[5] Pochi Yeh, "Dispersive magnetooptic filters," Appl. Opt. **21**, 2069–2075 (1982).

[6] Frank J. Loeffler, "A Faraday rotation experiment for the undergraduate physics laboratory," Am. J. Phys. **51**, 661–663 (1983).

[7] Frank L. Pedrotti and Peter Bandettini, "Faraday rotation in the undergraduate advanced laboratory," Am. J. Phys. **58**, 542–545 (1990).

[8] L. J. Aplet and J. W. Carson, "A Faraday effect optical isolator," Appl. Opt. **3**, 544–545 (1964).

[9] Daryl W. Preston and Eric R. Dietz, *The Art of Experimental Physics* (Wiley, New York, 1991), pp. 355–366.

[10] This labeling avoids the troublesome and contradictory conventions associated with right- and left-handed circular polarizations.

[11] Amnon Yariv, *Optical Electronics* (HRW, New York, 1985), 3rd ed., Chap. 5; this result omits the "counter-rotating" term, so it is valid anywhere near resonance, but not at "dc."

[12] A. M. van der Spek, J. J. L. Mulders, and L. W. G. Steenhuysen, "Vapor pressure of rubidium between 250 and 298 K determined by combined fluorescence and absorption measurements," J. Opt. Soc. Am. B **5**, 1478–1483 (1988).

[13] H. Becquerel, "On an explanation applicable to the phenomena of Faraday and Zeeman," C. R. Acad. Sci. **125**, 679 (1897).

[14] Jan Evetts (Ed.). *Concise Encyclopedia of Magnetic & Superconducting Materials* (Pergamon, New York, 1992), article on Magnetooptics.

[15] Robert W. Schmieder, Allen Lurio, W. Happer, and A. Khadjavi, "Level-crossing measurement of lifetime and hfs constants of the $^2P_{3/2}$ states of the stable alkali atoms," Phys. Rev. A **2**, 1216–1228 (1970).

[16] John R. Brandenberger, *Lasers and Modern Optics in Undergraduate Physics* (Lawrence University, Appleton, WI, 1989), pp. 33–58.

[17] D. A. Van Baak, "Temperature servomechanisms using thermoelectric modules," Am. J. Phys. **60**, 803–815 (1992).

[18] Lens LP-04 by Universe Kogaku (Glen Cove, NY).

[19] Cell supplied by Opthos, Inc. (Rockville, MD).

[20] Coils (Heath #40-694) from the Berkeley Physics course.

[21] Note that the polarizing efficiency of conventional Polaroid sheets is very low at these wavelengths.

[22] H. Adams, D. Reinert, P. Kalkert, and W. Urban, "A differential detection scheme for Faraday rotation spectroscopy with a color center laser," Appl. Phys. B **34**, 179–185 (1984).

[23] Polarizing beamsplitter 03 PBS 065 by Melles-Griot (Irvine, CA).

[24] Photodiodes VTB-6061 from EG&G Vactec (St. Louis, MO).

[25] Using dual op-amp LM833 from National Semiconductor, with feedback resistors of 3.9 kΩ (and parallel capacitors of 220 pF for high-frequency roll-off).

[26] G. P. Barwood, P. Gill, and W. R. C. Rowley, "Frequency measurements on optically narrowed Rb-stabilized laser diodes at 780 nm and 795 nm," Appl. Phys. B **53**, 142–147 (1991).

[27] Z. Wu, M. Kitano, W. Happer, M. Hou, and J. Daniels, "Optical determination of alkali metal vapor number density using Faraday rotation," Appl. Opt. **25**, 4483–4492 (1986). In this paper it is shown that an exact treatment gives a Faraday rotation (far from resonance) larger, by a factor of 7/6, than the one computed using the simple model described here.

[28] X. Chen, V. L. Telegdi, and A. Weis, "Magneto-optical rotation near the cesium D_2 line (Macaluso-Corbino effect) in intermediate fields: I. Linear regime," J. Phys. B **20**, 5653–5662 (1987).

[29] S. I. Kanorsky, A. Weis, J. Wurster, and T. W. Hänsch, "Quantitative investigation of the resonant nonlinear Faraday effect under conditions of optical hyperfine pumping," Phys. Rev. A **47**, 1220–1226 (1993).

[30] C. Wieman and T. W. Hänsch, "Doppler-free laser polarization spectroscopy," Phys. Rev. Lett. **36**, 1170–1173 (1976).

[31] Kazuyuki Muroo, Takeshi Matsunobe, Yukio Shishido, Yoshitaka Tukubo, and Manabu Yamamoto, "Resonant Voigt-effect spectrum of the rubidium D_2 transition," J. Opt. Soc. Am. B **11**, 409–414 (1994).

[32] Yat Ching Chan and Jerry A. Gelbwachs, "A Fraunhofer-Wavelength Magnetooptic Atomic Filter at 422.7 nm," IEEE J. Quant. Elec. **29**, 2379–2384 (1993).

[33] William J. Thompson, "Numerous neat algorithms for the Voigt profile function," Comput. Phys. **7**, 627–631 (1993).

[34] Milton Abramowitz and Irene K. Stegun, *Handbook of Mathematical Functions* (NBS, Washington, DC, 1964), 7.1.3.

[35] Reference 34, 7.4.13 and 14.

THE SAME OLD STUFF, YEAR AFTER YEAR

Instead of teaching the same old stuff year after year, [the teacher] will constantly enrich his knowledge, keep his teaching alive and dynamic, and prevent his mind from falling into the disease of authority and age, which is paralysis.

There is no other solution. Life is a process of constant change. No one can teach a subject in the same way two years running. Even if he uses the same books and teaches the same facts and conclusions, the second year he will have blurred a few outlines by repetition, cut a few corners because of age. The alternatives are only these: to allow your teaching to petrify by neglect, or constantly to refresh it by transfusions of new vitality and interest from your own reading. The choice is not too difficult, if it is clearly seen. One of the few consolations of age is that, while the body becomes weaker, the mind can grow stronger and richer.

Gilbert Highet, *The Art of Teaching* (Vintage Books, New York, 1989; originally published by Alfred A. Knopf, 1950), pp. 83–84.

DIODE LASER SPECTROSCOPY

APPARATUS SECTION

Chapter 5 - Apparatus
Table of Contents

I. Laser

I.A. 9 PIN CABLE AND CONNECTOR

The 9-pin cable provides electrical connections between the laser head and electronics box. A pin-out of the connector is shown in Figure 1. Your Laser diode head was shipped with a protective plug on the 9-pin connector on the laser head.   When you are ready to use the laser diode remove the protective plug and attach the 9-pin cable. Do not discard the protective shipping plug.   It can be used to protect the laser whenever the cable to the controller is removed. For both operational and safety reasons, it is important to keep the 9-pin electrical cable connected between the laser head and Laser Diode Controller box whenever possible.

There is protection circuitry inside the laser head, but large electrostatic voltages may still damage the laser diode. Ground yourself before removing the plug and attaching the cable. When the instrument is turned on there is also the possibility that high voltage is present on the cable (a maximum of 100 Volts that drives the piezo stack). Always connect the 9-pin cable before connecting the controller box to AC power. Figure 1 shows the pin out of the 9-pin connector and the protection diodes that are mounted inside the laser head.
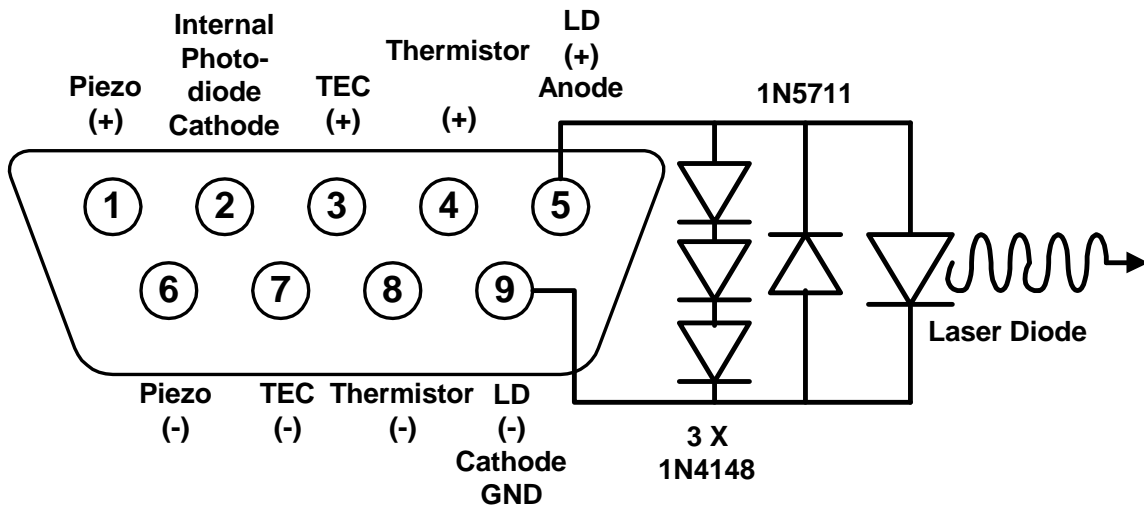

Figure 1: 9-pin Connector Pin-out

I.B. LASER TEMPERATURE

Temperature has several effects on the laser. The frequency of a "bare" diode laser changes with temperature for two reasons. First the wavelength dependence of the overall gain* changes with temperature. As shown in Figure 6 of Section 1, this change is reflected in the large-scale slope of the wavelength versus temperature graph ($\approx$ 0.23 nm/°C†). Secondly the optical length of the "bare" diode increases with temperature. This is shown in the small-scale slope of the individual "steps" in Figure 6. From this slope (0.05 nm/°C $\approx$ 25 GHz / °C) we can estimate that a temperature stability of 40 μ°C‡ is necessary for the variation in the laser frequency to be less than 1MHz. The temperature also changes the length of the external cavity formed by the grating. From the linear expansion coefficient of aluminum $\alpha \approx 2.5$ X 10-5 °C-1 we can estimate a change in wavelength of 0.015 nm °C-1, $\approx$ 7.5 GHz °C-1. §

Temperature also affects two other laser parameters. First, the threshold current increases with temperature. Second, if the current is kept constant, the laser intensity will decrease as the temperature is increased.

I.B.1. Specifications

Temperature Range	O to 60 °C
Temperature Stability	better than 0.05 °C
Control process	Proportional, Integral, Derivative
Adjustment	Back Panel Potentiometer
Thermo electric cooler	20 W @ 2.5 A
Sensor	10 kΩ thermistor
Modulation Input	12 kΩ Input Impedance
	+5 V in = -1 Volt Set Point Voltage Change

---

* The overall gain is the uppermost curve in figure 5 of section 1. (Diode Laser Physics)

† This is a useful number if you wish to tune the laser to a new wavelength.

‡ This estimate appears to be a severe restraint on the temperature. In practice the temperature stability needed is less restrictive. First, the external cavity modes "trump" the temperature variations of the internal modes. Secondly, there is a natural time scale for changing the temperature of any object. In an analogy to electronic circuits, a time constant may be defined as the product of the thermal resistance and the heat capacity. If we model the thermally connected parts as a cubic piece of aluminum, this leads to the following expression …. The mass of the mirror mount, cold plate, and collimation tube assembly is 168 grams which gives a time constant of about 20 seconds. Since we typically sweep through the absorptions in a time interval of about 0.1 sec, the amount of temperature change possible is small.

§ For an optical cavity, $\lambda = 2L/m$, where L is the cavity length and m is an integer. It is interesting that the change in wavelength with temperature depends only on the material and wavelength and not on the cavity length. $\Delta\lambda = \alpha\lambda$.

I.B.2. Laser Head

Figure 2 shows the Laser Head without the insulation between the cold plate and heat sink. The Thermo-electric cooler (TEC) is visible between these two aluminum pieces. The thermistor, located close to the diode laser in the collimation tube holder, is also shown. Four stainless steel screws secure the TEC between the cold plate and heat sink. These screws pass through nylon shoulder washers inside the heat sink, which provide electrical and additional thermal isolation between the cold plate and heat sink. (Note: stainless steel is a poor thermal conductor.) A 1/4-20 brass screw passes through the cold plate and mirror mount and threads into the collimation tube holder. This screw and the large aluminum contact area thermally link the cold plate with the diode laser. On the other side of the laser head (not visible in the picture), copper braid is used to thermally link the cold plate to the grating holder and the movable portion of the mirror mount.*
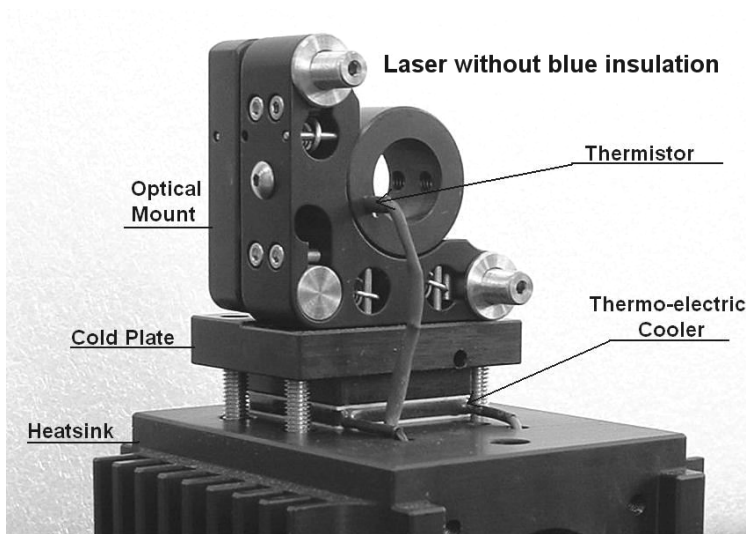
Figure 2: Picture of Laser Head

I.B.2-a. Plexiglas Cover

A Plexiglas cover over the laser provides isolation from air currents. There are two holes in the cover to allow the laser beam to exit both with and without the diffraction grating in place. When operating the laser at a temperature below the local dew point, condensation may be a problem. In such cases, it is advisable to put tape over the un-used hole and tape a piece of glass (microscope slide or cover slip) over the hole through which the laser beam exits.

---

* Though better than no braid at all, we believe that this is the weak link in the thermal stability chain as it relates to wavelength stability. When operating at temperatures far from room temp there is a significant temperature difference between the movable mirror mount section that holds the grating and the rest of the mirror mount (about 6 $°C$ at a 6 0 $°C$ set point).

I.B.3. Laser Temperature Electronics

The TEC is a Melcor, model CP1-127-08 with dimensions of 30 mm. by 30 mm., a maximum current/voltage of 2.3A/15.4V and a cooling power of 21.4 Watts.   The TEC transfers heat between the cold plate and heat sink. (When run in "reverse" direction, the cold plate becomes a hot plate and the heat sink a heat source.) Temperature is sensed with a 10k thermistor used in a bridge circuit (see Figure 3). An instrument amplifier generates an error voltage that is the difference between the set point voltage and the voltage across the thermistor. A PID circuit conditions the error signal into a control voltage that operates the TEC through a power amplifier. The entire circuit is bipolar so that both cooling and heating may be accomplished.

Analysis of the bridge circuit leads to the following relation between thermistor resistance (RT) and voltage (VT): $VT = 5.0\,RT / (10{,}000 + RT)$.

Values of thermistor resistance and voltage for temperatures from –10 to 60ºC are listed in Table 1, on the following page.

The set point voltage is adjusted using the ten-turn potentiometer, located on the back panel. The set point may also be controlled remotely with the temperature modulation input on the back panel.   The set point voltage is the difference between the voltage set by the potentiometer and the modulation voltage.
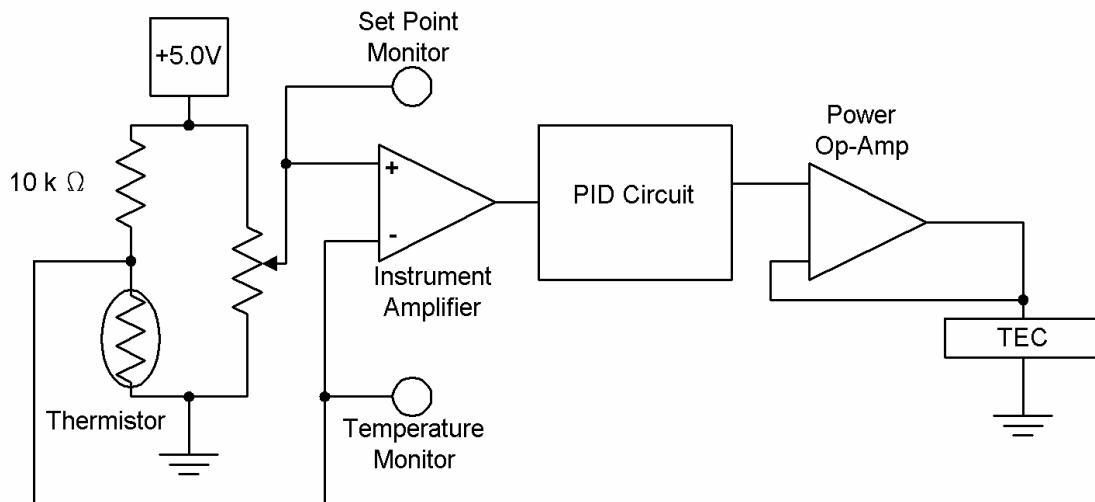
Figure 3: Laser Temperature Control Electronics

The voltage modulation circuit is not shown in Figure 3. Modulation input voltage is attenuated by one fifth so a five volt change in the modulation voltage leads to a minus one volt change in the set point voltage. In the MONITORS section of the front panel, the LASER DIODE TEMPERATURE and SET POINT voltages may both be measured. Two LEDs, mounted on the front panel, indicate when the laser head is above or below the set point temperature.

Thermistor Resistance and Bridge Voltage as a Function of Temperature

Temperature	Resistance	Voltage	Temperature	Resistance	Voltage
°C	Ohms	Volts	°C	Ohms	Volts
-10	55,330	4.2347	25	10,000	2.5000
-9	52,440	4.1992	26	9574	2.4456
-8	49,690	4.1623	27	9165	2.3911
-7	47,070	4.1239	28	8779	2.3375
-6	44,630	4.0848	29	8410	2.2841
-5	42,340	4.0447	30	8060	2.2315
-4	40,170	4.0034	31	7722	2.1786
-3	38,130	3.9611	32	7402	2.1268
-2	36,190	3.9175	33	7100	2.0760
-1	34,370	3.8731	34	6807	2.0250
0	32,660	3.8279	35	6532	1.9756
1	31,030	3.7814	36	6270	1.9269
2	29,500	3.7342	37	6017	1.8783
3	28,060	3.6863	38	5777	1.8308
4	26,690	3.6372	39	5546	1.7837
5	25,400	3.5876	40	5329	1.7382
6	24,170	3.5367	41	5116	1.6922
7	23,020	3.4858	42	4916	1.6479
8	21,920	3.4336	43	4725	1.6044
9	20,880	3.3808	44	4543	1.5619
10	19,900	3.3278	45	4369	1.5203
11	18,970	3.2741	46	4202	1.4794
12	18,090	3.2200	47	4042	1.4393
13	17,260	3.1658	48	3889	1.4000
14	16,470	3.1111	49	3743	1.3618
15	15,710	3.0552	50	3603	1.3243
16	15,000	3.0000	51	3469	1.2878
17	14,330	2.9449	52	3340	1.2519
18	13,680	2.8885	53	3217	1.2170
19	13,070	2.8327	54	3099	1.1829
20	12,500	2.7778	55	2986	1.1497
21	11,940	2.7211	56	2878	1.1174
22	11,420	2.6657	57	2774	1.0858
23	10,920	2.6099	58	2675	1.0552
24	10,450	2.5550	59	2580	1.0254
25	10,000	2.5000	60	2488	0.9962

Table 1: Thermistor Resistance and Bridge Voltage versus Temperature

I.B.4. Laser Temperature Electronics Advanced Details

The circuit is a modification of that described by C.C. Bradley et al Review of Scientific Instruments, 61, 2097 (1990). The PID control parameters were determined from the Zeigler-Nichols closed loop tuning method, and then tweaked to give better performance. These parameters give adequate performance but they are not guaranteed to be optimal, especially if you operate your laser at temperatures far from room temperature.

I.B.4-a. Changing the PID Control Parameters

To change the PID control parameters the top cover of the electronics box must be removed. Because of the high voltage in the box we require that you turn off the AC power and unplug the electronics from the wall outlet before removing the top cover. Four side screws hold the top cover in place. When looked at from the front, the temperature control board is located on the back left hand side. Three 1% metal film resistors are used to set the control parameters. These resistors are held in a series of terminal blocks, see picture below.
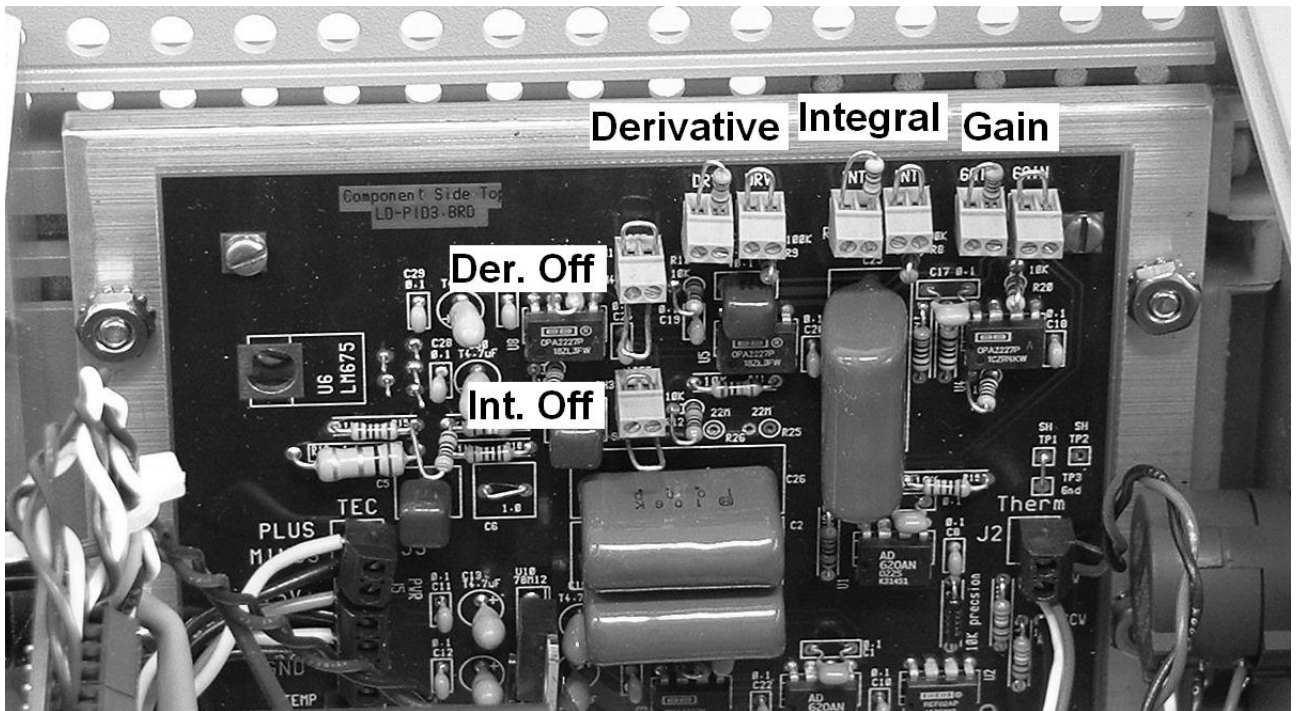
Figure 4: Picture of temperature control board showing terminal blocks

There are two terminal blocks wired in series for each parameter. The value is the sum of the resistances in each block. This allows for fine-tuning of the parameters. In the Zeigler-Nichols tuning method, both the derivative and integral term need to be disabled. The terminal blocks labeled (Der. Off) and (Int. Off) are used to enable or disable the derivative and integral control parameters respectively. To turn a parameter off you must remove the wire from the terminal block AND cut the wire loop that is located just underneath the block. To re-enable these terms the wire loops must be reinstalled. As shipped, the wire in the block and the loop underneath it are redundant. Both allow the parameter to be active.

Table 2 lists the various control terms and the standard values that the unit was shipped with. Once the changes have been made, the top cover should be reinstalled before the power is applied to the electronics.

Control Parameter	Equation	Standard Values	Value
Gain (P)	G= (Rxt1+Rxt6+10k)/10k	Rxt1 = 20 kΩ Rxt6 = 0	G = 3
Integral (I)	I = 20μF *(Rxt2+Rxt4+100k)	Rxt2 = 2.2 MΩ Rxt4 = 0	I = 44 sec.
Derivative (D)	D = 10μF *(Rxt3+Rxt5+100k)	Rxt3 = 1 MΩ Rxt5 = 0	D = 10 sec.

Table 2: PID Default values

I.C. LASER CURRENT CONTROLLER

The amount of current determines (in part) the gain of the laser. Below the threshold current, the overall gain is less than one, and the light coming from the diode is incoherent and broadband, similar to light from an LED.   At currents above the threshold, the light coming from the diode becomes coherent narrow-band laser light[*] and the intensity increases linearly with the current. Increasing the current also increases the temperature of the diode. This changes the wavelength of the laser in a manner similar to that of external heating.[†]   As discussed in Chapter 1, Section IIB, the small-scale local slope of the steps in Figure 7 makes it possible to estimate that a current noise of 0.5 µA would produce a laser line width of about 1 MHz. (See Chapter 1, pages 6 & 7, Figure 7, wavelength versus current for a "bare" diode).

I.C.1. Specifications

Current Range	0 - 100 mA
Current Noise[‡]	$< 50\ \text{nA}_{\text{RMS}}$ (3 Hz - 20 kHz. bandwidth)
Modulation	
Front Panel	
Gain	2 mA/Volt
Maximum Amplitude	± 11 mA
Frequency	DC to 1 MHz
RF on Laser Head	
Gain	20 mA/Volt
Frequency	100 kHz to 100 MHz[§]
Current Monitor Gain	100 mV / mA (10 mA = 1.0 V)
Current Limit	(50 – 100 mA) set at 80 mA
ESD protection	Schotty diode (reverse voltage)
	Three switching diodes 1N4148 (over voltage)

---

[*] Some fraction of the light remains LED like, at least for currents just above threshold where both types of light can be seen.

[†] Changing the current can be thought of a means of rapidly changing the diode temperature, for times longer than 1 µs. The current also changes the carrier density in the diode, which changes the index of refraction. This effect is smaller than the thermal effects and predominates only at time scales shorter than 1 us. This shortest response time is set by the relaxation oscillation frequency.

[‡] We measured the current noise with the Teachspin Signal Processor/ Lock-in Amplifier (SPLIA), configured in the amplitude detection mode, by detecting the voltage noise across a 100 Ω resistor in series with the diode. Unfortunately most of the noise measured was not current noise, but voltage noise from the Lock-in Pre-Amplifier (about 10 nV / $\text{Hz}^{1/2}$). A more sensitive front end would be needed to get an accurate measure of the noise.

[§] Most likely higher modulation frequencies are possible. This is highest frequency for which the laser has been tested.

I.C.2. Current Electronics

The ten-turn potentiometer of the CURRENT module is used to adjust DC laser current. One turn of the dial will change the current by about 10 mA. The BNC plug labeled modulation input is used for external modulation of the current. The attenuator dial is linked to the current modulation input. With a maximum modulation frequency of 1 MHz, and with the attenuator turned to 1 (full on), the input provides a modulation of 2 mA/Volt. The current itself can be measured using the BNC labeled laser current, which is in the MONITORS section of the front panel. The conversion factor is 1Volt = 10 mA.

I.C.2-a. Diode Protection

Currents injected in the wrong direction or in excess amounts can render your diode inoperable. The laser head is shipped with a protective shorting plug. This must be removed before attaching the 9-pin cable. Protective diodes are present in the laser head. (Refer to Figure 6 for details) When the laser is on, the three over-voltage diodes will conduct slightly, about 10% of the current from the electronics box will flow through these protection diodes. Current to the diode laser is shunted to ground when the front panel laser power toggle switch is in the off position. There is also a slow start circuit in the current controller that applies power to the electronics slowly after the AC power is switched on.

I.C.2-b. Current Limit

Diodes are specified by the maximum optical power that they will produce and not by the maximum current. For each individual diode, the current that will produce this specified power is different, with values ranging from 80 mA (min) 110mA (typ.) and 140mA (max.)* (See spec sheet in appendix.) Your instrument has a current limit that has been set to approximately 80 mA. This value has been chosen so that no diodes can be damaged by excess current from the controller. However this also means that the typical diode will not reach its maximum specified output power (70 mW). For the typical student experiment the current limit will not be a problem, because the diode has excess power and one is typically attenuating the beam when taking data. A user needing the full power may adjust this current limit. (See section I.B.2)

The current limit does not affect the currents injected either through the front panel current modulation input or through the SMA connector on the laser head. The front panel has a maximum modulation amplitude of 11 mA. This means that a maximum current of 91 mA (the sum of the modulation input and DC current) can be applied to the diodes by the students. It is possible that this may be enough current to damage a few select diodes. Please warn your students. There is no over-current protection limiting the amount of current that can be sent through the RF connector. *The RF input is for advanced users only.*

I.C.2-c.   Applying Power

Before turning on the AC line power to the electronics, make sure that the laser power toggle is off, that the Current ten-turn pot is set to zero, and that there is no external modulation.   Once AC power is applied you may turn on the laser power toggle and then finally increase the Current with the ten-turn pot. When shutting off the unit the steps should be followed in reverse. First set the current to zero, disconnect any external modulation, turn the laser power toggle off and finally shut off the AC power to the electronics box. All these steps are meant to ensure a maximum lifetime for your diode laser.

---

* This is for operation at 25 ℃. At higher tempera tures more current is needed to reach a specified output power. See Diode spec sheet.

I.C.3. Current Controller Advanced Details

The current control is based on the design of K.G. Libbrecht and J. L. Hall (Rev. Sci. Instrm. 64 (8) 2133 1993).
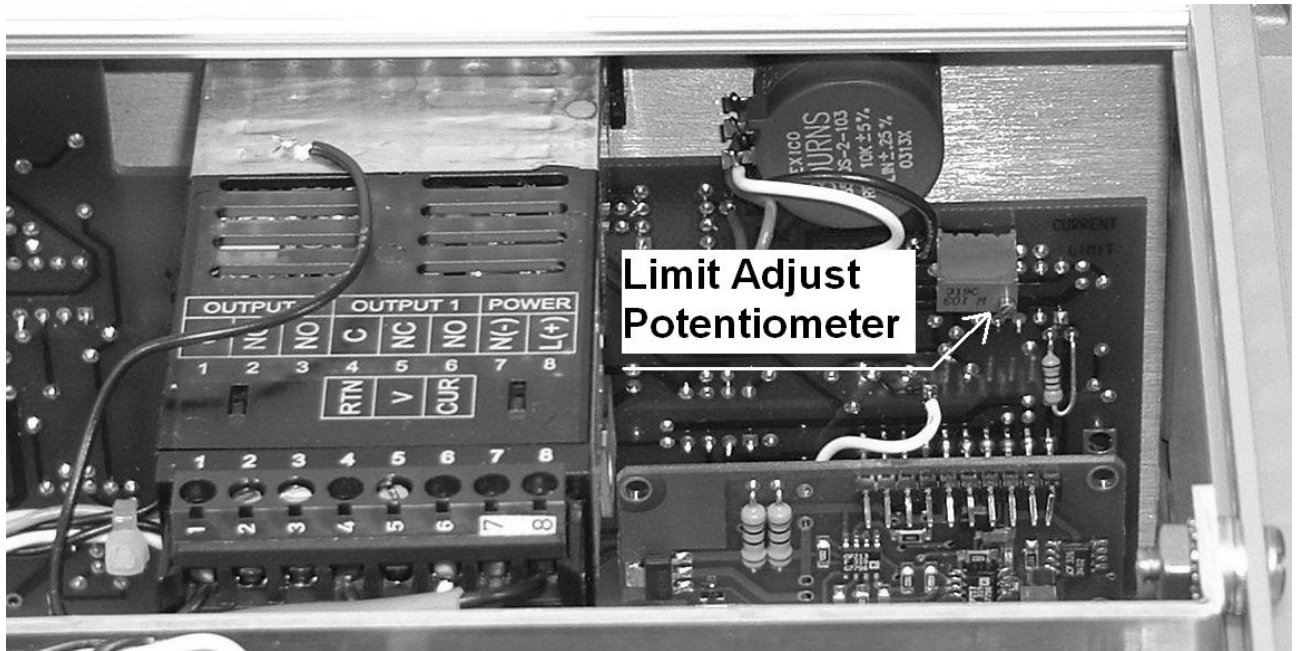

Figure 5:   Picture showing current limit trim pot and test points

I.C.3-a.   Current Limit Adjustment

Advanced users may want to change the current limit so that they can get more power from an individual diode. Increasing the current limit could lead to overdriving of the laser diode and permanent damage. This procedure is only for those who understand this and can set an appropriate current limit.

The circuit limits the current by setting the supply voltage. The supply voltage is dropped across the 50 ohm current sensing resistor, the 5 ohm current monitor resistor and then across the diode laser. Different diode lasers will have different forward biased voltage drops and hence the ultimate current limit will change slightly for different diodes. Turn off the power to the laser controller and unplug the AC power line from the wall. Turn the electronics box over and remove the four screws that hold the bottom cover of the electronics box in place and remove the cover. The current limit trim pot (potentiometer) is located on the front panel circuit board, underneath the cell heater controller.   Figure 5 shows a picture of the current control circuit board with the location of the supply voltage potentiometer and test point indicated. Turning the trim pot counter clockwise, when viewed as shown in Figure 5, will increase the supply voltage and current limit. One turn of the trim pot will increase the voltage by about 0.2 V and the current by about four milli-amperes (4 mA).

I.C.3-b. High Frequency Modulation

Figure 6 shows a schematic of the high frequency modulation circuit connected to the SMA connector on the laser head. A 0.033 μF capacitor is used to AC couple the RF into the diode. The RF is sent into the laser diode through the 50 ohm resistor. The resistor also acts as a 50 ohm impedance match for the RF. The connections are made on a small circuit board inside the laser head base right above the 9 pin connector. Also shown in the figure are the two sets of protection diodes on both sides of the 50 ohm resistor and 47 μH inductor. We included two sets of protection diodes to provide maximum electrostatic protection.
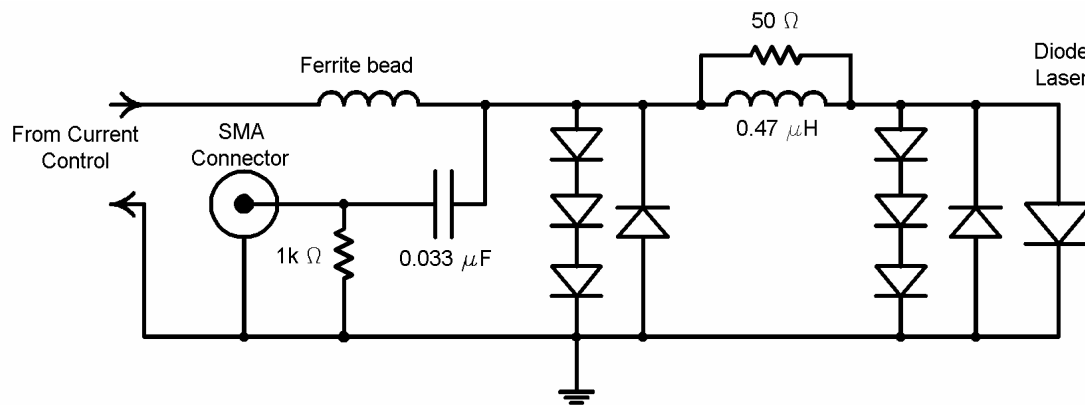
Figure 6: Schematic High Frequency Modulation Circuit. Also shown are two sets of protection diodes. The three diodes in series are 1N4148's and the diodes used to prevent reverse voltages are 1N5711's.

I.D. LASER OPTICS AND DIODE

Figure 7 is a diagram of the Laser Head as viewed from above. The diagram includes the diode, collimating lens, grating, PZT stack, ball tipped setscrew that provides contact between the mirror mount and grating holder, and the 6-32 socket head cap screws that fix the grating holder to the mirror mount. The basic design is from Arnold et al, Review of Scientific Instruments, 69, 1236 (1998). The only major change is the use of a flexure mount to hold the diffraction grating. The diode is held in a Thor Labs Collimation tube (LT230P-B), which also holds the aspheric collimation lens (C230TM-B) (f = 4.5 mm, 0.45 na). The holographic diffraction grating is from Edmunds Optics (R43-775) and has 1800 lines /mm. The actuators used for adjusting the grating and mirror mount have 100 threads per inch. From the grating equation ($\lambda = 2d\sin\theta$) and dimensions given above one can calculate the wavelength tuning rate of the actuators to be about 5.2 nm per turn.
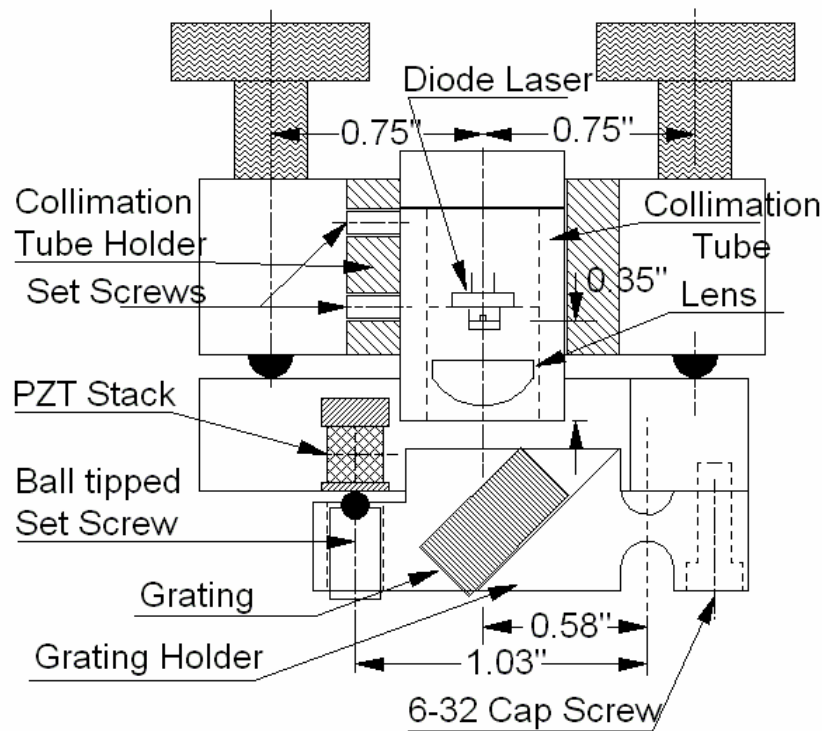

Figure 7: Overview of Laser Head

I.D.1. Laser Diode

The diode is a Sanyo DL-7140-201S infrared laser diode with a nominal wavelength of 785 nm and a maximum output power of 70 mW. The data sheet is included at the end of this section. The data sheet shows the output power as a function of current for different laser temperatures. The point where the power rises sharply is called the threshold current and is the start of lasing action. There are also graphs of the threshold current as a function of temperature.   When the diode is placed in an aligned optical system, the threshold current is reduced below that for the "bare" diode. When the laser beam is viewed on a white card with the CCD camera, you can observe the threshold as a sudden brightening of the beam spot. Measuring, or just observing, this threshold condition will be used in the following section for aligning the grating and correctly positioning the lens. (Section I.D.2-c)

If you notice that the laser experiments are not functioning properly, even though they did previously, you might have a damaged diode that needs to be replaced. Diode lasers rarely burn out completely before they lose the ability to function adequately in the laser lab. Thus, it is not always readily apparent when a laser needs to be replaced. The telltale signs of a damaged laser are: The laser power (as a function of current) is reduced from nominal values. The laser threshold is not abrupt and obvious at the nominal threshold current. The output beam profile of the diode may also change.

I.D.2. External Cavity

To align the external cavity you must adjust the angular orientation of the grating so that the beam diffracted from the grating is sent back into the diode. The beam labeled "Secondary Output" is also called the *retro-reflected* beam. Figure 8 diagrams the process.

Secondary Output Beam
Reflected from Grating and
Diode Front Facet

Primary
Laser Beam

Front Facet
R=15%

Back Facet
R=100%

Grating

Beam Diffracted
from Grating

Beams have been spacially separated for clarity
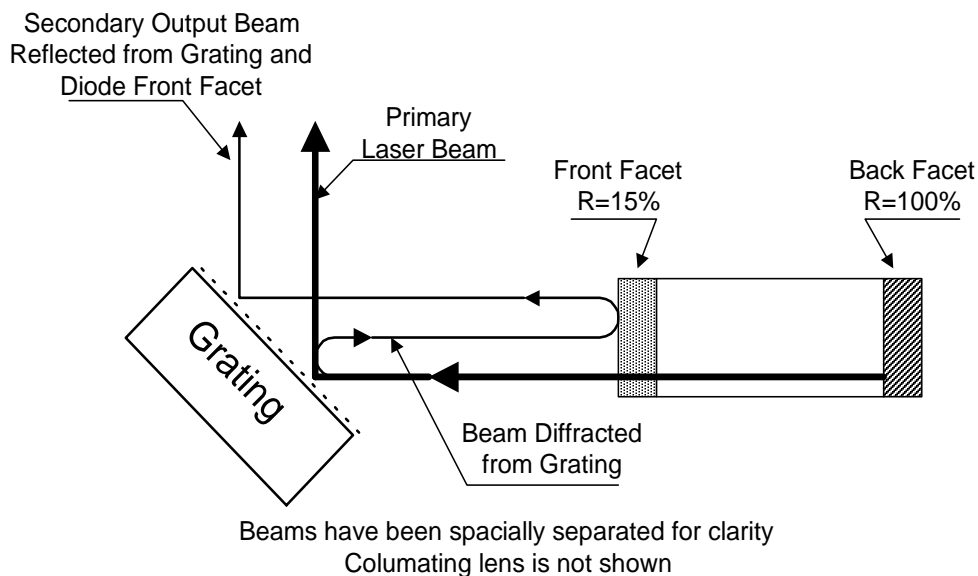Columating lens is not shown

Figure 8:   Diagram Showing Origin of both the Primary and Secondary (Retro-Reflected) beam Spots

I.D.2-a.   Finding the Retro Reflection

Use the blank backside of a business card as a viewing screen. Place the card in front of the laser and use the CCD camera and video monitor to view the output beam as shown in Figure 9. Turn on the laser power and set the laser current two to three milliamps above threshold. Check that the Laser TEMPERATURE SET POINT is correct (Refer to section I.B.3, Laser Temperature Electronics, for how to change temperature set point.)

The picture of the TV monitor in Figure 10 shows both the primary and retro-reflected beams. The intensity of the retro-reflected beam is only 2-3% that of the main beam. You will have to set the laser current a few milliamps above threshold to see the retro reflection. As discussed in Initial Setup of Chapter 3, Section II.D.5, the TOP knob is used to change the vertical position of the beam and the SIDE knob is used to change the horizontal position. See Figure 2 of Initial Setup on Chapter 3 page 6.

Use the TOP knob to set the beam height at 4.0". (If the grating has been removed refer to Section I.D.3.b and c; Installation of the grating and setting the beam height.) Dim the room lights. The retro reflected beam may appear above or below and to the right or left of the main beam spot. Be sure to position the viewing card with the main beam spot in the center.
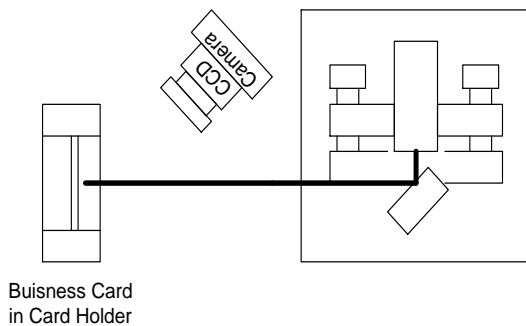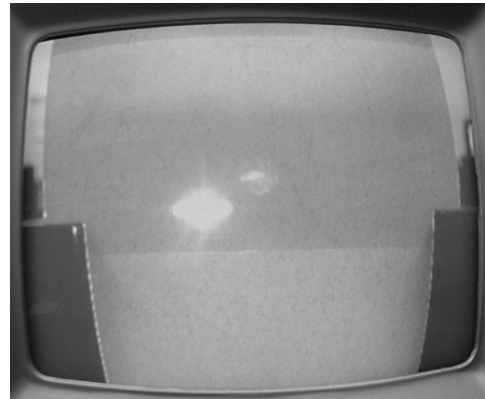

Figure 9:   Setup for Viewing Beam Profile and Retro-reflection.

Figure 10: Laser Beam Image Misaligned external cavity both main beam and retro-reflection are visible.

Turn the SIDE knob until you see the weak retro reflection on the monitor. You may have to make several turns of the SIDE knob in both directions. Reposition the viewing screen to keep the main beam centered on the screen. If you cannot find the retro reflection make sure that the laser is above threshold (Section I.C.3 or I.D.3-d). Increase the laser current by 2 mA and search again. If you still cannot find the retro reflection turn the TOP knob three turns in and search again. Then turn the TOP knob out six turns, (this gives a net of three turns out from the starting position), and search again.

I.D.2-b. Aligning the External Cavity

Once you see the retro reflection, adjust both the SIDE and TOP knobs so that the main beam and the retro reflection overlap. You should notice an increase in the laser intensity when this happens. You should also observe that, when turning the TOP knob, the main and retro beams move in opposite directions and when the SIDE knob is turned only the main beam moves.

I.D.2-c.   Measuring the Threshold Current

Threshold current measurements are used to set the lens position. Again use the setup shown in Figure 9. Dim the room lights and reduce the laser current to just above threshold. Connect a voltmeter to the laser current in the MONITORS section of the front panel. Adjust the TOP and SIDE knobs to find the region of maximum laser intensity.* Reduce the current until it is again just above threshold. Use the 5/64" Allen wrench, as shown in Figure 2 of Initial Setup, to gently change the knob positions. A flicker in the laser spot indicates that the laser is passing through a series of modes. You should be able to observe six or more vertical modes as you move the TOP knob and tens of modes as you move the SIDE knob. Position both knobs so that the laser is near the center of these mode patterns. Position the TOP knob so that you are at a mode maximum and reduce the current till you can just see the diode start to lase. We will define this as the threshold current. This procedure is a little subjective, but as long as you are consistent it will work fine.

I.D.3. Diffraction Grating Holder

The grating holder may be removed either to study aspects of the diode laser without the external cavity or to adjust the position of the collimating lens.

I.D.3-a. Grating Removal

Set the Laser Current to zero and turn off the Laser Power. Set the Piezo dc offset to zero and disconnect any cables from the Piezo modulation input. Loosen the ball tipped setscrew that contacts the piezo stack. (See Figure 7). Remove the two 6-32 socket head cap screws that hold the grating holder to the mirror mount. It will be necessary to hold the mirror mount with one hand as you loosen the 6-32 screws. Remove the grating holder and set it aside. Be careful not to touch the front face of the grating.

I.D.3-b. Installing the Grating

Place the grating holder on the mirror mount; insert and tighten the two 6-32 socket head cap screws. You will have to hold the movable end of the mirror mount while doing this.

There is a certain amount of "play" in the angular position of the grating holder. This "play" allows for the beam height to be set to 4.0" (See below). For the initial installation, press the grating holder from the side so that the holder makes contact with both 6-32 screws as you tighten the screws. See picture in Figure 11. This will approximately set the correct beam height.
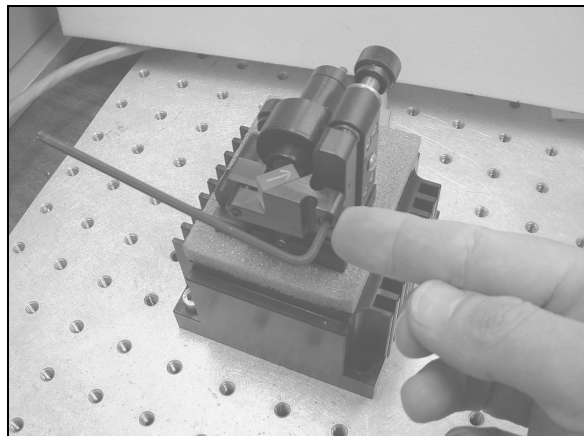
Figure 11:   Initial installation of the Grating: Grating holder is pressed against screws as screws are tightened

---

* This procedure is the same as outlined in Chapter 3, Section II.D, Aligning the Laser. The one difference is that you will now also adjust the SIDE knob.

I.D.3-c.   Setting the Beam Height

After the initial installation of the grating holder, turn on the laser and align the external cavity (See Section I.D.2-b). Place the viewing screen or IR viewing card at the far end of the optical table from the laser in a position to view the beam. Loosen the two 6-32 socket head cap screws and tilt the grating holder to set the beam height at four inches (4") above the optical table as seen on the viewing card. Retighten the 6-32 socket head cap screws. Align the external cavity once again and confirm that you have the correct beam height.

I.D.3-d.   Contacting Piezo Stack with Ball Tipped Setscrew

Once the beam height has been set, turn the ball tipped setscrew until it makes contact with the piezo stack. Once the ball tipped setscrew just makes contact, the screw should be tightened an additional one-quarter turn. *DO NOT tighten it more than one-quarter turn as this could lead to damage to the piezo stack when the high voltage is applied.* This preloads the piezo stack. If you find it difficult to tell when the setscrew has made contact, you can turn on the laser power and current and use the viewing screen and CCD camera to look at the beam spot as you tighten the ball tipped setscrew. When the beam spot starts to move, the setscrew is in contact with the piezo stack.

I.D.4. Collimation Tube

Figure 12 shows an exploded view of the collimation tube and associated parts. The aspheric lens threads into the front side of the collimation tube. The split aluminum adapter* and diode laser slide into the backside of the collimation tube. The black plastic retaining ring threads into the backside of the collimation tube and holds the diode in place. The printed circuit board (PCB) and 5.6 mm socket plug into the back of the diode. The strain relief body slides over the PCB and threads into the backside of the collimation tube. Three screws hold the strain relief cap onto the strain relief body.
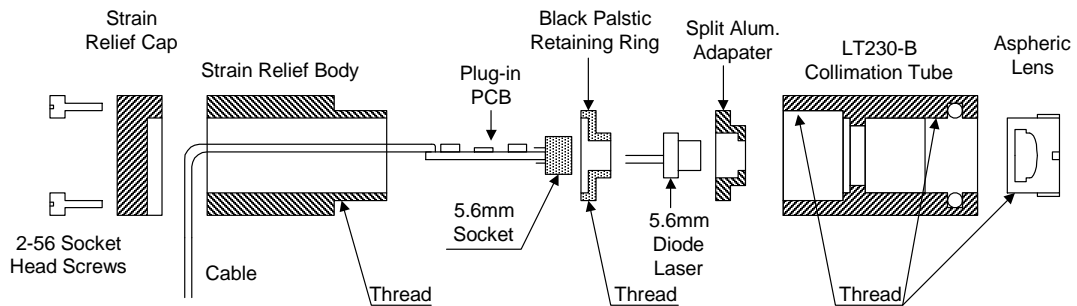

Figure 12: Exploded View of Collimation Tube

---

* The aluminum adapter and retaining ring are for use with 5.6 mm diode lasers. Included with your laser is a different retaining ring that can be used with 9 mm diodes if you ever want to try different makes of diode in your laser head. With 9 mm diodes the aluminum adapter is not used.

I.D.4-a. Replacing the Diode

First, turn off the AC power to the Laser Diode Controller. Before removing the diode from the laser you must set up an electrostatically safe place to work. This should include a grounded table surface and a grounded wrist strap.

Diode lasers are easily damaged by electrostatic voltages.

Loosen the two setscrews on the side of the collimation tube holder (see Figure 7) and slide the collimation tube out of the holder.   Remove the three 2-56 socket head cap screws from the strain relief cap and set the cap and screws aside. Unthread the strain relief body from the collimation tube and slide it over the cable. Do not allow the cable to twist with the strain relief body, but keep it fixed with respect to the collimation tube. You will have to unbend the cable somewhat to slide the strain relief body over it. Unplug the PCB and socket from the diode.
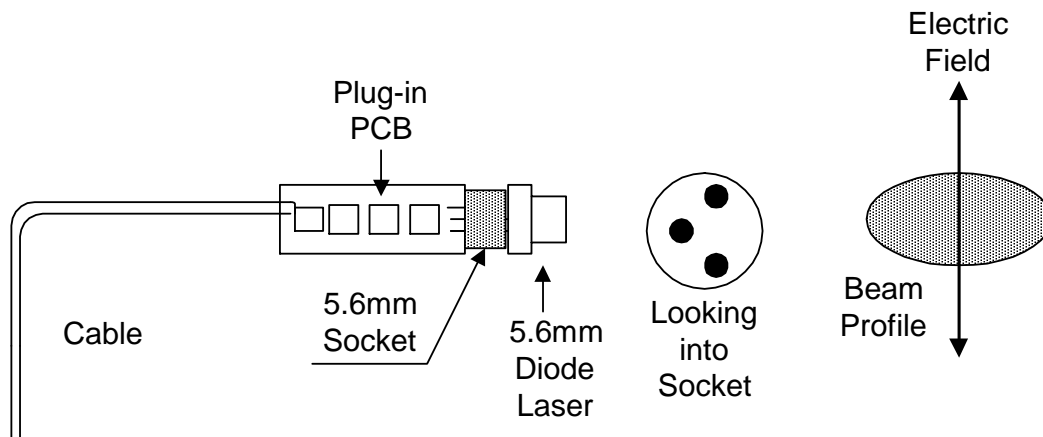

Figure 13:   **Diagram showing relation between cable bend, diode pin out, beam profile and laser light polarization.**

With the spanner wrench provided, unthread the retaining ring from the collimation tube and remove the diode laser and adapter. Place the old diode aside, perhaps in a bag marked, "old diode", and remove the new diode from its bag. Put the new diode into the collimation tube. Place the diode into the adapter. Then, drop the assembly into the collimation tube. The diode-adapter assembly should fit snugly into the tube without cocking. Now, thread the retaining ring into place. Attach the socket and PCB to the diode and screw the strain relief body over the PCB and into the collimation tube. As before, keep the cable fixed with respect to the collimation tube. Attach the cap to the back of the strain relief body. Note: The cap has a cutout to accept the bent cable.

Operating note: Figure 13 shows the relationship between the bend in the cable, the diode pin-out, the beam profile and the laser light electric field direction. In the next section, we will discuss how to orient the laser so that the long axis of the elliptical beam profile is horizontal. In this orientation, the grating provides the maximum resolution as the beam "covers" the largest number of lines in the grating.

I.D.4-b. Setting the Laser Orientation and External Cavity Length

Place the collimation tube assembly in the collimation tube holder and lightly tighten one of the setscrews. The position of collimation tube within the holder determines the cavity length. The major effect of the cavity length is to determine the external cavity mode spacing. (See diode laser physics section) It is found that a short cavity works best.* Position the tube so that there is a 2 to 3 millimeter gap between the collimation tube and diffraction grating. Do not let the collimation tube touch the grating. You need to leave space for the grating to move.

If not already connected, attach the 9-pin cable to the laser head and turn on the AC power to the Laser Diode Controller. The angular orientation of the laser within the collimation tube holder can be determined either by measurement of the polarization direction or observation of the beam profile. Figure 9 showed the setup to observe the beam profile as well as the retro-reflection. Figure 14 shows several images of the beam profile. In image 15c, the glass Neutral Density filter has been placed in the beam path so that the LED light from the diode does not interfere with imaging of the laser light. Turn on the Laser Power and increase the current till the laser is above threshold. Loosen the setscrew and rotate the collimation tube within the holder until the long axis of the beam imaged on the video screen is horizontal. (Figure 14c) You might also notice that two streaky features above and below the image that are from the LED light. Making these streaky lines vertical also sets the correct orientation.

To measure the polarization direction of the beam place a linear polarizer (available only with the complete optics package) after the glass ND filter and turn the polarizer until a minimum intensity image is observed on the video monitor. The electric field is polarized 90 degrees to the direction indicated on the polarizer.
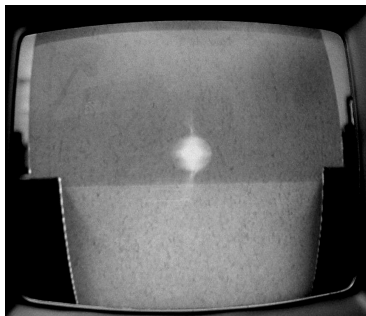

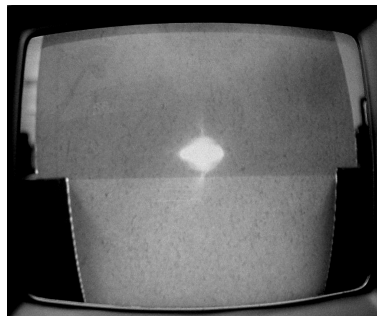**Figure 14a: Laser Beam with laser current *below* threshold, Only incoherent LED light is visible.**

Figure 14b: Laser Beam with laser current *just above* threshold, laser light and LED light visible

Figure 14c: Laser Beam with laser current *well above* threshold. An ND filter has been placed between laser and viewing screen, only laser light is visible

---

* There exists a "magic" cavity length for which, as the angle of the grating is changed, both the wavelength diffracted by the grating and the wavelength of an external cavity mode, (determined by the cavity length), change at the same rate with angle. This distance can be determined from the diffraction angle and distance from the grating pivot point to the center of the beam spot on the grating. For the TeachSpin laser head this distance is about 0.58 inches (=14.7mm).   This would seem to promise extremely long mode-hop-free scans. Unfortunately, the presence of internal cavity modes in the diode itself destroys the potential of long scans. (See Diode Laser Physics Section) A diode with an antireflection (AR) coating on its output facet would have no internal cavity modes and should show these long scans. The cost of AR coating a diode ($2,000.00) has precluded any investigations by TeachSpin.   We would be interested in hearing from anyone who has access to or has tried diodes with an AR coating.

I.D.4-c. Adjustment of Lens Position

Optimal alignment of the diode laser involves adjustment of the lens position within the collimation tube. We have found that proper lens position is crucial for obtaining long mode-hop-free scans of the laser. When installing a new diode, we have found that you have to adjust the lens position about half of the time. For some of the new diodes, the old lens position will work just fine. To determine whether the lens position needs to be adjusted, we observe the laser behavior as we scan with the piezo only (no current scan) through the rubidium absorption features. If, after careful external cavity alignment, you can sweep through the first three absorption features (87b, 85b and 85a) (See the diagram in Initial Setup section 27.), then the lens position is fine. If on the other hand you find that you cannot make a nice long sweep, the lens position may need adjustment.

Operating note: During the following procedures you will be turning the laser current on and off while you adjust the lens position. To adjust the position you will be looking almost directly into the output of the laser. We strongly urge you to exercise extreme caution and use proper laser safety. Keep your laser safety goggles on and always check that the laser current is set to zero and that the laser power has been turned off before you check the lens position.

I.D.4-c.1 Coarse Lens Adjustment: If you are installing a new diode into a collimation tube that has been previously used, you may skip the following step. Usually, this step is only necessary if you are installing a new collimation tube or if the lens position has been grossly misadjusted. Coarse adjustment involves collimating the laser beam so that the beam size does not change with distance. Turn the laser power on and adjust the laser current above threshold. Use the IR viewing card or the viewing screen, CCD camera, and TV monitor to observe the spot size first near the output of the laser and then at a point several meters away.   If the beam size changes, use the spanner wrench to adjust the lens until the beam is collimated.

I.D.4-c.2 Fine Lens Adjustment: Fine lens adjustment involves measuring the threshold current as a function of the lens position. At the optimal lens position, the threshold current is a minimum.   The following steps need to be repeated until the minimum threshold current is found: Align the external cavity and measure the threshold current (section I.D.2-b&c). Remove the grating (section I.D.3-a). Adjust and record the lens position (I.D.4-c.3). Reinstall the grating (I.D.3-b). Align the external cavity and then measure the new threshold current. You may be tempted to remove the collimation tube from the tube holder, adjust the lens position and then reinstall the collimation tube in the holder, thus skipping the removal and installation of the grating. However, the threshold current is a strong function of the electric field polarization direction and we have found it difficult to reinstall the collimation tube in a repeatable manner. This is why we favor the above procedure. When reinstalling the grating, it is not necessary to set the beam height or contact the piezo stack with the ball tipped setscrew. These steps need only be done at the end, once the correct lens position has been determined. However, you should attempt to install the grating holder in a reproducible manner, pressing the grating holder against the 6-32 cap screws before tightening the screws as shown in Figure 11.

I.D.4-c.3 The lens position may be determined by a mark that has been placed on the end of the collimation tube near one of the spanner wrench keyways. See the picture in Figure 15. Figure 15 also shows a series of measurements that were taken as a function of lens position. The pictures show the relative position of the mark and keyway. You should realize that the mark stays fixed as the lens and keyway are rotated, though the picture appears to show the opposite. You should notice in the picture that we are making very small changes in the lens position, only a few degrees, and that the threshold current is changing by a milliamp or less.
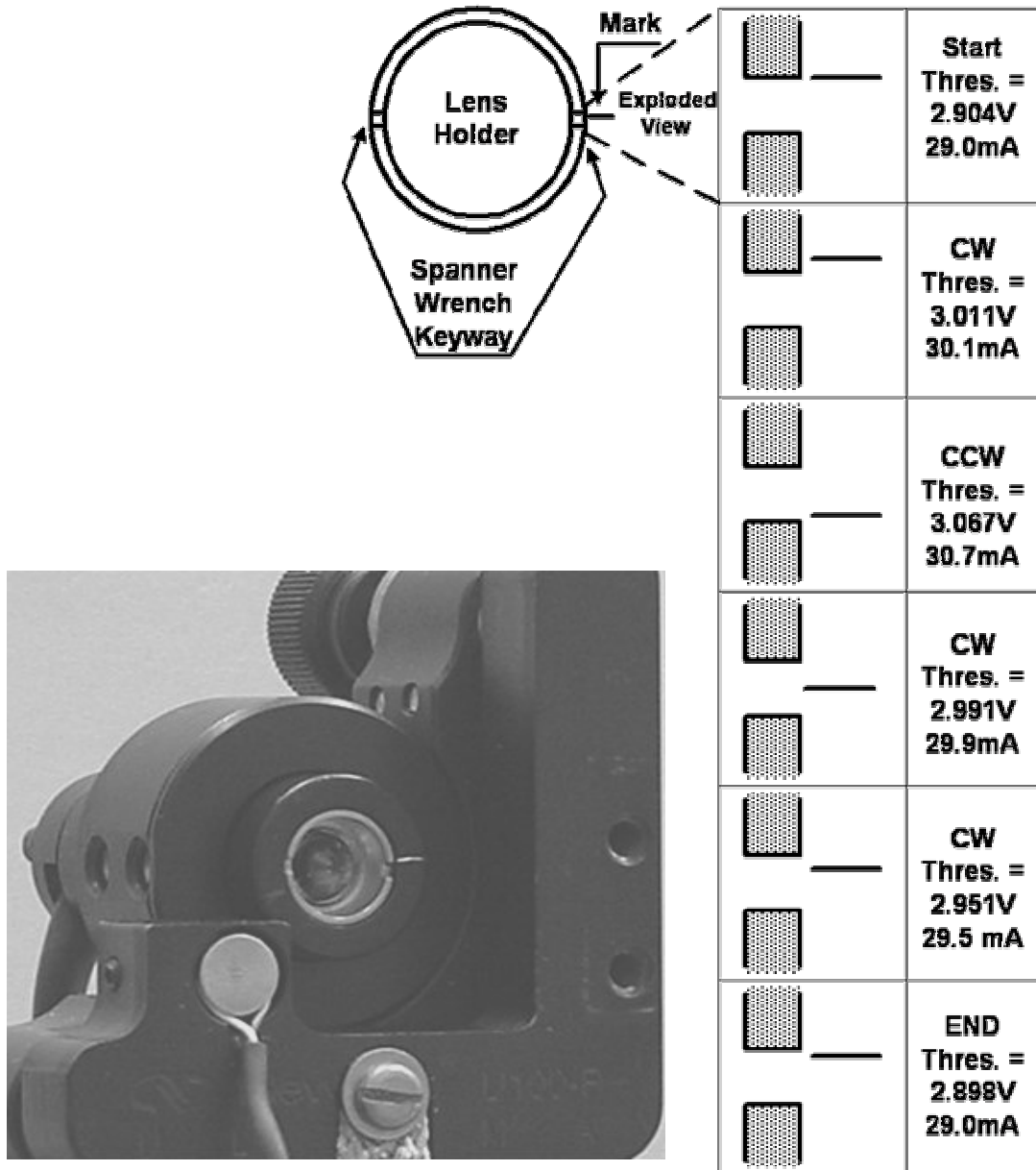

Figure 15: Picture of Scratch Mark on Collimation Tube and Diagram Showing Threshold Current Measurement as a Function of Lens Position.

I.E. PIEZO STACK

The piezo stack is an NEC / Tokin model AE0203D04, which has a nominal displacement of 3 μm at 100V. The piezo stack is polarized and voltage of only one polarity should be used. The stack is sandwiched between two metal plates. A setscrew contacts the bottom metal plate from the side and holds the stack in the movable portion of the mirror mount (See Figure 7). A ball tipped setscrew in the grating holder contacts the piezo stack. When voltage is applied to the piezo stack the ball tipped setscrew transmits the motion of the stack to the holder and grating, changing the grating position. Both the distance from the grating to the laser (the cavity length) and the angle of the grating are changed by the expansion and contraction of the piezo stack.

I.E.1. Electronics

Voltage is applied to the piezo stack through the 9-pin cable. The PIEZO CONTROLLER module in the electronics box adjusts the voltage applied to the stack.

Piezo Displacement	3.0 μm ± 1.5 μm @ 100 Volts
Piezo Maximum Voltage	150 volts
Piezo Frequency Response	DC to 1 kHz
DC OFFSET COARSE FINE	 Ten turn 0 to 100 Volts Single Turn 0 to 2 Volts

MODULATION INPUT
Input Impedance
ATTENUATOR
	1 V input = 5 V across piezo stack
	    10 kΩ
	    Reduces MOD. Input

MONITOR OUTPUT
OUTPUT OFFSET
	1/10th of voltage across stack
	    Changes DC level of monitor voltage 0 to -5V,
	    does not change piezo stack voltage

The voltage applied to the piezo stack is the sum of the voltage set by the DC OFFSET controls and the voltage from the modulation input. To avoid overdriving the stack, both positive and negative voltage clamps have been built into the electronics. These are +110V and -6V respectively. When used with the triangle wave from the Ramp Generator, the clamps may clip the triangle wave at the top or bottom, depending on the DC OFFSET of the Piezo Control. Thus, it is essential that you monitor the output on an oscilloscope.   The maximum amplitude change, when using the 10 V p-p Ramp output, is 50 Volts

The DC OFFSET FINE control and OUTPUT OFFSET are only needed when side locking the laser to a spectral feature. In normal operation, both these controls should be set to zero.

I.F. RAMP GENERATOR

The Ramp Generator provides a bipolar variable amplitude and frequency triangle wave. The frequency may be changed from 1 mHz to 7 kHz. The maximum amplitude is 10 Volts peak to peak, (plus and minus 5 volts about ground). The highest frequency output of the generator is 7 kHz. (Though the dials would lead you to believe that 10 kHz was the highest frequency.) At frequencies of 1 kHz and higher, the high frequency Fourier components of the triangle wave are attenuated and you will observe a "rounded" triangle wave.

The high frequencies have little use in taking data and are only used to investigate the frequency response of the Piezo and Current controller. The long sweep times were incorporated for use in slow temperature sweeps of the laser. The reset toggle switch stops the triangle wave generator and takes the output to the minimum value. This is useful in starting and stopping slow sweeps. The reset can also be used to disable the sweep. This is useful when you are trying to observe the fringes while setting up an interferometer. The SYNC output provides a -5 to +5 volt square wave that can be used to trigger an oscilloscope.

Ramp Generator Noise: The rms noise on the ramp generator output is about 50 μV rms. If you use the Ramp Generator to provide a simultaneous Current and Piezo sweep of the laser frequency, while observing very narrow Doppler-free features (12 MHz or less), the lines will be slightly broader than when doing only a Piezo sweep. If you wish to observe very narrow Doppler-free features, you should use the Ramp Generator to sweep the Piezo only!

II. Photodiode Detectors and detector/low pass/dc level Electronics

II.A. PHOTODIODE DETECTORS

Photodiodes	Photonic Detectors Model PDB-C108
Active Area	0.25" Diameter Circle
Responsivity	about 0.6 A/W (1.7 W/A) at 800nm
"Gain"*	10 MΩ to 333 Ω

The photodiode detectors contain a current to voltage converter. The switch on the back of the detector allows gain setting of 10 MΩ to 333 Ω in ten steps. Table 3 lists the high frequency 3dB points and noise for the different detector gains. The detectors have separate signal and power cables. Three detector power plugs are on the front panel. The signal is on the coax cable with BNC connector. The polarity of the signal is negative. If you plug the signal into an oscilloscope, the signal will be from 0 to -11.0 Volts. The detector voltage saturates at about -11 volts. **You should adjust the gain of the detector so that you are not near the saturation voltage.**

Gain	High Frequency 3dB.	Noise*
10 MΩ	5.8 kHz	1.57 μV / Hz$^{1/2}$
3.3 MΩ	10.3 kHz	0.90 μV / Hz$^{1/2}$
1.0 MΩ	20 kHz	0.42 μV / Hz$^{1/2}$
330 kΩ	28 kHz	0.20 μV / Hz$^{1/2}$
100 kΩ	54 kHz	91 nV / Hz$^{1/2}$
33 kΩ	88 kHz	48 nV / Hz$^{1/2}$
10 kΩ	165 kHz	24 nV / Hz$^{1/2}$
3.3 kΩ	260 kHz	16 nV / Hz$^{1/2}$
1.0 kΩ	480 kHz	13 nV / Hz$^{1/2}$
330 Ω	720 kHz	13 nV / Hz$^{1/2}$

Table 3: Photodiode Detector Parameters

* Measured in 3 Hz to 44 kHz. frequency range.

At high light intensities the response of the photodiodes becomes non-linear. (A doubling of the light intensity gives an output voltage that is less than double.) This occurs at an output current of about 0.5 mA. If you wish to use the photodiode as a power meter, you should make sure that the light current is below this value. If it is not, place a ND filter in front of the photodiode. Students will need to calibrate the Neutral Density filters using the photodiode detectors at low laser light levels.

---

* The current to voltage converter gain has units of ohms. $I_{IN} = V_{OUT} / R_{GAIN}$, from which the input power can found using photodiode responsivity (0.6 Amps/watt) .

II.B. DETECTOR / LOW PASS / DC LEVEL ELECTRONICS

Detector electronics on the front panel allow for conditioning of the signals. The BALANCE controls are two, input attenuating, potentiometers that can be adjusted to balance two signals from the photodiode detectors. The internal instrument amplifier can be used to take the difference of the two signals with a GAIN from 1 to 100. Table 4 lists the gain and high frequency 3dB point.

Gain	3dB. Freq. (Hz)
1	1.3 M
2	1.0 M
5	780 k
10	650 k
20	470 k
50	220 k
100	110 k

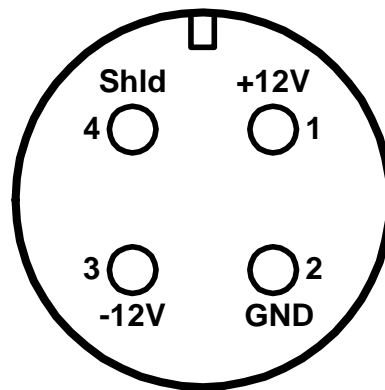**Table 4: High Frequency Response of Detector versus Gain**

Figure 16: Detector Power Pin-out (looking into connector on front panel

The LOW PASS filter and DC LEVEL controls are provided for side locking the laser to a spectral feature. The single pole low pass filter has switch selectable time constant from 10 µs to 0.1 seconds. The DC LEVEL has a ten-turn potentiometer that provides a DC offset from minus five volts to plus five volts.   For positive offset voltages, the voltage may be read off the dial directly. For voltages less that zero the voltage is found by subtracting ten from the number displayed on the dial. (9.0 dial = -1.0V, 7.2 dial = -2.8V). There is a final DC gain stage of 1 to 30 after the DC level adjustment. There are monitor outputs after the first difference and gain stage, and after the low pass filter. These can be used to record data or to check the function of the different sections.

III. Absorption Cell Assembly

The absorption cell assembly consists of an outer glass cylinder, several melamine foam insulation and support pieces, the heater assembly, a type T thermocouple sensor, a cold-finger, and the Rb cell. The heater is an aluminum cylinder about which is wound a bifilar heater wire. The heater has a resistance of about fifty ohms (50 Ω). Wires from the heater and thermocouple plug into the back panel of the electrical box.

III.A. SPECIFICATIONS

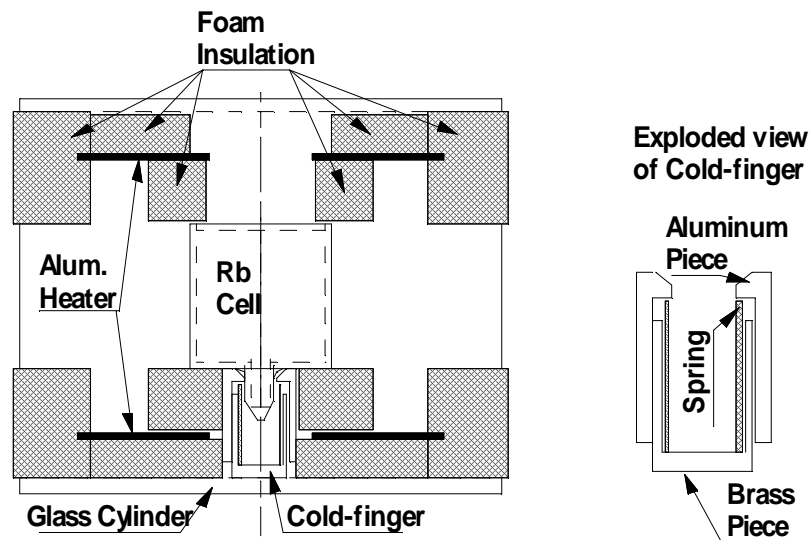|	
Maximum temperature	≈ 90 °C
	≈ 140 °C with ½" hole foam inserts
Temperature differential across Cell	
T= 50°C (min. on bottom max. on top)	10 °C
	2.0 °C with ½" hole foam inserts
Heater resistance	≈ 50Ω
Temperature Controller	1 Hz PWM* PID
Controller Resolution	0.1 °C
Regulation (no air currents)	0.2 °C
Rubidium Cell	25 mm Diameter and 25 mm Length natural isotopic Rb. (no buffer gas)

Figure 17: Cross section of Cell Heater Assembly

---

* PWD means Pulse Width Modulated output voltage (pulse rolled off with a maximum frequency of 1 kHz.), PID is Proportional, Integral, Derivative control algorithm.

III.B. CELL HEATER AND COLD-FINGER

III.B.1. Description

A cross sectional view of the Cell Heater is shown in Figure 17. The spring loaded cold-finger makes contact between Rb cell tip and the outer glass cylinder.   A white piece of thermal adhesive is placed around the cell tip to increase the contact area between the cell and cold-finger. The thermocouple temperature sensor has been placed between the cell and the foam near the cell tip. The junction is soldered together and the wires are covered with black heat shrink tubing.

III.B.2. Removal of Cell Heater and Cold-finger

To remove the cell and cold-finger, first turn off the power and let the unit cool to room temperature.

Loosen the Nylon setscrew on the side of the rotatable cell mount and remove the heater assembly with attached aluminum holder from the base. Set the assembly on the table. We will describe the removal of the cell and cold-finger while leaving the glass cylinder attached to the aluminum holder.

Remove the foam ends caps. When you remove the end cap with the wires for the heater and thermocouple (TC), the TC will come out with the end cap. Slowly push the foam and cell assembly out of the glass cylinder. Push towards the end where the heater wires come out. Be prepared to catch the bottom of the spring loaded cold-finger as it clears the end of the glass cylinder when the assembly is half way out.

When the foam and cell assembly is out of the glass cylinder, remove the remaining piece of the cold-finger. This is the aluminum piece that contacts the rubidium cell at the tip. You may need a pair of tweezers to pull this piece out of the foam.   Now push the Rb cell and foam support piece out of the aluminum heater. This completes the removal.

III.B.3. Installation

Installation is the reverse process of removal. Put the cell into the foam support piece. It is easy to tear the foam so be gentle. The small hole in the support piece is for the tip, and the larger hole is for viewing. Slide the cell and foam support into the aluminum heater. The large hole in the aluminum heater is for the cold-finger and the smaller hole is for the viewing window. Note, there is a little area of aluminum heater exposed around the viewing window; this is to keep the viewing window hot and prevent Rb metal condensation.

Place the aluminum cold-finger in the foam support piece so that it covers the cell tip. You should notice that the cold-finger pieces have been machined to fit the curve of the cell.

Slide the assembly into the glass cylinder. When the assembly is half way in, insert the spring and brass part of the cold-finger. Adjust the cell and foam pieces so that the cell is centered in the heater and also centered in the viewing window. Place the thermocouple sensor next to the cell just under the foam support near the cold-finger. We suggest that you keep the viewing window and cold-finger horizontal (Viewing window on one side and cold-finger on other.)

Figure 18: Insertion of Cold-finger into Cell Assembly

III.C. THERMOCOUPLE POSITION AND TEMPERATURE

There is a significant thermal gradient across the cell of about 10 °C at a set point of 50 °C. The thermal gradient is mostly vertical with the bottom cooler and the top hotter. The density of rubidium in the cell is determined by the temperature of the pool of excess rubidium that condenses in the tip near the cold-finger. If you need to have a reasonably accurate measure of the rubidium density, you should check that the thermocouple is placed close to the cold-finger. (For most experiments the exact temperature is not important) We have included some foam inserts that may be placed in the foam end caps for higher temperature operation.

III.D. CONDENSATION OF RB ON THE CELL WINDOWS

Rubidium metal condensed on the cell windows creates a silver, mirror-like layer on the inside of the cell. This reflects part of the laser beam and can lead to confusing results. Because there is a vertical temperature gradient across the cell the first condensation will probably be on the lower portion of the windows. The heater assembly has been designed to keep any excess Rb metal in the cell condensed in a hidden tip rather than the end windows. To accomplish this, equal areas of the aluminum heater must be exposed at each end of the assembly (See Figure 16 on page 5-25). If you notice Rb condensing on just one of the end windows of the cell, adjust the cell and foam support to expose slightly more of the heater on the side where the Rb is condensing. (Push gently on the foam and cell from the side where the metal is condensing.) See the addendum at the end of this section for detailed instructions on how to transfer the Rb from the end windows to the tip.

III.E. CELL TEMPERATURE CONTROLLER

III.E.1. Operation of Cell Temperature Controller

The Omega temperature controller is mounted on the front panel. (A manufacturer's manual for the controller has been included.) Reading from left to right across the face of the unit, the four keys used to program the controller are: MENU, UP, DOWN and ENTER. When the controller is in the normal or RUN mode, the temperature is displayed in degrees Celsius. Under normal operation, you will be changing only the temperature set point. In the RUN mode, the controller will display the current temperature. To get into the Configuration Mode, press the MENU key once. SP1 will be displayed. Now, press the ENTER key. The display will show the current "Setpoint1." Use the UP and DOWN arrow keys to change the value. Once the correct value has been selected, press the ENTER key again to store the value. The display will show "StRd" briefly indicating your value has been registered. Return to the MENU key and continue pressing until RUN is displayed.

III.E.2. Configuration of Cell Temperature Controller

The configuration of the controller has been done by TeachSpin. Unless the controller has been accidentally reset you should not need to change the configuration. The Instrument Configuration list, at the end of this section, includes only those items that have been changed by TeachSpin. The value in parenthesis is the main menu heading under which the changed settings are located. All other values are the factory default. See page 62 of the Controller Manual for details and additional explanations.

To change the Proportional, Reset or Rate values, enter the Instrument Configuration mode by pressing the MENU key until CNFG is displayed, and then press ENTER. Using the MENU key, scroll through the various options until OUT1 (Output 1) is displayed, then, press ENTER. Again scroll through the options with the MENU key until the CTRL option is displayed and ENTER.   Use MENU to set the CTRL to PID and ENTER.

Now that you are in the Configuration mode, use MENU to scroll until PROP, REST or RATE is displayed. Press ENTER, then use the UP and DOWN arrow keys to change the value of the selected parameter. Press ENTER again to save and store the value. Once all changes have been made, use the Menu key to return to RUN mode. Please refer to section 3, page 15, of the controller manual for a complete description.

Instrument Configuration List for Temperature Controller

Set Point 1 (SP1)	50.0
Input Type (INPT)	TC = t
Temperature Unit (RDG)	TEMP = C
Filter (RDG)	FLTR = 16
Control (OUT1)	CTRL = PID
Proportional Value (OUT1)	PROP = 005.8
Reset Value (OUT1)	REST = 0480 (Seconds)
Rate Value (OUT1)	RATE = 090.0 (Seconds)
Cycle period (OUT1)	CYCL = 0001
Damping Value (OUT1)	DPNG = 0005

We have chosen the PID values (P = Proportional, I = Integral (reset), D = Derivative (rate)) for reasonable temperature stability without the extra 1/2" hole foam inserts in place.

III.F. MAGNETIC FIELD COILS

The Helmholtz magnetic field coils were designed to provide a field of about 10 mT at a current of three amperes (3.0 A). The average radius of a coil is 3.44" (87.4 mm). There are 320 turns of 18 gauge copper wire on each coil (16 turns per layer and 20 layers). The room temperature resistance of each coil is about four ohms (4 Ω).   The terminal block on the side of the cell holder can be used to connect to the coils. You will have to provide your own power supply to energize the coils.

For the Helmholtz configuration we estimate the field in Gauss from,

$$B \text{ (Gauss)} \approx 0.9 * N \text{ (turns per side)} * I \text{ (A)} / R \text{ (cm)}$$

IV. Optics

Table 5 lists the optical components included in the complete instrument. The thin film components (Wratten neutral density filters, linear polarizers and quarter wave plates) can be damaged by the full power of the laser*. You should attenuate the beam before sending through one of these components.

OPTICS	SOURCE	STOCK NUMBER	MATERIAL	FLATNESS λ / INCH	OTHER
Mirrors (protected aluminum)	Thor Labs	ME1-G01	Float Glass	$< 5\lambda$	Scratch/ Dig 60 - 40
Beam Splitter 50/50 NIR	Edmunds Optics	Y45-853	BK7	$1\ \lambda$	Scratch/ Dig 60 - 40
Beam Splitter 2° Wedge	Red Optronics	RWP 101	BK7	$\lambda/4$	Scratch/ Dig 60 - 40
Beam Splitter 1° Wedge	Red Optronics	RWP 10X	BK7	$\lambda/4$	Scratch/ Dig 60 - 40
Beam Splitter 0.0° 1/4 " thick	Rolyn Optics	55.1025	Pyrex		Scratch/ Dig 80 - 50
Neutral Density Filter Glass	Thor Labs	NE10B	Schott NG4	$1\ \lambda$	≈15% trans. @ 780 nm.
Wratten Neutral Density Filter	Kodak	EK141 0042 filter #96	Gelatin ND 0.7		≈33% trans. @ 780 nm.
Linear Polarizer	American Polarizer (3M)	98-0440-0968-0	HN-32 0.03"		≈42% trans. @ 780 nm.
Quarter Wave Plate	American Polarizer (3M)	98-0440-1064-7			

Table 5: Optical components

---

* We have only noticed damage when using the laser at high current **without** the grating attached. There we have damaged both linear polarizers and the Wratten neutral density filters. You should be very careful using these components for this laser configuration. But this is not the normal mode of operation. When operating with the grating attached to the laser we have not noticed any damage, but we do observe some rather strange behavior at higher powers. (See discussion in section IVC on page 5-30))

IV.A. MIRRORS

Economy mirrors from Thor Labs have a reflectivity of about 85%. We have noticed no effects of the rather poor surface flatness of these mirrors in the interferometer setups.

IV.B. BEAM SPLITTERS

The NIR 50/50 Beam splitter has been coated so that the reflection and transmission are both about 50%. You should be aware that this is for unpolarized light and that there will be some polarization dependence. The other three beam splitters are uncoated pieces of glass. There will be reflections from both the front and back surfaces of the glass. With the wedged beam splitter, it is not easy to determine which surface a particular beam is coming from. It is sometimes easier to use a visible laser to identify the beams. The amount of reflection will also be polarization dependent.

IV.C. NEUTRAL DENSITY (ND) FILTERS

All the ND filters are absorptive rather than reflective. The glass ND filter can be used with any laser power. The thin film Wratten ND filters should only be used with low power laser light (2 mW or less). At laser powers up to 30 mW, there is no permanent damage to the filters. However, above 2 mW of laser power, we start to notice transient effects. The power transmitted fluctuates by about 0.5% in a way that is reminiscent of a damped harmonic oscillator with a time constant of tens of seconds. This is also true of the linear polarizers.

IV.D. LINEAR POLARIZER IN ROTATABLE MOUNT

The linear polarizers have been marked such that when the tick mark is at 0° the light transmitted by the polarizer has a vertically polarized electric field. The mark should be accurate to ±5°. Figure 19 shows the amount of light transmitted by the polarizer. The linear polarizers work well at laser powers of 2mW and below. At powers between 2 mW and 30 mW, they show transient behavior. With laser powers above 30mW, they can be permanently damaged
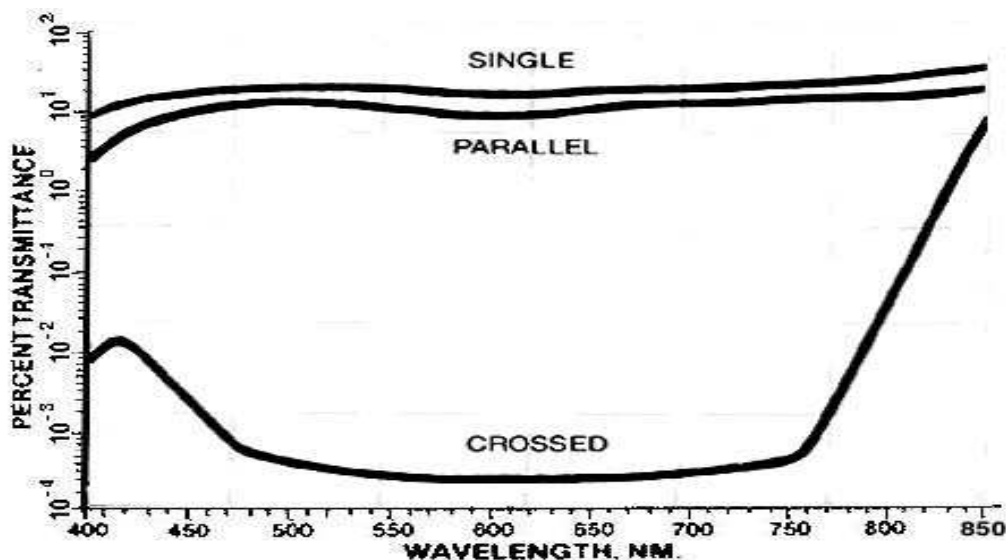

Figure 19: Percent Transmittance of Linear Polarizers

IV.E. QUARTER WAVELENGTH PLATE IN ROTATABLE MOUNT

Diameter 50 mm, "optical thickness" 200 ± 5 nm: When properly oriented, the quarter wave plate allows linearly polarized light to be converted to circularly polarized light. The plate has two optical axes (at 90 degrees to each other) with different indices of refraction along each axis. Light travels at different speeds along each axis. The axes are called the "fast axis" and "slow axis". To produce circularly polarized light, monochromatic, linearly polarized light is placed incident to the plate at 45° to each axis. If the plate is of the correct thickness, then the phase lag along the slow axis causes the light exiting the plate to be circularly polarized. The "optical thickness" of the plate may not be the desired value.

Tuning the optical thickness (retardation) can be accomplished by rotating the plate about the vertical axis.   Rotation about the slow axis increases the retardation, and about the fast axis decreases it.   See Figure 20. This tuning method requires either the fast or slow axis to be aligned vertically.
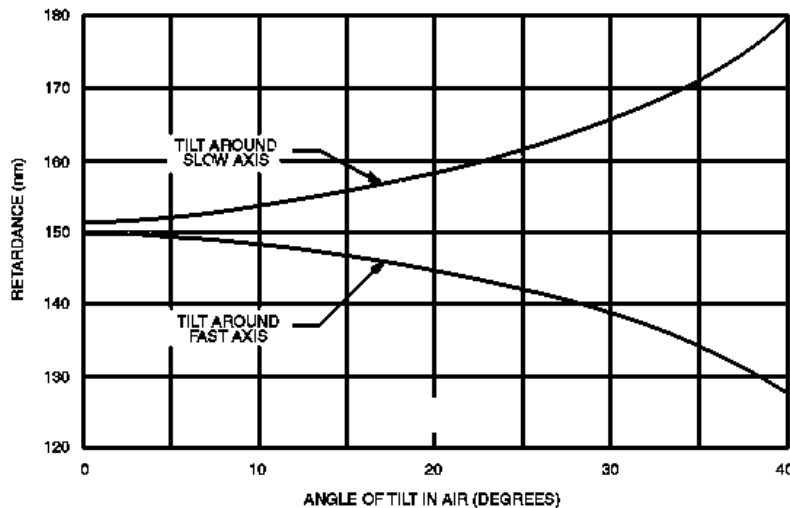

Figure 20: Tilt Tuning of Quarter Wave Plate

IV.F. ASSEMBLY AND CARE OF OPTICAL COMPONENTS

Loading optical elements into mirror mounts: You will have to place the various optical components into the mirror mounts. It is best to do this without touching the components with your fingers. If you must touch the components, wear protective gloves and touch the components only at the edges.

V. TV Monitor and CCD Camera

V.A. THE TV MONITOR

The TV monitor was shipped with its wall mounted AC to DC power supply in the box. The TV requires 12 V DC at 850 mA. The CCD camera power supply (12 V DC at 250 mA) plugs into the red plug on the cable attached to the back of the camera. The yellow plug on the same cable is the video output, which plugs into the back of the TV monitor. We have included an extension video cable for the camera and there may be an adapter plug attached to the extension cable, to make the cable compatible with the video input on the back of the TV.

VB Camera focus

V.B. CAMERA FOCUS

The CCD camera focus may be adjusted by turning the lens on the front of the camera. You may have to loosen a small setscrew to do this. The camera has an automatic gain control so that it adjusts to low and high light levels. To get a nice image on the TV monitor, it is often necessary to adjust either (or both) the background room light and laser intensity. Use the neutral density filters to adjust the laser intensity. This is particularly true if you are trying to image the laser beam profile or when you are looking for fringes while lining up an interferometer.

VI. Addendum

VI.A. CONDENSING RUBIDIUM IN THE TIP

When operating the cell at elevated temperatures (above the "normal" 40 – 50 °C.) it is possible that excess rubidium may move out of the cooled tip and condense on the windows. The following procedure may be used to evaporate the Rb off the windows and condense it back in to the tip.

1. Place the foam inserts into the open ends of the cell heater as shown in the figure below. (The smaller foam plug was only included in Diode Laser's with serial numbers DL154 and greater. If you have an earlier model Diode Laser, just use a piece of foam or insulation to block the opening in the cell heater.)

2. Increase the cell temperature set point to about 120 °C. The exact value is not important. See section A8-5 and A8-6 for details on cell temperature controller.

3. Let the cell heat up and stay hot for about 1 hour. (You can remove the foam plugs quickly and check to see if all the Rb has moved off the windows.)

4. After the Rb has been evaporated off the windows, return the cell temperature set point to its usual operating point (40 – 50 °C). Leave the foam plugs in place as the cell cools! This is critical. The windows must be kept warm to assure that the Rb will now condense in the tip.

5. Once the cell cools, the plugs may be removed and the cell heater returned to normal operation. If you are doing high-temperature experiments, it is always advisable to put the plugs into the open ends of the cell before turning off the power to the heater. This will prevent Rb from condensing onto the end windows as the cell cools.
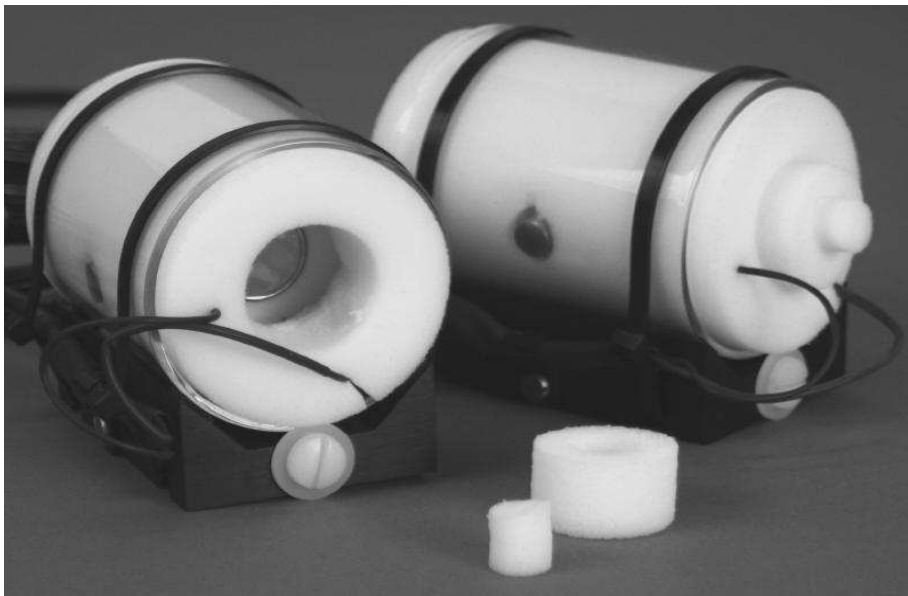

Figure 21: Cell assembly showing placement of foam plugs

APPENDIX

CONCEPTUAL INTRODUCTION to DIODE LASER SPECTROSCOPY

THINKING ABOUT SATURATED ABSORPTION and CROSSOVER TRANSITIONS

A Brief Introduction to Diode-Laser Spectroscopy

The ideal spectroscopic experiment would involve illuminating a free and unperturbed atomic system with perfectly monochromatic light, and then seeing what happens, to the light and to the atom, as a function of the frequency of the light. And nowadays it's feasible for undergraduates to get hands-on experience of this very scenario in a tabletop, real-time experiment.

The nearly-ideal monochromatic light comes most conveniently from solid-state diode lasers, mass-produced for the needs of the optical data-storage industry. The first technology to be commercialized, using aluminum gallium arsenide (AlGaAs) semiconductors, led to the establishment of the near-infrared 785 nm standard for CD readout. Such laser diodes are physically small, and need only a DC power supply to produce useful ($\approx$10-mW level) optical output. But astute physicists realized that the output wavelength could be varied by changing the laser's temperature, and further fine-tuned by changing the DC current operating the laser. Thus was born a wonderfully convenient spectroscopic light source.

To what atomic system might it be applied? Photons of wavelength 785 nm each convey an energy of only 1.58 eV, insufficient to excite most atoms from their ground states even to their lowest excited states. The exceptions are alkali metals, particularly rubidium (Rb) and cesium (Cs). In fact, rubidium's lowest excited states are split (by the spin-orbit interaction) into states accessible from the ground state by photons of wavelengths 780 and 795 nm.

Now these alkali metals are fiercely reactive to air or water, but compatible with glass, which brings up another convenience. A simple glass cell, evacuated and permanently sealed, with a bit of the solid metal inside, creates a great environment for spectroscopy. Light can get in and out through the glass, and (for temperatures in the range 20 - 50 °C) the metal will co-exist with its own vapor, in the form of a gas of freely-flying atoms of just the range of densities convenient for spectroscopic experiments.

Now it's time to imagine such an experiment -- what will happen when 785 nm light shines into such a cell? Answer: nothing at all; the light flies right through, because its wavelength is *not* resonant with rubidium atoms' allowed transitions at 780 and 795 nm. So the laser needs to be *tuned* to reach the resonant condition. In practice, this works through a hierarchy of mechanisms:

- 0) is to pick the right semiconductor;
- 1) is to hold the laser at the right temperature;
- 2) is to vary the current driving the diode-laser emission;
- 3) is to use a diffraction grating to create optical feedback into the laser, selectively for the desired wavelength;
- 4) is to use a piezoelectric element to tilt the grating ever so slightly.

In fact, mechanisms 2) and 4) are both electrically actuated, so it's possible to treat a working diode-laser system as a black box, with a variable control voltage going in, and a voltage-dependent optical wavelength coming out.

1

The application of a sawtooth waveform to this 'black box' will give an output beam whose optical frequency also undergoes a sawtooth in time, i.e. it scans up and down in optical frequency. And it's easy to accomplish the whole scan every 10 - 100 ms, so the laser's frequency is agile as well as variable.

Now it's rarely possible to get a diode-laser system to scan over any very long interval in wavelength -- even a scan from 780 to 795 nm for rubidium spectroscopy would be asking too much. In fact, it's time to think in terms of optical frequency instead -- such a scan would extend from 384,000 GHz down to 377,000 GHz. (Recall 1 GHz = 1000 MHz = 10^9 optical cycles per second.) In the simplest diode-laser systems, it's feasible to sawtooth-scan over only about 10 (not 7,000) GHz of optical frequency, which is only about a 30 part-per-million variation in frequency. Clearly, you want this relatively narrow scan to include the 780-nm target wavelength -- but once it does, what a wealth of spectroscopic information waits to be revealed!

How will it show up? The two mechanisms most easily displayed are absorption and fluorescence.

Absorption: that's the removal of energy from the beam of laser light as it passes through the cell. The exiting beam's power is easily measured, by conversion to an electrical current in a 'solar-cell' sort of photodiode, and it's easy to arrange a real-time oscilloscope display which shows transmitted power (on a vertical scale) as a function of the diode-laser's frequency-control voltage (a surrogate for its frequency, on a horizontal scale). Absorption will be indicated by a local *drop* in the amount of transmitted power. The process is easy to see, since fractional absorptions of 10 - 50% are easily achieved -- but only at the right wavelength!

Fluorescence: that's the production of light from inside the cell. For, if absorption happens, then assuredly energy is being removed from the light beam, transferred to the atoms as they are elevated to excited states. Since these atoms are in free flight in vacuum, there's no way for them to give up that energy except by 'radiative decay' -- they emit (in about 25 ns, on average) a photon of light in reverting to the ground state. These photons emerge in directions random with respect to the incident laser beam; in fact, a whole thread of atoms inside the cell, lying in the volume of the laser beam, *glows* as it emits into all directions this 'resonance fluorescence'. You can't see it by eye, only because your eyeball's sensitivity is so poor at these wavelengths. But simple solid-state CCD cameras have full sensitivity in the near infrared, so a monitor's display of the camera's view of the cell will image this fluorescence for you in real time.

One of the instructional pleasures of the diode-laser system is that the correlation of absorption and fluorescence can be seen in real time -- all that's needed is a slow scan in frequency over the resonance region, which will show that it's when (and only when) the transmitted power diminishes that the atoms are fluorescing.

But the next thing that appears in such scans, slow or fast, is that there are, as a function of frequency, *four* occurrences of absorption and fluorescence, not just one. This can be attributed to two causes:

1. There are two isotopes in natural rubidium, Rb-85 and Rb-87, and they have separate transitions frequencies.
2. Each isotope's atoms have 'two ground states', separated in energy by the tiny hyperfine interaction (the effect, on the valence electron, of the magnetic moment of the nucleus).

And, in fact, these ground-state hyperfine splittings are well known -- commercial rubidium atomic-frequency standards operate at the 6.834 GHz frequency corresponding to the energy difference between the two Rb-87 ground states. So that knowledge provides one way to calibrate the frequency scale along which the diode laser is being scanned. (There are direct optical methods for checking this calibration, such as unequal-arm Michelson interferometry, or the use of a Fabry-Perot resonator.)

Page 5 shows a detailed energy level diagram for the 780 nm, or D2, lines for both Rb-85 and Rb-87. The screen capture below it shows the transmitted power as a function of wavelength. You can match the "dips" to the transitions which caused them. (Our energy level diagram does not include the D1 transitions, which take place at 795 nm. They are the key to the phenomenon of Optical Pumping, another TeachSpin experiment.)

With a calibrated frequency scale, it also becomes clear that the four optical transitions you see are *not* infinitely narrow -- rather, they each have a 'spectral width' of about 0.5 GHz. In ordinary spectroscopy, such 'widths' are nearly always due to the imperfect resolving power of the spectrometer in question, but here it's not so -- the laser can be shown to be monochromatic to better than 0.01 GHz. So what is causing this width? It comes from the fact that the atoms being illuminated are *not* at rest, but instead are free-flying in vacuum. The relevant velocity is that component v_z of the atom's velocity along the direction of the light beam, because that motion causes a Doppler shift of the laser light's frequency. In the rest frame of the atom, the laser frequency is shifted from is lab value f_L to a received frequency of:

$$f_R = f_L (1 - v_z / c).$$

It is only when the received frequency f_R matches the atomic energy-level difference, according to $h\, f_R = \Delta E_{atom}$, that a transition will occur.

So a laser of fixed frequency in the lab frame will pick out only one 'velocity class' of atoms, namely the atoms having the v_z needed according to the equation above, and it will interact only with that class of atoms. Kinetic theory tells us how many atoms should have various v_z-values. In fact, there'll be a Gaussian distribution in v_z, with mean v_z-value of zero, but with mean-square value given by equipartition, according to:

$$(1/2)\, m < v_z^2 > = (1/2)\, k_B\, T$$

And that's why there's a Gaussian distribution in frequency, too, in the curve that gives the intensity of the fluorescence as a function of laser frequency.

3

Even here, the list of things to be observed spectroscopically is not nearly complete. Using the methods of laser spectroscopy, it is even possible to *surpass* the limits of Doppler broadening, and to achieve spectroscopic resolution far better than the 0.5-GHz Doppler width. The method involves splitting the laser beam into a strong 'pump beam' and a weaker 'probe beam', arranged to cross each other, at an angle of nearly 180°, at a location occupied by rubidium atoms. Now with milliWatt levels of optical power available, the pump beam is intense enough to cause a non-trivial depletion of the number of ground-state atoms in the particular velocity class with which it's in resonance. And the probe beam can sense this population depletion, as a decrease in the amount of absorption that would ordinarily occur. But that effect occurs *only* if the pump beam and the probe beam are interacting with the same sample of atoms; and because of the Doppler effect, that can only occur for atoms having $v_z = 0$. By this 'saturated absorption' effect, it's possible to resolve below the Doppler limit, and to see quantum transitions with a spectral width $\Delta f < 0.01$ GHz. This is occurring at a laser frequency $f \approx 384,000$ GHz, and so we can form a 'figure of merit' or quotient called the spectral resolving power, finding $f/\Delta f > 4 \times 10^7$.

Even at this superb resolution, it's *still* not the laser which limits the frequency width. Rather, the 'natural width' of the quantum transitions, related to the finite lifetime of the upper states, provides the next limit on resolution of $\Delta f \approx 0.006$ GHz. But at this higher level of resolution, there's yet more to be learned about atomic structure. With the Doppler limit surpassed, it becomes clear that the atom's *excited* states also display hyperfine splittings, formerly invisible because of the Doppler broadening, but now cleanly resolved.

Lots more can be done on a tabletop scale. Given this ultrahigh resolution, for example, it's very easy to see the Zeeman effect of even modest magnetic fields further splitting the atomic energy levels. And beyond these simple experiments, very glamorous things have been done with diode-laser spectroscopy, including laser cooling, magneto-optical trapping, and even Bose-Einstein condensation. What's truly remarkable is how far along this path one can proceed on *a tabletop scale* and *with real-time accessibility* of the optical phenomena. And it is all made possible by the techniques of diode-laser spectroscopy.

Rubidium Atomic Energy Level Diagrams

85 Rb (72%)   **87 Rb** (28%)
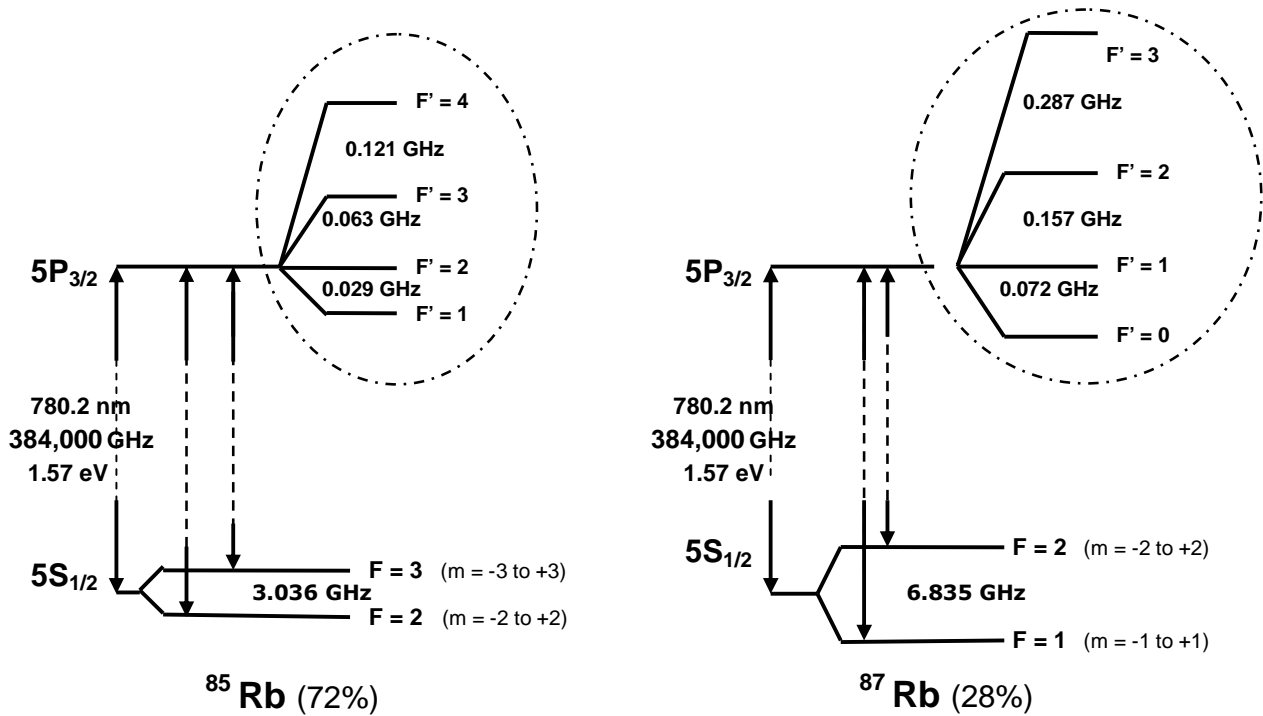
Energy Diagram shows D2 transitions only.   The D1 transitions at 794.8 nm are not shown
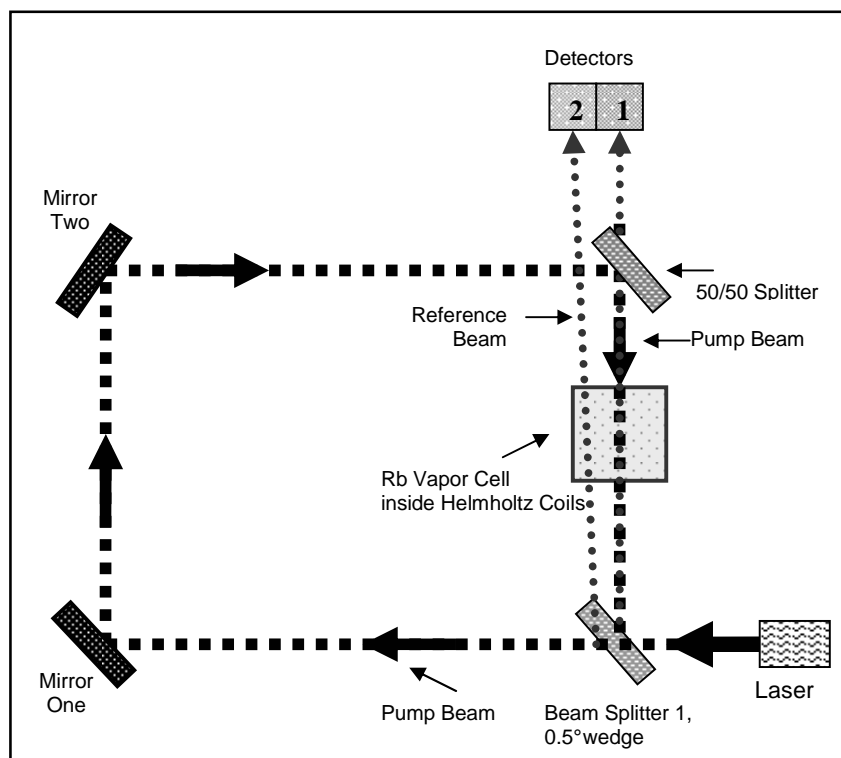
Transmitted Light vs. Laser Frequency
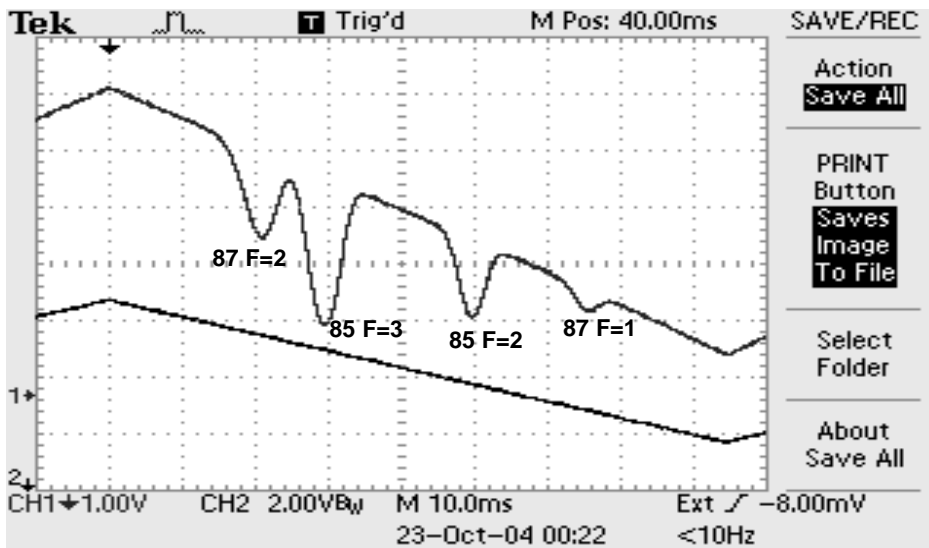
Lower Trace: Sawtooth ramp voltage which is creating a "sweep" of both the laser current and the grating angle. This, in turn, creates the change in the laser frequency.
Falling sawtooth indicates increasing frequency.

Upper Trace: Transmitted light received by the detector. In the section of the trace shown, frequency increases with time.

5

Optical Plan for Saturated Absorption

A schematic diagram of an optical layout suitable for performing diode laser pump-probe experiments in rubidium vapor.

Transmitted Light vs. Laser Frequency With Pump Beam On
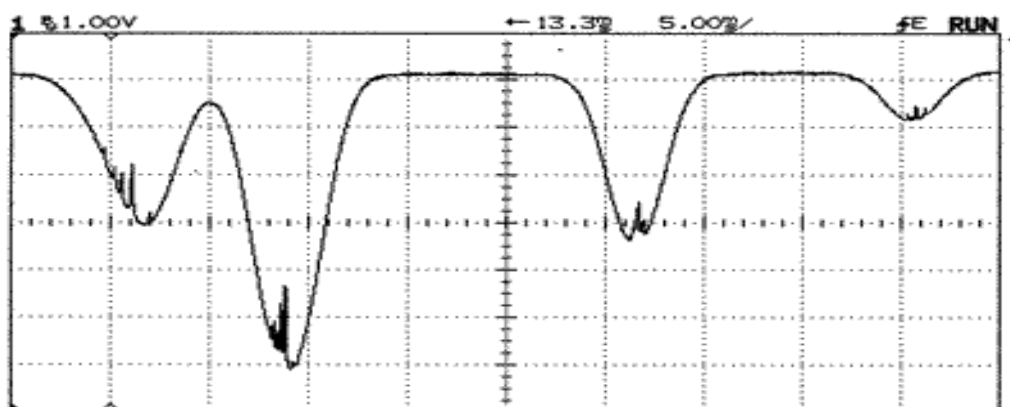
Trace showing features that appear when pump beam is introduced. In the section of the trace shown, frequency increases with time. For this trace, only the grating angle is being changed. The laser current is constant, as indicated by the flat base line.

Thinking about Saturated Absorption and Crossover Transitions

Barbara Wolff-Reichert – Rev 2.0 11/09

Any discussion of saturated absorption spectroscopy must begin with a reprise of the source of the Doppler broadening of absorption features. In absorption spectroscopy, a beam of laser light, which we will call a *probe beam*, is sent through a gas sample, in our case a mixture of ^{85}Rb and ^{87}Rb vapor, into a photodiode detector. The frequency of the light emitted by the diode laser is then modulated. As the frequency of the laser/probe beam sweeps through the frequency equivalent to the energy needed for a particular transition of the gas, photons from the beam will be absorbed and the atoms excited to a higher energy state. Of course, this energy is quickly reradiated as the atoms return to the ground state. The energy, however, is reradiated in all directions. This three-dimensional re-radiation creates a dual phenomenon – a line of fluorescence appears along the path of the photon beam and the intensity of light reaching the photodiode detector decreases significantly. For the TeachSpin Saturated Absorption experiment, the central frequency of the laser sweep is selected to stimulate a transition from the $S_{1/2}$ to $P_{3/2}$ energy state.

Were all the atoms at rest with respect to the beam, a graph of light intensity reaching the detector vs. the frequency of the laser would show a single sharp dip at the exact transition frequency f_0. The axes of an oscilloscope trace of photodiode detector voltage vs. time would be proportional to received light intensity vs. frequency and so would have the same shape. Because, however, atoms are in motion, atoms with a component of velocity toward the laser beam which we shall call $-v_{zA}$ will "see" the photons with a frequency f_A, which is actually an amount Δf below the transition frequency, as having a frequency f_0. These atoms will therefore absorb photons from the beam. In the same fashion, atoms moving away from the laser beam at speed $+v_{zB}$ will "see" photons of frequency f_B, (an equal amount above f_0) as being at the transition frequency. As a result of this phenomenon, the oscilloscope trace we see is a wide, smooth, curve, a Doppler broadening rather than a sharp dip.

Figure 1 offers a way to visualize this Doppler process. In the upper section of the Figure, the vertical axis of the "graph" indicates the magnitude of a particle's velocity in the direction of the laser beam. The horizontal axis is the frequency of the laser. The plotted line shows the velocity that a particle/atom must have in order to absorb the laser photons at that particular laser frequency within the sweep.

The lower section represents an oscilloscope trace of the detector signal vs. time as the frequency of the laser is swept from below to above the f_0 transition frequency of our imaginary gas. The vertical axis thus indicates the amount of laser light reaching the detector while the horizontal axis indicates frequency. On an actual oscilloscope trace, the transition frequency would be hard to determine with much accuracy.

When using saturated absorption spectroscopy (SAS), however, the oscilloscope trace for atoms with a single transition shows a sharp spike within the Doppler dip when the laser frequency matches f_0. The process of SAS, like many great insights, seems obvious in retrospect. The laser beam is split into two unequal portions. The weaker portion, the *probe beam*, with only 10% of the initial intensity, is directed through the gas cell to the detector. The stronger or *pump beam* is directed around the cell and sent back through it, in the opposite direction of but collinear to the probe beam. The upper section of Figure 2 shows the z-velocity vs. frequency plot for particles that will absorb pump photons as a heavy line while the plot for atoms that will absorb probe photons is thinner. Notice that the two lines cross at $v_z = 0$, $f = f_0$.

For most frequencies within the Doppler range, the pump and probe beams interact with groups of atoms moving in opposite directions. When the laser frequency is f_A, for instance, atoms moving toward the probe beam at a velocity we can call $-v_{zA}$ absorb the probe beam photons. However, for the pump beam, it is the atoms moving at $+v_{zA}$ which "see" the pump beam frequency as elevated to f_0. At this frequency, the presence of the pump beam has no effect on the amount of light reaching the detector. As the laser frequency sweeps through f_0, however, atoms with a $v_z = 0$ can absorb photons from either of the beams. The stronger pump beam saturates the transition, leaving far fewer atoms to interact with the probe beam. As a result, the intensity of the probe beam light reaching the detector increases significantly, creating the sharp spike shown in the lower section of Figure 2.

But what happens if there are two or more closely spaced transitions, transitions so close that the oscilloscope signal appears as single wide Doppler dip? As Figure 3 indicates, for a case of two closely spaced transitions, f_{01} and f_{02}, the oscilloscope trace will show not two but three spikes within the Doppler curve. While two spikes are at the expected frequencies, the frequency of the third spike is exactly halfway between the two actual transition frequencies. At this "halfway" frequency, f_{12}, two groups of particles have velocities which allow them to absorb photons from either beam. Because of their motion, atoms with velocity $+v_{z12}$ "see" the frequency of pump beam photons as elevated to f_{02} while the probe beam photons appear to have a frequency of f_{01}. For atoms of velocity $-v_{z12}$, the opposite effect occurs. For both sets of atoms, the absorption of probe beam photons decreases creating a spike in the Doppler curve.
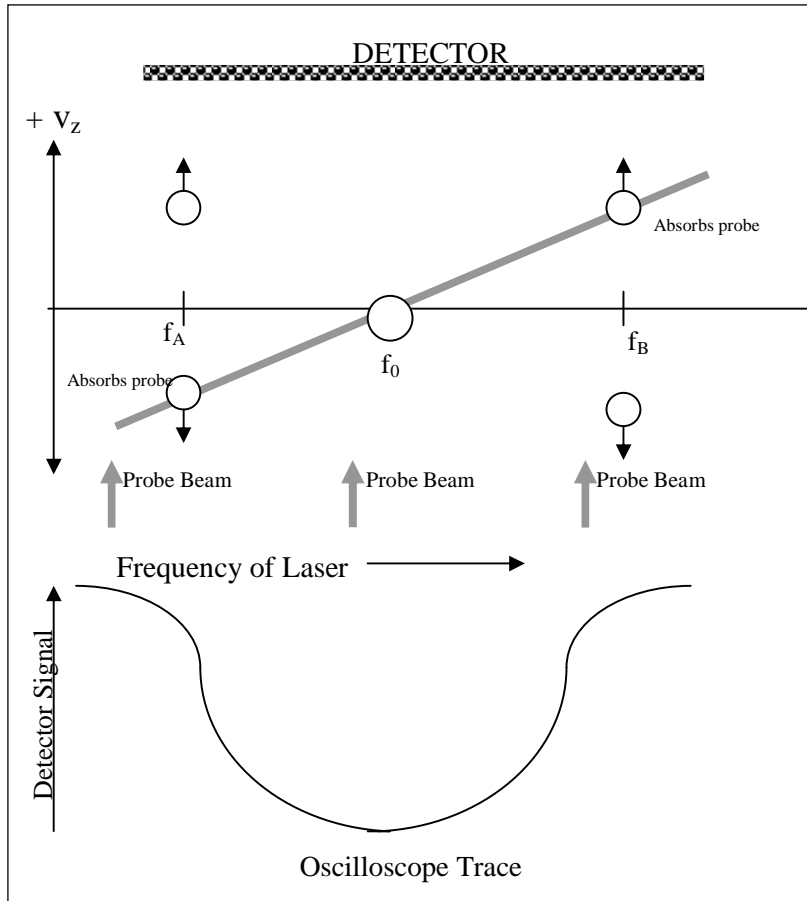
Doppler Broadened Signal

Figure 1

Saturated Absorption

Figure 2

Doppler broadening occurs when the frequency of the laser is swept on either side of the "true" absorption frequency f_0.

When the sweep frequency is below f_0 (as f_A) probe photons are absorbed by gas particles moving towards the probe beam at a velocity which Doppler shifts f_A to f_0. When the sweep frequency is above f_0, probe photons are absorbed by particles moving away at velocities that "see" f_B reduced to f_0. When the laser frequency is f_0, particles at rest or moving perpendicular to the beam absorb photons.
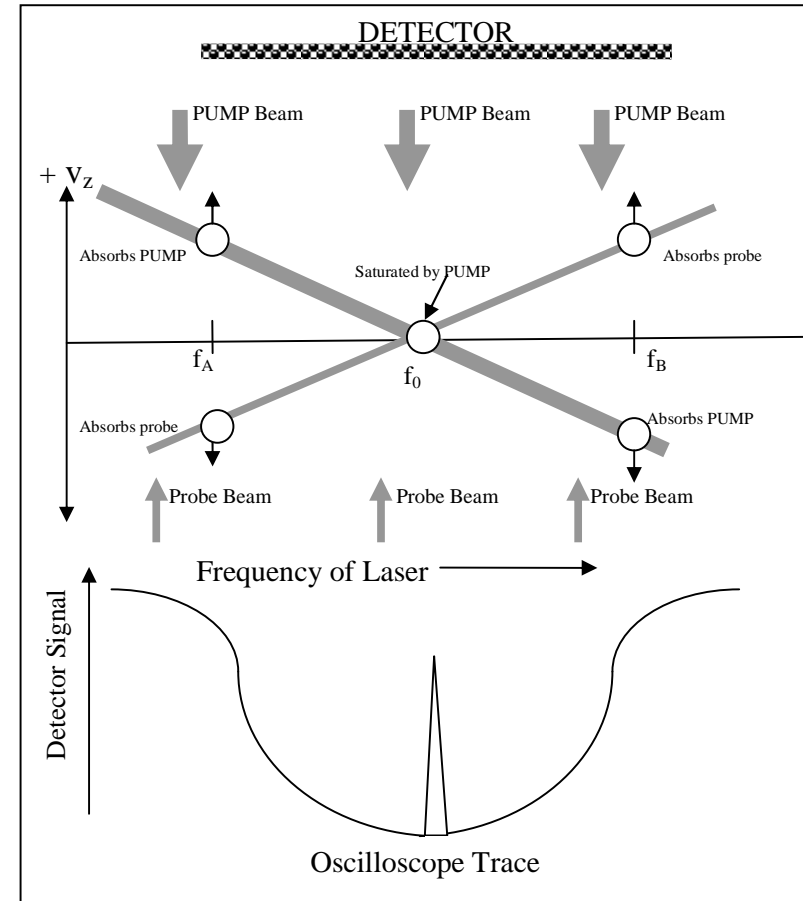
At frequency f_A, (below true absorption frequency f_0) probe and pump photons are absorbed by particles moving towards the each beam. These are completely different sets of particles so the probe signal is unchanged. With the laser frequency at f_B, which is above f_0, photons are absorbed by particles moving away from each beam.

When, however, the laser frequency passes through f_0, particles at rest or moving perpendicular to the beams can absorb photons from either beam. The PUMP beam 'saturates' the transition. Since fewer particles are available to absorb probe photons, the intensity of the probe beam reaching the detector is increased and the signal "spikes".
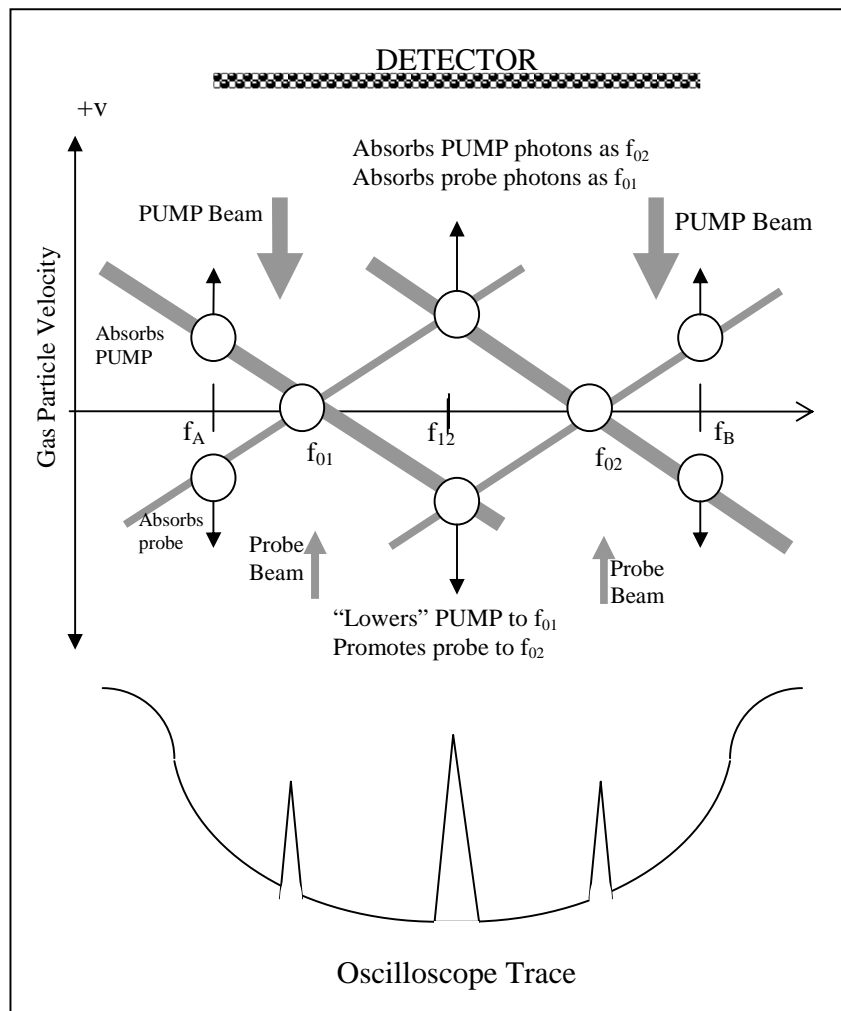
Crossover Transition

DETECTOR

+v

Gas Particle Velocity

Absorbs PUMP photons as f_{02}
Absorbs probe photons as f_{01}

PUMP Beam

PUMP Beam

Absorbs
PUMP

Absorbs
probe

f_A

f_{01}

f_{12}

f_{02}

f_B

Probe
Beam

Probe
Beam

"Lowers" PUMP to f_{01}
Promotes probe to f_{02}

Oscilloscope Trace

Figure 3

When a transition can be made from the ground state to two upper levels, adding the pump beam creates three "spikes" within the Doppler curve. Increases in transmission occur, as expected at the two actual absorption frequencies, f_{01} and f_{02}. The third spike, called the "crossover" transition, occurs exactly halfway between the two. At this frequency, an atom moving with the proper velocity in the $+v_z$ direction can either Doppler shift the probe beam photons down to f_{01} or the pump beam photons up to f_{02}. Thus at this crossover frequency f_{12} the atoms available for absorbing probe beam photons is reduced. More probe beam photons pass through the vapor and the detected intensity rises. Similar reasoning describes the fate of atoms moving at the proper velocity in the $-v_z$ direction.

When three possible transition frequencies fall within a Doppler curve, as in our rubidium vapor experiment, six spikes are produced. In addition to spikes at f_1, f_2, and f_3, there will be crossover spikes at f_{12}, f_{23} and f_{13}.

Fabry-Perot Cavity

FP1-A
INSTRUCTOR'S MANUAL

A PRODUCT OF TEACHSPIN, INC.

TeachSpin Inc.
FABRY-PEROT CAVITY

INSTRUCTOR'S MANUAL INDEX

Instruction Manual for TeachSpin's Fabry-Perot Cavity

Introduction

The Fabry-Perot Interferometer is a "resonant cavity" for light which has many uses in the world of optics.   TeachSpin's Fabry-Perot Cavity was designed specifically to calibrate the frequency scale of a tunable laser. It can be used with any tunable laser operating in a wavelength range of 740 - 820 nm.

As an appendix, we have included a manual written by California Institute of Technology Professors Kenneth Libbrecht and Eric Black of the California Institute of Technology, with whom TeachSpin collaborated in building both our Diode Laser Spectroscopy apparatus and this Fabry-Perot cavity. In it, you will find a detailed discussion of the physics of this instrument, as well as descriptions of a variety of student experiments.

Here we offer a brief *Overview of the Physics* of a Fabry-Perot Cavity, instructions for *Unpacking the Instrument* and detailed instructions for *Setting Up the Fabry-Perot Cavity for the First Time*.

Overview of the Physics

A Fabry-Perot cavity is created by mounting a matched pair of highly reflective mirrors at either end of a tube. As seems logical, light aimed at the back of the near end mirror is, generally, reflected immediately and not transmitted through its length and out the other end. However, as the analysis in the appendix explains, at certain "resonant" frequencies, monochromatic laser light is actually transmitted.

The distance between the mirrors mounted at the two ends of a Fabry-Perot cavity determine its resonant frequencies. A detector just past the far end monitors the transmission. Non-resonant light is scarcely transmitted.   As the frequency of a tunable laser is swept through the resonant frequencies of the cavity, distinct maxima in transmission occur.
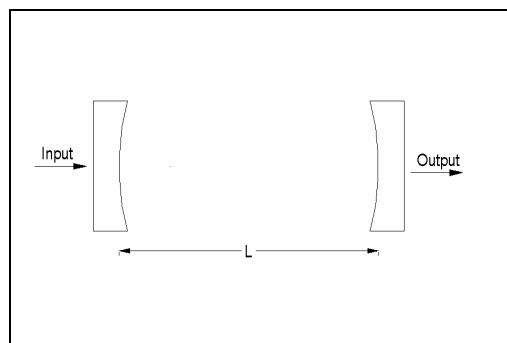
For a properly adjusted cavity, the resonant frequencies are given by:

$$f_j = j\frac{c}{4nL} \qquad\qquad 1\text{-}1$$

In this equation, j is an integer, c is the vacuum speed of light, L is the distance between the two mirrors defining the cavity, and n is the index of refraction of the air inside the cavity.

When the frequency of a tunable laser is scanned in time, a series of peaks in the transmitted light's intensity occur at

$$f_j = \ldots (j\text{-}1)\ \frac{c}{4nL},\ \ j\frac{c}{4nL},\ \ (j\text{+}1)\ \frac{c}{4nL},\ldots \qquad\qquad 1\text{-}2$$

As the series in equation 1-2 indicates, for any integer j, the transmission maxima will be equally spaced in frequency. The difference between adjacent maxima is defined as the *free spectral range* or FSR.

$$FSR = \Delta f = \frac{c}{4nL}$$ 1-3

For the TeachSpin cavity, the adjusted length, L, will be near 20 cm, which will give a free spectral range of about 0.38 GHz or 380 MHz.

The transmission maxima, of course, will not be perfect spikes. The narrowness of a peak is described in terms of its full width, in frequency units, at half the peak height of the signal. For a properly adjusted Fabry-Perot cavity, the width in frequency of the maxima peaks (δf) will be much smaller than the spacing between the maxima (Δf). The ratio $\Delta f/\delta f$ is called the *finesse* of the cavity, and you should be able to achieve a finesse of over 100.

To have an idea of the sensitivity of this instrument, we can look at the three different frequency ranges involved. Writing them all in MHz will make them easier to compare. First, there is the frequency equivalent of the particular light we are investigating. For light of wavelength near 780 nm, the optical frequency is about 384,000 GHz or 384×10^6 MHz. We have calculated that Δf, the free spectral range, of our cavity is about 380 MHz. This means that, as we sweep the laser frequency, whenever the frequency of the transmitted light changes by *one part in a million*, you'll get another transmission maximum. Now, let's look at the transmission peaks themselves. Since the finesse of our cavity is around 100, having a FSR (Δf) of 380 MHz means that the frequency width of the peak itself, δf, will be on the order of 4 MHz. Since δf is measured half way up the peak, we can easily see changes ¼ as great. Thus a Fabry-Perot interferometer can be sensitive to frequency changes on the order of 1 MHz, out of an optical frequency of 400 *million* MHz.

The optical cavity of a Fabry-Perot interferometer is created by the pair of high reflectivity concave mirrors mounted at the two ends. The TeachSpin mirrors have a (power) reflection coefficient of R > 0.995 or 99.5%. The experiment must adjust the distance between the mirrors so that the focal points of the two mirrors coincide in space at the center of the cavity – in other words, the mirrors must be arranged to be 'confocal'. When properly aligned, these mirrors define a cavity mode that is stable against the otherwise inevitable transverse spreading of a beam that bounces back and forth between the mirrors for hundreds of round trips. The mirrors used in the TeachSpin cavity have radii of curvature 20 cm, so as concave mirrors they have focal lengths of 10 cm. Therefore, when properly adjusted, the mirrors are 20 cm apart. Part of your task will be to find the 'confocal condition' experimentally.

The 'ray diagram' for a confocal cavity is quite simple: any ray leaving either mirror, at any (paraxial) angle, and reaching the other mirror, will return to its original point of departure after two round trips, for a total distance traveled that's very near 4*L. If the incident light reaches the cavity parallel to, but laterally displaced from, the common axis of the mirrors, then the rays inside the cavity follow a 'bow-tie' pattern.
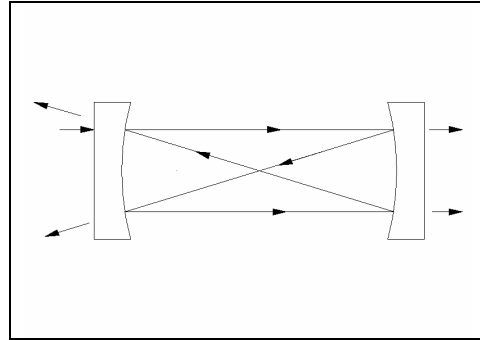
Emerging from the far end of the cavity are two transmitted rays, either of which will show the 'transmission maxima' you'll be studying. From the mirror at the input end of the cavity, there is also an immediate *reflection* from the cavity, which can be used in advanced applications of a Fabry-Perot interferometer. (At non-resonant frequencies, almost all of the light is reflected. At resonant frequencies, this immediate reflection reaches a minimum.)

Unpacking the Instrument

TeachSpin's Fabry-Perot Cavity comes with an iris for aligning the beam and a brass spanner wrench which can be used to remove the retaining ring if you wish to change or replace the mirrors.

The Fabry-Perot Cavity itself consists of an aluminum tube with a 0.5" ID. The tube is threaded at each end (0.535" by 40 threads per inch). These threads accept Thor Labs adjustable lens tubes (model SM05V05). High reflectivity curved cavity mirrors have been placed into each lens tube and are held in place with a threaded retaining ring. Both the lens tubes and the retaining rings have been shipped with the threads fully engaged and tightened. You will find removable plastic caps covering the ends of the lens tubes.

When you first unpack your cavity, remove the end caps and inspect the mirrors. Make sure the retaining ring has not become loose during shipping. (CAUTION: Do not scratch the mirrors with the retaining ring tool!) The lens tube should also be fully threaded in. The end caps should be used to protect the mirrors any time the instrument is not in use. You may want to keep them in place for the first part of the set up.

Setting Up the Fabry-Perot Cavity for the First Time

To set up the cavity, you will need to use the Diode Laser, the rubidium absorption cell and two photodiode detectors along with the Fabry-Perot system. Figure 1 shows a convenient layout. You are welcome to devise your own, but alignment will be simplified if you put the Fabry-Perot's input mirror close to the second steering mirror.

Before starting, be sure that the lens tubes are fully threaded in. This will mean that the cavity is set for its minimum length. The oscilloscope traces included in this manual were taken while a cavity was being set up for the first time. Because the photodiodes (PD) put out a negative voltage, both oscilloscope channels have been inverted. The transmission through the Fabry-Perot cavity (FP) is shown on Channel One.   Channel Two, when displayed, indicates the light intensity of a beam passing through a rubidium absorption cell. This means that dips the trace on Channel Two show the rubidium D$_2$-line's absorption signals.

Select area on the optical table for the cavity carefully. The cavity should be placed away from other beams and located so that there can be two steering mirrors before the cavity. (At this point, remove the vinyl end caps)
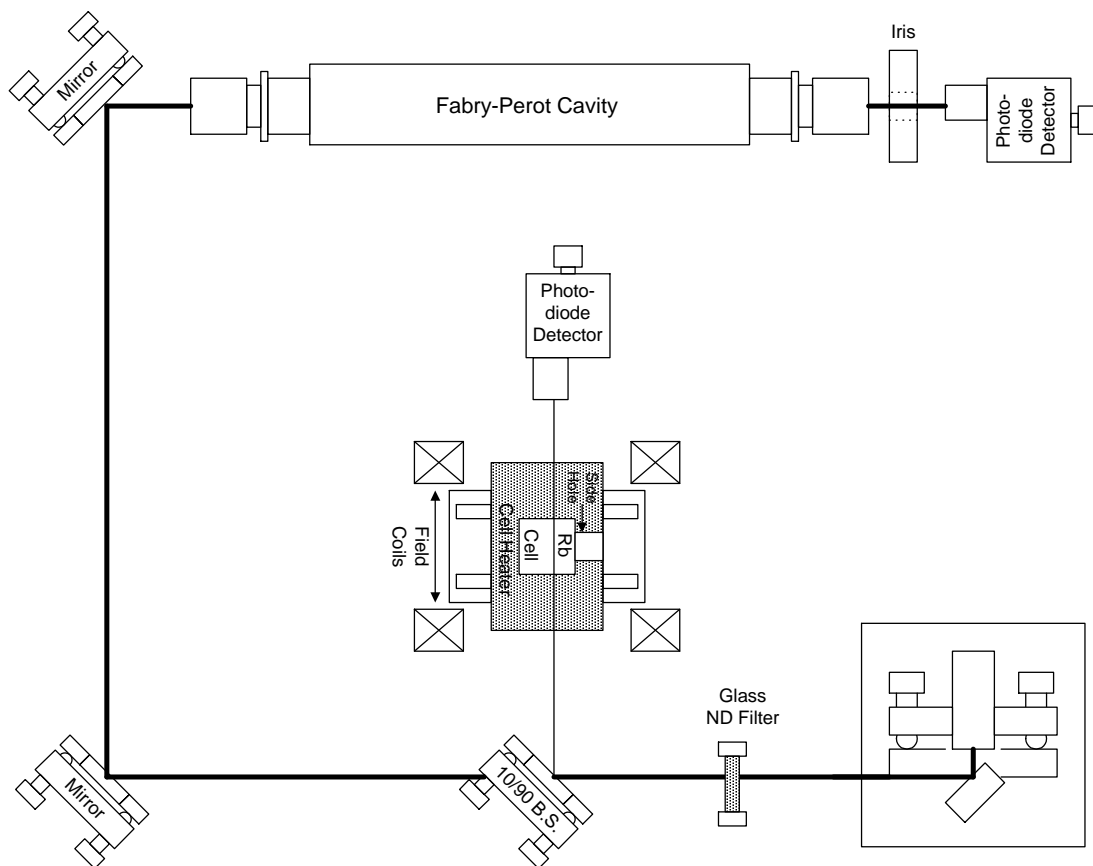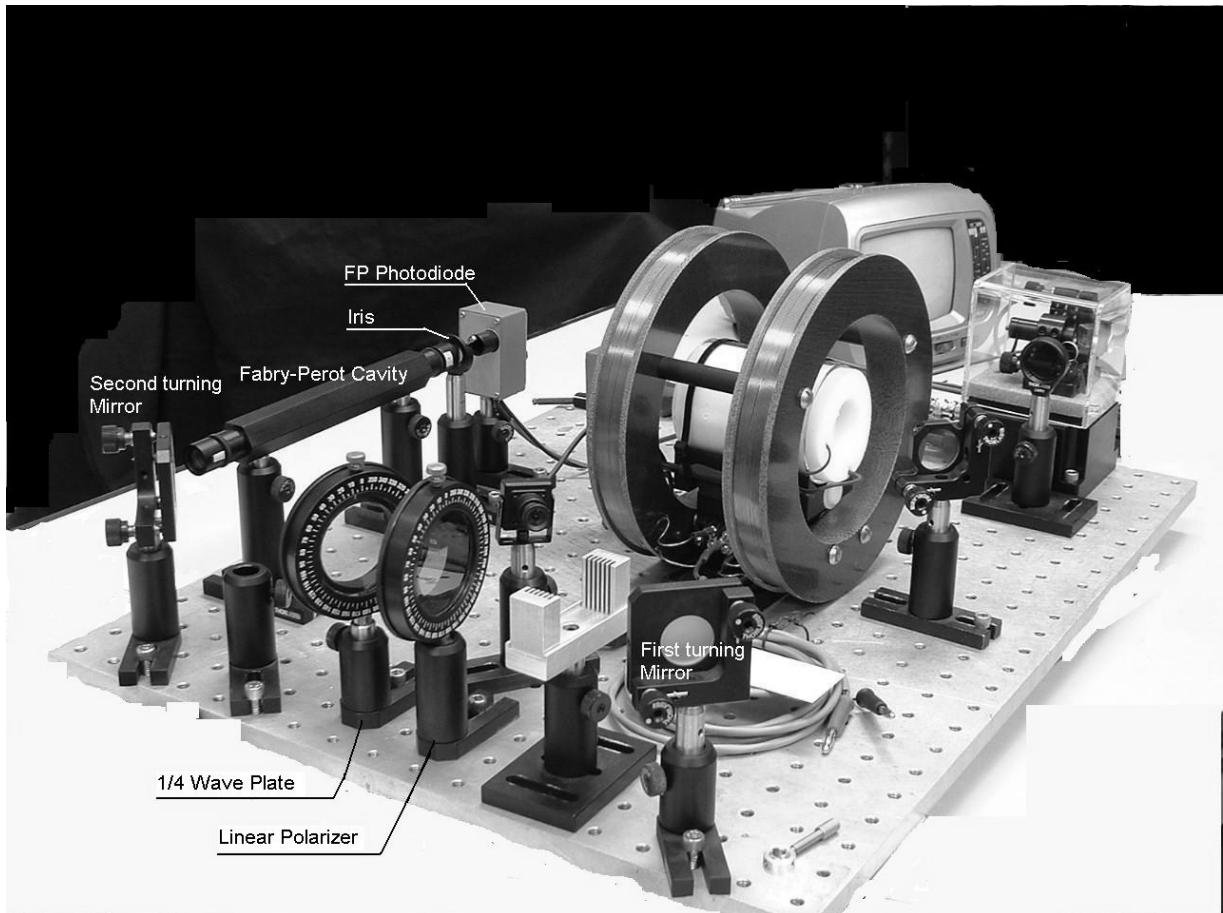

Figure 1   **This is a schematic of the setup used for aligning Fabry Perot cavity. The linear polarizer and quarter-wave plate which were placed between the two steering mirrors are not shown.**

One of Many Possible Configurations for Using the Fabry-Perot Cavity

This photograph shows only one possible arrangement of components for using TeachSpin's Fabry-Perot Cavity. We have shown a very compact version so that we could photograph it easily. Depending upon the space you have available, and the kinds of experiments you wish to do, other configurations may be far more useful.

The photograph shows the location of the linear polarizer and ¼ wave plate which were not included in the schematic. These are not used in the initial set up and are added somewhat into the process of tuning the cavity. As you can see, ¼ wave plate is tilted around its vertical axis. This is one of the degrees of freedom you can use when adjusting this "poor man's optical isolator" to prevent the light reflected off the Fabry-Perot surfaces from returning to the laser. (See page 9 of this discussion.)

Now it is time to turn on the laser and get the beam near center of two steering mirrors. Use the mirrors to make the beam parallel with the top of the breadboard and at a height of about 4 inches. The iris provided will make this task easier.

Tune the laser to the Rb spectrum and use one photodiode to monitor the absorption. This is not necessary to run the FP, but the cleanness of the absorption spectra will be used a diagnostic to tell you when reflections for the FP are getting back into the laser and changing its wavelength. The upper trace in Figure 2 is a normal spectrum; below is one corrupted by feedback. (Well-stocked optics labs may have an optical isolator that can be used to eliminate the back reflections.)   We will also describe later how the linear polarizer and quarter-wave plate may be set up as a "poor man's" optical isolator. Other techniques that can reduce the feedback are putting an attenuating filter in the beam path and keeping the optical path length between the laser and Fabry-Perot cavity as long as possible.   (The distance helps because the beam reflecting from the FP is diverging due to the curvature of the mirrors.)
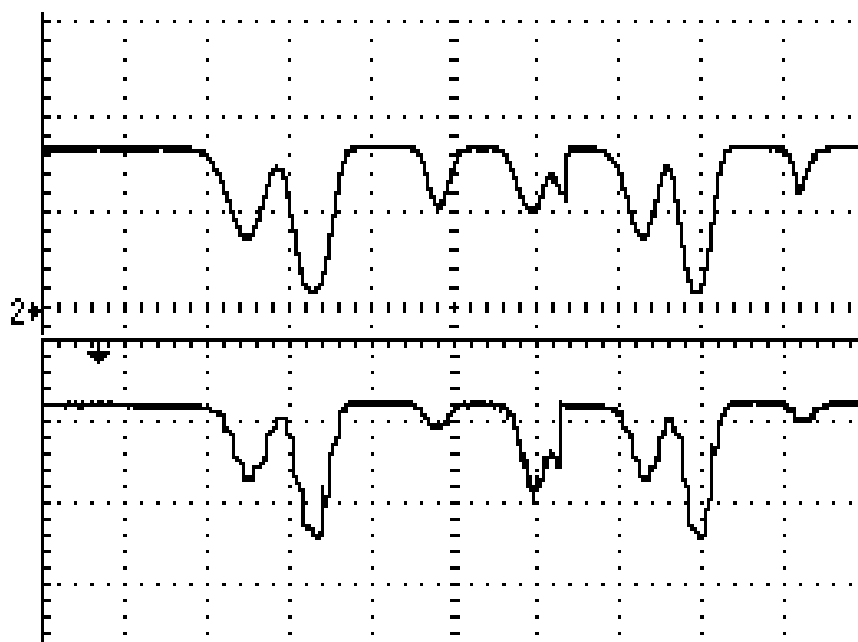

Figure 2   **The upper trace shows a normal absorption signal. The trace below is the same signal in the presence of optical feedback from the Fabry-Perot cavity to the diode laser.**

We now need to place the FP cavity in the beam such that the beam goes approximately down the center of the cavity. This is not a simple task because the highly reflecting mirrors mean that only a very small fraction of the light will pass through the cavity. (The mirrors are specified to be 99.5% reflective and we will make a power measurement to put an upper limit on this number.)   You can use the iris as an alignment aid.

Place the FP in its approximate position. Place the iris at a location on the table so that it will be just after the FP. Now remove the FP and position the iris so that the beam goes through the center. Reduce the iris size and use the IR viewing card or a photodiode detector (PD) to help in correct positioning. Even if you don't use the PD to help center the iris it's a good idea to place it on the table now and center the PD on the beam.   Keep the PD reasonably close to the iris and cavity. You will be making small changes in the position of the beam through the cavity; you don't want the beam to move off of the active area of the PD as you do this.

Now place the FP back in the beam path. Use the iris to center the downstream section of the FP on the beam and use the IR viewing card to position the upstream (input mirror) of the FP centered on the beam path.

Open up the iris so that the hole is at its largest opening and monitor the PD voltage on an oscilloscope as the diode is swept through the Rb absorption. Set the gain of the PD near its maximum value (1 to 10 Mohm). You should see an ugly signal on the 'scope. (See Figure 3 below -- note the evidence, in the Rb absorption signal, of feedback from the FP to the diode laser)
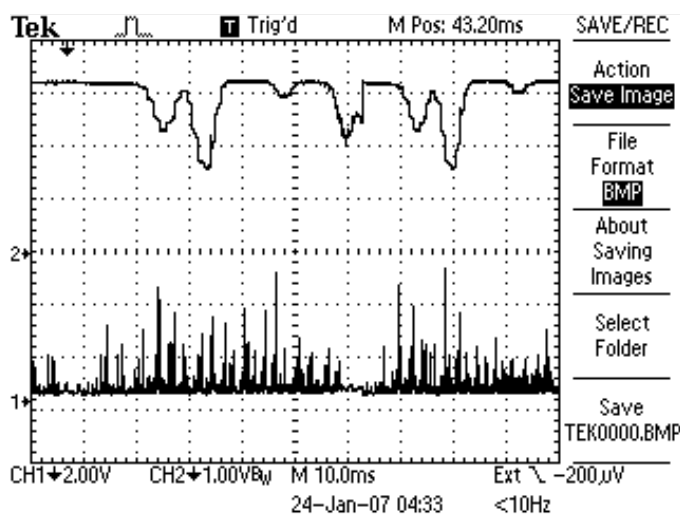

Figure 3 First view of F-P with no attenuation or isolator in beam path.
   Upper Trace is Rb detector. Lower trace shows transmission through F-P cavity.
   Gain in FP PD detector is 3.3M ohm. Gain Rb absorption detector is 10k ohm.

Now, place the glass neutral density filter in front of the laser. Adjust the photodiode and 'scope gains to display the signals again. The filter does a good job of reducing the back reflection because it attenuates the light both going from and returning to the laser. Figure 4 shows the 'scope trace with the feedback reduced. The PD gain of the FP PD has been increased to 10 MΩ and the room lights have been turned off. (If you cannot reduce the room lights you can also try putting a black cloth or paper "roof" over the gap between the end of the cavity and the snout of the photodiode detector to reduce the amount of stray light entering the PD.)

We can see from Figure 4 that the attenuator has reduced feedback to the laser. The rubidium absorption spectrum now shows that the laser is tuning smoothly and continuously in frequency.
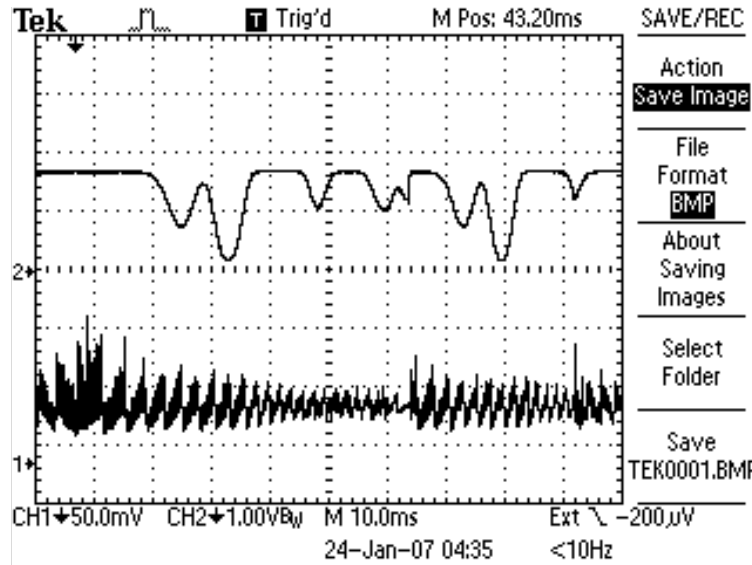

Figure 4   FP with a glass neutral density filter in beam path.
FP PD gain = 10 MΩ,   Rb abs PD gain = 100 kΩ, Room lights off.

Tweak the two steering mirrors to maximize the transmission signal through the cavity. Your oscilloscope traces should begin to look like Figure 5. We can now see some structure in the FP transmission signal. Each peak represents the excitation, by the laser, of a different resonant mode of the FP cavity. The transmission maxima occur in repetitions of a cluster of modes. Successive 'clusters' are spaced by the cavity's free spectral range, and differ in the 'longitudinal mode number' of the cavity mode. Within each cluster is a collection of modes, which occur because you are exciting various *transverse* modes of the cavity.
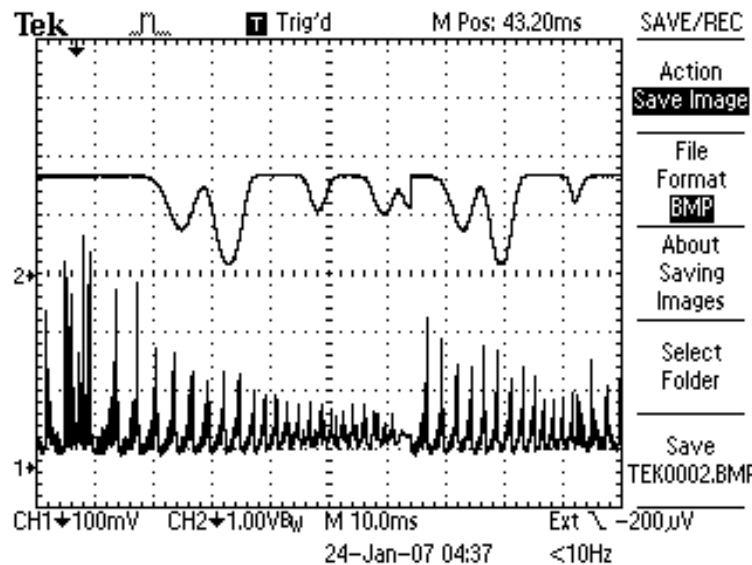

Figure 5 Same signal as Figure 4, but steering mirrors have been tweaked for maximum signal.

In Figure 5, we can see that these transverse modes are occurring at distinct frequencies. This is because the cavity length is not set to the confocal condition (where all the transverse modes become degenerate, and occur at the same frequency).

When tweaking the steering mirrors, you may notice that there is still some light feeding back into the laser. Now is a good time to use the linear polarizer and quarter wave plate to construct a "poor man's" optical isolator. See appendix A for one technique of adjusting these components.

Figure 6 shows a made trace after the linear polarizer and quarter wave plate were inserted and adjusted to reduce feedback into the laser. The horizontal scale has been expanded from Figure 5. The scan has been shifted so that the turning point of the piezo scan, which is shown by the arrow on the upper margin, is near the center of the trace.   In this section of the scan, the grating first lengthens, then shortens, the wavelength of the laser. You might notice that the long tails of cluster of modes stretch towards the *long* wavelength side of the spectrum. This tells us that the cavity length is not at the confocal condition and needs to be lengthened. (A tail to the *short* wavelength part of the scan would indicate a cavity that needed to be shortened.)
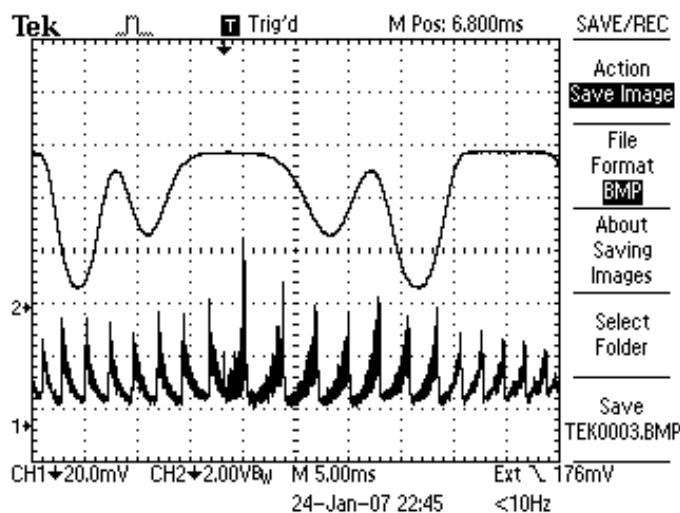

Figure 6   Oscilloscope trace with optical isolator in place. The turning point of piezo scan, shown by the arrow on the upper margin, is near the center of the 'scope trace.
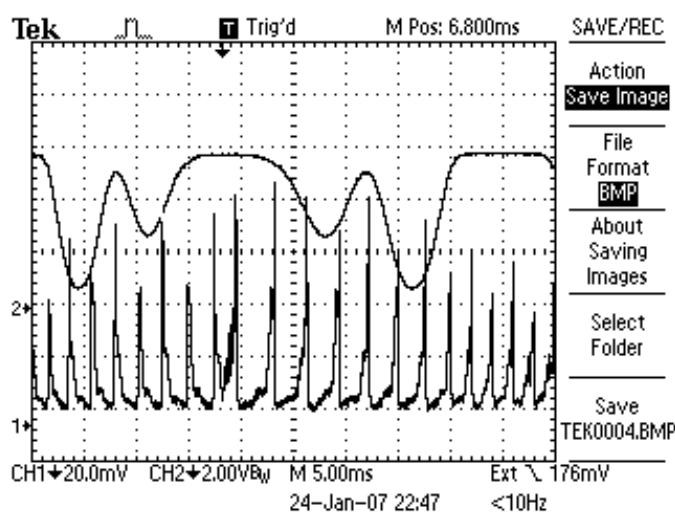
When you have determined whether the cavity is too long or too short, change the length by tuning one of the adjustable lens tubes on either end of the cavity. Watch the 'scope display as you do this.   Figure 7 shows the scan for our cavity with one adjuster rotated 5 turns. (You can put small pieces of masking tape on the lens tubes to keep track of how far you have turned them.)

Figure 7 Cavity length increased by five turns of one lens tube.

Before the next traces were made, the other end mirror was turned out four turns, making the cavity even longer. Note the change in scale of the y axis for the FP signal. It has changed from 20 to 200 mV per division. Evidently, as the cluster of modes coalesce, the intensity in the peaks increases dramatically. Here, the highest peak has gone from about 85 to 360 mV.

Figure 8 Cavity length increased by four turns at the other end of the cavity

Now you ought to check that you are not sweeping too fast through the Fabry-Perot transmission peaks. At a Gain of 10 MΩ, the PD has a 3dB bandwidth of about 5 kHz. We might estimate a resolvable pulse width to be about one half the period or about 100 us. In practice, we observe the FP transmission peaks on the scope and watch the peak heights while changing the sweep speed. As the sweep speed is reduced the peak height will increase. Keep reducing the sweep speed until no further increase in peak height is observed.

Figure 9 shows a scan through two transmission peaks. The tails have moved to the other side of the peaks, indicating that the cavity is now too long. You can convince yourself of this by increasing the cavity length further.

Figure 9 Scan for a slow sweep through two transmission peaks. Note that the "tails" are now to the short wavelength side indicating that the cavity is too long.

For the next screen captures, the cavity length was reduced by 1/4 turn. This gives the near optimal cavity length. See Figure 10 and 11.
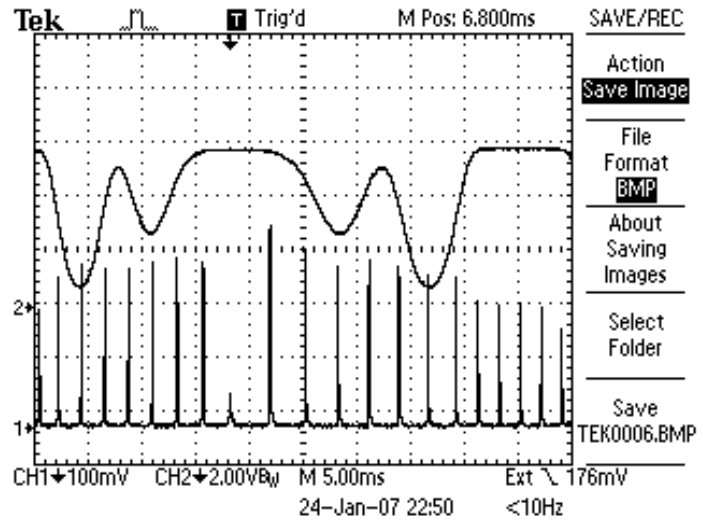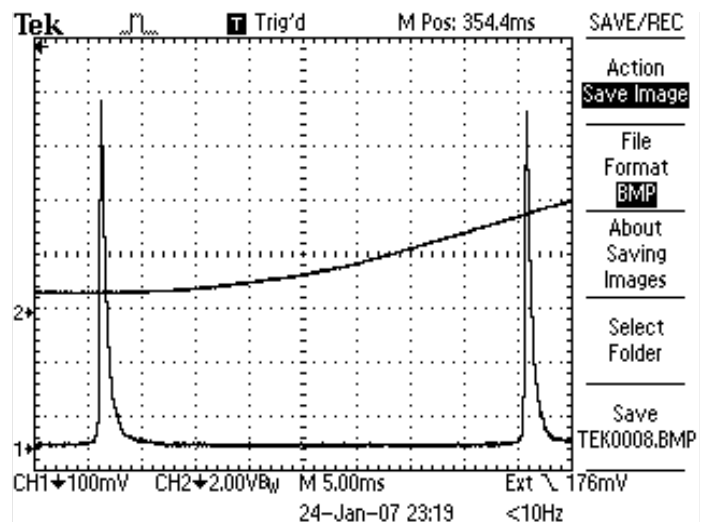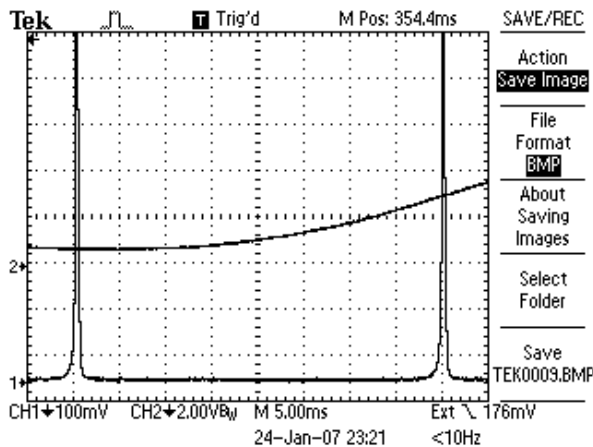
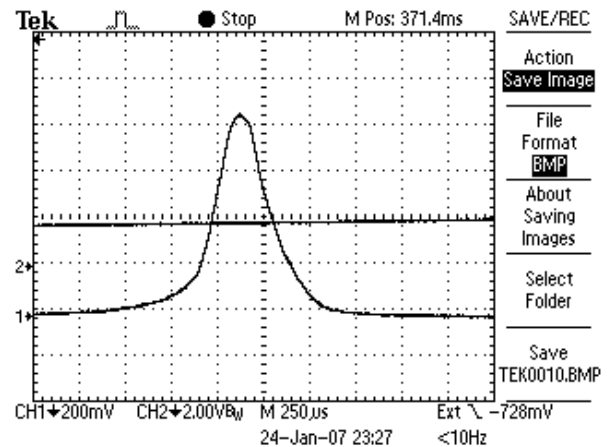**Figure 10   Near optimal cavity length**

Figure 11   Expanded view of single peak from Figure 10.

Figure 11 shows an expanded view of one of the peaks in Figure 10. Traversing one free spectral range (FSR) occupies about 40 ms of time. The full width at half maximum of the peak shown in Figure 10 is about 300 us, giving a finesse slightly greater than 100. If you try and reproduce this data, you will find that vibrations in the air and room will distort the line shape.

Now you are seeing 'markers' equally spaced on the optical frequency scale, and they can serve to calibrate the frequency scale as soon as you can assign a numerical value to the free spectral range. If you could measure L well enough, you could compute this FSR from the equation $\Delta f = c/(4nL)$, but there is a better method. It involves modulating your diode laser, to put 'sidebands' on its heretofore monochromatic signal.

The TeachSpin diode laser is equipped with a special electrical input, in the form of an SMA connector right on the diode-laser head, at which a modulating current can be injected. We have used an RF signal generator which delivers a maximum RF power of 0.7 Volts peak to peak (into 50 ohms) or about 0 dBm. (1 mW of power into 50 ohms) It may be possible to damage the diode if more RF power than this is applied.

The laser current may be modulated at frequencies from 100 kHz to over 150 MHz through the SMA connector on the laser head. [Lower frequency modulation, (DC to 500 kHz), is possible via the current-modulation input on the front panel of the electronics box.] We have also provided a SMA to BNC adapter. Though we have not experienced any problems, you should always use extreme caution when modulating the laser via the direct SMA input. We always worry about turn-on transients damaging the diode. *Before applying AC power to the RF signal generator we make sure that the output amplitude has been set to its smallest value. Then, after AC power is applied, the output amplitude can be increased.*
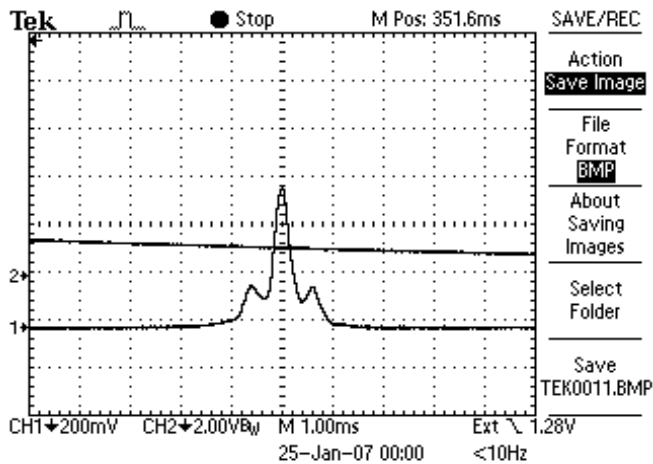
Figure 12a Low Amplitude Current Modulation

Modulation of diode-laser current at low amplitude, and 5 MHz frequency, has put sidebands on the laser's optical frequency. These are separated from the 'carrier frequency' by ±5 MHz, and are revealed by their ability to excite the FP cavity
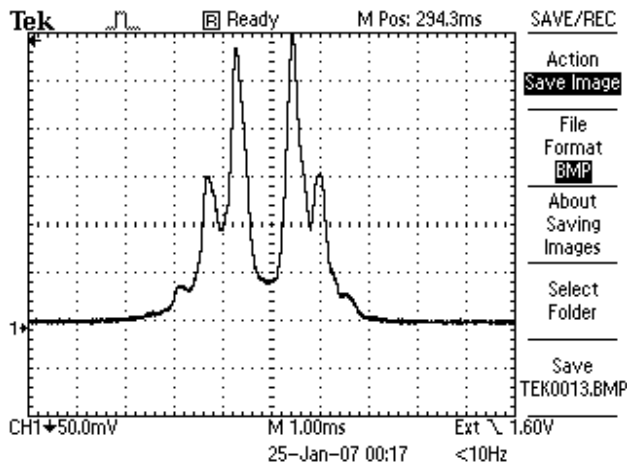

Figure 12b Increased Amplitude

Modulation with larger amplitude. Note that sidebands of order ±1 are now dominant, and sidebands of orders ±2 and ±3 are also visible. For this 'magic' choice of modulation amplitude, the original 'carrier frequency' now has a vanishing amplitude.
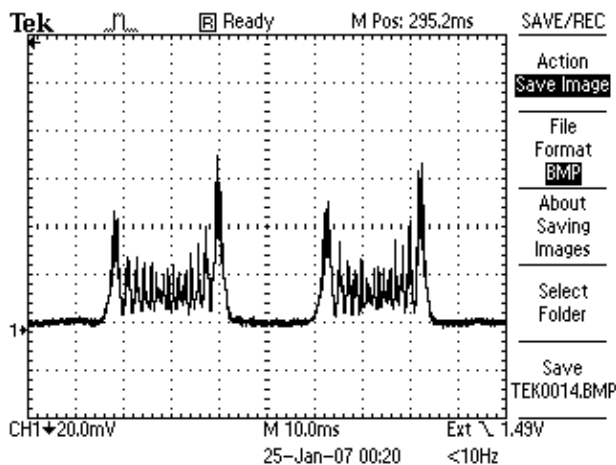

Figure 12c Maximum Amplitude

Maximum Amplitude trace shown using expanded time scale.

Two successive traces of the Fabry-Perot transmission over the spectrum of the laser when it is frequency modulated by a 5 MHz wave form of maximum amplitude.

Figure 12 Modulation of diode-laser current at low, medium, and maximum amplitude and 5-Mhz frequency

Thus far, you have seen the results of exciting the 'bow-tie modes' of the cavity which are spaced at $\Delta f = c/4L$. Figure 13 shows the scan for a well tuned cavity.

If your isolation between laser and cavity is good enough so that feedback is minimal, you can try exciting the on-axis modes. A ray-diagram for an on-axis beam would show a round-trip distance of 2L. In that case, the modes should occur at frequency spacing $c/2L$ which is twice as big as what we have been seeing.

By tweaking your steering mirrors, you may be able to find this on-axis condition. As the beam becomes closer to on-axis, you will see a *drop* in the intensity of every other mode of the $c/4L$ spacing. At the same time, as we can see from Figure 14, the magnitude of the alternate peaks increases. If you were able to be exactly on-axis, you would be exciting even, but not odd, transverse modes, and you would get complete suppression of every other peak in the mode spectrum.

In addition to doubling the free spectral range, exciting these on-axis modes also maximizes feedback to your laser. (Can you explain why?) This places the highest demands on isolation of the laser from the cavity.
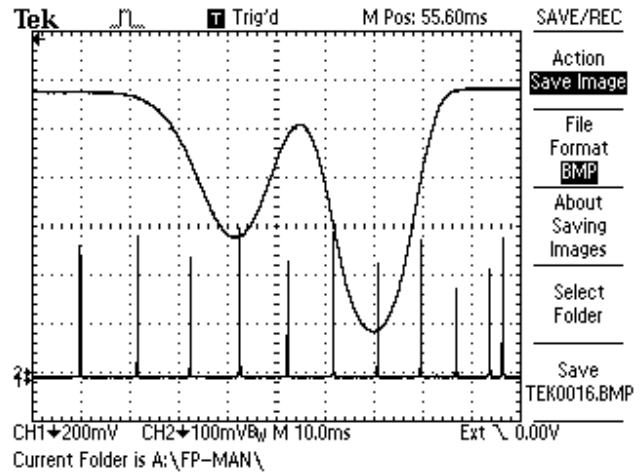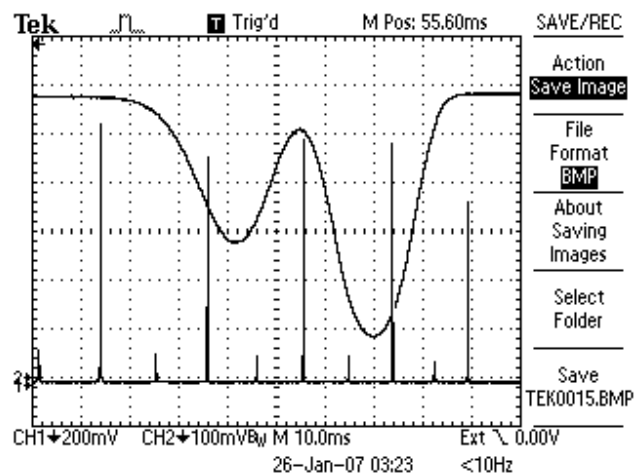

Figure 13 Normal input signal, FSR = c/4L

Figure 14 On-axis input, FSR = c/2L

Appendix A –` The "Poor Man's Optical Isolator"

The "poor man's optical isolator" is a means by which specular reflections may be reduced. It consists of a linear polarizer followed by a 1/4 wave plate. If the axis of the polarizer is placed at 45 degrees with respect to the axes of the 1/4 wave plate, the light beam will emerge from the 1/4 wave plate circularly polarized. The isolator works because when light is specularly reflected from a surface, there is a change in the momentum vector, but not the angular momentum! Thus a light beam that is right hand circularly polarized (RHCP) when approaching a mirror is left hand circularly polarized (LHCP) after a 180-degree reflection from the mirror. (See Figure 1 below.)

When the reflected light passes through the 1/4 wave plate in the reverse direction, the beam again becomes polarized. Because of the change in "handedness," the plane of polarization of the returning light is at a 90° angle to the Linear Polarizer and so its passage is blocked. We have optically "isolated" the source of the incoming light. In the case of a laser, this is extremely important because light re-entering a laser cavity significantly disturbs its performance.
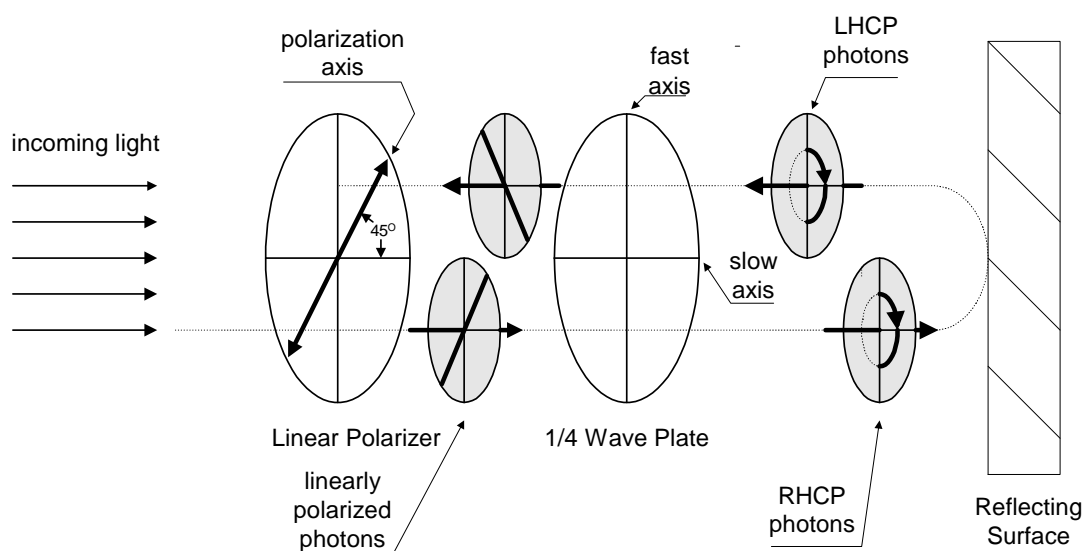
Figure 1: **Schematic showing the change in the direction of circular polarization at reflection and the resulting change in linear polarization which prevents the light from passing back through the Linear Polarizer.**

The 1/4 wave plates that come with your diode laser are not specified to be exactly a quarter wavelength for 780 nm light. Fortunately, it is possible to tune the optical thickness (retardation) of the wave plate by tilting the wave plate about either its fast or its slow axis. Rotation about the slow axis causes an increase in the retardation, and about the fast axis causes a decrease. In practice, one does not know which axis is the fast or slow, or whether the retardation needs to be increased or decreased. Happily, the optimal setting of the wave plate can be found empirically.

Set up the isolator near the source of the unwanted reflection. Position the 1/4 wave plate so that its 0 mark is at the top, making one of its axes vertical. Orient the linear polarizer so that its polarization axis is at 45 degrees with respect to the vertical. (It is best to NOT have any mirrors between the isolator and reflection optics because the mirror will cause a change in the polarization state of circularly polarized light.) You may observe that I did not follow this advice in the set-up shown in the photograph on page 5 of the manual. The reason for this was that I wanted to keep the second steering mirror close to the input of the F-P cavity for ease of alignment. [*]
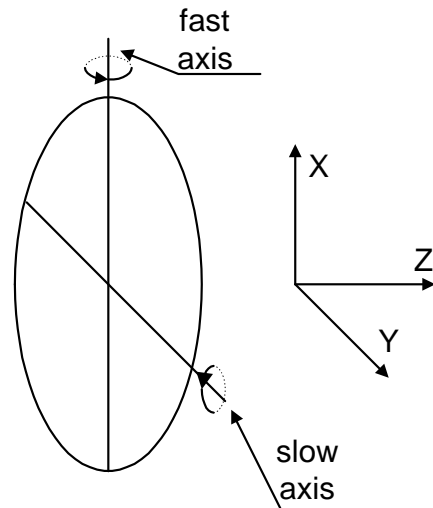
Figure 2: **Diagram of 1/4 wave plate showing reference axes.**

Alignment of the isolator involves two separate rotations: first, rotation of the wave plate in its own plane in the 360-degree mount that is provided, and secondly, rotation of the wave plate about the vertical axis using the optical mount that holds the wave plate to the table. The diagnostic you will use for alignment will be to minimize the intensity of the unwanted reflection. Punch a hole in one of the viewing cards and place it upstream of the isolator. Position the viewing card so that the incoming light goes through the hole. Use the CCD camera to observe the reflection. Warning: there will be several reflections! You should be able to see additional reflections for the linear polarizer and wave plate. By tilting the elements in their optical mounts you can identify which reflection belongs to which element. It is the reflection from the Fabry-Perot mirror that we wish to reduce. The other elements can be angled such that their reflections do not travel back into the laser.

Now that you have identified the reflection you wish to reduce, rotate the wave plate in its own plane to minimize this reflection. (You will be rotating around the Z-axis in the figure above.) By this process you will have adjusted the relative angles of the wave plate and polarizer to be 45 degrees. Now, try twisting the whole wave plate about the vertical axis using the optical mount that holds the optic to the table. (You will be rotating around the X-axis in the figure above.) If you find a point were the reflection becomes a minimum then you are done. You may however observe that the reflected spot only gets brighter as the wave plate is rotated. You have the "wrong" axis in the vertical direction. Rotate the wave plate in its own plane by 90 degrees, bringing the other velocity axis into the vertical position. Once again, try to minimize the reflected beam's intensity by adjusting both the X and Z rotations. This time you should find a nice minimum. The alignment of your "poor man's optical isolator" is now optimized. The isolation is far from perfect, but it is good enough to perform all the measurements that have been outlined in the Fabry-Perot manual.

---

[*] It may also be the case that, by empirically adjusting the isolator, I was able to compensate for the polarization change caused by the mirror.

Fabry-Perot Cavities and FM Spectroscopy

Student Laboratory Manual (Pg. 1-12)

California Institute of Technology

Dr. Eric Black and Professor Kenneth Libbrecht

Followed by:

Scanning Spherical-Mirror Interferometers
for the
Analysis of Laser Mode Structure

(Spectra-Physics Laser Technical Bulletin Number 6)

Ph 77 ADVANCED PHYSICS LABORATORY
– ATOMIC AND OPTICAL PHYSICS –

Expt. 71 – Fabry-Perot Cavities and FM Spectroscopy

I. BACKGROUND

Fabry-Perot cavities (also called Fabry-Perot etalons) are ubiquitous elements in optical physics, and they are used for such applications as sensitive wavelength discriminators, as stable frequency references, and for building up large field intensities with low input powers. Also, lasers are all made from optical cavities. For our diode lasers, the cavity is made from a semiconductor material a few millimeters in length, and the light propagates inside the semiconductor. Cavities are often made from two curved mirrors as shown in Figure 1.

In this lab you will investigate some cavity properties, and you will see how a cavity can be used as an "optical spectrum analyzer" to measure the spectral content of a laser. In this capacity, you will use the cavity to observe radio-frequency (RF) sidebands on the laser output.

A basic Fabry-Perot cavity consists of two reflectors separated by a fixed distance L, as is shown in Figure 1; curved reflectors are typically used because such a configuration can trap light in a stable mode. (Two flat mirrors can also make a cavity of sorts, but it is not stable; the light "walks off" perpendicular to the cavity axis.) An excellent detailed discussion of the properties of Fabry-Perot cavities is given by Yariv (1991), and you may want to look through Chapter 4 of this text to better understand the details of cavity physics. Another useful, although somewhat dated, reference is attached as an appendix at the end of this hand-out.

Much of the physics of optical cavities can be understood by considering the flat-mirror case, which reduces the problem to 1D. Physically, this case can be realized if the flat mirrors have effectively infinite extent and the input light can be approximated by a perfect plane wave. For two identical mirrors, each with reflectivity R and transmission T ($R + T = 1$), the amplitude of the transmitted and reflected electric field amplitudes (which you will calculate as a prelab problem) are given by

$$E_t = \frac{Te^{i\delta}}{1 - Re^{2i\delta}}E_i$$

$$E_r = \frac{(1 - e^{i2\delta})\sqrt{R}}{1 - Re^{i2\delta}}E_i$$

where E_i is the amplitude of the incident light and $\delta = 2\pi L/\lambda$ is the phase shift of the light after propagating through the cavity (we assume the index of refraction is unity inside the cavity). The transmitted light intensity is then

$$\frac{I}{I_0} = \left|\frac{E_t}{E_i}\right|^2 = \left|\frac{Te^{i\delta}}{1 - Re^{2i\delta}}\right|^2$$

The cavity transmission peaks when $e^{2i\delta} = 1$, or equivalently at frequencies $\nu_m = mc/2L$, where m is an integer, c is the speed of light. At these frequencies the cavity length is an integer number of half-
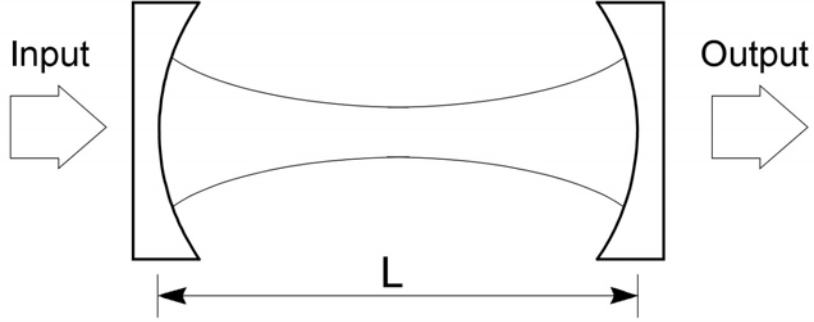
Figure 1. The basic Fabry-Perot cavity. The curved surfaces of the mirrors are coated for high reflectivity, while the flat surfaces are anti-reflection coated and have negligible reflectivity. The curved lines inside the cavity represent the shape of the resonance optical mode.

wavelengths of light. Note that the peak transmission is $I/I_0 = 1$, regardless of R.

The separation between adjacent peaks, called the *free-spectral range,* is given by

$$
\begin{aligned}
\Delta\nu_{FSR} &= \nu_{m+1} - \nu_m \\
&= \frac{c}{2L}.
\end{aligned}
$$

If the mirror reflectivity is high (for our cavity mirrors it is approximately 99.5 percent) then the transmission peaks will be narrow compared with $\Delta\nu_{FSR}$. The full-width-at-half-maximum, $\Delta\nu_{fwhm}$, (*i. e.* the separation between two frequencies where the transmission is half the peak value) is written as

$$
\Delta\nu_{fwhm} = \Delta\nu_{FSR}/F,
$$

where F is called the cavity "finesse." If $T \ll 1$ the finesse can be shown from the above to be approximately

$$
\begin{aligned}
F &\approx \frac{\pi\sqrt{R}}{1-R} \\
&\approx \frac{\pi}{T}
\end{aligned}
$$

The results so far describe an ideal cavity, in which there is no absorption or other loss of light inside the cavity. The peak transmission of such an ideal Fabry-Perot cavity is unity, as can be seen above. Introducing small losses in the cavity leads to the expression

$$
E_t = \frac{T\alpha e^{i\delta}}{1 - R\alpha^2 e^{2i\delta}} E_i
$$

where α is a loss parameter (the fractional intensity loss from a single pass through the cavity is equal to $\varepsilon = 1 - \alpha^2$). This gives a peak cavity transmission

$$
\frac{I_{peak}}{I_0} \approx \frac{T^2(1-\varepsilon)}{(T+\varepsilon)^2} \approx \frac{T^2}{(T+\varepsilon)^2}
$$

and a finesse

$$F \approx \frac{\pi \alpha \sqrt{R}}{1 - \alpha^2 R}$$
$$\approx \frac{\pi}{T + \varepsilon}$$

It is sometimes useful to think of the Fabry-Perot cavity as an interferometer, and it is also useful to think of it as an optical resonator. If the input laser frequency is not near ν_m, the beam effectively just reflects off the first mirror surface (which after all does have a high reflectivity). If the input is equal to ν_m, however, then light leaking out from inside the cavity destructively interferes with the reflected beam. Right after turning on the input beam, the power inside the cavity builds up until the light leaking out in the backward direction exactly cancels the reflected input beam, and the beam leaking out in the forward direction just equals the input beam (neglecting cavity losses). Thus at ν_m the total cavity transmission is unity, and the light bouncing back and forth in the cavity is $\sim 1/T$ times as intense as the input beam.

Problem 1. Derive the above expressions for E_r and E_t as a function of δ when $\varepsilon = 0$. [Hint: write down a series expression that describes the sums of all the transmitted and reflected beams. Use reflected and transmitted amplitudes r and t, where $r^2 = R$ and $t^2 = T$. Then sum the series. Use the fact that if the reflected amplitude is r for light entering the cavity, then it is $r' = -r$ for light reflecting from inside the cavity (why? in one case, light is going from in air into glass; in the other case, light is going from glass into air).] Also derive the peak cavity transmission I_{peak}/I_0, and finesse F, in the limit $T, \varepsilon \ll R$. Plot the transmitted and reflected intensities, I_{tran}/I_0 and $I_{reflect}/I_0$, of a cavity as a function of δ for $R = 0.9$, 0.95, 0.99 and $\varepsilon = 0$.

The Optical Spectrum Analyzer. If we can scan the cavity length, for example by attaching one mirror to a piezo-electric transducer (PZT) tube, as shown in Figure 2, then we can make an interesting gadget called an optical spectrum analyzer. Scanning the spacing L (which equivalently scans the phase δ you used in your calculations) then scans the cavity resonant frequencies ν_m. If the laser beam contains frequencies in a range around some ν_0, then by scanning the PZT one can record the laser spectrum, as is shown in Figure 2. Note that there is some ambiguity in the spectrum; a single laser frequency ν_0 produces peaks in the spectrum analyzer output at $\nu_0 + j\Delta\nu_{FSR}$, where j is any integer. If a laser contains two closely spaced modes, as in the example shown in Figure 2, then the output signal is obvious. But if the laser modes are separated by more than $\Delta\nu_{FSR}$, then the output may be difficult to interpret.

In the lab, you will scan the laser frequency while keeping the cavity length fixed, but the resulting measurements are basically the same as if you scanned the cavity length.

Laguerre-Gaussian Modes. The above analysis strictly holds only for the 1D plane-wave case, and real cavities must have mirrors of finite extent. In this case, it's best to thing of Fabry-Perot cavities as full 3D optical resonators, rather than simply a set of two mirrors. By curving the mirrors, the cavity supports a set of trapped normal modes of the electromagnetic field, known as *Laguerre-Gaussian modes*. As long as the cavity has cylindrical symmetry, the transverse mode patterns are described by a combination of a
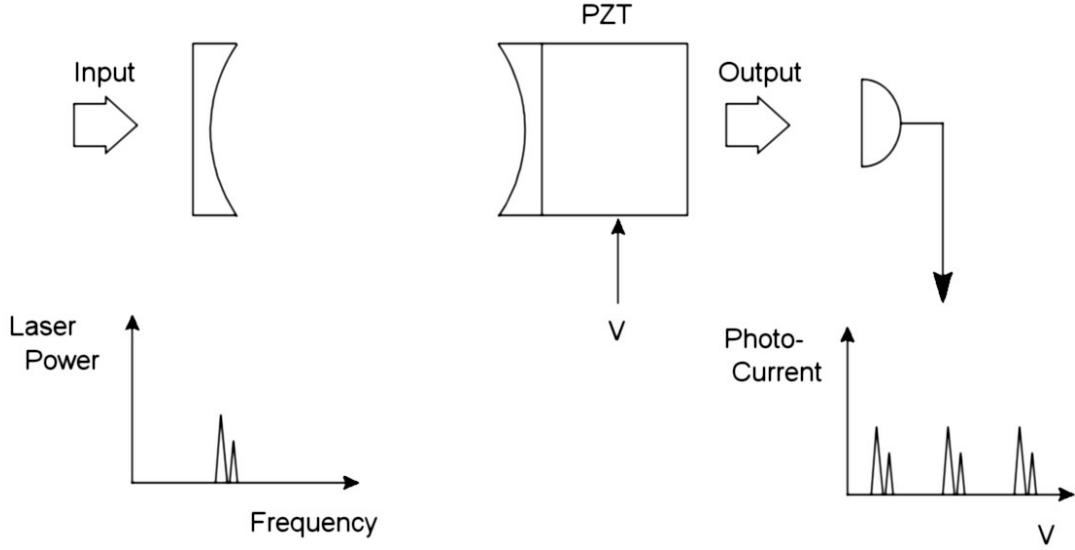
Figure 2. Using a Fabry-Perot cavity as an optical spectrum analyzer. Here the input laser power as a function of frequency $P(f)$ is shown with a multi-mode structure. By scanning the cavity length with a piezoelectric (PZT) tube, the laser's mode structure can be seen in the photodiode output as a function of PZT voltage $I(V)$. Note the signal repeats with the period of the cavity free-spectral range.

Gaussian beam profile with a Laguerre polynomial. The modes are labeled by $\text{TEM}_{p\ell}$, where p and ℓ are integers labeling the radial and angular mode orders. The intensity at a point r, ϕ (in polar coordinates) is given by

$$I_{p\ell}(r, \phi) = I_0 \rho^\ell \left[L_p^\ell(\rho) \right]^2 \cos^2(\ell\phi) e^{-\rho}$$

where $\rho = 2r^2/w^2$ and L_p^ℓ is the associate Laguerre polynomial of order p and index ℓ. The radial scale of the mode is given by w, and modes preserve their general shape during propagation. A sample of some Laguerre-Gaussian modes is shown in Figure 3.

This figure displays the transverse mode profiles; the longitudinal profile of the mode is that of a standing wave inside the cavity, which has some number n of nodes. The various modes with different n, p, and ℓ in general all have different resonant frequencies. The TEM_{00} mode has a simple Gaussian beam profile, and this is the mode one usually wants to excite inside the cavity. Lasers typically use this mode, and thus generate Gaussian output beams. As you will see in the lab, however, it is not always trivial to excite just the TEM_{00} mode inside a cavity.

Note that the mode shape shown in Figure 1 essentially shows w for a TEM_{00} mode as a function of position inside the cavity. The mode has a narrow *waist* at the center of the cavity, and diffraction causes the beam to expand away from the center. At the waist, the wavefronts of the electric field (or equivalently the nodes of the standing wave) are flat and perpendicular to the cavity axis. At the mirrors, the wavefronts are curved and coincide with the mirror surfaces, so the wave reflects back upon itself.
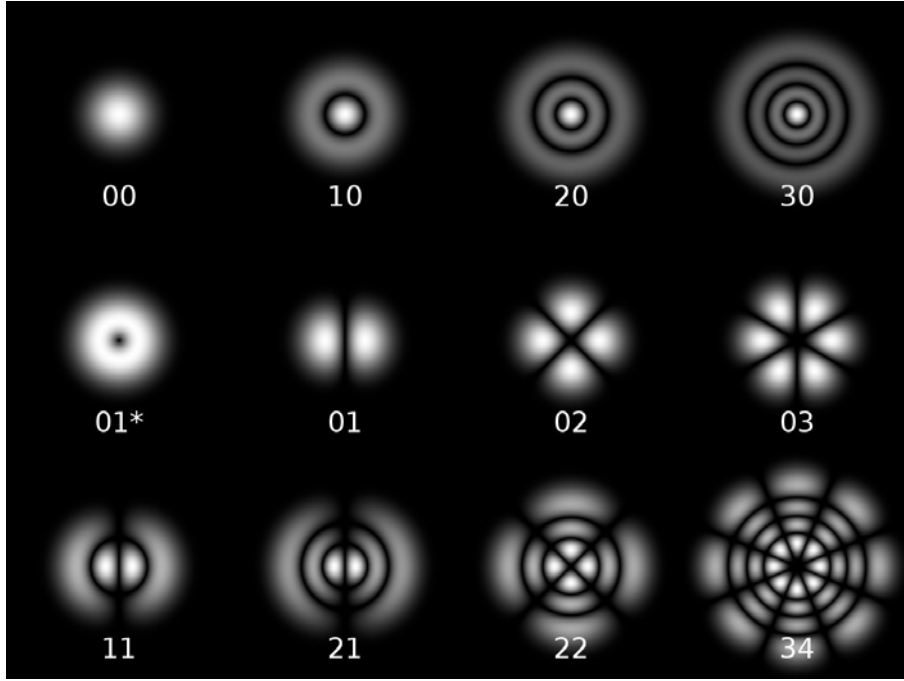
Figure 3. Several Laguerre-Gaussian modes, which are the electromagnetic normal modes inside a Fabry-Perot cavity. The TEM^*_{01} mode, called a doughnut mode, is a superposition of two (degenerate) TEM_{01} modes rotated $90°$ with respect to one another.

Confocal Resonators. An interesting (and useful) degeneracy occurs if we choose the cavity length to be equal to the radius of curvature of the Fabry-Perot mirrors, $L = R_{mirror}$. In this case, the mode frequencies of the various transverse modes all become degenerate with a separation of $c/4L = \Delta\nu_{FSR}/2$ (see Yariv, Section 4.6, for a derivation of this). For this special case, called a "confocal" cavity, the spectrum will look just like that shown in Figure 2, except the mode spacing will be $\Delta\nu_{confocal} = c/4L$. The width of the transmission peaks $\Delta\nu_{fwhm}$ stays roughly the same in principle, but in practice $\Delta\nu_{fwhm}$ depends on how well the cavity is aligned, and how precisely we have $L = R_{mirror}$.

Another nice feature of the confocal cavity is that the cavity transmission is insensitive to laser alignment. Figure 4 shows that each resonant mode in the confocal cavity can be thought of as a "bow-tie" mode, which traverses the cavity twice before retracing its path – hence $\Delta\nu_{confocal} = c/4L$. This is a crude picture, but it can be helpful in understanding the confocal cavity. It shows you in a rough way how the output spectrum might be insensitive to alignment, since the bow-tie modes are excited no matter where the beam enters the cavity. You will work with a confocal and non-confocal cavity in the lab, and hopefully this will all make good sense once you see it all in action.

FM Spectroscopy. In the radio-frequency domain, there exists a substantial technology built up around amplitude-modulation and frequency-modulation of an electromagnetic carrier wave (which gives us, for example, AM and FM radio broadcasting). If one boosts the typical carrier wave frequency from 100 MHz
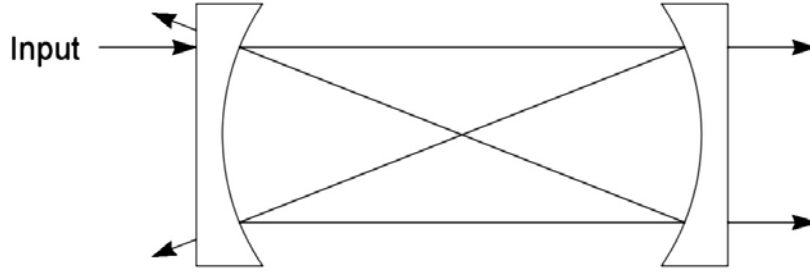
Figure 4. Ray paths for a confocal Fabry-Perot cavity (the off-axis scale is exaggerated).

(FM radio) to 500 THz (optical), the same ideas apply to AM and FM modulation of lasers. The resulting optical technology has many applications, the most dominant one being fiber-optic communications.

Modulating the injection current to the diode laser is a very simple way to modulate the laser output, both in frequency and amplitude. (Using non-linear crystal modulators is another way to modulate a laser beam.) The basic idea is that one drives the laser with an injection current which consists of a large DC part and a small high-frequency AC part on top. The AC part produces both AM and FM modulation of the laser, but we will ignore the smaller AM part for now.

For pure frequency modulation, we can write the electric field of the laser beam at some fixed location as:

$$\vec{E}(t) = \vec{E}_0 \exp(-i\omega_0 t - i\phi(t))$$

where $\phi(t)$ is the modulated phase of the laser output. We always assume that $\phi(t)$ is slowly varying compared to the unmodulated phase change $\omega_0 t$, since ω_0 is at optical frequencies, and our modulation will be at radio frequencies. If we're putting in a single sinusoidal phase modulation we have

$$\phi(t) = \beta \sin(\Omega t)$$

where Ω is the modulation frequency, and β, called the modulation index, gives the peak phase excursion induced by the modulation. If we note that the instantaneous optical frequency is given by the instantaneous rate-of-change of the total phase, we have

$$
\begin{aligned}
\omega_{\text{instant}} &= \omega_0 + d\phi/dt \\
&= \omega_0 + \beta\Omega\cos(\Omega t) \\
&= \omega_0 + \Delta\omega\cos(\Omega t)
\end{aligned}
$$

where $\Delta\omega$ is the maximum frequency excursion. Note that $\beta = \Delta\omega/\Omega$ is the dimensionless ratio of the maximum frequency excursion to frequency modulation rate.

It is useful to expand the above expression for the electric field into a carrier wave and a series of

sidebands

$$
\begin{aligned}
\vec{E}(t) &= \vec{E}_0 \exp[-i\omega_0 t - i\beta \sin(\Omega t)] \\
&= \vec{E}_0 \sum_{n=-\infty}^{n=\infty} J_n(\beta) \exp[-i(\omega_0 + n\Omega)t] \\
&= \vec{E}_0 \left\{ J_0(\beta) \exp(-i\omega_0 t) + \sum_{n=1}^{n=\infty} J_n(\beta) \left[\exp[-i(\omega_0 + n\Omega)t] + (-1)^n \exp[-i(\omega_0 - n\Omega)t]\right] \right\}
\end{aligned}
$$

This transformation shows that our original optical sine-wave has now developed a comb-like structure in frequency space. The J_0 term at the original frequency ω_0 is the optical "carrier" frequency (in analogy with radio terminology), while the other terms at frequencies $\omega_0 \pm n\Omega$ form sidebands around the carrier. The sideband amplitudes are given by $J_n(\beta)$, which rapidly becomes small for $n > \beta$. Note that the total power in the beam is given by

$$
\bar{E} \cdot \bar{E}^* = E_0^2 \left[J_0^2(\beta) + 2 \sum_{n=1}^{n=\infty} J_n(\beta)^2 \right] = E_0^2
$$

which is independent of β, as it must be for pure frequency modulation. Often one wishes to add two small sidebands around the carrier, for which one wants $\beta << 1$, and the sideband power is then given by $\sim J_1(\beta)^2 \approx \beta^2/4$. Evaluating the above sum, and convolving with a Lorentzian laser+cavity spectrum gives an output power

$$
I(\omega) = J_0^2(\beta) L(\omega; \omega_0) + \sum_{n=1}^{n=\infty} J_n(\beta)^2 [L(\omega; \omega_0 + n\Omega) + L(\omega; \omega_0 - n\Omega)]
$$

where $L(\omega; \omega_0)$ is a normalized Lorentzian function centered at ω_0.

Problem 2. Evaluate and plot the above optical spectrum, as you might expect to see it using your Fabry-Perot optical spectrum analyzer (remember that a photodiode measures optical *power*, not electric field amplitude). Plot versus frequency $\nu = \omega/2\pi$, which is what a frequency meter reads. Assume a Lorentzian laser+cavity linewidth of $\Delta\nu = 10$ MHz. Plot three curve with: 1) $\Omega/2\pi = 120$ MHz, $\beta = 0.5$; 2) $\Omega/2\pi = 30$ MHz, $\beta = 1.5$; and 3) $\Omega/2\pi = 1$ MHz, $\beta = 20$. Note for the last plot you will have to evaluate the sum up to fairly high n, at least to $n > \beta$. For $\beta \gg 1$, note that the spectrum looks much like what you would expect for slowly scanning the laser frequency from $\omega_0 - \beta\Omega$ to $\omega_0 + \beta\Omega$.

II. LABORATORY EXERCISES.

Your first task in this lab is to look at the light transmitted through a simple cavity using the set-up shown in Figure 5. Use the ramp generator in the laser controller to scan the laser frequency (ask your TA how), and monitor the photodiode output on the oscilloscope.

In order to get any light through the cavity, you need to align the incoming laser beam so that: 1) the beam hits the center of the first mirror, and 2) the beam is pointed down the cavity axis. The mirrors M1 and M2 provide the necessary adjustments to align the incident beam, and note that the different degrees of freedom are nicely decoupled – M1 mostly changes the laser position at the cavity, and M2 mostly changes the angle of the entering beam.
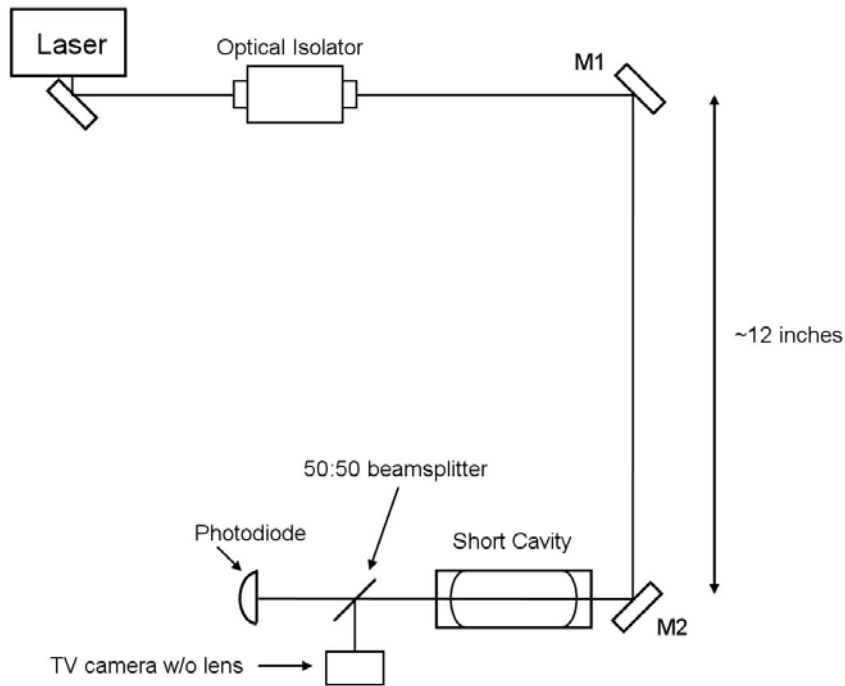
Figure 5. Optics set-up to view the light transmitted through the short cavity.

First adjust M1 so the beam is centered on the cavity, and then adjust M2 so the backreflected beam coincides with the incident beam. Use a white card with a hole in it to see the position of the backreflected beam. Iterate as necessary.

When this looks good, place a white card behind the cavity to view the transmitted beam. It will be faint, but you should be able to see a pair of bright spots, or perhaps a bright ring, on the card. To bring the transmitted beam to a single spot, you will probably need to "walk" the input beam, which is a way to systematically sample the 4-dimensional alignment space defined by the four adjustments of M1 and M2. Your TA can show you how. Once you have the transmitted beam down to a single, sharp spot, place the photodiode to intercept the beam, and place the TV camera to view the shape of the beam.

With the sweep on, you should see a forest of peaks on the transmitted signal. Each peak corresponds to a single cavity mode you are exciting with the laser. Each $\text{TEM}_{np\ell}$ mode has a slightly different frequency, so each gives a separate peak. In addition, the spectrum repeats with a period of $\Delta\nu_{FSR}$. If you tweak the alignment of the incoming beam slightly, you will see the peaks all change height. This is because you excite different modes with different alignments.

With the sweep off, you can examine the shapes of the different modes using the TV camera. Move the piezo DC offset adjust to select different modes. Compare with Figure 3 above. **Print out an oscillo-scope trace showing a typical scan, and tape it into your notebook.**
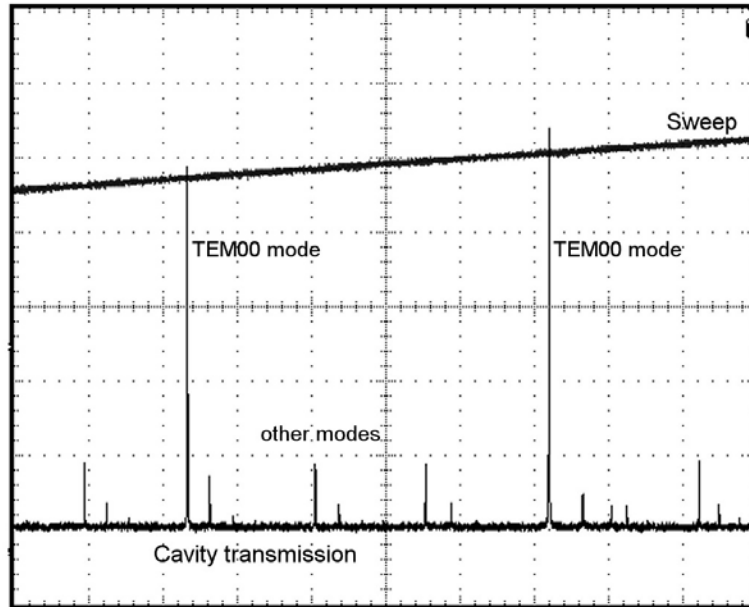
Figure 6. The cavity transmission with fairly good mode matching. Note the dominant TEM$_{00}$ modes separated by $\Delta\nu_{FSR}$. The peaks heights are very sensitive to alignment and even to vibration.

Mode Matching. Now you should try to excite just the TEM$_{00}$ mode of the cavity, which means you have to *mode match* the incoming beam to the cavity mode. If you think about the mode inside the cavity (see Figure 1), you can see that the beams leaking out of the cavity diverge in both directions. You can see this if you use a white card with a hole in it placed far from the cavity. The reflected beam from the cavity will make a large spot on the card, much larger than the incoming beam. Thus the input beam is not well matched to the cavity modes.

To match the TEM$_{00}$ mode, the incoming beam should be converging. You can achieve this by placing a 500mm focal length lens about 11 inches in front of the cavity. Before aligning the cavity, note that the size of the reflected beam is now about equal to the incoming laser size, so the mode match is better than before.

Align the cavity with the lens in place and view the transmitted signal. You should see fewer large modes. Turn the sweep down to identify the different modes on the TV. Find the TEM$_{00}$ mode, and tweak the mirror alignment to maximize this mode while minimizing the others. With some effort, you can produce a transmitted signal that looks something like that shown in Figure 6, with dominant TEM$_{00}$ peaks separated by $\Delta\nu_{FSR}$. You cannot do much better than this, even in theory, for two reasons: 1) the mode-matching lens is actually not quite right to match to the cavity, so you are bound to excite some other modes; and 2) the incoming laser beam is itself not a perfect TEM$_{00}$ mode (expand the beam with a lens and you can see that it doesn't have a perfect Gaussian shape), which means it contains other modes

at some level. **Print out a trace showing your best TEM$_{00}$ modes.**

The Confocal Cavity. The next task is to set up the confocal Fabry-Perot cavity as shown in Figure 7 and to look at some of its properties. Unlike the previous cavity, the confocal cavity is insensitive to the precise alignment and mode matching of the input beam, because the different transverse modes are degenerate in frequency (see the discussion in Section I above). Nevertheless, you still have to align things reasonably well, using the same procedures described above.

Observe the Mode Structure of the Cavity. Align the input beam and adjust the cavity length until the transmitted signal shows a series of sharp peaks (much different than with the non-confocal cavity!). Tweak the cavity length so the peaks are narrow and symmetrical, which should maximize the transmitted peak intensity. Once that looks good, change the cavity length by a large amount (say 10 turns of the mounting tube) and observed the transmitted spectrum. As the cavity length is changed away from the confocal length, the transverse modes are no longer degenerate. At first, you see the peaks broaden and become asymmetrical. Then, as you change the length more, you can see individual mode peaks show up. Change the input beam alignment to see the different modes change in amplitude. **Print out a few spectra with different cavity lengths.**

Measure the Transmitted and Reflected Intensities. Adjust the cavity length to its confocal value, and align the input beam to maximize the height of the transmitted peaks. Tweak the length and alignment with some care to produce sharp, symmetrical peaks with the highest possible amplitude. When that looks good, insert a "pick-off" mirror somewhere in the beam and send it to the second photodiode. Use the mirror to maximize the photodiode signal on the oscilloscope (so the beam is centered on the photodetector), and measure the output voltage (and note the photodiode gain). It works well to use the "measure" feature on the oscilloscope to measure the average output voltage. With care, you could convert this voltage to milliwatts of laser power, but you will be taking power ratios, so you don't need this conversion.

Without changing the cavity alignment, set up the second lens and photodiode as shown in Figure 7. Again make sure the beam is centered on the photodetector and measure the output signal. The value should be about 25% of what you measured previously (because the beam intensity was diminished twice by the 50:50 beamsplitter). If you don't get within a few percent of that value, something is wrong (probably the alignment).

Next send the first photodiode signal directly into the oscilloscope along with the second. Note that the dips in reflected light correspond to the peaks in transmitted light, as you would expect. Measure the peak widths and make sure they are greater than 20 μsec, so that the photodiode is fast enough to record the full peak. If not, use a slower scan. **Measure the height of the transmitted peaks and compare with the input beam intensity, to produce a peak transmitted fraction**. Keep in mind the photodiode gains, which may be different, and how many times the various beams went through the beamsplitter. You should be able to produce a transmitted fraction between 5% and 10%. If your measurement is above 10%, you probably made an error somewhere (or your cavity alignment is amazingly good). If
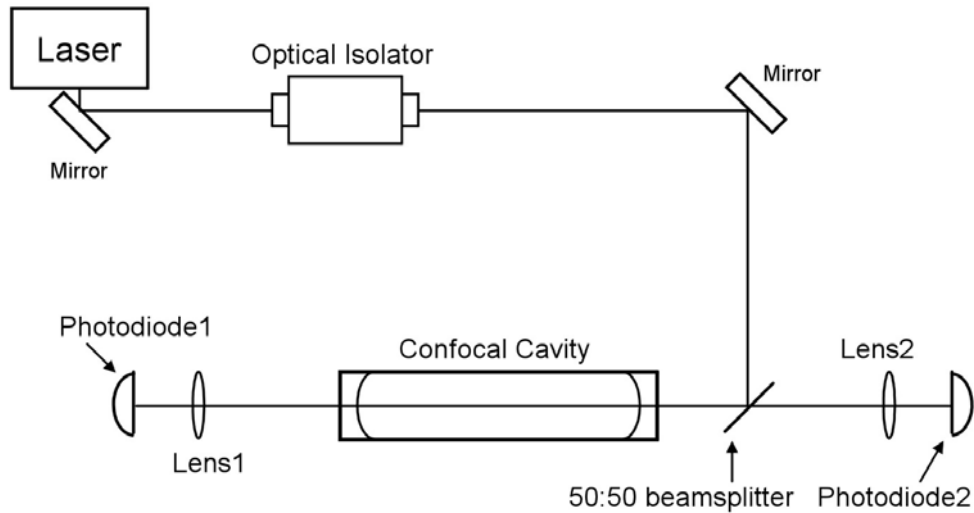
Figure 7. Optics set-up for the confocal cavity.

your measurement gives you something below 5%, again check for simple errors. If that's not it, tweak the cavity length and alignment until the peak transmitted fraction is above 5%. When everything looks good, **print out the spectrum showing sharp peaks.**

Measure the Cavity Finesse. Capture a single sweep on the oscilloscope and use the built-in cursors to measure the effective finesse of the cavity. Measure the spacing between the peaks (the free spectral range) and then change the time-base on the 'scope and measure the full-width at half-maximum of the peaks. The effective finesse is then $F = \Delta\nu_{FSR}/\Delta\nu_{FWHM}$. You should get $F > 100$ or even $F > 200$ if the cavity is well aligned.

Why is the transmitted peak intensity only 5%, when in principle it could be 100%? Part of the reason is losses inside the cavity, as described in the discussion in Section I, but that's only a small part. Calculate about how great the losses would have to be to produce a 5% transmitted intensity, assuming a mirror transmission of 1%. The actual mirror losses are probably less than 0.1% per bounce (unless the mirrors are very dirty, which they shouldn't be).

The main reason for the low transmitted intensity is that the mode degeneracy is not perfect. If you change the cavity length or input beam alignment only slightly, you can see the peak height drop quickly. Since the input beam is not mode-matched to the cavity, the transmitted intensity of any given mode is fairly low. And if the modes are not perfectly degenerate, they don't overlap well, resulting in a low peak intensity. With a non-confocal cavity and a well mode-matched beam, it is possible to achieve a peak transmitted intensity close to 100%. However, for simply looking at the frequency structure of a laser (i.e., with an optical spectrum analyzer), the confocal cavity is quite convenient to use, even with its lower transmitted intensity.

FM Spectroscopy. Next you should observe the FM spectra you calculated in the prelab exercises, using the confocal Fabry-Perot cavity as an optical spectrum analyzer. With the transmitted signal showing nice sharp peaks, reduce the sweep to zoom in on a single peak. Then take the RF function generator, turn it on, and feed it into the RF Input BNC of the diode laser. (NOTE: Do not disconnect the cable from its connection at the laser. The laser is sensitive to static discharge, which can easily burn out the diode. Also turn the RF generator on *first*, and then feed the output into the laser. This helps avoid voltage spikes that may occur when you turn the generator on.)

As you vary the oscillator frequency $\Omega/2\pi$ and the amplitude (which changes $\Delta\omega$ and thus β), you should observe the range of behavior you calculated. **Record several traces that correspond as closely as you can achieve to your three calculated plots.** You should get pretty good agreement (if not, check with the TA). One significant difference between calculated and measured spectra is that the measured spectra may be asymmetric. This is due to residual *amplitude* modulation of the laser, which we did not include in our pure FM calculation.

Measure the Free-Spectral Range. Finally, put two high-frequency sidebands on your laser, **print out a spectrum**, and use the known sideband frequency to measure the free-spectral-range of the Fabry-Perot cavity. Compare with what you expect for a cavity length of 20 cm (equal to the radius of curvature of the mirrors).

III. REFERENCES

Yariv, A. 1991, *Optical Electronics*, Saunders College Publishing, 4th ed.

Spectra-Physics Laser Technical Bulletin Number 6

Ⓢ

Scanning Spherical-Mirror Interferometers For The Analysis of Laser Mode Structure

I. Introduction

Scanning spherical-mirror interferometers[1] have become common tools for the analysis of laser radiation. They are very high-resolution spectrometers, and can be used to provide information concerning laser mode structure that is difficult to obtain using any other instrument.

For a variety of practical reasons, scanning spherical-mirror interferometers have been difficult to use. Recently, however, it has been found that certain special types of these interferometers are comparatively easy to use: these special types of interferometers are "mode-degenerate" interferometers. Of the mode-degenerate interferometers, the most useful is the confocal interferometer, first described, in a somewhat different form than is now common, by Connes[2].

The principal reason for the interest in using scanning spherical-mirror interferometers to study laser radiation is, of course, that the light emitted by most ordinary gas lasers is not perfectly monochromatic. The beam from a typical gas laser contains several discrete optical frequencies, separated from each other by frequency differences of "radio-frequency" magnitude ($10^6 - 10^9$ Hz). These different optical frequencies can be associated with different modes of oscillation of the laser.

It is common practice to distinguish two types of laser modes: "longitudinal" modes differ from one another only in their oscillation frequency; "transverse" modes differ from one another not only in their oscillation frequency, but also in their field distribution in a plane perpendicular to the direction of propagation. Corresponding to a given transverse mode are a number of longitudinal modes which have the same field distributions as the given transverse mode but differ in frequency; it is not customary, however, to associate different transverse modes with a given longitudinal mode.

Most applications of gas lasers require that the laser operate in a single transverse mode. Moreover, in most cases, the laser must operate in the lowest order (TEM_{oo}) transverse mode. The reason for this concerns the amount of power that can be focused in a diffraction-limited beam: more power can be focused in such a beam when the laser operates in the lowest-order transverse mode than when it operates in high-order transverse modes[3].

In many applications of gas lasers, the longitudinal mode structure of the laser beam is also important. In holography, for example, the presence of several longitudinal modes limits the coherence length of the emitted light, and hence the depth of field of holograms made with it. In many communications experiments, the presence of several longitudinal modes may give rise to distortion effects. In some spectroscopic applications, the resolution is limited by the number of oscillating longitudinal modes.

As mentioned above, the scanning spherical-mirror interferometer is a powerful tool for studying the mode structure of gas lasers. There are, however, other methods which are used to study laser mode structure. The most common of these employs a radio-frequency spectrum analyzer. When a laser beam is detected by a photodetector, the output current from the photodetector will contain signals at the difference frequencies between the various modes of the laser beam. By measuring the frequencies and amplitudes of the various difference-frequency signals, some characteristics of the optical spectra can be deduced.

Radio-frequency measurements have some advantages and some disadvantages over direct optical-frequency measurements, such as those obtained from scanning spherical-mirror interferometers. Radio-frequency measurements usually have higher resolution than optical-frequency measurements.

On the other hand, conventional radio-frequency measurements do not give complete information about the optical mode spectra.

Consider the case of a laser beam containing two modes, one large in amplitude, and one small in amplitude. If such a beam is detected by a photodetector, the output current will contain a signal which oscillates at a frequency equal to the difference frequency between the two modes. However, there will be no way to determine whether the strong mode is the higher-frequency mode or the lower-frequency mode. Both situations will give the same radio-frequency output signal. With direct optical-frequency spectroscopy, this ambiguity does not occur: the output signal gives complete information regarding the spectrum.

Radio-frequency measurements are most useful when it is only necessary to detect the presence or absence of certain modes in a laser beam. In general, direct optical-frequency measurements are easier to interpret and easier to perform.

II. The Fabry-Perot Interferometer

Scanning spherical-mirror interferometers belong to the general class of multiple-beam interferometers. The most common multiple-beam interferometer is the Fabry-Perot etalon, which consists of two plane mirrors which are placed parallel to one another, separated by a distance d. The resonance condition for such an interferometer is that the spacing between the mirrors be equal to an integral number of half wavelengths of the incident light. If the interferometer is illuminated at normal incidence with a collimated beam of frequency v_o, the resonance condition is

$$v_o = \frac{mc}{2d} , \qquad (1)$$

where m is an integer and c is the velocity of light.

More generally, it can be shown that the transmittance of the etalon is given by the famous Airy formula

$$\frac{I}{I_o} = \frac{1}{\left(1 + \dfrac{A}{T}\right)^2} \; \frac{1}{1 + \dfrac{4R}{(1-R)^2} \sin^2 \dfrac{2\pi vd}{c}} , \qquad (2)$$

where I_o is the intensity of the beam incident on the interferometer, I is the intensity of the beam emerging from the interferometer, R is the reflectance of the mirrors, T is the transmittance of the mirrors, and A is the "dissipative" loss of the mirrors.

For high-reflectance mirrors (typical of modern Fabry-Perot etalons) the transmission "fringes" are extremely sharp. Under these conditions, the transmittance of the Fabry-Perot etalon will be

negligible unless the sine term is nearly zero. We may thus use the approximations $\sin \theta \approx \theta$ and R ≈ 1 to write the Airy formula as

$$\frac{I}{I_o} = \frac{1}{\left(1 + \dfrac{A}{T}\right)^2} \; \frac{1}{1 + \left(\dfrac{4\pi d}{c(1-R)}\right)^2 (v-v_o)^2} . \qquad (3)$$

This formula is illustrated graphically in Figure 1. We see that near a transmission fringe, the transmittance of a Fabry-Perot etalon is a Lorentzian function of frequency having a full-width at half maximum of

$$\Delta v = \frac{c(1-R)}{2\pi d} . \qquad (4)$$

The quantity Δv is called the "instrumental bandwidth" of the etalon.
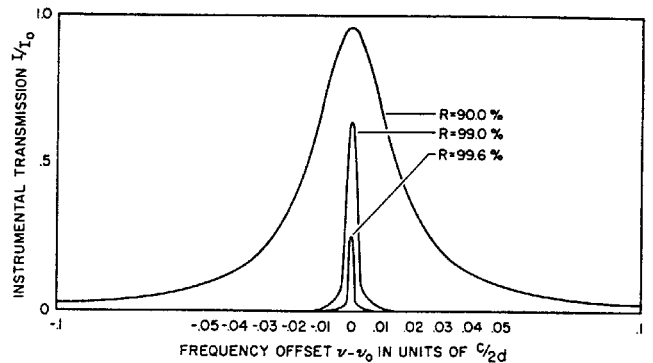
1. Transmittance of a Fabry-Perot etalon for various mirror reflectances. The "dissipative" loss of the mirrors is assumed to be 0.2%.

Note from (1) that the difference in frequency between two transmission fringes, called the "free-spectral-range" of the etalon, is given by

$$\text{FSR} = \frac{c}{2d} . \qquad (5)$$

The ratio of the free-spectral-range to the instrumental bandwidth is called the "finesse" of the etalon. Using (4) and (5), we find for the finesse

$$F = \frac{\pi}{(1-R)} . \qquad (6)$$

The ratio of the transmission frequency to the instrumental bandwidth is known as the resolving power, or "Q" (quality factor) of the etalon. We thus have

$$Q = \frac{2\pi vd}{c(1-R)} . \qquad (7)$$

The Fabry-Perot etalon, although it is a versatile tool for the high-resolution spectroscopy of ordinary light sources, is of limited usefulness in analyzing laser mode structure. The reason for this is that an ordinary Fabry-Perot etalon does not have

sufficient resolving power to be very useful in analyzing laser beams.

A typical gas-laser transition has a Doppler linewidth of a few gigahertz. The various modes of the laser are typically separated by a few tens of megahertz. In order for an interferometer to be useful in analyzing laser mode spectra, it should have a free-spectral-range which is larger than the Doppler linewidth and an instrumental bandwidth which is small compared to the frequency differences between the various modes of the laser; in short, it should have a high finesse. For analyzing laser mode spectra, it is usually desirable to employ an interferometer having a finesse of at least one hundred.

It is very difficult to make Fabry-Perot etalons which have a finesse of 100. A typical value for the finesse of a Fabry-Perot etalon is ≈ 30, although it is possible to obtain somewhat higher values with high-quality instruments.

Two principal factors limit the finesse of Fabry-Perot etalons. The surface figure of the mirrors must be flat to approximately the transmission wavelength divided by the finesse of the interferometer. Thus, an interferometer having a finesse of 100 must have mirrors which are flat to 1/100 wavelength over the useful aperture. If the aperture of the interferometer is small enough, the mirrors may indeed appear flat to within 1/100 wavelength. However, if the aperture is made small, diffraction effects which limit the finesse of the interferometer become important.

The Airy formula given above neglects the effects of diffraction. If the diameter of the interferometer mirrors is large compared to their separation, diffraction is not important. However, if a small aperture is placed within the interferometer in an attempt to improve the effective figure of the mirrors, diffraction effects at the edges of the aperture cause a "loss" in the interferometer which is equivalent to a reduction in the reflectance of the mirrors. This equivalent reduction in reflectance limits the finesse of the interferometer.

III. Spherical-Mirror Interferometers

The diffraction effects which are characteristic of Fabry-Perot etalons can, to a large extent, be eliminated by using spherical mirrors in the interferometer. The radii of curvature of the mirrors (which, for the sake of simplicity, we assume to be equal) must be greater than one half their separation.

The diffraction loss of a spherical-mirror interferometer is orders of magnitude lower than that of a Fabry-Perot interferometer, and is usually small enough to be negligible. In addition, the surface figure on the mirrors of a spherical-mirror interferometer is considerably less critical than the figure on the mirrors of a Fabry-Perot interferometer. The reason for this comparatively large figure tolerance is that only a small area (typically < 1 mm²) of the spherical-mirror interferometer mirrors is useful. Thus, mirrors which are good to within 1/10 wavelength over their entire area may contain small areas having a figure of better than 1/100 wavelength.

The salient characteristic of a general spherical-mirror interferometer is that it must be illuminated with a narrow, diffraction-limited beam to work properly. In laser terminology, it must be "mode-matched" to the laser which is to be analyzed.

The various modes of a spherical-mirror cavity resonate at frequencies given by

$$\nu_0 = \frac{c}{2d} \left[q + \frac{1}{\pi} (1 + m + n) \cos^{-1} \left(1 - \frac{d}{R} \right) \right],$$

(8)

where c is the velocity of light, d is the separation of the mirrors, R is the radius of curvature of the mirrors, q is an integer denoting the longitudinal-mode number, and m and n are integers denoting the transverse-mode numbers.

A spherical-mirror interferometer will have a high transmission for frequencies which satisfy the resonance condition (8). The resonance frequencies corresponding to different values of q define the different longitudinal modes of the interferometer. The resonance frequencies corresponding to different values of m and n define the different transverse modes of the interferometer. Note that to any specific transverse mode there correspond a number of longitudinal modes.

The frequency separation of any two interferometer resonances defines the free-spectral-range of the interferometer. In order for the free-spectral-range of the interferometer to be large enough to be useful, it is necessary to restrict the excitation of the interferometer to a single transverse mode. The various longitudinal modes corresponding to that transverse mode then determine the free-spectral-range to be c/2d, as is the case for the Fabry-Perot etalon. In practice, the only transverse mode of the interferometer which is convenient to excite is the lowest-order (TEM$_{00}$) mode.

The requirement that a general spherical-mirror interferometer be excited in a single transverse mode causes considerable complication in practical applications of the device. In order to match the laser beam into the TEM$_{00}$ mode of the interferometer, the laser itself must operate in the TEM$_{00}$ mode. In addition, the interferometer must be carefully aligned so that its axis corresponds to the propagation axis of the incoming laser beam. When such alignment is accomplished, light reflected

from the interferometer travels back into the laser and perturbs the modes of the laser. It is thus necessary to use an optical isolator between the laser and the interferometer. Finally, the beam diameter and divergence of the incoming laser beam must be matched to the beam diameter and divergence of the TEM_{oo} mode of the interferometer.

If the above conditions are not fulfilled, the interferometer will not work properly. The most serious defect of general spherical-mirror interferometers is that if they are not properly mode-matched to the incoming laser beam, they will have "spurious" transmission fringes. These fringes are caused by the excitation of high-order transverse modes of the interferometer, which generally resonate at different frequencies than the TEM_{oo} mode.

The above requirements make the general spherical-mirror interferometer rather difficult to use. Fortunately, by using special forms of spherical-mirror interferometers, these requirements can be considerably relaxed. These special forms of spherical-mirror interferometers are called "mode-degenerate" interferometers.

IV. Mode-Degenerate Interferometers

For practical applications, mode-degenerate interferometers are more useful devices than are general spherical-mirror interferometers. The fundamental reason for this is that mode-degenerate interferometers do not need to be mode-matched to the incident laser beam. This fact permits considerable simplification in the experimental use of mode-degenerate interferometers. Specifically:

1. Since the transverse modes of the laser do not need to be matched to the transverse modes of the interferometer, it is not necessary that the laser operate in a single transverse mode.

2. There are no "spurious" resonances in mode-degenerate interferometers.

3. Since mode-matching is not required, the interferometer need not be accurately located on the axis of the incident laser beam; this reduces the required alignment tolerance of the interferometer.

4. When the axis of the interferometer does not coincide with the axis of the incident laser beam, the light reflected by the interferometer does not travel back into the laser and perturb the laser oscillation. It is thus usually desirable to use the interferometer with off-axis illumination.

A mode-degenerate interferometer is a spherical-mirror interferometer whose transverse modes are degenerate in frequency. The operation of such interferometers can be understood by considering that, if the radii of curvature and separation of the mirrors of a spherical-mirror interferometer satisfy the equation

$$\cos^{-1}\left(1 - \frac{d}{R}\right) = \frac{\pi}{l} , \qquad (9)$$

where l is an integer, then the resonance equation (8) can be written as

$$v_0 = \frac{c}{2ld} [lq + 1 + m + n] . \qquad (10)$$

Since increasing the sum $(m+n)$ by l and decreasing q by one leaves the resonant frequency of the interferometer unchanged, it follows that the interferometer will have l "sets" of degenerate transverse modes. These l "sets" of modes will be equally separated in frequency.

The best-known mode-degenerate interferometer is the confocal interferometer, which corresponds to $l = 2$. The confocal interferometer has "even-symmetric" modes corresponding to $(m+n)$ even, and "odd-symmetric" modes, corresponding to $(m+n)$ odd. The even-symmetric mode resonances fall exactly halfway between the odd-symmetric mode resonances. Thus the free-spectral-range of a confocal interferometer, when it is illuminated simultaneously in several transverse modes, is $c/4d$, rather than $c/2d$.

In general, the free-spectral-range of an l-fold mode-degenerate interferometer is given by

$$FSR = \frac{c}{2ld} . \qquad (11)$$

The transmittance of an l-fold mode-degenerate interferometer is given by

$$\frac{I}{I_o} = \frac{T^2 \sum\limits_{j=1}^{l} R^{2(j-1)}}{(1-R^l)^2} \frac{1}{1 + \frac{4R^l}{(1-R^l)^2} \sin^2 \frac{2\pi vld}{c}} . \qquad (12)$$

Note that, if $l = 1$, the above equation reduces to the Airy formula (2). If the reflectance of the mirrors is close to unity, we find for the transmittance of the interferometer near a resonant frequency:

$$\frac{I}{I_o} = \frac{1}{l\left(1 + \frac{A}{T}\right)^2} \frac{1}{1 + \left(\frac{4\pi d}{c(1-R)}\right)^2 (v - v_0)^2} . \qquad (13)$$

The instrumental bandwidth is thus given by

$$\Delta v = \frac{c(1-R)}{2\pi d} ; \qquad (14)$$

the resolving power by

$$Q = \frac{2\pi v d}{c(1-R)} ; \qquad (15)$$

and the finesse by

$$F = \frac{\pi}{l(1-R)}.\qquad(16)$$

We thus see that the instrumental bandwidth and Q of a mode-degenerate interferometer are the same as for a general spherical-mirror interferometer or a Fabry-Perot etalon, but that the free-spectral-range, finesse, and peak transmission are reduced by a factor l. We can also see why the confocal interferometer is the most useful mode-degenerate interferometer: it has the highest finesse of any mode-degenerate interferometer. (The concentric interferometer, which corresponds to $l = 1$, is not mode-degenerate; the theory leading to equation (8) is not valid in the concentric limit.)

Mode-degenerate interferometers can also be analyzed in terms of geometrical optics[4]. The condition expressed in equation (9) is equivalent to the condition that a ray launched in the cavity retrace its path after l complete traversals of the cavity. Thus, from the standpoint of geometrical optics, an l-fold mode-degenerate interferometer appears to have an effective length which is l times the actual distance between the mirrors. A typical ray path for a confocal interferometer is shown in Figure 2.
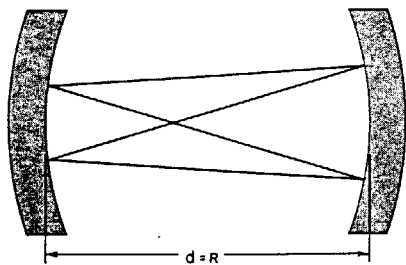
2. Ray paths in a confocal interferometer.

The factors which limit the performance of mode-degenerate interferometers are the reflectance of the mirrors, the surface figure of the mirrors, and the spherical aberration of the mirrors.

The limitation imposed by the reflectance of the mirrors is not usually serious. It is now possible to obtain mirrors having a reflectance of greater than .998. In a confocal interferometer, this corresponds to a finesse (c.f. equation 16) of more than 750. Such values of finesse have been realized experimentally.

The surface figure requirement on the interferometer mirrors presents a somewhat more serious problem. As is the case for a Fabry-Perot etalon, the surface figure must be accurate to roughly the transmission wavelength divided by the finesse. In order to minimize the requirements on the surface figure of the mirrors, the diameter of the incoming laser beam should be approximately equal to the diameter of the TEM$_{oo}$ mode of the interferometer.

Spherical aberration of the mirrors gives rise to a fundamental limitation on the amount of mode-mismatch that can be tolerated in a mode-degenerate interferometer. The theory of Hermite-Gaussian mode structure in spherical-mirror interferometers is based on the paraxial-optics approximation. If a mode-degenerate interferometer is illuminated too far off-axis, the paraxial-optics approximation cannot be used to describe its behavior. The dominant aberration which enters the theory is spherical aberration. The amount of spherical aberration in the interferometer depends on the radius of curvature and separation of the mirrors.

For a confocal interferometer, one can show that the path-difference variation, caused by spherical aberration, for rays entering the interferometer parallel to the axis, but displaced from it by a distance h, is given by

$$\Delta = -\frac{h^4}{d^3}.\qquad(17)$$

If we demand that this path-difference variation be less than the transmission wavelength of the interferometer divided by the finesse, we find that the incoming beam must have a radius h given by

$$h < \left(\frac{\lambda d^3}{F}\right)^{1/4}.\qquad(18)$$

V. Experimental Properties of Mode-Degenerate Interferometers

In this section, we consider some of the practical aspects of mode-degenerate interferometers. As discussed in the preceding section, the confocal interferometer is the most useful of the mode-degenerate interferometers, because it has the highest finesse. Most of the discussion in this section is specifically, but not inevitably, related to the confocal interferometer.
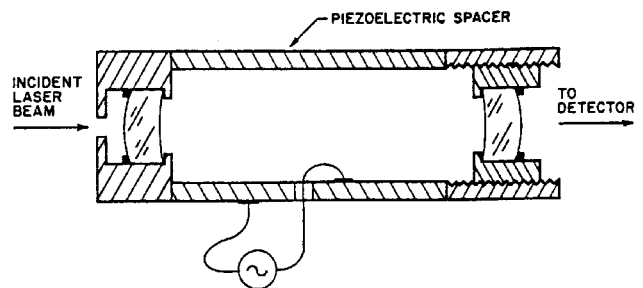
3. Scanning confocal interferometer.

Figure 3 shows a typical scanning confocal interferometer. It comprises two spherical mirrors, separated by a distance equal to their radius of curvature. The back surfaces of the mirrors are made such that the mirrors are self-collimating: that is, a plane wavefront incident on the interferometer will be transformed into a spherical wavefront whose radius of curvature matches that of the transverse modes of the interferometer. The concave surfaces of the mirrors are coated with high-reflectance multilayer films, and the convex surfaces are coated with anti-reflection films to eliminate spurious interferometer resonances involving the back surfaces of the mirrors.

The mirrors are mounted in cells which are separated by a piezoelectric spacer. By applying a potential difference of a few hundred volts to the piezoelectric spacer, the separation of the mirrors can be varied by a few wavelengths. In practice, a sawtooth or sinusoidal waveform is usually applied to the piezoelectric spacer to scan the separation of the interferometer mirrors. For a confocal interferometer, a change in separation of the mirrors of one-fourth wavelength scans the interferometer through one free-spectral-range.

An aperture is placed outside the entrance mirror to limit the diameter of the incident beam. The upper limit on the aperture size can be determined using equation (18). If the beam entering the interferometer is collimated, no further apertures are required. However, if the interferometer is used with non-collimated beams, it is also necessary to use an aperture on the exit of the interferometer to eliminate the reduction in finesse caused by spherical aberration in the mirrors. The use of this second aperture will reduce the peak transmission of the interferometer, and it is generally more desirable to focus the incoming beam properly, rather than use a second aperture.

The light transmitted by the interferometer is detected by a photocell or photomultiplier, and the output signal of the photodetector is recorded on an oscilloscope, as a function of the voltage applied to the piezoelectric spacer. The oscilloscope thus displays a signal which is equivalent to the laser mode intensity vs. optical frequency.

It is important that the mirror separation be quite close to confocal. The tolerance on the mirror spacing depends on the length of the interferometer and its finesse. For very short, high-finesse interferometers, the mirror spacing should be set to within a few wavelengths. In practice, the adjustment of length is quite easy to make. The mirror spacing should be set so that it is approximately confocal. By observing the mode structure of a laser on an oscilloscope, the final adjustment of the mirror spacing can then be made to maximize the finesse of the interferometer. Once the separation of the interferometer mirrors is set, it needs no further adjustment.

The actual use of confocal interferometers is quite simple: basically, they need only be placed in a laser beam and adjusted so that the beam is reflected more or less back on itself. With a relatively crude alignment, fringes will be obtained. To achieve the maximum finesse, the angle should be adjusted fairly carefully to ensure that the interferometer axis is close to the axis of the incident beam. To perform the fine-angle adjustment, it is convenient to mount the interferometer on an adjustable-angle mirror mount.

It is usually desirable to put an optical isolator, such as a circular polarizer, in the beam between the laser and the interferometer, even when the interferometer is illuminated off-axis. The reason for this is that there is usually a certain amount of back-scatter from the interferometer mirrors. Although the specular reflection from the interferometer mirrors does not retro-reflect into the laser, the back-scatter can, in some cases, perturb the modes of the laser.

VI. Applications of Scanning Spherical-Mirror Interferometers

As stated in the introduction, scanning spherical-mirror interferometers are useful for studying the general mode structure of gas lasers. In this section, we consider two specific applications.

The first application of scanning spherical-mirror interferometers that we consider is their use in adjusting a laser so that it operates in a single transverse mode. The conventional method for making such an adjustment consists of visually observing the intensity distribution in the output beam of the laser while adjusting the mirrors. When the output beam has an apparently Gaussian intensity distribution, the laser is assumed to be oscillating in the TEM_{oo} transverse mode.

The above method for adjusting a laser is somewhat unreliable; often lasers which appear to be operating in a single transverse mode actually are oscillating simultaneously in two transverse modes. This double oscillation can be detected easily using a scanning (mode-degenerate) spherical-mirror interferometer. Figure 4 shows the mode spectra obtained when a typical helium-neon laser is operating in (a) two transverse modes, and (b) a single transverse mode.
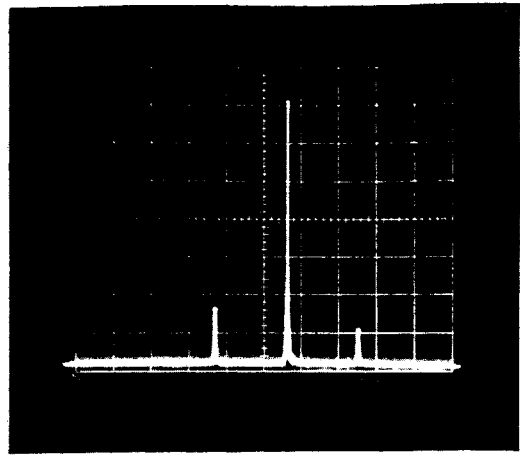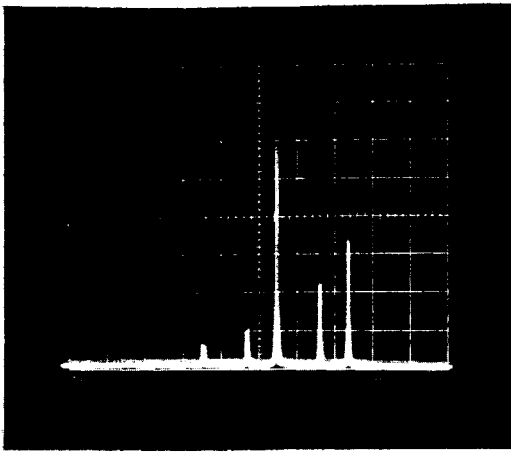
4. (a) Output spectrum of a helium-neon laser operating simultaneously in two transverse modes.

(b) Output spectrum of a helium-neon laser operating in a single transverse mode.

The vertical sensitivity and horizontal dispersion are the same for both (a) and (b).
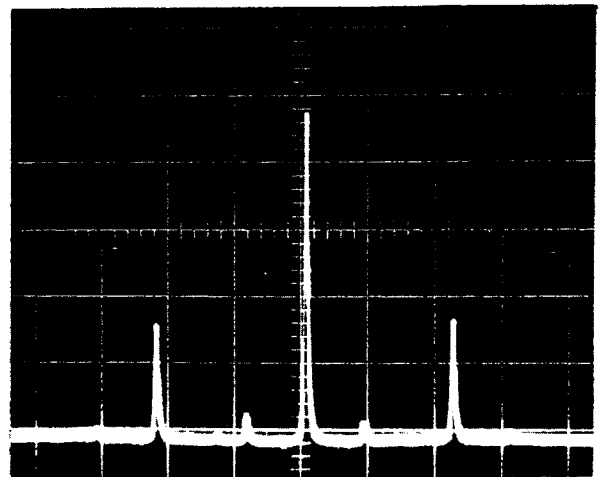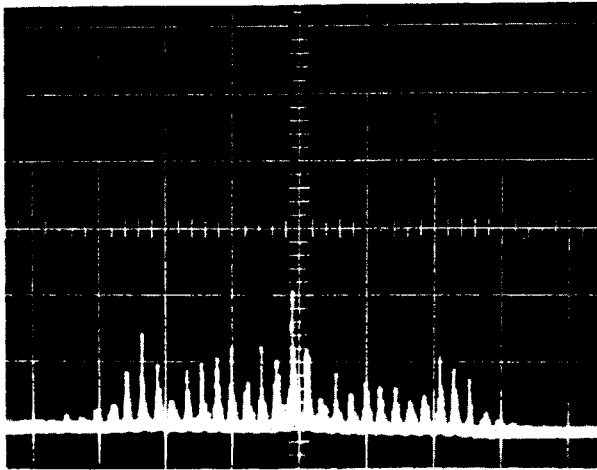
5. (a) Output spectrum from a free-running argon ion laser.

(b) Output spectrum from a self-phase-locked argon ion laser.

The vertical sensitivity and horizontal dispersion are the same for both (a) and (b).

The other application of scanning spherical-mirror interferometers that we consider is their use in studying phase-locking phenomena. Figure 5 shows the output spectrum of a single transverse-mode argon-ion laser when it is (a) free running, and (b) self phase-locked. Note that the output spectrum is quite different for the two cases. The spectrum shown in Figure 6(a) is somewhat blurred because of the erratic mode-hopping during the exposure time. This mode-hopping is characteristic of lasers whose mode spacing is less than the homogeneous linewidth. In Figure 6(b), the output spectrum is constant in time.

Douglas C. Sinclair

April, 1968

7

References

1. R. L. Fork, D. R. Herriott, and H. Kogelnik, "A Scanning Spherical Mirror Interferometer for Spectral Analysis of Laser Radiation," Appl. Optics *3*, 1471 (1964).

2. P. Connes, "Increase of the Product of Luminosity and Resolving Power of Interferometers by Using a Path Difference Independent of the Angle of Incidence," Revue d'Optique *35*, 37 (1956).

3. A. L. Bloom, "Properties of Laser Resonators Giving Uniphase Wave Fronts," Spectra-Physics Laser Technical Bulletin No. 2, Mountain View, California (1963).

4. D. R. Herriott, H. Kogelnik, and R. Kompfner, "Off-Axis Paths in Spherical-Mirror Interferometers," Appl. Optics *3*, 523 (1964).